Technische Universität München

Lehrstuhl für Raumfahrttechnik

In Situ Consumable Production for Mars Missions

Kristian Pauly

Vollständiger Abdruck der von der Fakultät für Maschinenwesen der Technischen Universität München zur Erlangung des akademischen Grades eines

Doktor-Ingenieurs

genehmigten Dissertation.

Vorsitzender: Univ.-Prof. Dr.-Ing. Boris Laschka

Prüfer der Dissertation:

1. Univ.-Prof. Dr.-Ing. Eduard Igenbergs, i.R.
2. Univ.-Prof. Dr.-Ing., Dr.-Ing. habil. Johann Stichlmair

Die Dissertation wurde am 17.01.2002 bei der Technischen Universität München eingereicht und durch die Fakultät für Maschinenwesen am 15.07.2002 angenommen.

Technische Universität München
Fachgebiet Raumfahrttechnik

NASA - Johnson Space Center
Propulsion Systems Branch

"Roald Amundsen and a crew of six in the 70 foot, 47 ton Gjøa were the firsts to find the Northwest Passage to Asia through North America. There had been some hundred previous failed attempts, all involving at least an order of magnitude greater effort than the success. The British Navy, at the height of its power, tried thirty times without success. The Franklin expedition, with two specially adapted steam frigates […] had one of the deepest penetrations into the passage. All 130 men died of starvation on or near King William Island. Amundsen's crew spent more than two years at the same place, hunting caribou for food and doing valuable scientific research instead of starving.

What was the difference?

Carrying all provisions versus living off the land."

[Olson, 1997]

ACKNOWLEDGEMENTS

I would like to thank for their continued support:

My Family
Dr.-Ing. Peter Eckart
Hugh Ronalds
The German National Merit Foundation (Studienstiftung des dt. Volkes)

as well as

Prof. Eduard Igenbergs	Dr. Howard Wagner	John Connolly
Prof. Johann Stichlmair	Scott Baird	Constantin Corsten
Todd Peters	Gerald Sanders	Nadeeka Cyril
Martin McClean	Joe Trevathan	Kennda Lynch
Tom Simon	Donn Sickorez	Andrea Ross

Dedicated to Thidarat

อวกาศ รัก ธิดารัตน์

TABLE OF CONTENTS

1 Introduction 15
2 Background 19
2.1 Definitions 19
2.1.1 In Situ Resource Utilization (ISRU) 19
2.1.2 In Situ Consumable Production (ISCP) 19
2.1.3 In Situ Propellant Production (ISPP) 20
2.1.4 Mars In Situ Consumable Production Elements 20
2.2 NASA's Long-Term Planning 21
2.2.1 Mars Surveyor Program 21
2.2.2 The NASA Design Reference Mission 23
2.2.3 Where does ISRU fit in? 32
2.2.3.1 Mass Reduction 35
2.2.3.2 Cost Reduction 35
2.2.3.3 Risk Reduction 35
2.2.3.4 Expansion of Human Exploration and Presence 35
2.2.3.5 Enabling of Space Commercialization 35
2.3 Propulsion and Fluid Systems Branch 37
2.3.1 Mars ISRU Systems Test Facility 37
2.3.2 Mars ISPP Precursor Experiment (MIP) 39
2.4 The Sabatier Reaction 40
2.4.1 The Sabatier Reaction in Chemistry 40
2.4.2 The Sabatier Process in Life Support Systems 43
2.5 Requirements and Constraints for Space Applications 44
2.5.1 Launch Environment 44
2.5.2 Space Environment 45
2.5.3 Mars Environment 47
2.6 Scope of Ph.D. Work 49
3 Modeling 53
3.1 Outline 53
3.2 The Reverse Water Gas Shift Reaction 54
3.3 Methanol Synthesis 63
3.4 Excel Model 69
3.5 MATLAB Model of the Sabatier Reactor 72
3.5.1 Pressure Loss within the Reactor 72
3.5.2 Enthalpy, Heat of Reaction, Gibbs Energy 74
3.5.3 Actual Heat of Formation 81
3.5.4 Lagrange's Undetermined Multipliers Method 82
3.5.5 Relaxation Method 86
3.5.6 Modified Relaxation Method 89

3.5.7 Modified Relaxation Method in Cylinder Coordinates 90
3.5.8 Relaxation Method with Internal Heat Sources 91
3.5.9 Influence of Catalyst on Mass and Heat Transport 92
3.5.10 Reaction Rate 97
3.6 MATLAB/SIMULINK Model of the Overall System 102
3.6.1 Modeling of Fluid Properties 102
3.6.2 Atmosphere Acquisition System 103
3.6.3 Pipes 105
3.6.3.1 Heat Transfer at Inner Wall 105
3.6.3.2 Heat Flow due to Convection 109
3.6.3.3 Heat Transfer due to External Airflow 110
3.6.4 Condenser 114
3.6.5 Electrolyzer 118
3.6.6 Overall Model 119
4 Testing 123
4.1 Outline 123
4.2 Test Setup 124
4.2.1 Atmosphere Simulation and Acquisition 127
4.2.2 Chemical Processing 128
4.2.3 Liquefaction and Storage 130
4.3 Safety and Environmental Impact 132
4.4 Integrated Tests under Ambient Conditions 133
4.4.1 Flow Schematic 133
4.4.2 Measurements and Controls 133
4.4.3 Test Plan for Tests under Ambient Conditions 134
4.5 Integrated Tests in Simulated Martian Environment 137
4.5.1 Flow Schematic 137
4.5.2 Measurements and Controls 137
4.5.3 Simulation of Martian Environment 138
4.5.4 Test Plan for Tests under Simulated Martian Environment Conditions 139
4.6 Results of Integrated Tests under Ambient Conditions 142
4.7 Results of Integrated Tests in Simulated Martian Environment 145
5 Validation / Comparison of Model and Tests 149
5.1 Outline 149
5.2 Evaluation of Model Predictions of Atmosphere Acquisition 151
5.3 Evaluation of Model Predictions of Tests under Ambient Conditions 152
5.4 Evaluation of Model Predictions of Tests in Simulated Martian Environment 153
6 Next Steps 155
6.1 Learned Lessons of the 1st Generation Breadboard 155
6.1.1 Filling and Draining of Water into and from the Breadboard 155
6.1.2 Flooding of Reactor 156
6.1.3 Vent Path for Trace Gases 157

6.1.4 COTS vs. Martian Requirements 158
6.1.5 Pressure Control throughout the System 159
6.1.6 Check-Valve Problems 160
6.1.7 Corrosion of Brass 3-Way Valve 160
6.1.8 Carbonic Acid Production 160
6.1.9 Loading of Reactor and Dryers 160
6.1.10 Sample Port Location 161
6.1.11 Storage Vessel Evacuation 162
6.1.12 Water Level Measurements 162
6.1.13 Over-sizing of Condenser Tank 162
6.1.14 Static Electricity Problems 163
6.1.15 Sabatier Reactor Heat Management 163
6.1.16 Water Supply for Electrolyzer 164
6.2 Second Generation Breadboard 164
6.3 Sabatier ISRU Demonstrator for Mars Surveyor Program Missions 171
6.4 ICONPROM - Integrated Consumables Production on Mars 173
6.4.1 Drawbacks of current Planning 173
6.4.2 IconProM – The Concept 174
6.4.3 Beyond Sabatier and Mars 179
7 Conclusions 183
Appendix A: Breadboard Flow Sheet for Tests under Earth Ambient Conditions 185
Appendix B: Breadboard Flow Sheet for Tests in Simulated Mars Environment 187
Appendix C: Test Procedure 193
References 207

LIST OF FIGURES

Figure 2-1: Typical Martian ISCP Production Elements 20
Figure 2-2: Mars Surveyor Program (Status before MCO/MPL Failures) 21
Figure 2-3: Revised Mars Surveyor Program (Status October 2000) 22
Figure 2-4: DRM Mission Architecture 24
Figure 2-5: DRM Mission Sequence 26
Figure 2-6: Shuttle C and Magnum Launch Vehicle 27
Figure 2-7: Payload Stacks for Nuclear Thermal Propulsion 28
Figure 2-8: Solar Electric Propulsion System Layout 29
Figure 2-9: Deployed ISRU Plant 30
Figure 2-10: Long- and Short-Stay Missions 31
Figure 2-11: Fast Transit Trajectory 31
Figure 2-12: Comparison of Different ISRU Options 33
Figure 2-13: Rationale for ISRU 36
Figure 2-15: NASA-JSC Energy Systems Test Area 38
Figure 2-16: The MIP Experiment during Flight Acceptance Testing at NASA-JSC 39
Figure 2-17: Simplified Sabatier / Water Electrolysis System Overview 42
Figure 2-18: Longitudinal Static, Acoustic and Shock Loads of Launch Environment 46
Figure 2-19: Progress and Uncertainties of ISRU Development 50
Figure 2-20: Procedure pursued in this Thesis 52
Figure 3-1: Sabatier / Water Electrolysis Breadboard 54
Figure 3-2: Effect of Pressure and Input Ratio on Conversion 57
Figure 3-3: Equilibrium Constants as a Function of Temperature 60
Figure 3-4: Reaction Triangle of Methanol Synthesis 64
Figure 3-5: Solving of non-linear Equations for the Extents of Reaction 69
Figure 3-6: Coefficient Matrix representing the non-linear RWGS equations 69
Figure 3-7: Excel Model of a RWGS / Methanol Synthesis Reactor 71
Figure 3-8: Pressure Loss Estimates 73
Figure 3-9: Modeled C_p (red) vs. actual C_p (blue) 77
Figure 3-10: Comparison of different Approximations for the Standard Heat of Sabatier Reaction 79
Figure 3-11: Modeled Gibbs Energy and Enthalphy vs. Actual Values 80
Figure 3-13: Working Scheme of Finite Element Modeling of Reactor 82
Figure 3-14: Fugacity of Water 83
Figure 3-15: Reaction Equilibrium as a Function of Temperature 84
Figure 3-16: Reaction Equilibrium as a Function of Temperature and Pressure 85
Figure 3-17: Reaction Equilibrium of Sabatier Reactor 86
Figure 3-18: Two-Dimensional Finite Element Grid 87
Figure 3-19: Convergence of Relaxation Method 89
Figure 3-20: Effective Heat Conductivity as a Function of Porosity and $\lambda_{solid}/\lambda_{fluid}$ 95

Figure 3-21: Reactor Bed Porosity Distribution 96
Figure 3-22: Sabatier Reaction Equilibrium Constant 100
Figure 3-23: H_2 Viscosity Model – Accuracy 103
Figure 3-24: Pipe Temperature Loss Calculations Overview 113
Figure 3-25: Condenser Calculations Overview 117
Figure 3-26: MATLAB Model - Overview over Simulation Program Elements 119
Figure 3-27: Simulink Model of the Overall Breadboard with User Interface 121
Figure 4-1: Sabatier / Water Electrolysis Breadboard in the 20ft Vacuum Chamber of the MISTF Facility 124
Figure 4-2: Breadboard Overview 125
Figure 4-3: Overall Sabatier / Water Electrolysis Breadboard Layout 126
Figure 4-4: Breadboard Frontplate Subsystem Overview 126
Figure 4-5: Flow Sheet of Breadboard Atmosphere Simulation Subsystem 127
Figure 4-6: Flow Sheet of Breadboard Atmosphere Acquisition Subsystem 128
Figure 4-7: Sabatier Reactor, with Copper Strap, with Insulation 129
Figure 4-8: Flow Sheet of Breadboard Chemical Processing Subsystem 130
Figure 4-9: Flow Sheet of Breadboard Liquefaction and Storage Subsystem 131
Figure 4-10: Test Procedure for Earth Ambient Tests 136
Figure 4-11: Flow Sheet of Breadboard Process Sampling Subsystem 137
Figure 4-12: Residual Gas Analyzer User Interface 138
Figure 4-13: Test Procedure for Tests in Simulated Martian Environment 141
Figure 4-14: Successful Ambient Test Run (Series D, Test 2, 22.09.1999 – Reaction Achieved) 143
Figure 4-15: Failed Ambient Test Run (Series C, Test 1, 16.09.99 – No Reaction) 144
Figure 4-16: Successful Environment Test Run (Series K, Test 1, 05.12.2000 – Reaction Achieved) 146
Figure 5-1: Temperature Distribution in the Reactor 150
Figure 5-2: CO_2 Adsorption of Sorption Bed as a Function of Pressure and Temperature 151
Figure 5-3: Comparison of measured vs. calculated Temperatures under Earth Ambient Conditions 153
Figure 5-4: Comparison of measured vs. calculated Temperatures in simulated Martian Environment 154
Figure 6-1: Reactor Top with Thermocouple 161
Figure 6-2: Installation of Copper Strap 164
Figure 6-3: Conceptual Design of 2nd Generation Sabatier Reactor (Initial Design) 165
Figure 6-4: 2nd Generation Sabatier Breadboard - Draft Design 166
Figure 6-5: Grid Structure of 2nd Generation Breadboard Reactor 168
Figure 6-6: Massflow Analysis 2nd Generation Breadboard 169
Figure 6-7: Latest Layout of 2nd Generation Breadboard 170
Figure 6-8: Model User Interface - Vital Parameters of 2nd Generation Breadboard 171
Figure 6-9: PUMPP ("Propulsive Use of on Mars Produced Propellant") Experiment - Preliminary Layout with Lander Shroud 172

Figure 6-10: Micro-Channel Technology 173
Figure 6-11: Elements of Current Program Architecture 174
Figure 6-12: Integrated Consumable Production for/on Mars 176
Figure 6-13: IConProM in Practice – Application in a DRM Scenario 178
Figure 6-14: IConProM - Integrating ECLSS and ISPP Functions 179
Figure 6-15: Stability of Sub-Surface Ice on Mars 180

LIST OF TABLES

Table 2-1: Earth vs. Mars Environment 48
Table 3-1: Critical Molecule Diameters 57
Table 3-2: Heat Capacities of Gases 63
Table 3-3: Heat Capacity Constants 78
Table 3-4: Values for rate constant, activation energy, and catalyst coefficient 101

ABBREVIATIONS

BPR	Back Pressure Regulator
COTS	Commercial off the Shelf
CH	Cold Head
CV	Check Valve
DART	Dust Accumulation and Repulsion Test
DRM	Design Reference Mission
ER	Electronic Regulator
ERV	Earth Return Vehicle
ESA	European Space Agency
EV	Electronic Valve
EVA	Extravehicular Activity
FCV	Flow Control Valve
F	Filter
FC	Flow Controller
FM	Flow Meter
HE	Heat Exchanger
HLLV	Heavy-Lift Launch Vehicle
HRP	Hydrogen Recovery Pump
HTR	Heater (electrical)
HV	Hand Valve
IConProM	Integrated Consumable Production on/for Mars
IDE	Integrated Design Environment
IMLEO	Initial Mass in Low Earth Orbit
ISCP	In Situ Consumable Production
ISPP	In Situ Propellant Production
ISRU	In Situ Resource Utilization
JSC	Johnson Space Center
LEO	Low Earth Orbit
LHHW	Langmuir-Hinshelwood-Hougen-Watson (Rate Expression Model)
LMO	Low Mars Orbit
LSS	Life Support System
LS	Level Sensor
MAAC	Mars Atmosphere Acquisition and Compression (Part of MIP)
MATE	Mars Array Technology Experiment (Part of MIP)
MAV	Mars Ascent Vehicle
MGS	Mars Global Surveyor
MIP	Mars ISPP Precursor (2001 Lander Experiment)
MISTF	Mars ISRU Systems Test Facility
MOI	Mars Orbit Insertion
MPF	Mars Pathfinder
MTERC	Mars Thermal Environment and Radiator Characterization (Part of MIP)
MTV	Mars Transfer Vehicle
NASA	National Aeronautics and Space Administration
NC	Normally Closed
NERVA	Nuclear Engine for Rocket Vehicle Application
NIST	National Institute of Standards and Technology
NO	Normally Open
NTR	Nuclear Thermal Rocket
OGS	Oxygen Generator Subsystem (Sub-Experiment of MIP)
PEM	Proton Exchange Membrane
PEMFC	Proton Exchange Membrane Fuel Cells or Polymer Electrolyte Membrane Fuel Cells (Polymer Electrolyte Membrane is the generic term)
Ph.D.	Philosophiae Doctor
PID	Proportional-Integral-Differential Control
PT	Pressure Transducer
PUMPP	Propulsive Utilization of on Mars Produced Propellant (Experiment planned to be flown aboard the 2003 Mars Lander)
RGA	Residual Gas Analyzer
RKA	Russian Aerospace Agency (Российским Авиационно-Космическим Агентством)
RTG	Radioisotope Thermoelectric Generator
RV	Release Valve
RWGS	Reverse Water Gas Shift Reaction
SEI	Space Exploration Initiative
SOEC	Solid Oxide Electrolysis Cell
SOFC	Solid Oxide Fuel Cell
SOV	Solenoid Valve
STS	Space Transportation System (Space Shuttle)
SV	Solenoid Valve
T	Thermocouple / Temperature Sensor
TEI	Trans-Earth Injection
TMI	Trans-Mars Injection
TRR	Technical Readiness Review
TRL	Technology Readiness Level
WGS	Water Gas Shift Reaction

SYMBOLS / UNITS

In order to prevent the loss of more space probes, English units are avoided as far as possible; SI units are preferred. Every symbol is also explained at its point of usage. The decimal point is written as for example as in "0.01". In order to reduce the potential for confusion, commas for parting thousands, millions, etc. (American notation) are not used.

α	Heat Transition Coefficient	$[W/(m^2K)]$
η	Concentration Polarization	[V]
ρ	Density	$[kg/m^3]$
η	Dynamic Viscosity	$[Ns/m^2]$
λ	Heat Conductivity	[W/(mK)]
ν	Kinematic Viscosity	$[m^2/s]$
η_{ohm}	Ohmic Polarization	[mV]
u	Stoichiometric Number	[-]
a	Acceleration	$[m/s^2]$
A	Area	$[m^2]$
c_P	Specific Heat Capacity	[J/(kgK)]
C_{Pm}	Molar Heat Capacity	[J/(molK)]
D	Diameter	[m]
D_i	Inner Diameter	[m]
D_o	Outer Diameter	[m]
E	Energy	[J]
e	Elementary Charge	$1.602 \cdot 10^{-19}$ [C]
E^o	Standard Potential (Nernst current)	[V]
F	Faraday's Constant	$9.648 \cdot 10^4$ [C/mol]
F	Force	[N]
G^o	Standard Free (Gibbs) Energy	[J]
g_E	Norm Gravity Factor on Earth	9.80665 [N/kg]
g_M	Norm Gravity Factor on Mars	3.73 [N/kg]
H^o	Standard Enthalpy	[J/mol]
i	Current Density	$[A/m^2]$
I	Electric Current	[A]
i_L	Limiting Current Density	$[A/m^2]$
k	Heat Transition Number	$[W/(m^2K)]$
K_H	Film Height Coefficient	[-]
K_T	Film Temperature Coefficient	[-]
m	Mass	[kg]
n	Number of Electrons	[-]
n	Substance Quantity	[mol]
N_A	Avogadro's Constant	$6.0221367 \cdot 10^{23}$ [1/mol]
Nu	Nußelt Number	[-]

This page was intentionally left blank

P	Power	[W]
p	Pressure	[bar = 10^5Pa]
Pr	Prandtl number	[-]
Q	Heat	[J]
q	Specific Heat	[J/kg]
Q_m	Molar Heat	[J/mol]
R	Total Cell Impedance	[Ωcm^2]
R	Electric Resistance	[Ω]
$R_{(X)}$	Specific Gas Constant (of substance X)	[J/(kgK)]
Re	Reynolds number	[-]
Re_c	Critical Reynolds number	2300 [-]
R_m	Universal (molar) gas constant	8.31451 [J/(molK)]
T	Temperature	[K]
t	Time	[s]
U	Circumference	[m]
U	Voltage	[V]
v	Velocity	[m/s]
V	Volume	[m^3]
V_{mn}	Molar Norm Volume	22.4141 [m^3/kmol]
w	Specific Work	[J/kg]
W	Work	[J]
W_m	Molar Work	[J/mol]
X	Length	[m]

Dots on variables mean differentiation over the time; e.g. $\dot{m} = \frac{dm}{dt}$ stands for mass flow, $\dot{V} = \frac{dV}{dt}$ for volume flow.

1 INTRODUCTION

Since the very first plans for a human Mars mission, like the studies of [von Braun, 1956], it has been evident that this project would definitely be one of the biggest endeavors that man has ever undertaken, maybe requiring even more man-hours than the construction of the pyramids or the great wall [von Puttkamer, 1996]. Since then it has also become obvious that this project will consume a considerable amount of money, too. Several attempts in the past were made to reduce the cost of a human Mars mission. However, in the decades following the von Braun study, the amount of really new ideas in this context remained comparatively low [Portree, 2001]. And none of the few new ideas that were brought forward (e.g. aerocapture [Himmel et al., 1961], nuclear propulsion [Ruppe, 1963], recurrent trajectories [Friedlander et al., 1986], etc.) could reduce the costs significantly below the costs of a conventional, all chemical Mars Mission. In the course of the Space Exploration Initiative (SEI) of President Bush Sr. in 1990, and as part of the infamous "90-days-report" [Cohen et al., 1989], a group at the Johnson Space Center (JSC) estimated the cost for such a "conventional" mission to be in the order of some $235 \cdot 10^9$US$[1] [Cohen et al., 1989] - approximately half of the total cost of the initiative. These plans had to be given up due to lack of political support.
Without receiving much attention however already in the Sixties [Steinhoff, 1963], the Seventies [Ash et al., 1978], and in the Eighties [Richter, 1981] methods were suggested and investigated which dealt with Mars **in situ resource utilization (ISRU)**, that means using the resources found on the Red Planet. After the sudden demise of the Space Exploration Initiative, Robert Zubrin, a member of Martin Marietta Astronautics, proposed the so-called "Mars Direct" plan, a plan that involved the extensive use of in situ resources [Zubrin & Wagner, 1996]. This was the first time ISRU entered the perception of a large audience.

Since then, numerous studies have been performed, we which show that **ISRU can significantly reduce mass, cost, and risk of exploration missions** (both, robotic and human). Consequently, the Exploration Office at JSC altered its "Design Reference Mission" (DRM)[2], which since then has been based on the ISRU philosophy.

Mass can reduced mainly by in situ propellant production, since for space missions the propellant is typically the largest mass fraction of the overall system. The benefit of ISRU comes into play especially for return missions. Usually, these missions are of greater effort than normal missions, since they not only have to carry the payload itself, but also

[1] In 1989's dollars

[2] The DRM [Hoffmann & Kaplan, 1997] describes the currently preferred plan for the first human Mars missions. Every new proposal is compared to the current DRM to see whether it is preferable or not. In the case of the former, the DRM is changed accordingly (compare e.g. [Schaefer, 1997]).

the means to return it. The Saturn 5 is an embodiment of this effect. The hugeness of this launcher is mainly caused by the fact that it did not only have to bring the astronauts to the moon, but also the (much more massive) return propellant and return capsule. And for each kilogram of propellant brought to the moon, a multiple of that had to be launched from Earth. With the help of in situ propellant production however, the "multiplication chain" that usually aggravates return missions can be avoided.

Cost is to a large degree influenced by the mass of space systems. ISRU systems introduce mass to the system, too, however the (propellant mass) savings more than make up for their mass. Thus, even taking into account the additional cost introduced via ISRU systems, total mission cost savings of considerate extents are possible. The same group at JSC that had estimated the costs for the 90-days-study calculated the cost for the ISRU-based "Semi Direct Mission" to be less than *one eighth* of the cost based on the 90-days-study [Cyr, 1998].

Risk is reduced by providing a functional backup to the life support system, reducing dependence on Earth supplied logistics, providing mission flexibility, and increasing radiation protection using indigenous materials.

Many of the ISRU-related studies, however, are just theory – work based on theoretical deliberations rather than on hardware testing. The Johnson Space Center as NASA's lead center for human space exploration and thus human Mars mission design has therefore decided to fill this gap and initiate a test facility as well as a development program with hardware that brings these technologies from theory up to a level from where they can help set the way for Human Mars Missions. The work described in this document is embedded into this effort and was mainly conducted during an research stay at the Propulsion Branch of the Johnson Space Center lasting from January 1999 to May 2001.

Goal of this thesis is to firstly model an ISRU system (in particular the so-called Sabatier process) end-to-end and with all its essential chemical and physical processes included, something that has not been attempted yet in this form. Secondly, the thesis will attain concrete hardware data from tests conducted with an Sabatier / water electrolysis breadboard under Earth ambient and simulated Martian environment. It will then try to validate the computer model using this data.
Based on the model and the tests, the modeling capability as well as the gained experience will be utilized to derive recommendations for new generations of hardware, ranging from 2nd generation breadboards over demonstration experiments for robotic Mars landers to consumable production units to be used in the context of human missions to the Red Planet. The developed and validated tools are – like the concept of ISRU itself, too – not only applicable to the Sabatier process or Mars respectively. They are *generic*, meaning that many of their elements can be employed in other areas, too, such as for example for the modeling of other processes and systems, as well as applications on

celestial bodies other than Mars. Hence, they aim at serving as a stepping-stone for further development in this area.
The thesis is structured as follows:

Chapter 2 describes the background of this dissertation. It depicts current ISRU activities, how this thesis fits into the "big picture" of Mars exploration, how NASA plans to send humans to Mars, how the human missions are to be prepared by robotic precursor missions, as well as the expertise of the Propulsion and Fluid Systems Branch, the host institution for the author's research work at NASA Johnson Space Center.

Chapter 3 describes the development of the author's computer model as well as the theory that stands behind it.

Chapter 4 deals with the test setup, the test execution as well as the test results that were obtained in the course of tests within the Mars ISRU Systems Test Facility.

Chapter 5 is the synthesis of the previous two chapters: here the theoretical predictions of the computer model meet the real data. Differences are highlighted and the model's usefulness is evaluated.

Chapter 6 looks into the future: what experiences can be derived from the work done? Which design guidelines can be derived for future test hardware? What is the best approach for ISRU systems to be flown on robotic missions, and on human missions, respectively?

Chapter 7 summarizes the thesis and its results.

2 BACKGROUND

In this chapter, information is given that is necessary to understand the content of succeeding chapters.
First, some basic terms will be defined. Then, a brief overlook over the current NASA long-term planning for the human and robotic exploration of the Red Planet is given. With this context in mind, the rationale of in situ resource utilization and its placement in the overall setting is discussed. The thesis work presented in this paper is embedded in this setting and was mainly conducted at the Propulsion Branch of the Johnson Space Center, NASA's lead center for in situ resource utilization. The expertise and the activities of the host institution are thus described, too. Then, the use of the Sabatier process in related areas, as well as requirements and constraints of its use for space applications are discussed. Finally, in light of this background, the scope of the Ph.D. is defined and outlined.

2.1 Definitions

The following definitions are crucial for the understanding of the content of this thesis. They will be outlined in this chapter in order to eliminate the risk of confusion and misunderstandings.

2.1.1 In Situ Resource Utilization (ISRU)

ISRU covers all aspects of using or processing local resources for the benefit of robotic and human exploration. It represents a paradigm shift away from the classical approach of "take everything with you" towards a philosophy of "living off the land". An example of the classical approach are the Apollo missions, which did not make use of the local resources, but relied solely on assets imported from Earth. Examples for ISRU are:

- Using regolith for radiation shielding
- Making surface habitats / structures and solar cells from processed resources
- Making propellants or other consumables

2.1.2 In Situ Consumable Production (ISCP)

ISCP is a subset of ISRU that covers all aspects of producing consumables from local resources. Consumable products and needs include substances that are consumed in order to assist space missions such as:

- Propellant for ascent / Earth return vehicles and hoppers
- Reagents for fuel cells
- O_2, H_2O, and N_2 for environmental control & life support systems (ECLSS)
- Gases for purging, inflating habitats/structures, & pneumatic equipment
- Heat for spacecraft/habitat thermal control

The focus of this thesis is on systems for Martian In Situ Consumable Production.

2.1.3 In Situ Propellant Production (ISPP)

ISPP is a subset of ISCP that covers all aspects of producing propellants from local resources. This propellant may be used e.g. in ascent vehicles, hoppers, as well as in rovers and other surface mobility systems. ISPP requires the least amount of infrastructure to support and provides immediate benefits to mission plans. Therefore it will probably be the first area, in which ISRU will be put to use. Consequently, most of the work currently performed in ISRU research is conducted in the area of ISPP.

2.1.4 Mars In Situ Consumable Production Elements

The elements of a typical Martian ISCP system utilizing the Mars atmosphere are outlined in the following figure:

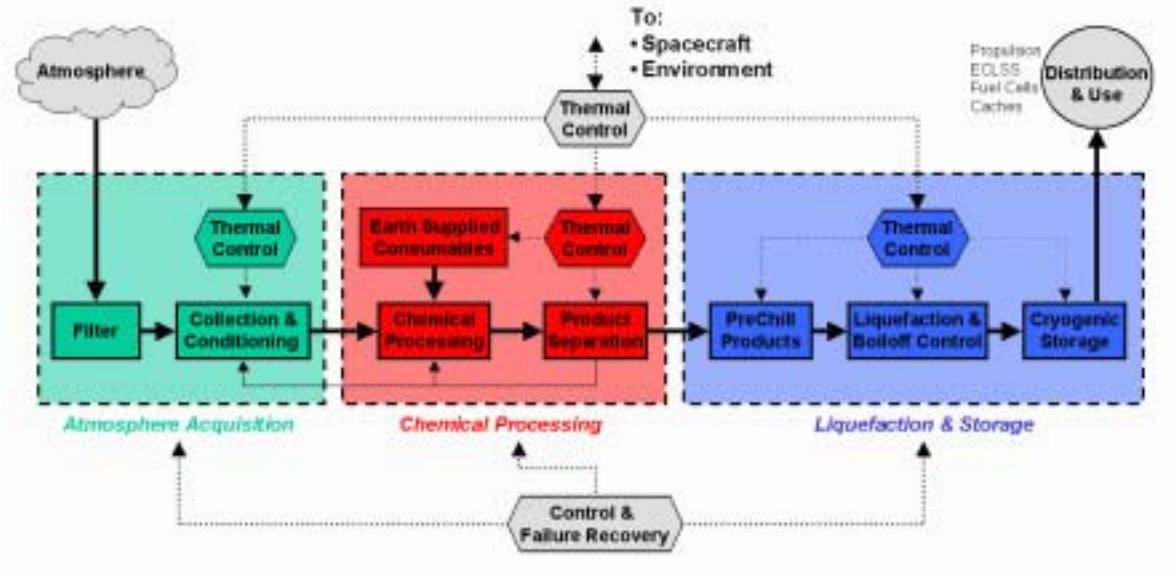

Figure 2-1: Typical Martian ISCP Production Elements

Such a system would typically consist of the three main subsystems:

Atmosphere Acquisition

which filters and compresses the atmosphere from the very low pressures in the Martian atmosphere (some 6 mbar) to the internal process pressures (typically few bars). This can be achieved with the help of adsorption beds, mechanical pumps, chemical acquisition, or freezers.

Chemical Processing

which represents the core of ISCP systems. Here, the reactants are transferred into products via chemical (or physical) processes. For a review of a variety of different process options, see [Pauly, 1998a]. Some processes require "seed" reactants which have to be imported from Earth, in most cases hydrogen. Following the processing of reactants, the produced consumables are separated from the product streams. The unreacted reactants and unwanted products are re-inserted into the reactant stream (or dumped).

Liquefaction & Storage
where the propellants are cooled down and liquefied. They are then stored, however in some cases (e.g. for life support applications) the products may well be directed towards their utilization directly without this interim step.

In all three phases of ISCP, process control (in particular thermal control) of the processes is of crucial importance. This is especially true for turn-on and turn-off transient phases [Lauterbach, 1998].

2.2 NASA's Long-Term Planning

2.2.1 Mars Surveyor Program

All of NASA's robotic exploration efforts to the Red Planet are placed into the overall "Mars Surveyor Program". The different missions serving to this common goal are summarized in Figure 2-2.

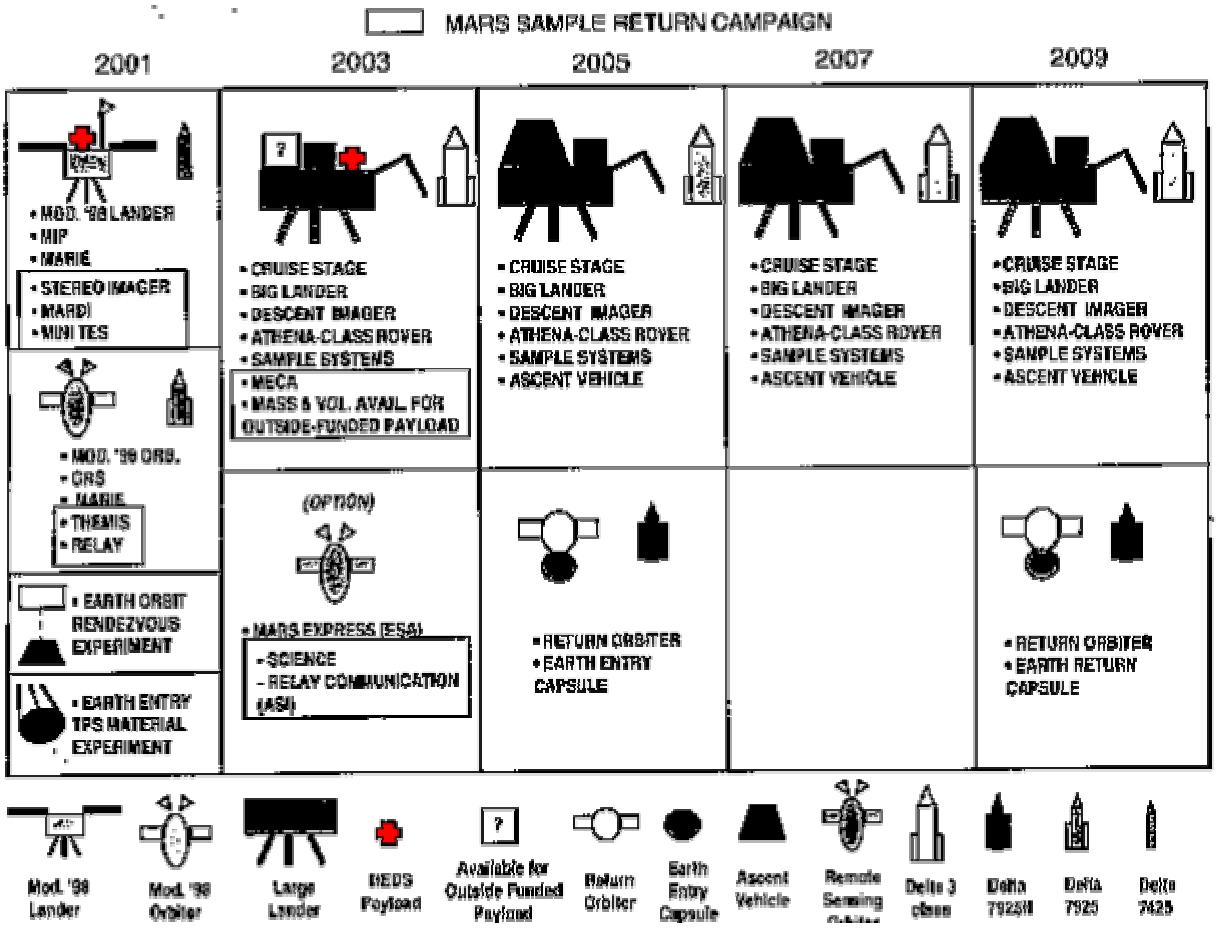

Figure 2-2: Mars Surveyor Program (Status before MCO / MPL Failures)
[Connolly,1998]

In this overall concept, it was planned to send one lander and one orbiter towards Mars in every launch window for at least ten years, starting with Mars Pathfinder and Mars Global Surveyor in 1996. Aboard the 2001 Lander, according to this plan, the very first ISPP experiment should have flown to and been activated on Mars. This experiment (the "Mars ISPP Precursor" – MIP) was developed under the lead of the Propulsion and Fluid Systems Branch of NASA Johnson Space Center in Houston Texas. This group also planned a follow-on experiment "PUMPP" (Propulsive Utilization of on Mars Produced Propellant) to be launched the succeeding launch window in 2003. Here, for the first time, an end-to-end Sabatier / water electrolysis system was to be demonstrated. The demonstrator was supposed to produce methane and oxygen from the Martian atmosphere, as well as to liquefy, store, and utilize them in a small rocket engine. The work described in this thesis started in the Propulsion and Fluid Systems Branch under the premise that its effort would later be an integral part of the follow-on experiment; however all these plans and activities – as well as the whole Mars Surveyor Program - were harshly impacted by the failures of both, the Mars Climate Orbiter in September 1998 and the Mars Polar Lander in January 1999. In the latter case, design flaws and inadequate testing led to a complete mission failure. Due to the close resemblance of the spacecraft bus designs of the '98 and the '01 lander, NASA decided not to launch the latter one and to alter the entire Mars Surveyor Program. The revised architecture is shown in Figure 2-3.

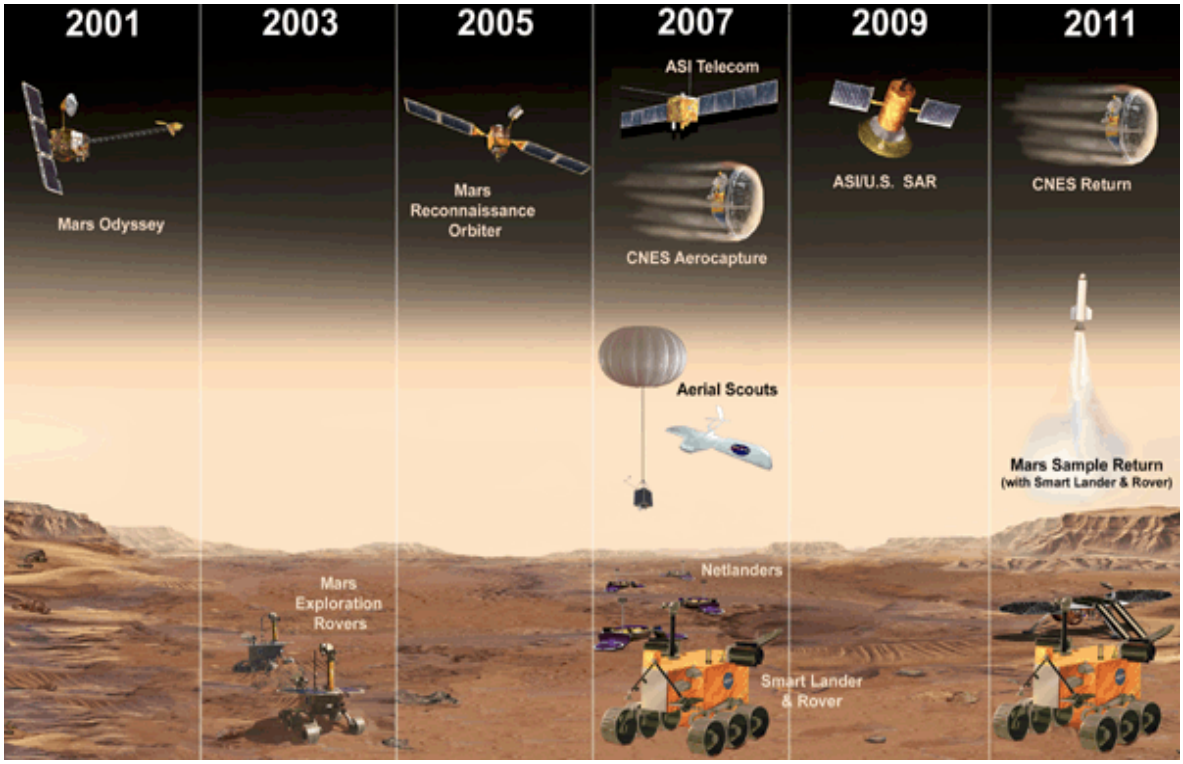

Figure 2-3: Revised Mars Surveyor Program (Status October 2000) [JPL, 2000]

This decision at the highest level also had a direct effect on the work of the Propulsion Branch and on the presented thesis. Although the flight version of the MIP experiment (as well as many other 2001 experiments) had already passed the flight-qualification tests,

neither them nor the follow-on experiment will fly (at least not before 2007). As a result, the scope of the activities of the Propulsion Branch shifted towards the preparation of an interim step, a 2nd Generation Sabatier / Water Electrolysis Breadboard, which is described later in this thesis.

Shortly before the completion of this thesis, a new NASA administrator was called into office. He has already outlined his aim of significant changes within NASA, which will undoubtedly also impact NASA's Mars program.

2.2.2 The NASA Design Reference Mission

The various Mars-related efforts of agencies all around the world have to be seen not just as isolated missions, but in their context. Many of these efforts are intended to culminate in the first human mission to Mars. In order to be able to understand why agencies like NASA, as well as ESA, have started to invest into ISRU, and in order to get an appreciation of the role of ISRU in the big picture of future Mars exploration efforts, the current mission scenario of the Human Mars Mission Study Team is described. According to the Version 3.0 of the Design Reference Mission [DRM V3.0, 1998] (see also [Hoffmann & Kaplan, 1997], [Schaefer, 1997], [Joosten et al., 1997], [Drake, 1998]), the different aspects of the first human Mars mission architecture will look as outlined in the following graphic (see also Figure 2-4):

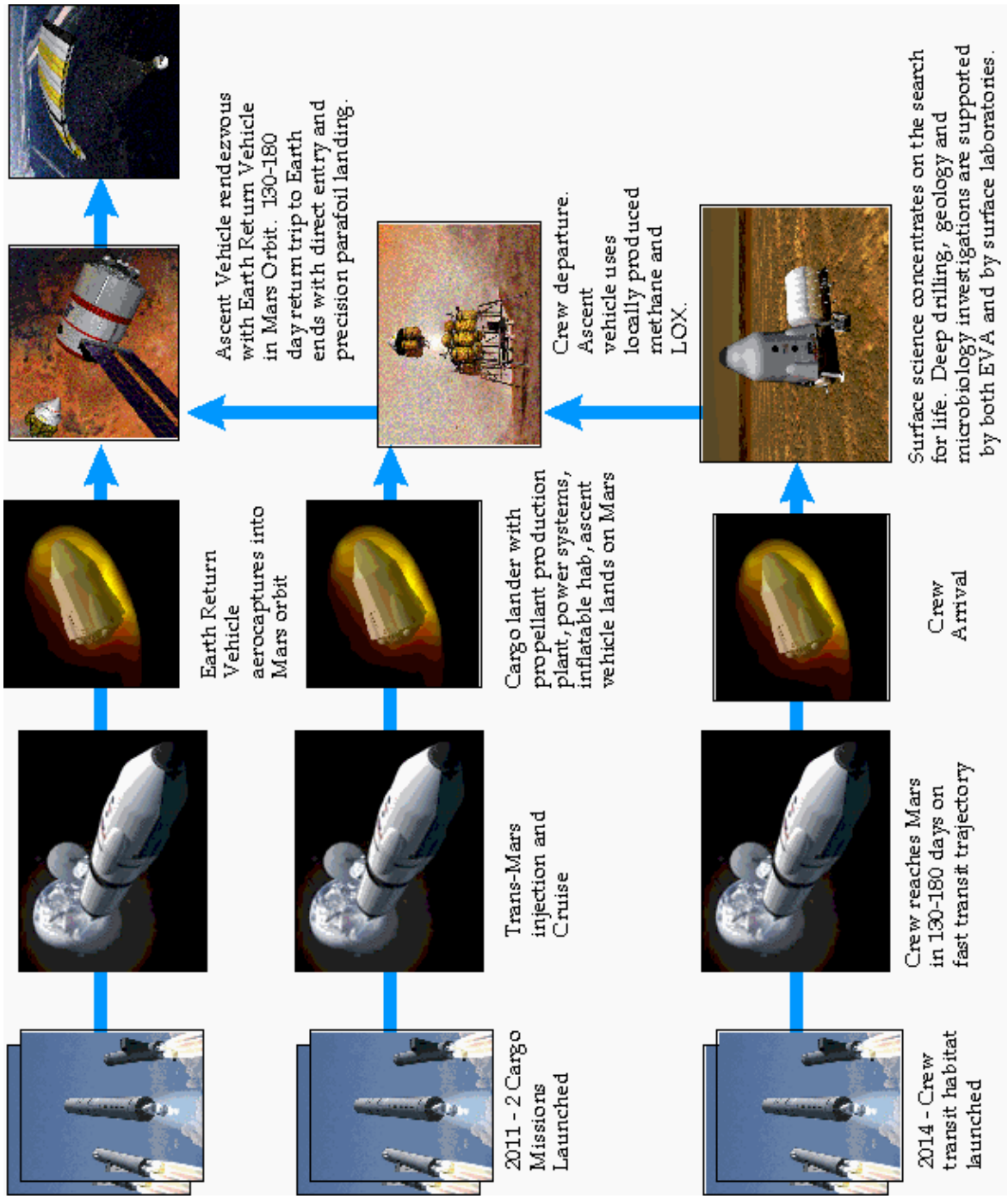

Figure 2-4: DRM Mission Architecture [DRM V3.0, 1998]

- In opposition to other mission architecture, this design reference mission document pays special attention to the fact that the first human Mars mission will likely be not just a stand-alone mission, but rather embedded in a whole set of robotic precursor/outpost missions, pre-deployment/cargo missions, and follow-on human missions, meaning an overall context or framework. It is important to not overlook the importance of this interrelationship between succeeding missions since these missions can greatly benefit from each other. This is possible, since the celestial mechanics of the Earth and Mars orbits allow an Hohmann Transfer roughly every 25 months.

Transit times to Mars are in the order of 8 months on Hohmann trajectories (which would be used for cargo missions), and 6 months for the faster Typ I "fast" trajectories (which would be used for crew transfers). Together with some 550 days stay on the Martian surface (waiting for the Earth return launch window to open), this results in a total mission duration for the crew of over 900 days[1]. Previous concepts involving short stay strategies (see Figure 2-10b) are not pursued by NASA any more, mainly because they mean little reduced mission size at the cost of a almost completely scrubbed surface stay (typically less than a month).

- Per outbound launch window, three spacecrafts are sent en route to Mars. Two of them are cargo ships on slow Hohmann trajectories, the third one is a crew transit ship on a fast trajectory. The crew ship launches after the two crew ships, but overtakes them on the way and therefore lands on the Red Planet first. The two cargo ships actually do not carry the cargo for the first human mission, but already in support of the follow-on crew, that will set sail towards Mars one launch window later. Consequently there are only two unmanned launches in the first launch window (see Figure 2-5).

[1] The actual duration can - due to the high eccentricity of the Mars orbit - vary greatly. The exact numbers therefore depend mainly on the on the true anomaly of Mars at the moment of launch. The exact calculations of these values even decades in advance however impose no problem. All Hohmann opportunities in the years from 2001 to 2030 to all planets in the solar system are listed in [Eckart / Pauly et al, 2001]

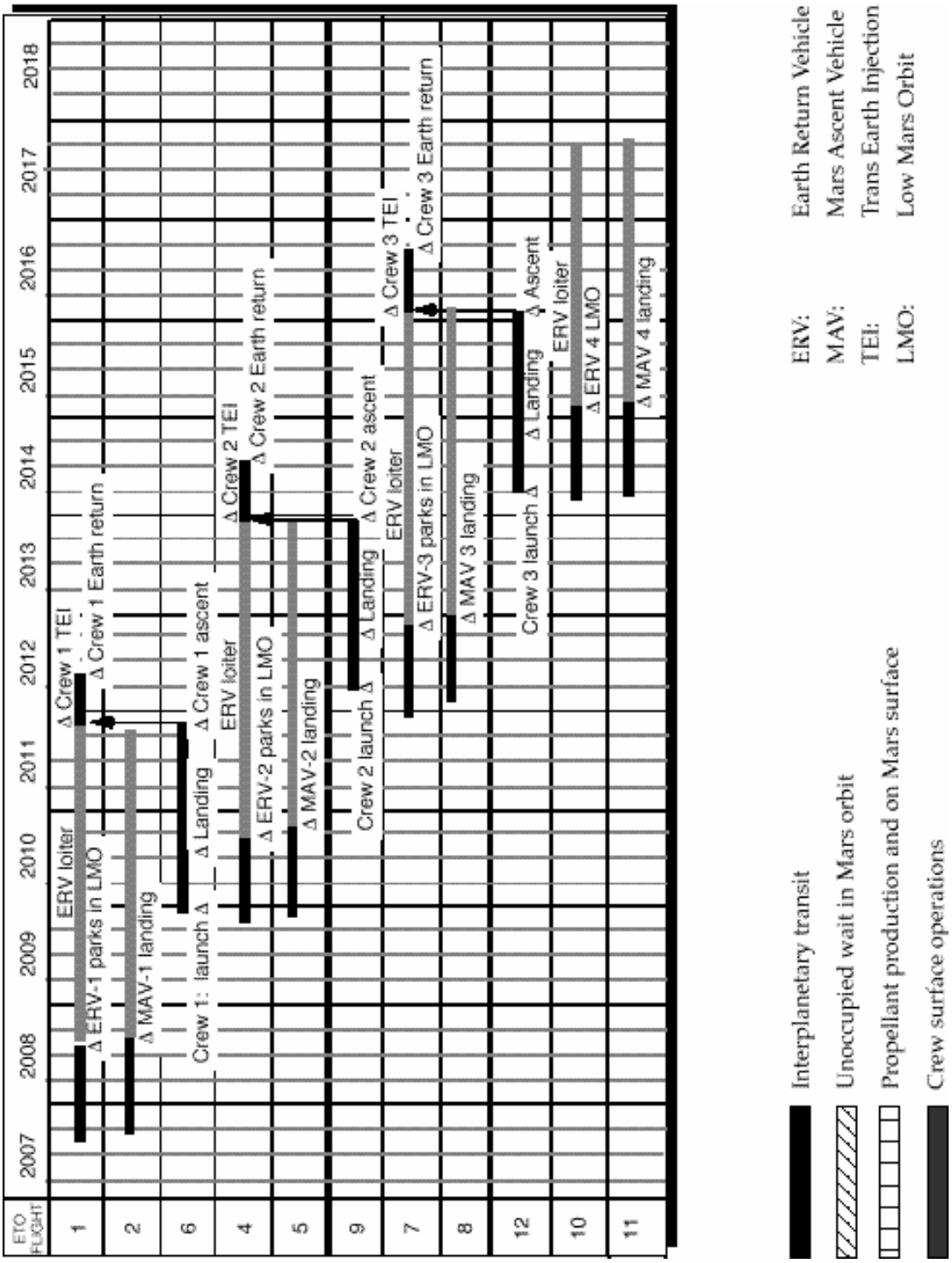

Figure 2-5: DRM Mission Sequence [Drake, 1998]

- This means however, that the first crew will land on Mars only some days before the cargo for their successor crew arrives on Mars, too. This has the great benefit of firstly an additional redundancy for them in case some of their own hardware fails and secondly of being able to assist the set-up of the assets for the other crew, which increases greatly the probability of a successful deployment.

Before manned and unmanned spacecrafts can leave Earth en route to Mars, the spacecrafts have to overcome the gravity well of Earth. They are thus carried into low Earth orbit with an unmanned heavy lift launch vehicle based on the Shuttle Transportation System (STS, see Figure 2-6a) or a new developed launch system with liquid propellant fly-back boosters, the so called "Magnum" launcher (see Figure 2-6b). The idea of increasing the payload of the STS by taking off the orbiter was already brought forward in the Seventies in [Ruppe, 1979].

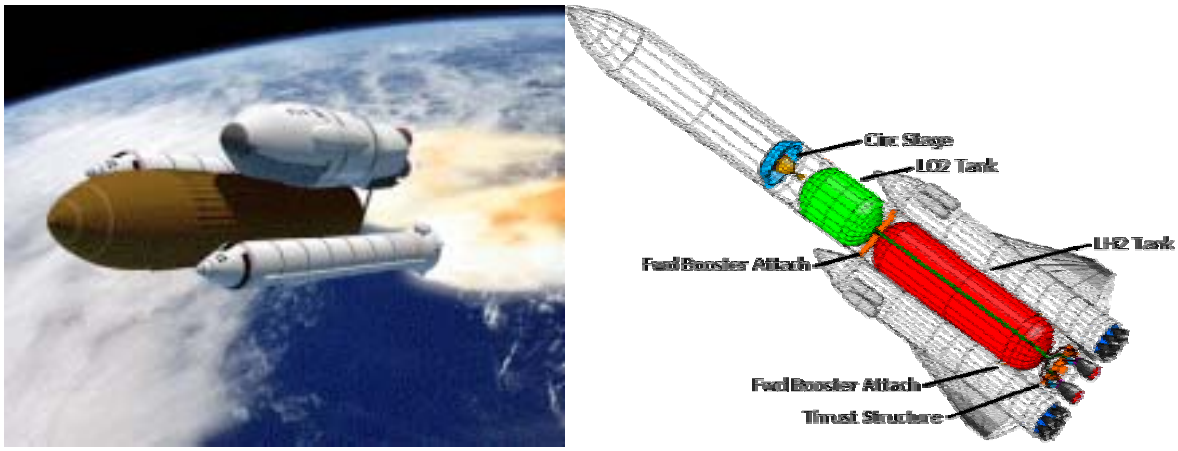

Figure 2-6: Shuttle C and Magnum Launch Vehicle [DRM V3.0, 1998]

- With the help of such a launcher, which would bring approximately 85t into low Earth orbit, the DRM tries to avoid extensive on-orbit assembly operations. The logistics that presumably would be connected to such an approach are immense and costly, as shown vividly by the example of the International Space Station. The three spacecrafts on the other hand can be brought into orbit with only six launches, with the total payload mass however still being comparable to the total mass of the International Space Station. Each spacecraft is brought by two launches, typically one for each of the three trans-Mars injection (TMI) stages and one for each, the cargo lander, the Earth return vehicle, and the crew lander. Once in orbit, each of the three docks to its TMI stage and sets sail for Mars.
- For the propulsion system of the TMI stage, the DRM foresees three options: nuclear-thermal (based on NERVA[1] derived engines, see Figure 2-7), nuclear electric, or solar electric propulsion (see Figure 2-8). The TMI propulsion system choice has only little impact for the further progress of the missions after the injection.

[1] "Nuclear Engine for Rocket Vehicle Application" - designed, built and tested from 1955 until 1973.

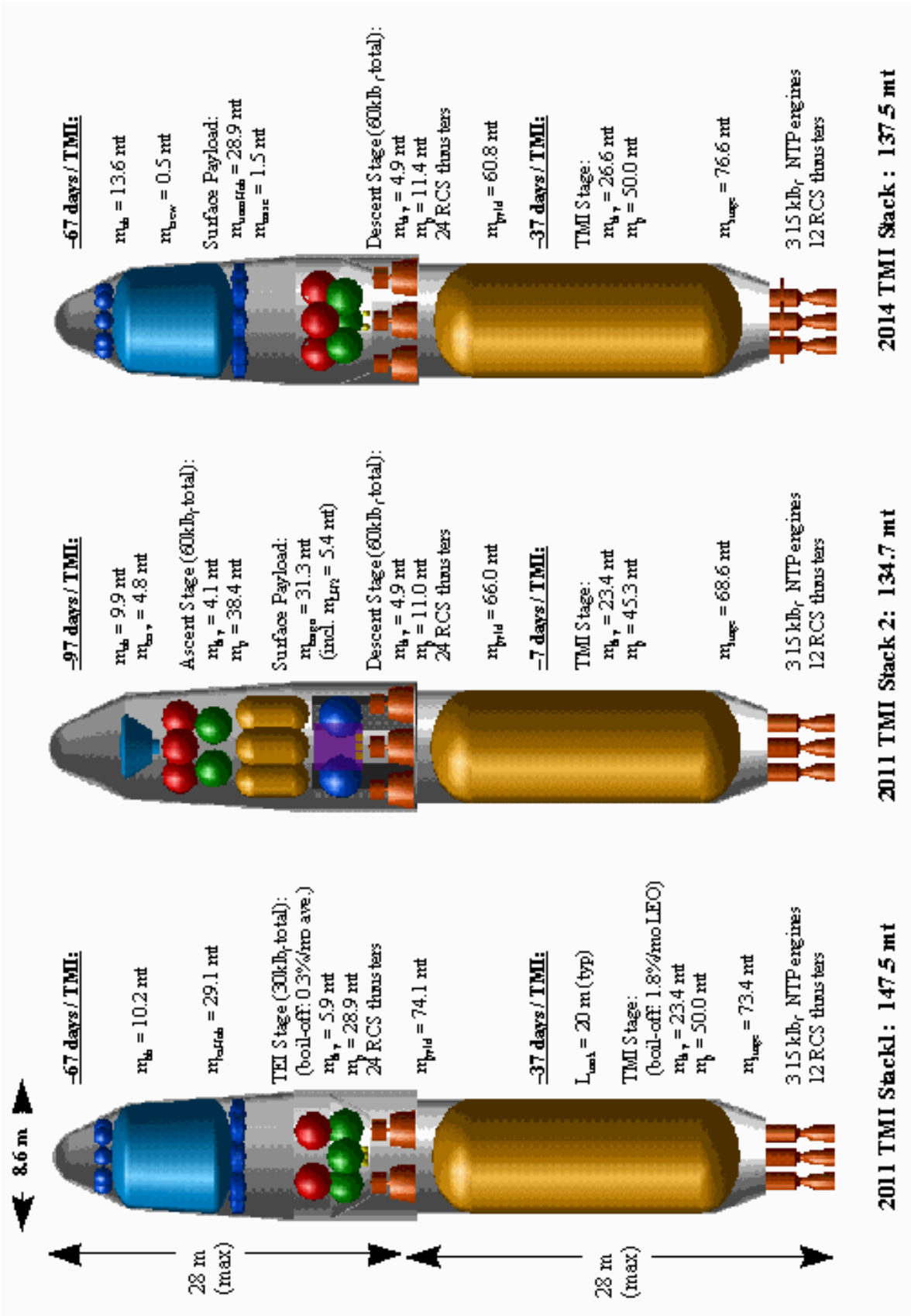

Figure 2-7: Payload Stacks for Nuclear Thermal Propulsion [DRM V3.0, 1998]

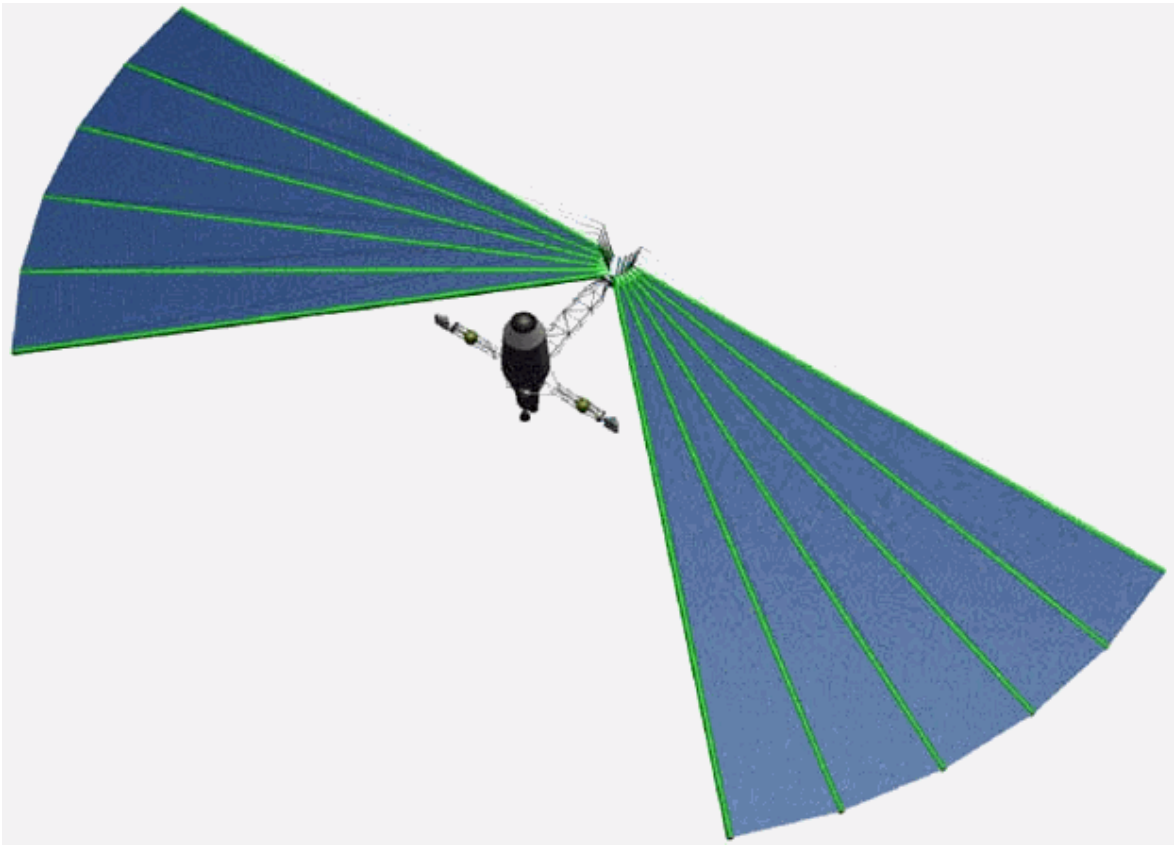

Figure 2-8: Solar Electric Propulsion System Layout [DRM V3.0, 1998]

- After aerocapture in the Martian atmosphere, the Earth return vehicle (ERV) stays in orbit, whereas the cargo lander descents to the surface of Mars. The ERV contains a habitat for the journey back to Earth as well as the Earth crew capture vehicle for the entry into the terrestrial atmosphere. The cargo lander carries the scientific payload, the in-situ resource utilization unit and the Mars ascent vehicle (MAV), that will latter carry the astronauts from the Martian surface to the ERV in orbit. When it lands, the MAV propellant tanks are empty. During the months succeeding the landing propellant is produced with the help of the ISRU unit (see Figure 2-9).

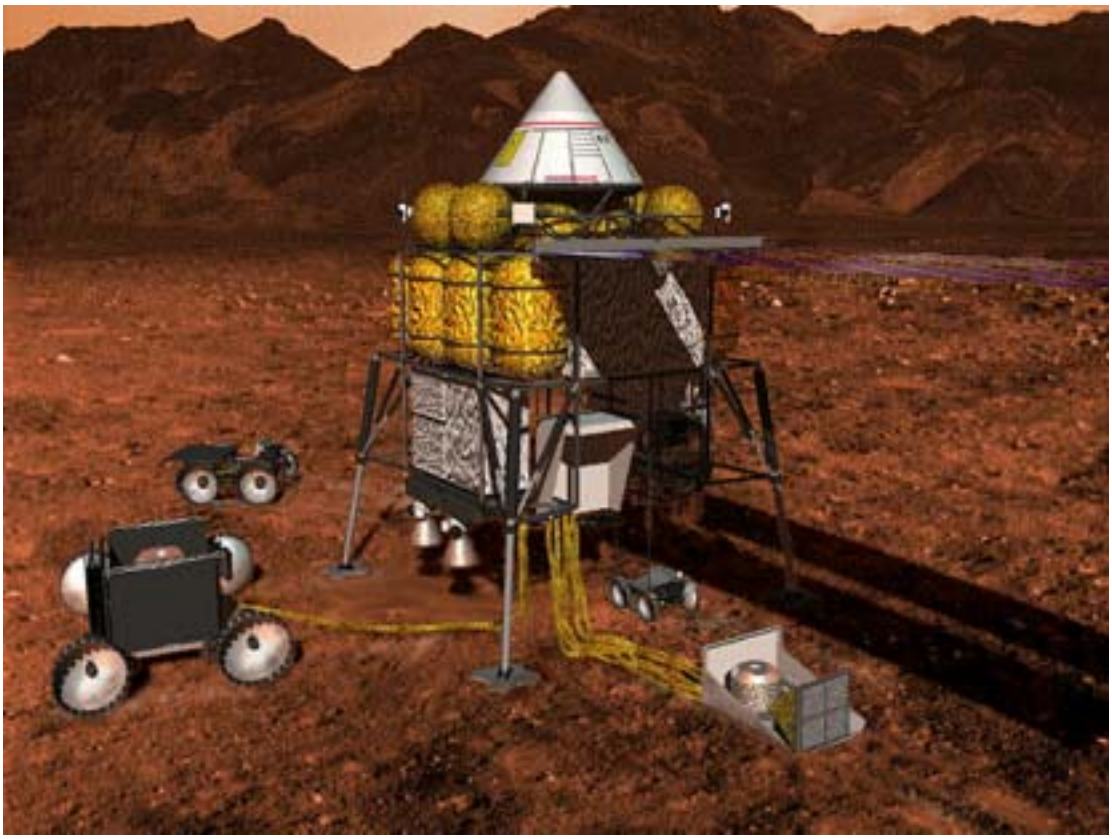

Figure 2-9: Deployed ISRU Plant [Frassanito et al., 1993]

- **Only if both, Earth return vehicle and cargo lander, have arrived on Mars safely, the crew will be sent to Mars during the next launch window.** Their spaceship is the so called "hab", the crew habitat for the journey from Earth to Mars as well as for the stay on the surface of the Red Planet. In the same launch window, another cargo lander plus another Earth return vehicle will be launched to Mars. They are supposed to be used by the second crewed mission, but they can also serve as a system backup for the first crew in the case of a severe malfunction. Apart from the manned vehicles, all spacecrafts use low energy / Hohmann transfer trajectories to reduce the Δv-requirement (conjunction class instead of opposition class trajectories). A comparison of the numbers shown in Figure 2-10 makes obvious that the difference in mission duration of these two options results almost entirely from the different surface stay times. The accumulated flight time of a "short" mission is thus actually longer than the flight time of the "long" mission. This, together with the fact that a "short" mission flies at a relatively close distance to the Sun on the way to and from the Venus swing-by, results in a significantly increased radiation load, which many people do not realize when they underline their promotion of short stay missions with the pointer to allegedly *decreased* risks to the crew.

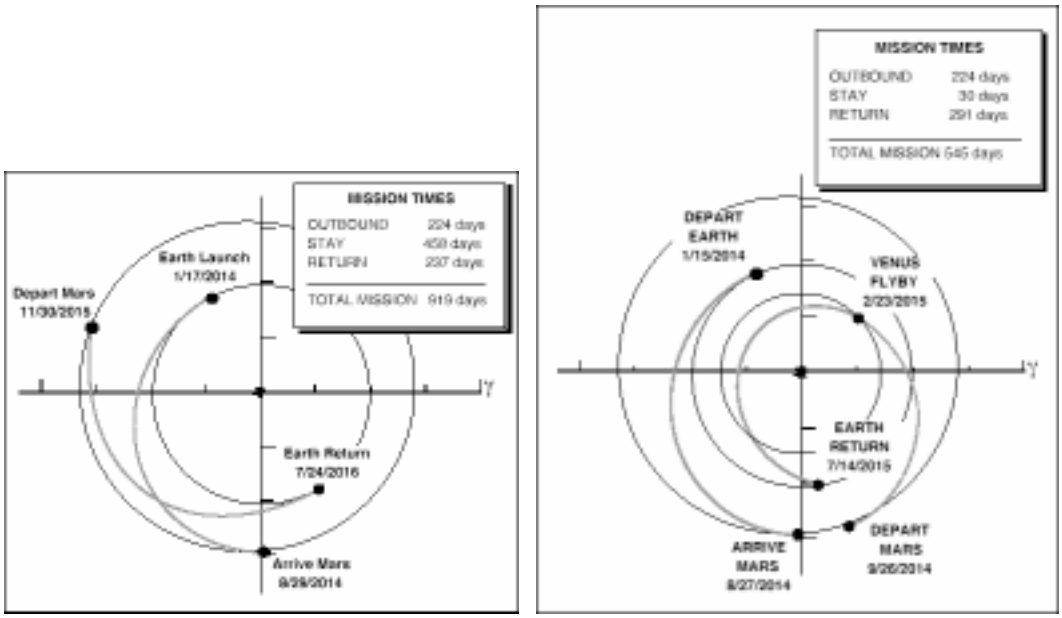

Figure 2-10: Long- and Short-Stay Missions [Drake, 1998]

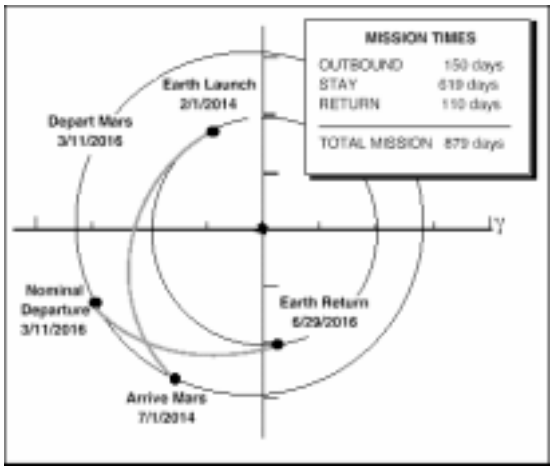

Figure 2-11: Fast Transit Trajectory [Drake, 1998]

- The crew flies on a so-called fast transit trajectory (see Figure 2-11). The overall mass of the hab is smaller than the masses of ERV and the cargo lander, but it must reach a higher Δv. Thus, the same TMI-stage is used for all injections to Mars, the only difference is a fourth engine in the case of the human mission (in the nuclear-thermal scenario) in order to achieve a higher thrust level. The crewed mission launches some weeks after the unmanned missions of the second launch window, but because of the fast trajectory it arrives some weeks sooner at Mars. The flight time for the crew is, depending on the launch window, some six months.
- After aerocapture at Mars, the hab lands in the vicinity of the cargo lander. The Mars outpost is established. To increase the usable habitat volume, a "TransHab"-derived inflatable habitation volume is deployed. The following 500 days are used for exploration of Mars with the help of pressurized and unpressurized rovers. The ISRU

plant produces not only the propellant for the Mars ascent vehicle but also water and oxygen which can be used in an open loop backup system in the case of a malfunction of a closed loop life support system.

- When the time for departure has come, the crew gets into the MAV and lifts off from the Martian surface, thereby using the propellant produced on Mars itself. After arriving Mars orbit and docking to the Earth return vehicle, the crew leaves Mars with the help of chemical engines and heads home.
- After some six months the crew enters the Earth crew capture vehicle that brings them down to the surface. The overall mission time for the crew is over 900 days.

A more detailed discussion of the question "Why use ISRU?" is the focus of the following chapter.

2.2.3 Where does ISRU fit in?

For the ISRU propellant production, several methods for production were investigated by different authors (e.g. by [Peters, 1998] or [Pauly, 1998a] respectively). An analysis of these investigations is given in [Sanders, Pauly, et al., 2000], which describes the rationale for ISRU as follows:

"Numerous analytical studies have been performed over the past several decades that all show ISRU can significantly reduce the mission mass, cost, and risk of both robotic and human exploration missions. Most of these studies have focused on the production of propellants [ISPP] due to the fact that the greatest improvement in a mission results from reducing the largest mass component, typically propellant, which can make up as much as 80% of the landed vehicle's mass. Specific system analyses of robotic and human Mars missions show that producing propellants by processing Mars carbon dioxide with hydrogen brought from Earth can reduce the initial mission mass required in low Earth orbit by 20% to 45% as compared to carrying all of the propellant for a round trip mission to the Mars surface from Earth. ISRU systems can also significantly reduce the risk of human exploration as well as enhance the capability of crews to explore the surface. Risk is reduced by providing a functional backup to the life support system, reducing dependence on Earth supplied logistics, providing mission flexibility, and increasing radiation protection using indigenous materials. ISRU systems and capabilities can significantly enhance and expand robotic and human exploration by increasing surface mobility through production of Extra Vehicular Activity (EVA) consumables, use of ISRU-supplied hoppers and fuel cell powered vehicles, and growth in outpost habitation and infrastructure (including electrical power)."

An example of typical results is displayed in Figure 2-12:

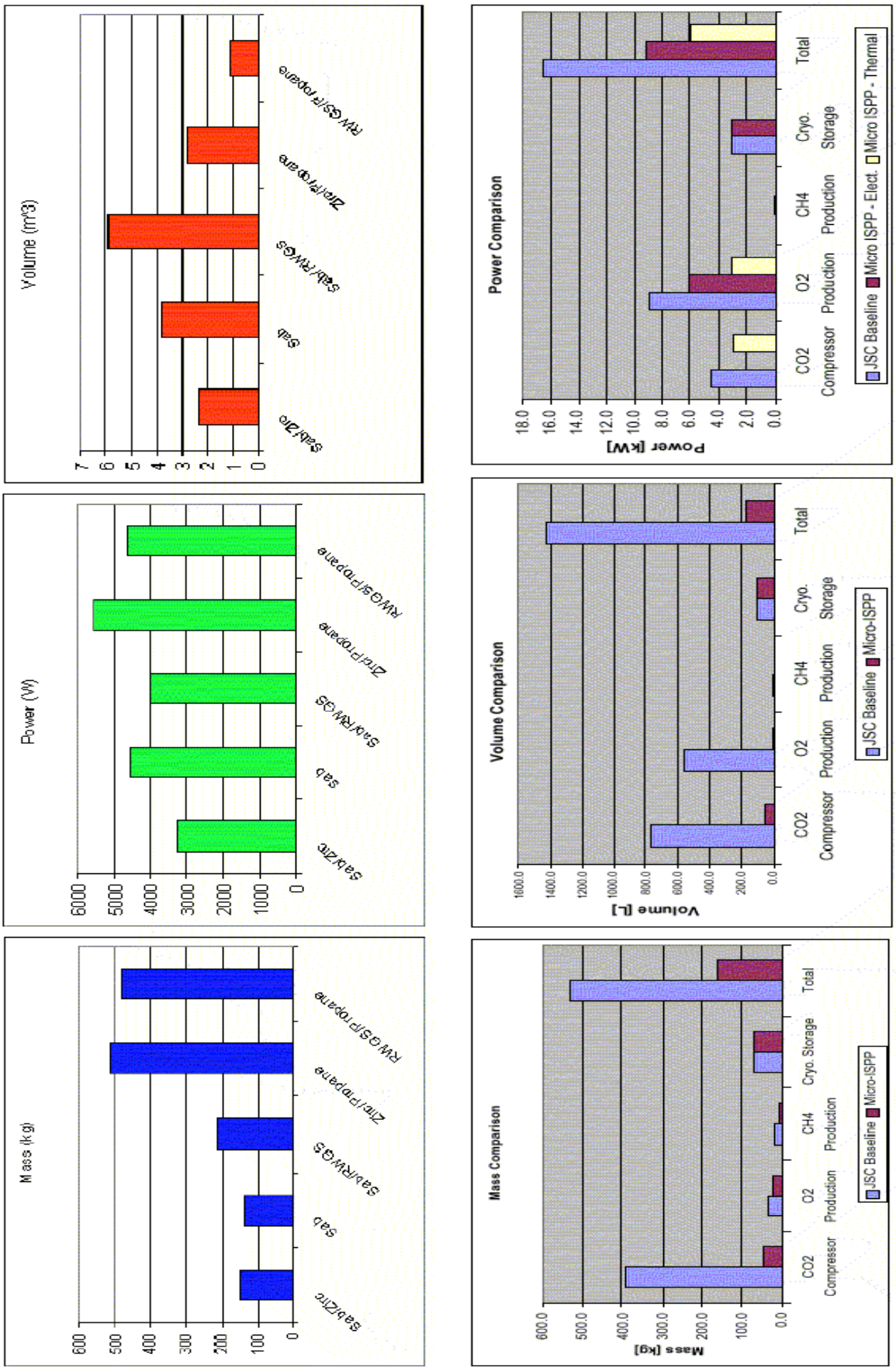

Figure 2-12: Comparison of Different ISRU Options [Sanders, Pauly, et al., 2000]

Results like these led to the choice of solid oxide electrolysis and Sabatier / water electrolysis as the premier choices. It were also exactly these technologies that had been selected as the most useful ISRU options in [Pauly, 1998a].

By contrast, the conventional approach without enabling technologies like e.g. aerocapture and ISRU requires more launches from Earth since the vehicles are heavier. The development of a completely new launch vehicle with unprecedented payload mass capabilities is nearly inevitable in these designs, whereas the DRM uses a launcher based on the existing Shuttle Transport System, a concept already proposed forward by H.O. Ruppe in the Seventies [Ruppe, 1979].

Apart from that, classical proposals often require intensive on-orbit assembly operations to integrate spacecrafts, since portions of the spacecraft must be delivered to Earth orbit by several separate launch vehicles. The major mass reduction afforded by ISPP is made possible by producing the Mars ascent vehicle's propellant oxidizer from the Martian Atmosphere, rather than bringing it from Earth. In addition to that the wet mass of the Mass ascent vehicle, which must be landed on the surface of Mars, is reduced, so all the systems in the TMI-stage and in the cargo lander required to place the MAV on the surface of Mars (e.g. propulsion, structure, aerocapture heat shield, parachutes, etc.) are reduced. Both of these effects result in significantly less mass being launched from Earth [Frisbee, 1987]. In other words: the benefit of ISRU lies not only in the reduction of propellant mass that has to be imported to Mars, but also in the cutting of the "multiplication chain" that seemed to be an inherent part of space travel up until today.

In contrast to the common prejudice that ISRU automatically means an increase in Mission risk, this design has more backups and thus less risk than the original "classic", all chemical designs:

- The crew leaves Earth not before both, Mars ascent vehicle as well as Earth return vehicle, are fully fueled, checked and ready to fly.
- In the case that at Mars arrival a landing is not possible, an Earth return vehicle is already waiting in Orbit with consumables for additional 500 days: within some weeks a second ERV arrives.
- If the first hab should not land in the vicinity of the first MAV, then it is possible to direct the second MAV (that arrives shortly after the Hab-1) to the landing site of the first hab
- If either the MAV or the hab fail during the stay at Mars, the crew can switch to the systems supposed to be used for the second crew.
- In the case of an ERV - malfunction, there is a second ERV already waiting in Mars orbit.
- If all closed loop life support systems should fail, there is also a backup feedstock, an open loop system produced by the ISRU unit.

This last paragraph gives a glimpse at the plethora of reasons why ISRU has been implemented in the DRM. In summary, the benefits of ISRU that were discussed in this chapter can be divided in the following groups [Baird, 2000]:

2.2.3.1 Mass Reduction

- Reduces Earth-to-orbit mass by 20 to 45%
- Estimated 300 t/yr reduction in Earth logistics

2.2.3.2 Cost Reduction

- Reduces number and size of Earth launch vehicles
- Allows reuse of Mars landers (e.g. as shuttles or hoppers)

2.2.3.3 Risk Reduction

- Reduces dependence on Earth supplied logistics
- Enables self-sufficiency
- Provides backup options & flexibility
- Radiation Shielding

2.2.3.4 Expansion of Human Exploration and Presence

- Increase surface mobility and extends mission life
- Habitat & infrastructure construction
- Propellants, life support, power, etc.

2.2.3.5 Enabling of Space Commercialization

- Develops material handling and processing technologies
- Provides infrastructure to support space commercialization
- Earth, Moon, & Earth-Moon space manufacturing, and product/resource development, resupply, & transportation

This list of reasons is summarized in the following NASA graphic:

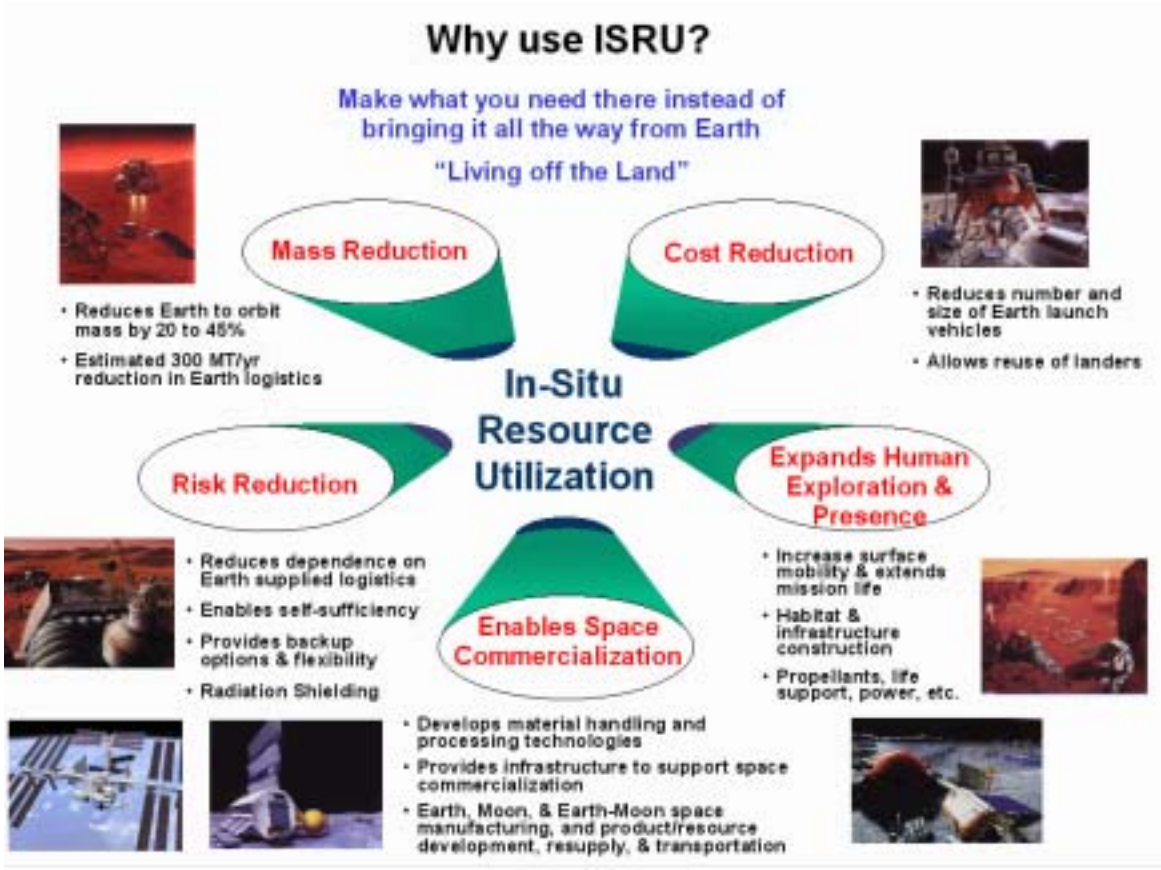

Figure 2-13: Rationale for ISRU [Baird, 2001]

2.3 Propulsion and Fluid Systems Branch

2.3.1 Mars ISRU Systems Test Facility

The Johnson Space Center in Houston, Texas, is not only NASA's lead center for human spaceflight, but also for ISRU development. This mission involves a variety of tasks, such as:

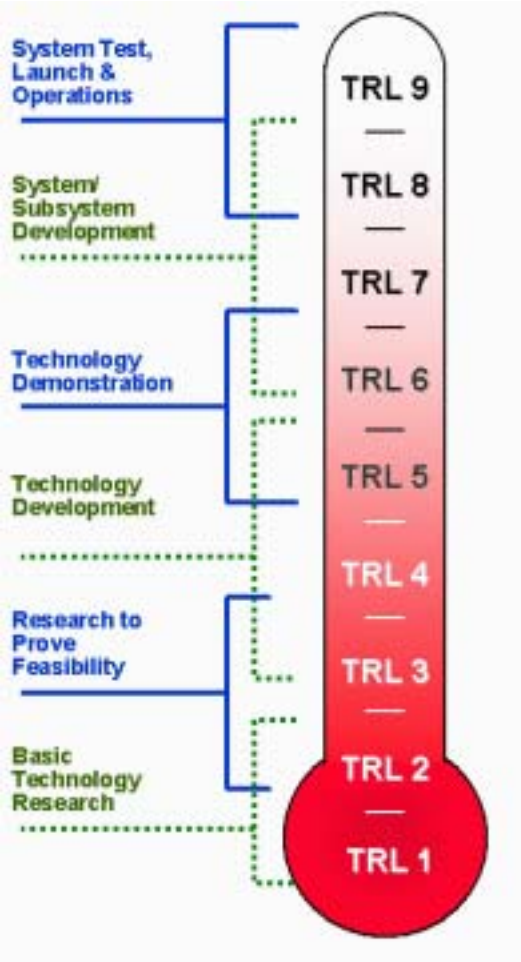

Figure 2-14:Technology Readiness Levels [Baird, 2001]

- the characterization of technology and subsystem performance,
- the enhancing of subsystem and component technology readiness,
- the reduction of risks and concerns for missions utilizing ISRU, and
- the demonstration of environmental suitability of ISRU processes and systems.

Main goal is to evaluate the technologies that come into question, select the ones that are promising, and to increase their Technology Readiness Level[1] (TRL, see Figure 2-14).

In order to fulfill this mission, a variety of different simulation and test chambers has been employed (see Figure 2-15).

[1] The Technology Readiness Level is a measure for the development status of a technology. The scale reaches from 1 to 9 with 1 corresponding to theoretical deliberations and 9 corresponding to applied and well-established technologies.

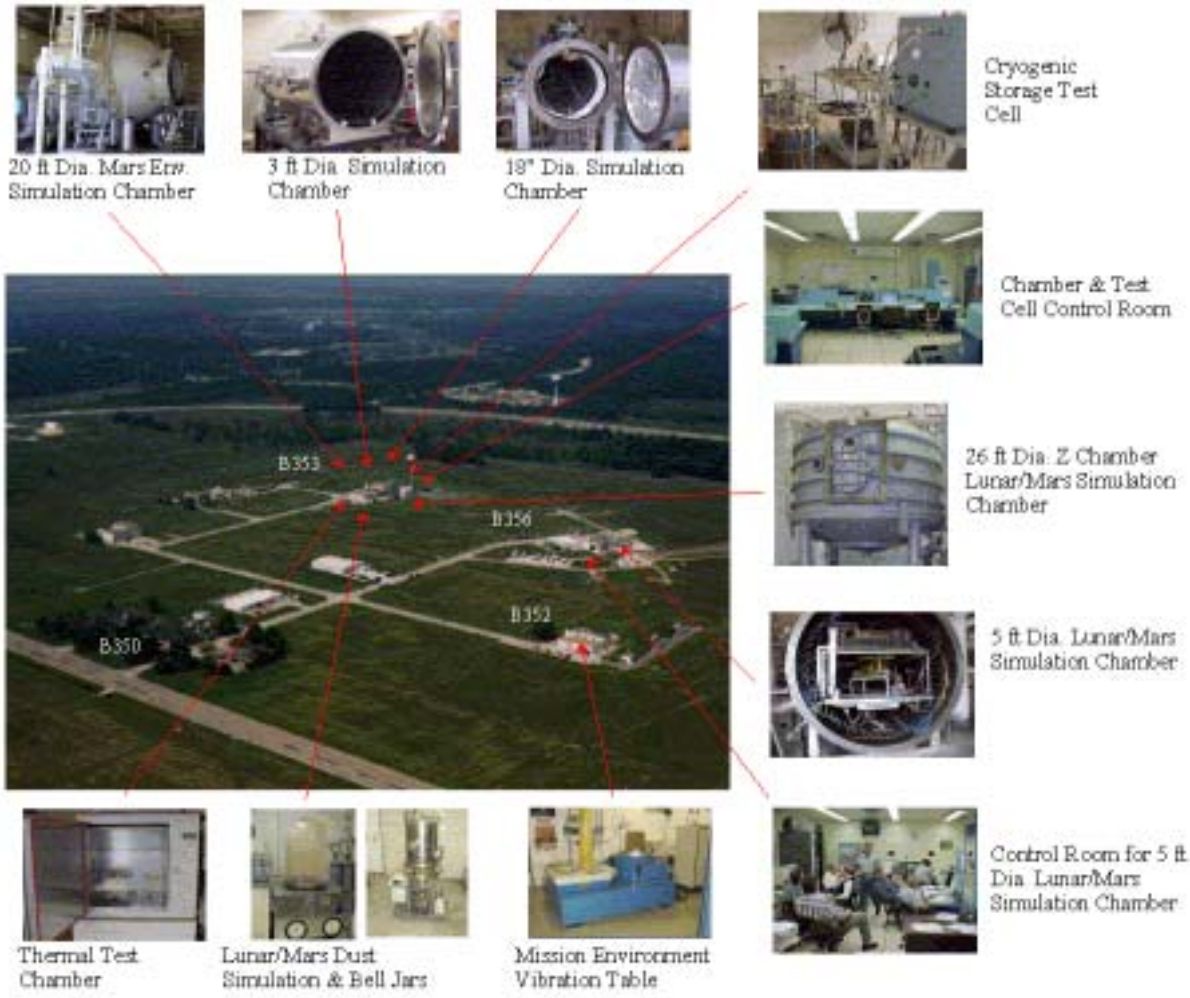

Figure 2-15: NASA-JSC Energy Systems Test Area [Baird, 2001]

Building 353

This building was used for the development and testing of the Sabatier / water electrolysis breadboard. The testing described in chapter 4 was entirely carried out in this building. The heart of this system is the 20ft (6.1m) diameter chamber for Mars environment testing, in which the integrated breadboard was located during the test campaign from December 1998 to April 2001. In this chamber atmosphere, pressure, and temperature conditions comparable to the Martian environment can be obtained. The chamber, built originally as testing facility for the qualification of the Apollo Command Module in the Sixties, is designed for hazardous operation testing (explosion and fire hazards). Currently, the addition of solar flux and dust condition capability is in work. In order to further extent the current capabilities, a so-called "Z Chamber" for Lunar & Mars surface simulations is currently also being set up (to be operational by 2004).

The building hosts six ambient test cells for subsystem and system testing, too. They are also designed to simulate Mars environment conditions, however on a smaller scale. In these chambers the Sabatier / water electrolysis breadboard subsystem testing was carried out (prior to system integration).

Building 356

This facility was used for the development, qualification, and flight unit testing of the MIP experiment (see next chapter). It hosts a 5ft (1.5m) diameter chamber for Mars environment testing for both, atmosphere, pressure, and temperature emulation on the one hand, as well as night sky temperature simulation (down to -300F/90K) on the other hand.

2.3.2 Mars ISPP Precursor Experiment (MIP)

As already outlined in chapter 2.2 the NASA-JSC Propulsion and Fluid System Branch successfully led the development and flight certification of the Mars ISPP Precursor Experiment (MIP), a project that was undertaken in collaboration with the Jet Propulsion Laboratory and the University of Arizona (Prof. K.R. Shridar). The flight hardware passed flight acceptance tests on schedule in January 2001 (however the hardware had then to be mothballed at Lockheed Martin Denver due to the reasons described in chapter 2.2.1). It consists of five sub-experiments looking at different ISPP technology aspects related to later (including human) missions. Hence, MIP (see Figure 2-16) will be described briefly at this point.

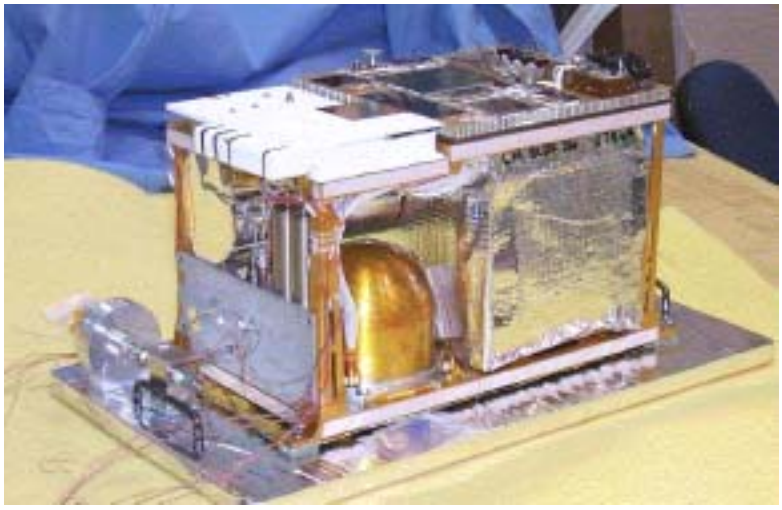

Figure 2-16: The MIP Experiment during Flight Acceptance Testing at NASA-JSC [McClean, 2001]

MIP is comprised of five distinct experiments; their names and key objectives are:

- Mars Atmospheric Acquisition and Compression (MAAC): to selectively absorb and compress carbon dioxide from the Martian atmosphere;
- Oxygen Generator Subsystem (OGS): to produce propellant-grade, pure oxygen;
- Mars Array Technology Experiment (MATE): to measure the spectrum at the Mars surface and to test several advanced photovoltaic solar cells;
- Dust Accumulation and Repulsion Test (DART): to investigate the properties of dust and to test techniques to mitigate the settling of airborne dust onto solar arrays; and

- Mars Thermal Environment and Radiator Characterization (MTERC): to measure the night sky temperature and to demonstrate the performance of radiators.

The MIP package will be small and lightweight. Its overall external envelope is approximately 40 x 24 x 25 cm, and its mass is 8.5 kg, 1kg of which is the mass of the OGS. The OGS is sized to produce 0.5 standard cubic centimeters of oxygen per minute (sccm) while operating.
The long-term effects of operating in the Martian environment is one of the key information being sought by MIP. Therefore, MIP aims at a lifetime of 90 sols or more on Mars.

Apart from the system lead role, the team at JSC also provided the Oxygen Generator Subsystem (OGS) hardware. This experiment package is the predecessor of the experiment planned for 2003, which has been the focal point for the efforts of this thesis. The overall MIP flight experiment package was also integrated at JSC. Furthermore, the JSC civil servants and JSC ISRU test facilities, combined with previous MIP breadboard development and test activities, were critical in resolving design issues during development and qualification. It was the same team that conceived, built, tested and verified design solutions to deficiencies in the JPL provided Mars Atmosphere Acquisition and Compression (MAAC) experiment. They were also critical in the resolution of thermocouple manufacturing and installation problems with the Oxygen Generator Subsystem (OGS) experiment.

2.4 The Sabatier Reaction

The Sabatier process will play a central role in this thesis. Therefore, its background shall be briefly introduced here.

2.4.1 The Sabatier Reaction in Chemistry

Like its biggest competitor in the field of ISCP, the solid oxide electrolysis cell [Nernst, 1899], the Sabatier reaction is based on a some hundred year old discovery, too. It was first investigated in 1902 by the French chemist Paul Sabatier, who studied the hydrogenation of hydrocarbons using a nickel catalyst [Sabatier & Sendersen, 1902]. He received, together with Victor Grignard, the 1912 Nobel Prize for chemistry for their method of hydrogenating organic compounds in the presence of finely divided metals [Nobel Foundation, 2000]. The Sabatier reaction describes the hydrogenation of carbon dioxide to methane and water:

$$CO_2 + 4H_2 \rightarrow CH_4 + 2H_2O + 164.6 \frac{kJ}{molCO_2}$$

The process is exothermic and typically occurs at temperatures greater than 600K in the presence of a catalyst. A variety of catalysts was evaluated over several decades in terms of their usefulness for the Sabatier reaction; Paul Sabatier himself, as well as [Dew et al., 1955] studied this reaction using a nickel catalyst, whereas [Kern et al., 1965] were the first ones to focus on ruthenium, which up to this day continues to be the most promising Sabatier catalyst (typically in the form of ruthenium on alumina pellets) with efficiencies in excess of 99.5%. Since methane (in the form of natural gas) and water are readily available on Earth, the reaction has been of limited interest for today's industry. On Mars however, methane and water would be invaluable resources while carbon dioxide builds 96% of the Martian atmosphere (see chapter 2.5.3). Although the extraction of water from subsurface resources is conceivable (see chapter 6.4.3), it would probably be too risky to gain the hydrogen this way. Consequently, no agency planning currently foresees in situ hydrogen production in the course of a precursor mission. Nevertheless, even with imported hydrogen, the in situ production of methane can be beneficial, as can be seen from the following overview:

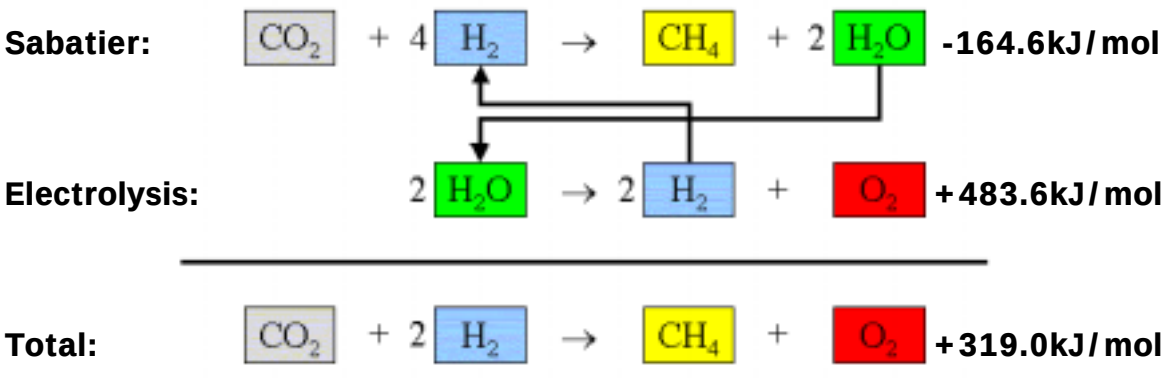

This last equation can be looked at from the point of view of molar mass units:

$$44u + 2 \cdot 2u \rightarrow 16u + 32u$$

In essence that means that with just 4 tons of hydrogen, one can produce 48 tons of rocket propellant on Mars, which then can be utilized, e.g. in support of a human mission to Mars. Taking into account the fact that savings of just a few pro mille are usually considered already significant in space business, a ratio of 12 (48/4) represents a "serious" number. This ratio of total mass of the in situ produced propellant and imported "seed" hydrogen is called "leverage". In comparing different ISRU technologies, the leverage is used as means of evaluating the different efficiencies [Zubrin & Wagner, 1996][1].

Obviously, the production unit will have a mass of its own, however studies have shown that such a production unit can produce a multiple of its own mass the course of 300 to

[1] However, as pointed out in [Pauly,1998], the leverage is the not only parameter which should be considered in such a comparison of different ISRU strategies.

500 days. How the Sabatier process, together with a water electrolyzer unit, can be employed for ISCP purposes is shown in Figure 2-17 (compare also with Figure 2-1!):

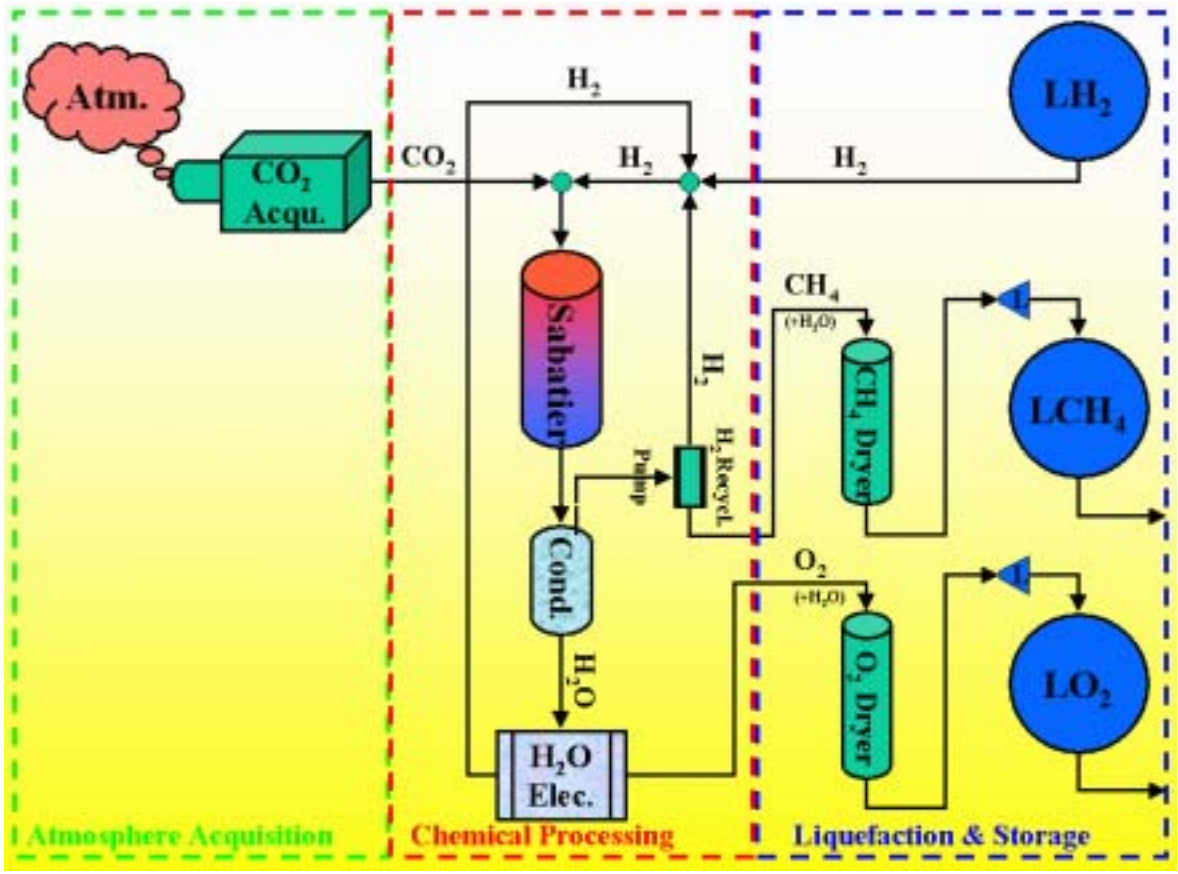

Figure 2-17: Simplified Sabatier / Water Electrolysis System Overview[1]

The Sabatier process combined with water electrolysis produces an oxygen to methane ratio of 32:16 or 2:1 (see last page). To achieve an efficient combustion in a rocket engine, however, it needs to take place in a near-stoichiometric fashion, meaning a ratio in the order of 3.5:1 to 4.0:1 (see [Pauly, 1998a]). Thus, it might very well prove useful to employ a third chemical process that is able to adjust the oxygen to methane ratio. This third chemical process can also further increase the leverage ratio (up to 20 and more), which can be achieved either by increasing the amount of oxygen, e.g. via the solid oxygen electrolysis cells ($2CO_2 \rightarrow 2CO + O_2$), or by reducing the amount of methane, e.g. via pyrolysis ($CH_4 \rightarrow C + 2H_2$).

Of course it has also to be stated that importing hydrogen to and providing additional power on Mars is everything but an easy undertaking. Nevertheless it remains as a promising fact that the mass numbers are significantly reduced compared to the classical approach – a statement which is underlined by the analyses listed in 2.2.3.

[1] The "L" in the fluid labels stands for "liquid"; "LO_2" is liquid oxygen, "LCH_4" liquid methane, and so forth.

2.4.2 The Sabatier Process in Life Support Systems

The Sabatier process is not new to space exploration. ESA [Tan, 2000], NASA [Boyda et al., 1992] as well as the Russian Space Agency (RKA) [Mitchell, 1993] have been developing concepts for use in a different area for many years: as a regenerative removal system for metabolic carbon dioxide. For the use of the Sabatier process in ISRU, the aspect of methane production is paramount. However, when applied in life support systems, the main interest lies on removing the CO_2 out of the space vehicle's atmosphere with the help of hydrogen, which results in the production of methane and water. The water is electrolyzed into (breathing) oxygen and hydrogen (which is recycled), whereas for the methane - in this context a waste product - the following three different scenarios come into question:

- **dumping** overboard (leads to a loss of hydrogen from the system, which has to be made up for),
- storage and **use as a fuel**, e.g. in a propulsion system, which requires an oxidator, and
- **pyrolysis**, to recover the hydrogen ($CH_4 \rightarrow C + 2H_2$), a reaction which requires high temperatures (ca. 1000°C).

Pyrolysis may very well have significant applications in ISRU, too, as an alternative means to solid oxide electrolysis for increasing the oxygen-to-methane mass ratio. This scheme is discussed and evaluated with respect to its applicability in ISRU system [Pauly, 1998a].

During short duration space missions (up to a few weeks), the relatively high system mass of the Sabatier CO_2 removal system makes it less competitive compared with non-regenerative systems like lithium hydroxide (LiOH) canisters, which have been in use already since the early Mercury days. However, with the mission length extending up to several months aboard Mir and ISS, Sabatier actually surpasses non-regenerative systems and turns out to be de facto a better choice, since it makes a significant fraction of the re-supply requirement obsolete[1]. For long duration missions (beyond some 200days [von Puttkamer, 1986]), Sabatier is also favorable in terms of mass compared with the Bosch process ($CO_2 \rightarrow C + O_2$), although this process - in theory - makes use of only one

[1] The trade-off between regenerative and non-regenerative life support systems is subject of many publications, e.g. [von Puttkamer, 1986, p.132-142].

chemical reaction[1]. These various aspects led to the decision in favor of a Sabatier removal system for the ISS [Boyda et al., 1992][2].
In this scheme, it is planned to dump the methane that will be produced on ISS overboard. Using methane as a propellant would require an oxidator – and this is where the dog bites his tail, since the goal of the whole system is to produce oxygen (for life support), not to consume it. However, on a planet's surface where additional indigenous oxygen might be available, the situation could be different – an important fact that has to be kept in mind. Schemes for opportunities to make use of "waste" methane on Mars are presented in the outlook in chapter 6.4.

The Sabatier based systems envisioned, developed and used in the field of regenerative life support systems up to now differ significantly from the ISRU-related systems discussed in this thesis. The reason for that however is almost solely due to the fact that ISRU systems have to be designed for Martian environment, whereas the LSS Sabatier systems are all designed for micro-gravity and 1bar environment. This however hides the fact that there is a big potential for synergy between these two areas (as well as others) on the Martian surface; methods for utilizing this potential will also be discussed in chapter 6.4.

2.5 Requirements and Constraints for Space Applications

Processes that are employed for space applications, no matter whether they are of a physical or chemical nature, such as for example the Sabatier Process, have not only to work; they also have to be able to cope with the different environments during launch, in space, and on Mars. These environments will be discussed briefly.

2.5.1 Launch Environment

From the viewpoint of mechanical stresses, the launch is the most serious phase in the mission life of most space hardware. Similar environmental conditions can also be found during Mars entry, decent and landing.

Axial and Lateral Loads

Going to space is mostly a problem of achieving momentum. In order to orbit around planet Earth for example, a spacecraft has to exceed the first cosmic velocity (7.9km/s).

[1] [Eckart, 1999] quotes 1840kg (102.1kg) as the expected on-orbit mass for an ISS-LSS regenerative life support system based on the Bosch process, whereas a system of similar performance based on the Sabatier process is estimated to have a mass of just 500kg (17.9kg).

[2] Although a Sabatier-based removal system is currently the baseline for planning, it remains unclear whether it will actually be installed, since the cost overruns of the station currently even puts the completion of the ISS as a whole into question.

Thus today's launchers, which are propelled by chemical combustion engines, inherently subject their payload to lateral accelerations (see Figure 2-18a), which are typically around 30 m/s² for manned missions, and some 50m/s² or more for robotic missions. All payloads have to be able to withstand these stresses, which are accompanied by axial loads.

Acoustic Vibrations

All of today's launchers are, as already mentioned, propelled by chemical propulsion, more specific liquid propellant engines and solid rocket motors. These propulsion systems typically convert some 1% of their inherent energy into acoustic energy. All payloads are subject to these stresses to a certain degree (see Figure 2-18b). Again, any payload launched to space has to be able to cope with these stresses. The proof of this ability usually is obtained in finite element computer analyses and random vibration tests prior to launch.

Shock

During ascent and payload deployment, explosive devices, so-called "pyro-actuators", are used, most commonly to separate spacecraft elements (e.g. rocket stages, fairings, payloads, etc.). The shocks resulting from this also subject the payload to stresses (see Figure 2-18c), which it again has to be able to withstand.

2.5.2 Space Environment

Once the spacecraft is separated from its launcher, it has to be injected onto its trans-Mars trajectory. In space, another set of environmental requirements has to be fulfilled in order to enable a successful mission.

Vacuum

The lack of an atmosphere in space leads to many problems, such as outgassing, increased leakage rates, as well as mechanical stresses and failures. Thus, space hardware is typically subjected to this environmental condition prior to launch in thermal-vacuum test chambers.

Micro-Gravitation

Micro-g (also known as zero-g or weightlessness) does not necessarily describe a state of gravity absence. Actually it is a situation which describes the absence of differential forces between the spacecraft and its payload (this is also why this state can be reached for example aboard a plane flying parabolas, too). During its transfer to Mars, spacecraft as well as payload are subject to weightlessness.

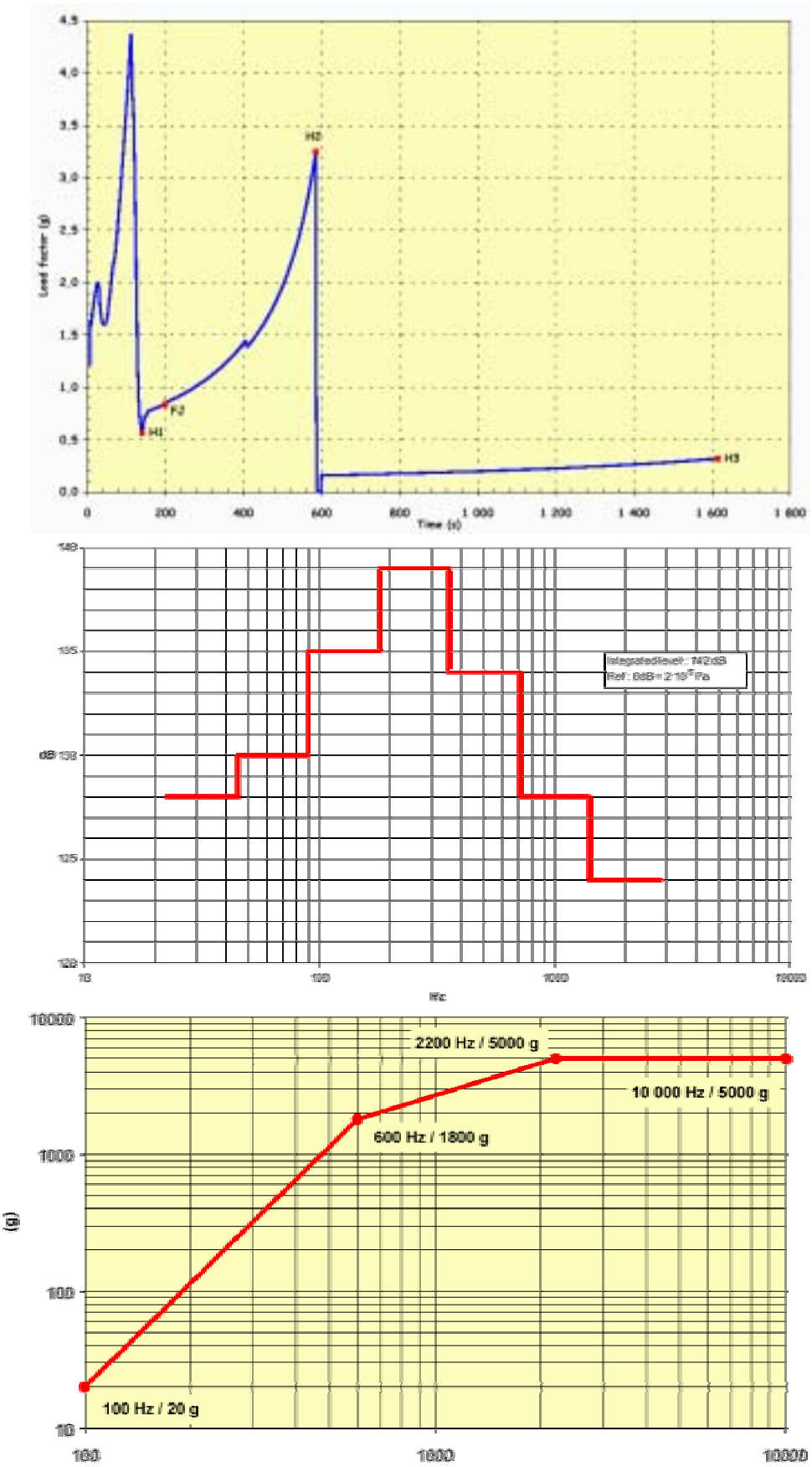

Figure 2-18: Longitudinal Static, Acoustic and Shock Loads of Launch Environment [Arianespace, 2000]

Thermal Cycling

The vastness of deep space is very cold, with temperatures down to 3K. Also, in space, the protective influence of an atmosphere is missing, which leads to high temperature gradients between the parts of a spacecraft in shadow and the parts in line of sight relative to the sun. The thermal control system of a spacecraft has to ensure that the internal temperature remains within an ambient temperature range. This temperature range typically covers a few tenths of degrees Kelvin, which simultaneously defines the temperature range which the payload has to be able to withstand.

Radiation

The lack of the protective influences of atmosphere and magnetosphere imposes further problems on payloads and spacecrafts during interplanetary transport. Solar galactic radiation, together with cosmic galactic radiation, can lead to serious impacts on humans and hardware. This is especially true in the case of solar proton events that normally occur during the maximum of the eleven year cycle of our sun. Some of the solar proton events are so vigorous that they could easily subject a crew en route to Mars with lethal radiation doses in an instant, unless they are protected e.g. by a special "storm-shelter" aboard the spacecraft.

2.5.3 Mars Environment

The Red Planet's environment is a vital driver for the design of Mars in situ resource utilization systems. In the following, the main aspects of the environmental conditions on Mars will be discussed, summarized, and then compared with the terrestrial parameters in Table 2-1.

Gravity

On the Martian surface, with 3.7m/s² the gravitational acceleration is less than that on Earth (9.8m/s²), but more than that on the Earth's Moon (1.6m/s²). This has of course an impact on the spacecraft design, but also on chemical and physical processes. The influences of gravity on chemical processes will be discussed in chapter 3.

Table 2-1: Earth vs. Mars Environment

Parameter	Earth	Mars
Surface Gravity [m/s²]	9.8	3.7
Temperature [K] min. max.	 230 320	 150 190-240
Solar Flux [W/m²] min. max.	 1352 1370	 490 690
Atm. Pressure Surface [hPa] min. max.	 990 1030	 6 10
Atm. Wind Speed [m/s]	2..7 30 (Hurricanes)	2..7 (Summer) 5..10 (Fall) 17..30 (Dust Storm)
Atm. Composition [%] CO_2 N_2 Ar O_2 H_2O	 79 19 0 to saturated	 95.5±0.65 2.70±0.30 1.60±0.50 0.15±0.50 0 to saturated

Atmosphere

The atmosphere of Mars is the main basis of in situ resource utilization on the Red Planet. It consists mainly of carbon dioxide, with small amounts of nitrogen and argon, as well as traces of other gases. The carbon dioxide in the Martian atmosphere thus represents a resource which is in reach globally on Mars.

Dust

The Martian atmosphere is loaded with fine sand. Its grain size can be as low as 1μm or less. The small size enables the particles to reach extreme altitudes during the global dust storms, which sometimes enshroud the planet in a redish haze. For future Mars hardware, in particular for systems related to extra-vehicular activities, this fine dust will pose a major technical challenge. Due to its highly oxidizing character, the dust might very well also pose a threat to astronauts' health if it inhaled. Consequently, two of the five experiments of the MIP platform that was outlined in chapter 2.3.2 focus on dust mitigation technologies

Thermal Cycling

Due to the thin atmosphere, from the viewpoint of thermal control, the harshness of the Martian surface temperatures takes a middle position between the ones found on Earth and the ones found on the moon. However, the deployment of e.g. radiator areas is a technological challenge not to be underestimated.

Mass Limitation

Going to space is inherently expensive. The launch cost to low Earth orbit alone is in the order of several thousand US$ per kilogram launched. For interplanetary mission, the specific cost can well be in the order of several tens (or even hundreds in the case of lander missions) of thousand $/kg. Thus, like in no other technological field, space engineers are forced to reduce mass in order to reduce cost. Consequently, only technologies that can be realized within the tight mass limitations of space missions, are of interest.

Power Limitations

Providing power is another hurdle in the exploration of space. Long-term space exploration missions were, are, and will be based either on nuclear (e.g. RTGs) or solar power sources (e.g. photovoltaic arrays). The requirement of providing power means additional masses. Thus, for space missions (in particular Mars missions), power is, like mass, always limited and poses significant constraints on the systems.

2.6 Scope of Ph.D. Work

A proverb says: "it's hard to make predictions – especially if they are about the future". Some of the people that have to face this problem of making accurate predictions are engineers that work on Mars ISRU systems. They are aware of many of the theoretical publications and reports on ISRU, however they also know very well that the number of sources discussing real ISRU hardware tests is ever so limited. These breadboards usually feature comparatively small mass flow rates compared to what would be required for e.g. a Mars ISRU sample return mission or even a human Mars mission. The question now is: how do such systems scale up? Over the coming years and decades, ISRU systems will undoubtedly evolve in mass flow rates. High mass flow rates will result in higher ISRU plant masses and higher power requirements. But how much mass? How much power? Will the complexity of such systems explode in higher mass flow ranges or will the level of sophistication more or less stay the same? Will the up-scaling of techniques that have proven useful at small scales turn out to be dead-ends further down the road, because material, heat dissipation, side reaction, or other problems surfaced, that were not anticipated before? How can these questions be answered, not only in a qualitative, but also in a quantitative fashion?

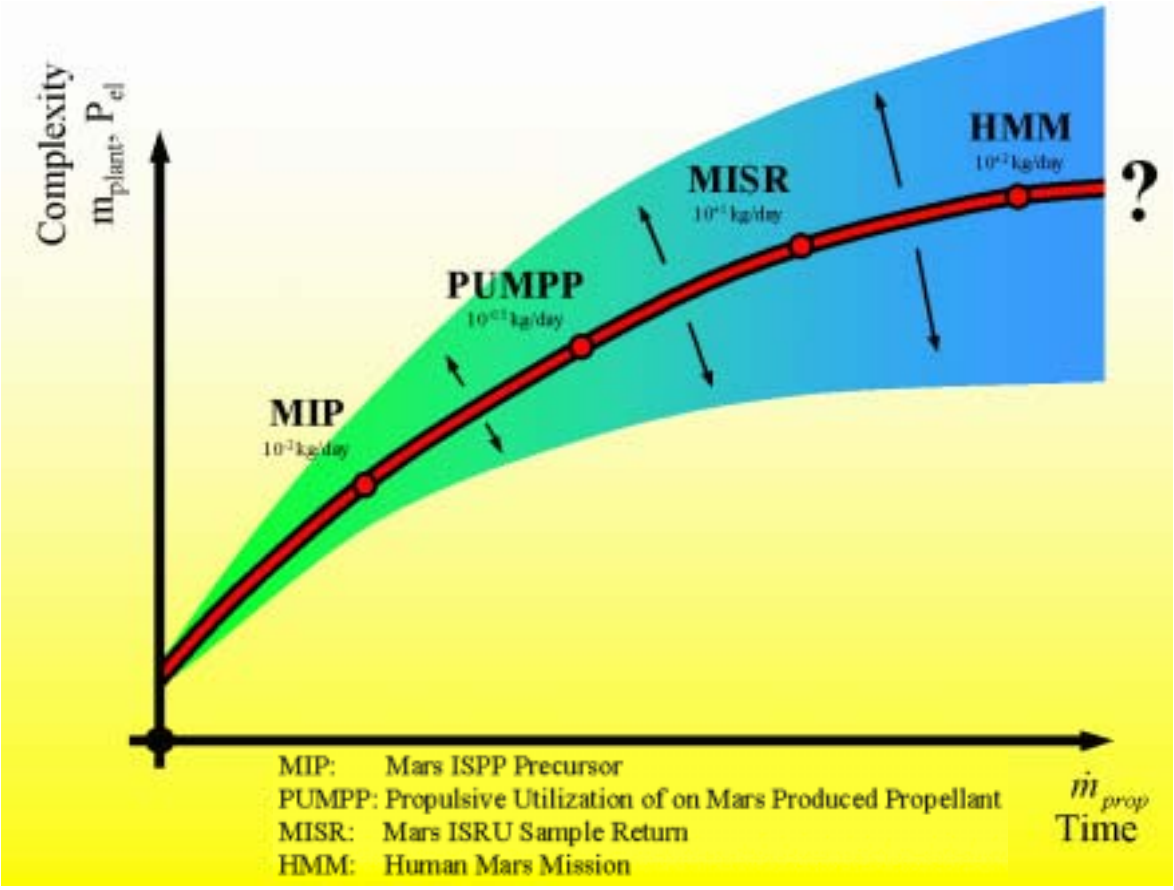

Figure 2-19: Progress and Uncertainties of ISRU Development

In this situation (see Figure 2-19), the creation of computer models seems to be a feasible way out of the dilemma. Today, computer models can accurately simulate even complex the most phenomena and systems. This is where this thesis comes into play.

In the previous chapters the background setting for this thesis has been described. The objective for the thesis in view of this background can be summarized as follows:

Based on theory, models will be derived that will simulate the performance behavior of chemical reactions and other phenomena as well as the systems that employ them, or that are subject to them, respectively.
However, like most computer models, it can only be an enabling tool for the design of ISRU systems if it is validated prior to further use. Therefore, the second of the two main focuses of this thesis is to conduct tests in Earth ambient and simulated Martian environment and to compare the results obtained in this test with the predictions previously made by the computer models. If the models turn out to be in accordance with the reality that assumes a definite form during the tests, then - and only then - this model can become a design tool. Once this tool is in hand however, it can be used together with the experience gained in the test campaign to derive design guidelines and design recommendations for the development of future hardware (such as breadboards, demonstrator experiments, or production plants for use on Mars).

In order to achieve this goal, the following procedure or series of steps is pursued (see Figure 2-20). This procedure is also the basis for the structuring of the thesis itself.

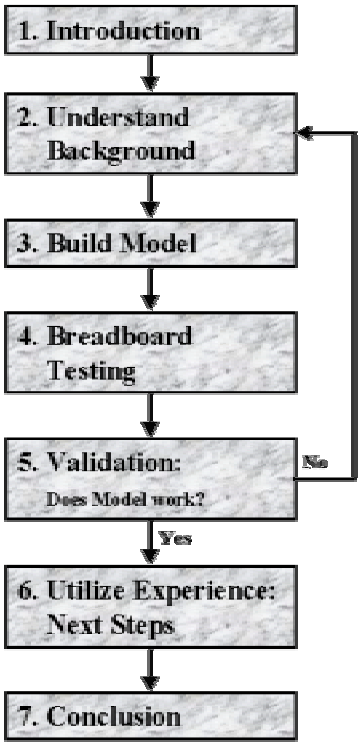

Figure 2-20: Procedure pursued in this Thesis

First, it is attempted to adequately understand the underlying theory of related chemical and physical processes, in particular the processes within the reactor. Based on this theoretical foundation, the computer model of the hardware is built. In the next step, based on this computer model, the performance of the hardware during tests is simulated / predicted. Then, the testing is conducted in order to be able to validate the computer model predictions with the actual hardware performance. This testing is divided in Earth ambient and simulated Martian environment test. After the termination of the tests, the predicted results are compared with the actual test. If necessary, meaning if the sufficient accordance is not achieved, the model has to be altered. This iteration has to be repeated until predicted and actual performance are in satisfactory concurrence. Once the model is validated, it can be used to design follow-on breadboards, demonstrator experiments for robotic missions, as well as production plants that serve to prepare human missions to Mars etc.

In the second chapter, the setting of this thesis has been outlined, consisting of NASA's current Mars exploration plans, the role and benefits of ISRU, as well as the activities and the expertise of the Johnson Space Center Propulsion Branch. The chapter then continued with a description of the applications of the Sabatier process in related areas, as well as the requirements and constraints of space. Finally, the scope of the Ph.D. was defined and outlined.

3 MODELING

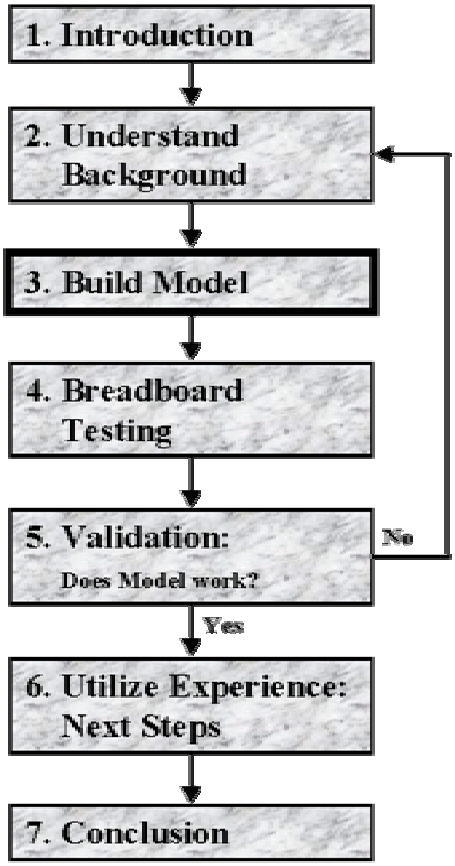

The main focus of the succeeding chapter is the construction of computer modeling tools intended to assist NASA, in particular the Johnson Space Center Fluid Systems Branch, in her effort to built, test and fly ISCP hardware, an effort which was outlined in the previous chapter. The modeling of such an ISCP breadboard with all the physical and chemical phenomena involved has not been attempted in this form yet.

Hence, the aim of this chapter lies in the derivation of correct models of the Sabatier reaction, as well as accompanying and related processes. Furthermore, the other main elements of the overall breadboard are modeled.

Many of the tools developed in this chapter are not only of use in the context of this particular breadboard, but also in the design and optimization of future hardware.

3.1 Outline

The Sabatier reaction depicted in chapter 2.4 is an exothermic reaction that proceeds at a useful rate (required for high yields) already at comparatively low temperatures[1] of just some 600K. The higher the temperatures get, the more likely becomes the occurrence of unwanted side-reactions, such as the reverse water gas shift reaction (RWGS, see chapter 3.2), as well as the formation of unwanted side-products, such as carbon monoxide. On the other hand, the temperature has to exceed a certain minimum reaction temperature in order to allow the reaction to take place. Thus it is the goal of a good reactor layout to avoid large temperature gradients over the reactor vessel radius, as well as to provide an adequate temperature gradient over the length of the reactor, with the maximum temperature within the reactor over the required minimum reaction temperature and with an outlet temperature slightly over the boiling temperature of water (in order to avoid the wetting of the catalyst, see chapter 6.1.2). The design should make maximum use of the

[1] compared e.g. to the solid oxide electrolysis cell, which is used in the MIP experiment (see chapter 2.3.2).

catalyst material, while it minimizes mass and volume of the reactor. The same statements are true for the other components of the breadboard (see Figure 3-1).

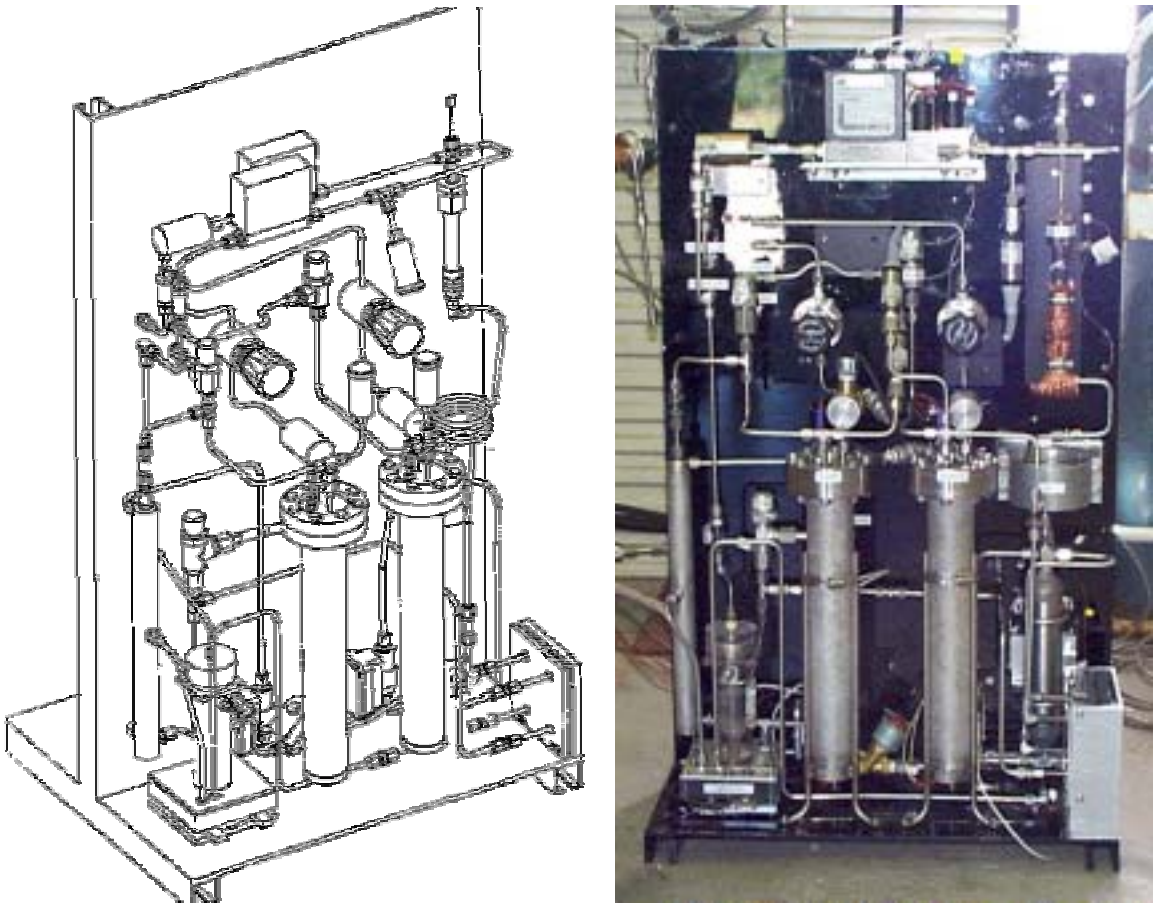

Figure 3-1: Sabatier / Water Electrolysis Breadboard [McClean, 2001]

The modeling of those processes involved is complicated by the fact that reaction equilibrium constants, reaction product stream composition, reaction temperatures, as well as fluid properties are all a function of inlet stream composition, reactor pressure, inlet temperature, and reactor vessel properties. Only computer modeling can take into account all these complex interrelationships. Correspondingly, it is the goal of the overall system computer model to correctly predict the breadboard performance behavior, not only in a qualitative fashion, but also with concrete quantitative statements. Once these tools are validated to correctly model the breadboard, they can be utilized in optimizing existing hardware and in the design of future hardware.

3.2 The Reverse Water Gas Shift Reaction

The reverse water gas shift reaction (RWGS) is the most likely unwanted side-reaction that may take place in a Sabatier reactor. Already due to this fact, an evaluation of the RWGS is necessary if one wants to correctly model the processes which occur within the

reactor. But there is also a second good reason why the RWGS reaction is worth to be modeled: it has also been proposed as a chemical reaction which – in collaboration with the methanol synthesis discussed in chapter 3.3 - could be employed for the purpose of ISCP. With just a few alterations (some of which are described in chapter 3.3), parts of the developed simulation tool can be key for the simulation of an RWGS / Methanol Synthesis reactor, thus contributing to a truly generic set of computer models.
The RWGS reaction has been known to chemists since the middle of the 19th century. Although this technology was suggested as a potential technique for Mars propellant manufacture already in [Zubrin & Wagner, 1991] there had been no experimental work done to demonstrate its viability for such application until Tom Meyer of the University of Boulder, Colorado, set up a breadboard in 1997 [Meyer, 1997].

The RWGS reaction is given by the equation

$$CO_2 + H_2 \rightarrow CO + H_2O$$

This reaction is mildly endothermic and occurs rapidly in the presence of an iron-chrom catalyst at temperatures of 400°C or greater. At 400°C the equilibrium constant K_p

$$K_p = \frac{c_{CO} \cdot c_{H_2O}}{c_{CO_2} \cdot c_{H_2}}$$

is driving the reaction to the right side of the equilibrium reaction with a value of about 0.1, and even at much higher temperatures K_p remains in the same order of magnitude. For a stochiometric reaction with $c_{CO_2} = c_{H_2} =: x$ the above formula leads to the equation

$$K_p = \frac{(1-x)\cdot(1-x)}{x^2} = \frac{x^2 - 2x + 1}{x^2} \Rightarrow$$

$$(1-K_p)x^2 - 2x + 1 = 0 \Rightarrow$$

$$x_{1/2} = \frac{+2 \pm \sqrt{4 - 4(1-K_p)}}{2(1-K_p)} = \frac{1 \pm \sqrt{K_p}}{1-K_p}$$

and since x can obviously not be more than one (mass conservation!):

$$x = \frac{1-\sqrt{K_p}}{1-K_p} = \frac{1}{1+\sqrt{K_p}}$$

For for an equilibrium constant of 0.1 this leads to a x of

$$x = 0.76$$

and thus to a concentration ratio of carbon dioxide to carbon monoxide of

$$\frac{c_{CO_2}}{c_{CO}} = \frac{c_{H_2}}{c_{H_2O}} = \frac{x}{1-x} = \frac{3.16}{1}$$

This means that even at e.g. 400°C only 24% of the carbon and hydrogen atoms decide to go to the left side of the equilibrium reaction. There is thus a significant problem in driving the RWGS reaction to completion. The goal therefore is to find a way to drive the RWGS to the right. To achieve this goal, [Meyer, 1997] suggests four different ways to do that, apart from increasing temperature and pressure:

"1. Overload the reactor with CO_2 to force the complete consumption of the H_2 and then recycle the excess CO_2 in the exhaust stream back into the reactor.
2. Overload the reactor with H_2 to force the complete consumption of the CO_2 and then recycle the excess H_2 in the exhaust stream back into the reactor.
3. Operate a system that removes water vapor from the reactor, thereby driving the reaction to the right. Such a system could be a desiccant bed or a condensing apparatus.

Way 1 and 3 respectively 2 and 3 could be combined to increase the yield even more.

The effect of increasing pressure as well as an off-stoichiometric H_2 to CO_2 input ratio of 2:1 can be seen in Figure 3-2:

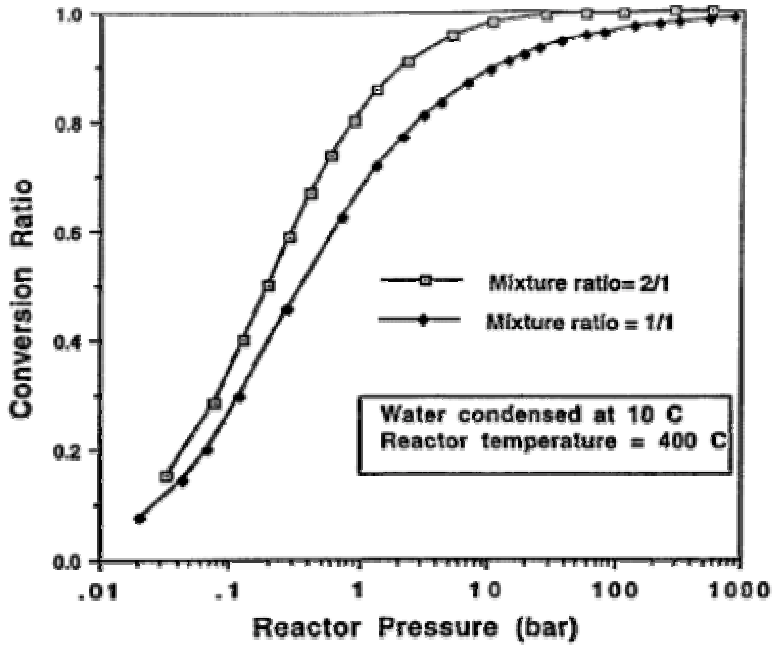

Figure 3-2: Effect of Pressure and Input Ratio on Conversion [Meyer, 1997]

However, assuming that this reaction can be driven as written, an 'infinite leverage oxygen machine' can be created by simply tying reaction in tandem with the water electrolysis. That is, the CO produced by the RWGS is discarded while the water is electrolyzed to produce oxygen (the net product), and hydrogen which can be recycled to reduce more CO_2. Since all the hydrogen is recycled, barring leakage losses this can go on forever allowing the system to produce as much oxygen as desired. The only important reagent needed is a small amount of water, which is endlessly recycled."

This is certainly not as easy as described. Especially condensing the water in the reactor is hard, since the reactor temperature of 400˚C is 26˚C above the critical point of water, and even at that lower temperature the vapor pressure is at 22.064 MPa, way beyond the pressures that seem feasible. In order to stay below a pressure of 5MPa in the reactor, the reactor temperature would have to be reduced to 264˚C. Therefore water condensing within the reactor can be ruled out.

On the other side a molecular sieve of 3 Ångstrøm could be capable of separating the water from the rest of the stream. A comparison of critical molecule diameters (Table 3-1) however shows that this will not be easy either, since the molecule diameters are quite similar:

Table 3-1: Critical Molecule Diameters

Molecule	Critical Diameter [Å]
H_2	2.4
O_2	2.8

CO	2.8
CO_2	2.8
H_2O	3.2
CH_4	4.0
CH_3OH	4.4

In order to verify the numbers quoted by [Meyer, 1997], the RWGS was modeled. He and his co-authors looked only at a CO_2 / H_2 inlet feed without any water or carbon monoxide traces. But since the carbon monoxide and the water cannot be completely separated from the recycle stream the reactor model has also to take this into account.

Again, the RWGS reaction is given by the equation:

$$CO_2 + H_2 \rightarrow CO + H_2O$$

with an equilibrium constant:

$$K_p = \frac{c_{CO} \cdot c_{H_2O}}{c_{CO_2} \cdot c_{H_2}}$$

If we call the concentrations of the reactants at the inlet x and the concentrations of the products at the outlet y and assuming that the mixture coming out of the RWGS is in a chemical equilibrium one can write:

$$K_p = \frac{y_{CO} \cdot y_{H_2O}}{y_{CO_2} \cdot y_{H_2}}$$

If ε is the amount of water molecules that is built within the reactor, than one can write:

$$\varepsilon = y_{H2O} - x_{H2O}$$

The oxygen atom that is required to build the water molecule is split from the carbon dioxide molecule. Therefore, one can write:

$$y_{CO} = x_{CO} + \varepsilon$$
$$y_{CO_2} = x_{CO_2} - \varepsilon$$
$$y_{H_2} = x_{H_2} - \varepsilon$$

With that the equilibrium constant can be rewritten as:

$$K_P = \frac{y_{CO} \cdot y_{H_2O}}{y_{CO_2} \cdot y_{H_2}} = \frac{\left(x_{CO} + \varepsilon\right) \cdot y_{H_2O}}{\left(x_{CO_2} - \varepsilon\right) \cdot \left(x_{H_2} - \varepsilon\right)}$$

If now we define the molar feed ratio Φ as:

$$\Phi = \frac{x_{CO_2}}{x_{H_2}}$$

then the inlet rate of hydrogen is the only unknown remaining in the formula for the equilibrium constant:

$$K_P = \frac{\left(x_{CO} + \varepsilon\right) \cdot y_{H_2O}}{\left(x_{CO_2} - \varepsilon\right) \cdot \left(x_{H_2} - \varepsilon\right)} = \frac{\left(x_{CO} + \varepsilon\right) \cdot y_{H_2O}}{\left(\Phi \cdot x_{H_2} - \varepsilon\right) \cdot \left(x_{H_2} - \varepsilon\right)}$$

This formula can also be written as:

$$\underbrace{\Phi}_{a} \cdot x_{H_2}{}^2 \underbrace{- \left(\Phi + 1\right)\varepsilon}_{b} \cdot x_{H_2} + \underbrace{\varepsilon^2 - \frac{\left(x_{CO} + \varepsilon\right) \cdot y_{H_2O}}{K_P}}_{c} = 0$$

The variables a, b, and c can then be put in the binomic formula:

$$x_{H_2} = \frac{-b \pm \sqrt{b^2 - 4ac}}{2a} = \frac{\left(\Phi + 1\right)\varepsilon + \sqrt{\left(\Phi + 1\right)^2 \varepsilon^2 - 4 \cdot \Phi \cdot \left(\varepsilon^2 - \frac{\left(x_{CO} + \varepsilon\right) \cdot y_{H_2O}}{K_P}\right)}}{2\Phi}$$

The minus in the plus minus can be neglected since only positive concentrations make sense.

The equilibrium constant is dependent on the standard Gibbs energy change of reaction and the reaction temperature:

$$\ln K = -\frac{\Delta G^0}{RT}$$

The change of the equilibrium constant over temperature is shown in Figure 3-3:

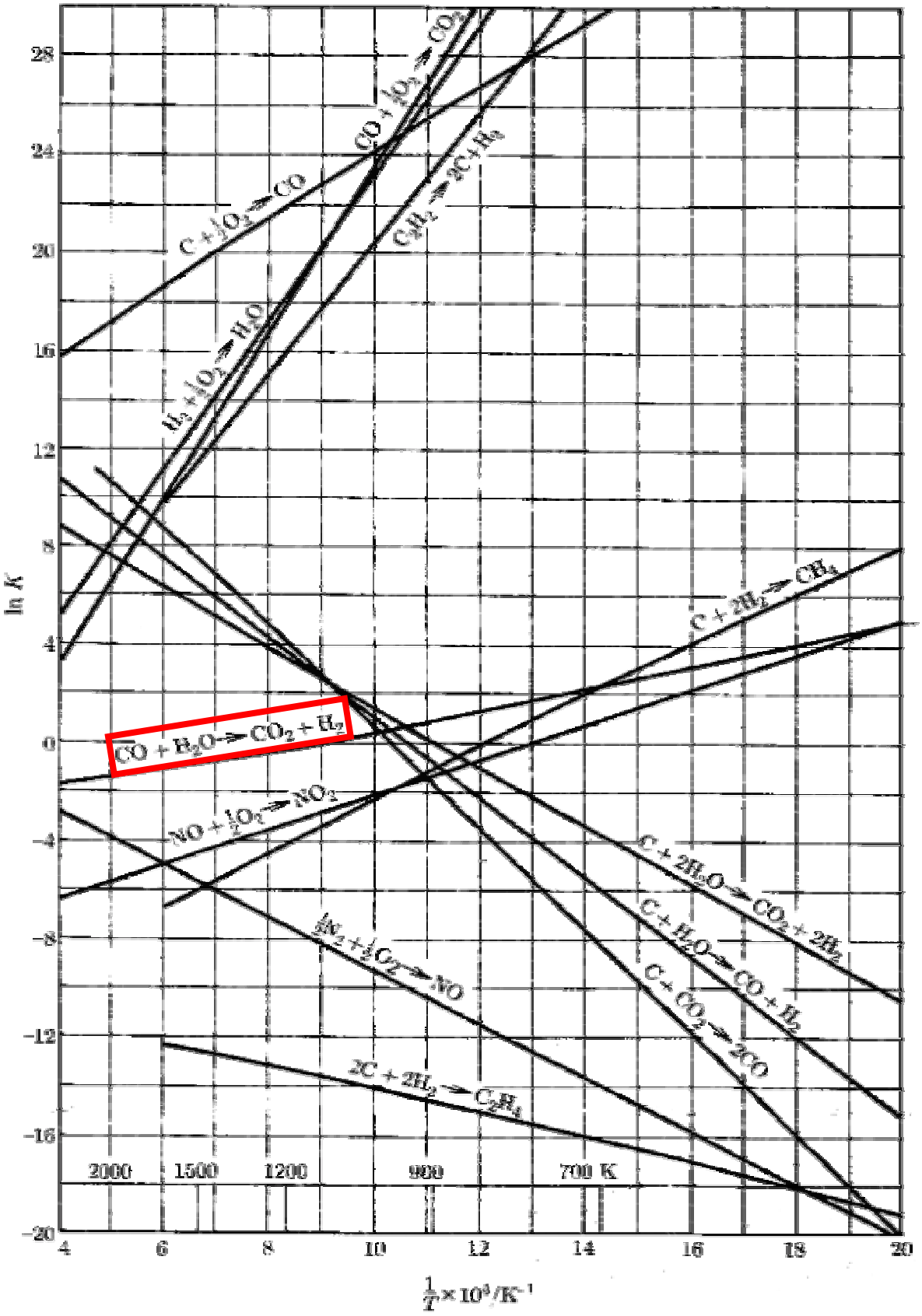

Figure 3-3: Equilibrium Constants as a Function of Temperature
[Smith et al., 1996]

The lines in Figure 3-3 are only an approximation. The exact relation between the equilibrium constant and the temperature is given by the formula:

$$\frac{d \ln K}{d\left(1/T\right)} = -\frac{\Delta H^o}{R}$$

The graph implies that a plot of K vs. the reciprocal of absolute temperature is a straight line. This is often the case, since ΔH^o is often nearly constant over a limited temperature range. This method is known as the *"second law method"*.

To get more precise estimations of K, [Smith et al., 1996] recommend the use of the general relation:

$$\Delta G^o = \Delta H^o - T \cdot \Delta S^o$$

whereas

ΔG^o = standard Gibbs energy change of reaction
ΔH^o = standard enthalpy change (standard heat) of reaction
T = temperature [K]
T_0 = standard temperature [K]
ΔS^o = standard entropy change of reaction.

The standard heat of a reaction with constant pressure is related to temperature by the equation:

$$dH = C_P \, dT$$

whereas

ΔC_P^o = heat capacity.

The heat capacity ΔC_P^o is defined as:

$$C_P = \left(\frac{\partial H}{\partial T}\right)_p$$

hence:

$$\Delta H = \int_{T_1}^{T_2} C_p \, dT \qquad \text{(p = const.)}$$

This formula applies to any process for which $p_2 = p_1$, whether or not it is actually carried out at constant pressure. However, only for the mechanically reversible, constant-pressure process heat and work can be calculated by the equations:

$$Q = n \cdot \Delta H = n \cdot \int_{T_1}^{T_2} C_p \, dT$$

$$W = -p \cdot n \cdot \Delta V$$

If we arbitrarily set the standard-state enthalpies of all elements equal to zero as the basis of calculation, then the standard-state enthalpy of each compound is its heat of formation. We therefore can write:

$$\Delta H^o = \sum_i \upsilon_i \cdot \Delta H_{f_i}$$

$$\Delta H^o = \Delta H_0^o + R \int_{T_0}^{T} \frac{\Delta C_P^o}{R} dT$$

The temperature dependence of the standard entropy change of reaction is developed in a similar way, resulting in the equation:

$$\Delta S^o = \Delta S_0^o + R \int_{T_0}^{T} \frac{\Delta C_P^o}{R} \frac{dT}{T}$$

Combined, the above equations result in the formula:

$$\Delta G^o = \Delta H_0^o + R \int_{T_0}^{T} \frac{\Delta C_P^o}{R} dT - T\Delta S_0^o - RT \int_{T_0}^{T} \frac{\Delta C_P^o}{R} \frac{dT}{T}$$

However:

$$\Delta S_0^o = \frac{\Delta H_0^o - \Delta G_0^o}{T_0}$$

hence:

$$\Delta G^o = \Delta H_0^o - \frac{T}{T_0}\left(\Delta H_0^o - \Delta G_0^o\right) + R \int_{T_0}^{T} \frac{\Delta C_P^o}{R} dT - RT \int_{T_0}^{T} \frac{\Delta C_P^o}{R} \frac{dT}{T}$$

Finally, division by RT yields:

$$-\ln K = \frac{\Delta G^o}{RT} = \frac{\Delta G_0^o - \Delta H_0^o}{RT_0} + \frac{\Delta H_0^o}{RT} + \frac{1}{T}\int_{T_0}^{T} \frac{\Delta C_P^o}{R} dT - \int_{T_0}^{T} \frac{\Delta C_P^o}{R} \frac{dT}{T}$$

The values for the standard changes can be found in tables. The heat capacity ΔC_P^o within a range from T_0 = 298 K to T_{max}. can be approximated with a curve fit of the form:

$$C_P = \left(A + BT + CT^2 + DT^{-2}\right) \cdot R$$

The values for the eligible substances are summarized in Table 3-2:

Table 3-2: Heat Capacities of Gases

Substance	T_{max} [K]	A [-]	$10^3 \cdot B$ [K^{-1}]	$10^6 \cdot C$ [K^{-2}]	$10^{-5} \cdot D$ [K^{-3}]
H_2	3000	3.249	0.422	0	0.083
O_2	2000	3.639	0.506	0	-0.227
H_20	2000	3.470	1.450	0	0.121
CO_2	2000	5.457	1.045	0	-1.157
CO	2500	3.376	0.557	0	-0.031
CH_3OH	1500	2.211	12.216	-3.450	0
CH_4	1500	1.702	9.081	-2.164	0

3.3 Methanol Synthesis

Due to the reasons outlined at the commencement of chapter 3.2, the formation of methanol was further investigated. This was done in support of the efforts of the JSC Fluids Systems Branch with respect to the potential establishment of a RWGS / methanol synthesis breadboard similar to the Sabatier / water electrolysis breadboard which is subject of this thesis, as well as in continuation of the work started in [Pauly, 1998a]. Parts of the tools developed in this sub-chapter will also be of use later in chapter 3 for the modeling of the Sabatier breadboard.

Today, methanol (CH_3OH) is the third most common hydrocarbon produced in the world with a total work production at about 27 million tons per year [Chinchen et al., 1990]. The principal feedstocks on Earth for making methanol are natural gas, coal, and wood.

The RWGS process described in the previous chapter is more complicated in reality. Actually, side reactions have to be taken into account, too. For the RWGS, these can be neglected in the first level of approximation.

With methanol this is not the case. For a first approach to the problem the formation and other hydrocarbons apart from methanol are not taken into account. Thus, the three main reactions that may take place in the reactor are:

$$CO + 2H_2 \rightarrow CH_3OH \quad (1)$$
$$CO + H_2O \rightarrow CO_2 + H_2 \quad (2)$$
$$CO_2 + 3H_2 \rightarrow CH_3OH \quad (3)$$

The second reaction is familiar. It is nothing else but the “reverse” reverse water gas shift or simply water gas shift (WGS).

Although methanol synthesis is widely used in chemical industry today, until 1990 methanol was one of the least understood of the major catalytic processes. In particular a big quarrel remained unsolved for many years, that is whether methanol is actually built out of CO (first reaction) or out of CO_2 (third reaction) or both. The reason why the answer to that problem is so hard to give is because the WGS reaction (or RWGS respectively)(second reaction) is always accompanied the other two reactions. This reaction changes CO into CO_2 and vice versa. These three reactions thus built a “reaction triangle”, shown in Figure 3-4:

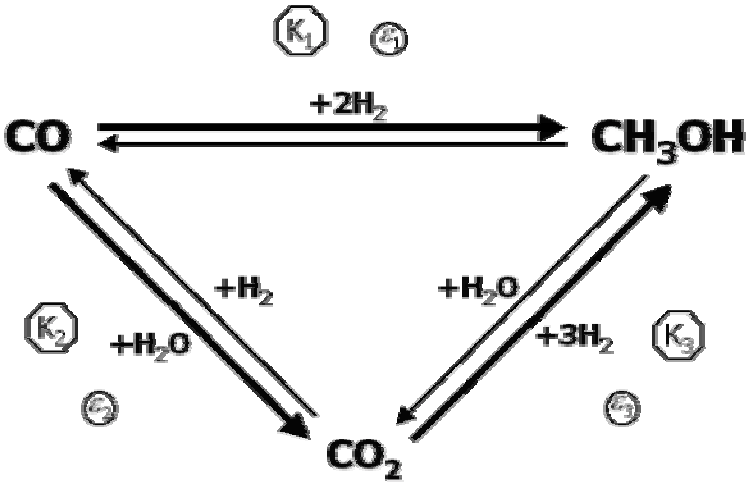

Figure 3-4: Reaction Triangle of Methanol Synthesis

But since in industry methanol is produced out of “syngas” or synthesis gas, a mixture of CO and CO_2, the answer to the question is secondary. In the case of methanol production on Mars, the answer is important, since all reactants apart from CO_2 have to be either imported from Earth or be produced in situ before the actual methanol synthesis.

The study of [Chinchen et al., 1990] proved with the help of radioactive markers that with a $Cu/ZnO/Al_2O_3$ catalyst (copper / zinc oxide / alumina) at 50 bars and 250°C, basically all methanol is built out of CO_2. The question now is, whether or not and how far this is applicable also to other catalysts, temperatures, and pressures.

In order to optimize these processes for an ISCP plant based on the RWGS reaction, these processes have to be modeled.

In general, a chemical reaction can be written in the form

$$|\nu_1| \cdot A_1 + |\nu_2| \cdot A_2 + ... \rightarrow \quad |\nu_3| \cdot A_3 + |\nu_4| \cdot A_4 + ...$$

whereas

ν_i = stoichiometric number [-]
(positive for products, negative for reactants)
A_i = species (chemical formula).

The absolute of a stoichiometric number is the so-called “stoichiometric coefficient”.

For the first reaction

$$CO + 2H_2 \quad \rightarrow \quad CH_3OH$$

the stoichiometric numbers are:

$$\nu_{CO} = -1 \qquad \nu_{H_2} = -2 \qquad \nu_{CH_3OH} = +1$$

The stoichiometric number for any inert species is zero.

With this reaction the changes in the numbers of moles of the species present are in direct proportion to the stoichiometric numbers. Thus, if one mole of carbon monoxide disappears by reaction, two moles of hydrogen have also to disappear. Simultaneously one mole of methanol is formed. Applying this principle to a differential amount of reaction, we can write:

$$\frac{\Delta n_{CO}}{\nu_{CO}} = \frac{\Delta n_{H_2}}{\nu_{H_2}} = \frac{\Delta n_{CH_3OH}}{\nu_{CH_3OH}}$$

or in general:

$$\frac{\Delta n_1}{\nu_1} = \frac{\Delta n_2}{\nu_2} = \frac{\Delta n_3}{\nu_3} = \frac{\Delta n_4}{\nu_4} = \frac{\Delta n_i}{\nu_i}$$

With all terms being equal, they can be identified collectively with a single quantity representing an amount of reaction. Thus a definition of $\Delta\varepsilon$ is provided by the equation:

$$\frac{\Delta n_1}{\nu_1} = \frac{\Delta n_2}{\nu_2} = \frac{\Delta n_3}{\nu_3} = \frac{\Delta n_4}{\nu_4} = \frac{\Delta n_i}{\nu_i} = \Delta\varepsilon$$

The new variable ε, called the *reaction coordinate* (or *extent of reaction*), characterizes the extent or degree to which a reaction has taken place.

Integration from an initial unreacted state where $\varepsilon = 0$ and $n_i = n_i^o$ to a state in which the equilibrium is reached:

$$\int_{n_i^o}^{n_i} dn_i = \int_0^{\varepsilon} d\varepsilon$$

or:

$$n_i = n_i^o + \nu_i \cdot \varepsilon$$

Summation over all species yields

$$n = \sum_i n_i = \sum_i n_i^o + \varepsilon \cdot \sum_i \nu_i$$

or

$$n = n^o + \nu \cdot \varepsilon$$

whereas:

$$n = \sum_i n_i \qquad n^o = \sum_i n_i^o \qquad \nu = \sum_i \nu_i$$

The mole fractions y_i of the species present are related to ε by:

$$y_i = \frac{n_i}{n} = \frac{n_i^o + \nu_i \cdot \varepsilon}{n^o + \nu \cdot \varepsilon}$$

With the stoichiometric numbers for the reaction being:

$$\nu_{CO} = -1 \qquad \nu_{H_2} = -2 \qquad \nu_{CH_3OH} = +1$$

The final numbers of moles for the different species therefore are:

$$n_{CO} = n_{CO}^{o} - \varepsilon_1 - \varepsilon_2$$

$$n_{H_2} = n_{H_2}^{o} - 2\varepsilon_1 + \varepsilon_2 - 3\varepsilon_3$$

$$n_{CH_3OH} = n_{CH_3OH}^{o} + \varepsilon_1 + \varepsilon_3$$

$$n_{CO_2} = n_{CO_2}^{o} + \varepsilon_2 - \varepsilon_3$$

$$n_{H_2O} = n_{H_2O}^{o} - \varepsilon_2 + \varepsilon_3$$

ν can be calculated as:

$$\nu = \sum_i \nu_i = \nu_{CO} + \nu_{H_2} + \nu_{CH_3OH} = -2$$

The reaction within the reactor will at all times take place in the gaseous phase. Thus the fluids within the reactor vessels shall be modeled as mix of gases.

If the assumption that the equilibrium mixture is an ideal solution is justified, then the real gas coefficent $\hat{\Phi}_i$ becomes Φ_i, the fugacity coefficient of pure species i at temperature T and pressure p. In this case, the last equation becomes

$$\prod_i \left(y_i \cdot \Phi_i\right)^{\nu_i} = \left(\frac{p}{p^o}\right)^{-\nu} \cdot K$$

The Φ_i of each specie can be evaluated from a generalized correlation once the equilibrium T and p are specified.

For pressures sufficiently low or temperatures sufficiently high, the equilibrium mixture behaves essentially as an ideal gas. In this event, each $\hat{\Phi}_i = 1$, and the equation reduces to

$$\prod_i (y_i)^{\nu_i} = \left(\frac{p}{p_o}\right)^{-\nu} \cdot K$$

That means that for a gas with close to ideal gas behavior we can calculate the mole fractions as:

$$y_i = \frac{n_i}{n} = \frac{n_i^o + \nu_i \cdot \varepsilon}{n^o + \nu \cdot \varepsilon}$$

In order to get the equilibrium mole fractions y_i, the extent of reaction ε must somehow be derived from the equilibrium constant equations. For the three reactions

$CO + 2H_2$	$\rightarrow$	CH_3OH	(1)
$CO + H_2O$	$\rightarrow$	$CO_2 + H_2$	(2)
$CO_2 + 3H_2$	$\rightarrow$	CH_3OH	(3)

these equations are:

$$K_1 = \frac{y_{CH_3OH}}{y_{CO} \cdot y_{H_2}^2} \cdot \left(\frac{p}{p_o}\right)^2 = \frac{n_{CH_3OH} \cdot n^2}{n_{CO} \cdot n_{H_2}^2} \cdot \left(\frac{p}{p_o}\right)^2 \quad (1)$$

$$K_2 = \frac{y_{CO_2} \cdot y_{H_2}}{y_{CO} \cdot y_{H_2O}} = \frac{n_{CO_2} \cdot n_{H_2}}{n_{CO} \cdot n_{H_2O}} \quad (2)$$

$$K_3 = \frac{y_{CH_3OH} \cdot y_{H_2O}}{y_{CO_2} \cdot y_{H_2}^3} \cdot \left(\frac{p}{p_o}\right)^2 = \frac{n_{CH_3OH} \cdot n_{H_2O} \cdot n^2}{n_{CO_2} \cdot n_{H_2}^3} \cdot \left(\frac{p}{p_o}\right)^2 \quad (3)$$

The task now is to find right values for ε_1, ε_2, and ε_3 so that the equations for the given K_1, K_2, and K_3 are fulfilled.
This task can be completed if it one manages to solve a set of non-linear equations for the extents of reactions (see Figure 3-5).

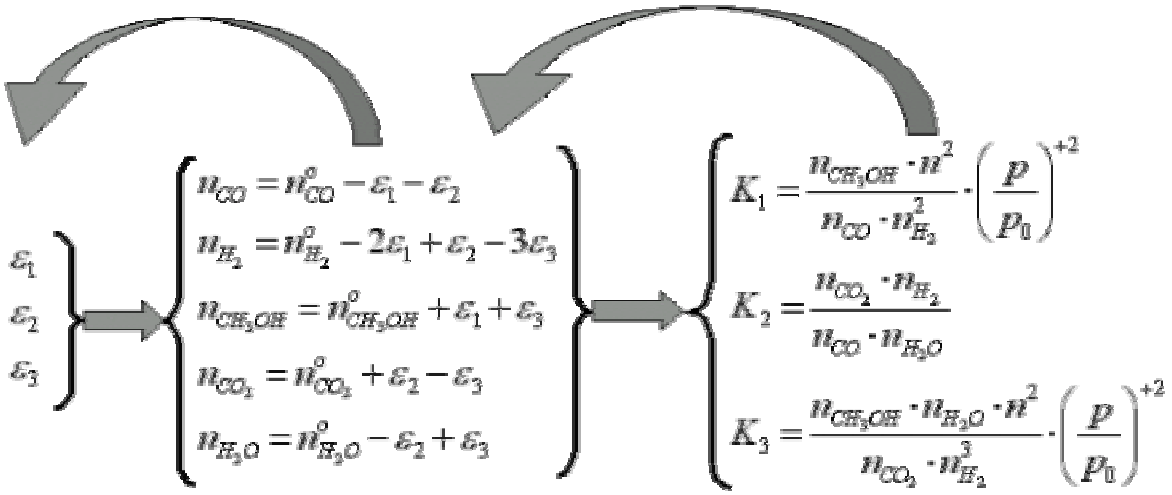

Figure 3-5: Solving of non-linear Equations for the Extents of Reaction

For three reactions and five species, this set will feature 8 unknown variables. The coefficient matrix representing this set of non-linear equations is shown in Figure 3-6:

$$\left(\begin{array}{cccccccc|c}
\frac{R\cdot T}{n_{CO}}-\ln\frac{n_{CO}}{n_T} & 0 & 0 & 0 & 0 & 1 & 1 & 0 & -\Delta G^o_{CO} \\
0 & \frac{R\cdot T}{n_{H_2}}-\ln\frac{n_{H_2}}{n_T} & 0 & 0 & 0 & 0 & 0 & 2 & -\Delta G^o_{H_2} \\
0 & 0 & \frac{R\cdot T}{n_{CH_3OH}}-\ln\frac{n_{CH_3OH}}{n_T} & 0 & 0 & 1 & 1 & 4 & -\Delta G^o_{CH_3OH} \\
0 & 0 & 0 & \frac{R\cdot T}{n_{CO_2}}-\ln\frac{n_{CO_2}}{n_T} & 0 & 1 & 2 & 0 & -\Delta G^o_{CO_2} \\
0 & 0 & 0 & 0 & \frac{R\cdot T}{n_{H_2O}}-\ln\frac{n_{H_2O}}{n_T} & 0 & 1 & 2 & -\Delta G^o_{H_2O} \\
1 & 0 & 1 & 1 & 0 & 0 & 0 & 0 & n^o_C \\
1 & 0 & 1 & 2 & 1 & 0 & 0 & 0 & n^o_O \\
0 & 2 & 4 & 0 & 2 & 0 & 0 & 0 & n^o_H
\end{array}\right)$$

Figure 3-6: Coefficient Matrix representing the non-linear RWGS equations

This can be done numerical or via Lagrange multipliers respectively.

3.4 Excel Model

At the beginning of the modeling efforts in the course of this thesis, it was tried to integrate it as seamlessly as possible into the ongoing modeling activities at NASA JSC, in particular the Exploration Office and the Fluid Systems Group. These two are significantly influenced by the Integrated Design Environment (IDE) Facility, the concurrent

engineering design center at JSC. Here, the expertise from various different subsystems comes together with the goal of a concurrent development of new designs. With this as background and raison d'être, it was decided to base this Integrated Design Environment on MicroSoft Excel®. The rationale behind this decision being that Excel is a widely used software, which significantly reduces the training time for the experts that take part in IDE sessions. Therefore, it was first tried, to also base some of this thesis' calculation work on Excel.

The field in which Excel proved most helpful was the derivation of scaling models, meaning models that can quickly give a first estimation of the elements sizes of an ISCP system (see Figure 3-7).

In order to arrive at an overall system layout with a sizing of the major components, the program has to follow through a set of iteration steps. An example of such a set of iteration steps will be discussed with the following example of an RWGS / methanol synthesis reactor (see Figure 3-7s):

1. The wanted total liquid oxygen mass after the production phase is entered
2. The wanted total liquid methanol mass after the production phase is entered
3. The daily input into the oxygen tank is calculated
4. The required oxygen output of the electrolyzing unit is calculated
5. The hydrogen output of the electrolyzing unit is calculated
6. The water traces in both, hydrogen and oxygen output mass flows are calculated
7. The required water input mass flow into the electrolyzing unit is calculated
8. With the total methanol mass the daily input into the methanol tank is calculated
9. With that the methanol reactor in- and output mass flows are calculated
10. With the water inlet mass flow into the electrolyzing unit minus the water outlet mass flow of the methanol reactor, the water outlet mass flow of the RWGS unit is calculated
11. With that, the inlet mass flows into the RWGS are calculated
12. With the carbon dioxide inlet mass flow of RWGS and methanol reactor and the recycled carbon dioxide mass flows, the fresh carbon dioxide input into both systems is calculated
13. With that the sorption pump atmosphere input mass flow is calculated
14. With the hydrogen input mass flow of RWGS and methanol reactor and the hydrogen output of the electrolyzing unit, the required hydrogen input into the methanol unit is calculated (the RWGS is supplied by the electrolyzing unit solely)
15. With that the amount of seed hydrogen to be imported to Mars is calculated

Based on such a set of iteration steps, the program easily allows for the user to conveniently obtain estimates for mass flows and flow compositions at any point within the system, as well as power, mass, and volume requirements of any subsystem with just a click of a mouse or the insertion of a number (via pop-up windows, see Figure 3-7). In this function, it also proved useful later in the layout of future systems (see chapter 6, in particular Figure 6-7).

However, after some weeks and months of utilization, it became obvious that the advantage of the familiarity of Excel was outweighed by its disadvantages: first, Excel is a very general program, meaning it is by no means dedicated to take on modeling problems of chemistry and chemical engineering. Its abilities turned out to be rather limited, in particular with respect to numerical simulation. Similar negative experiences were made using CHEMCAD®, a dedicated chemical engineering software. It was thus decided to design more capable tools, some of which will be outlined in the succeeding subchapters.

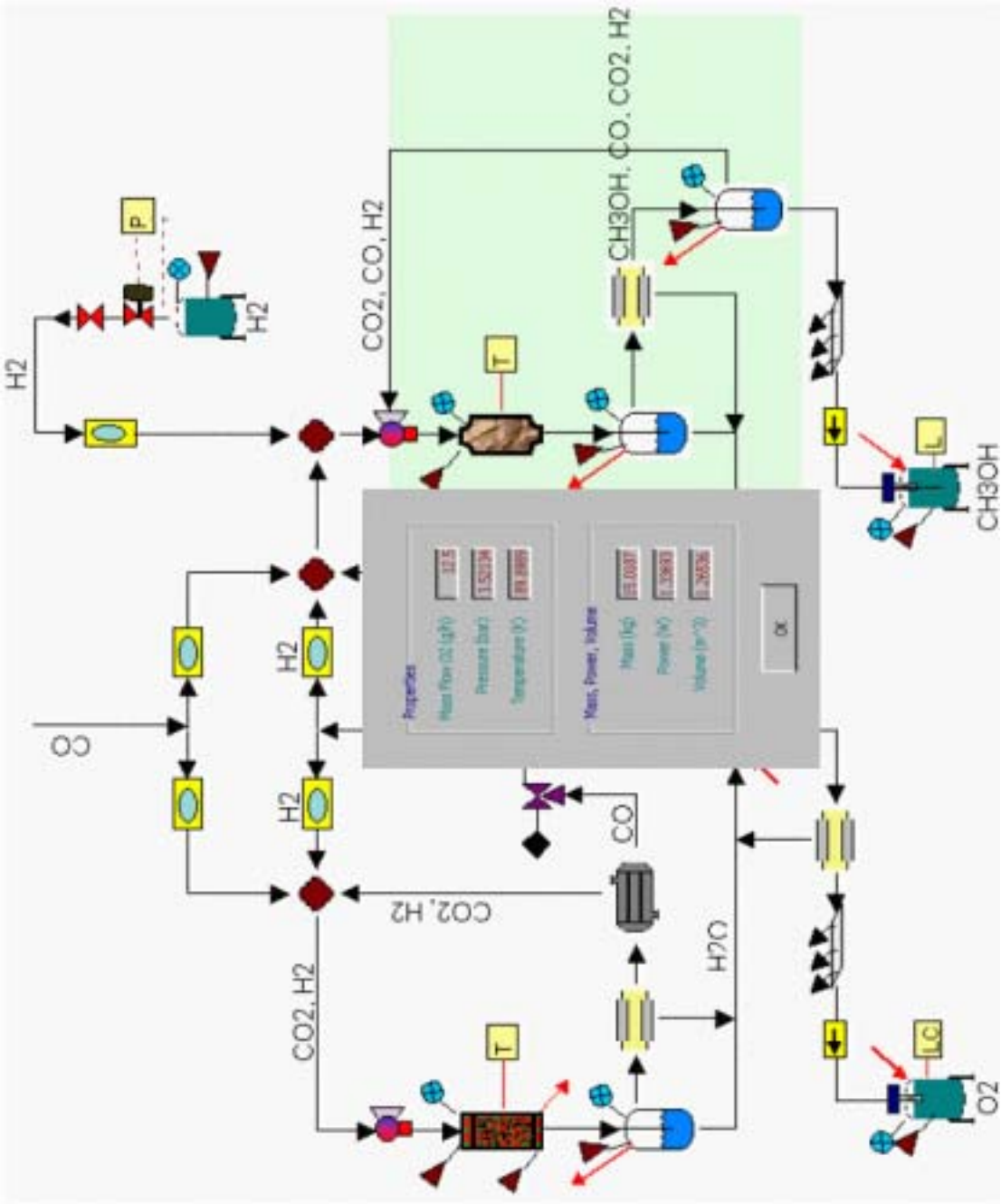

Figure 3-7: Excel Model of a RWGS / Methanol Synthesis Reactor

3.5 MATLAB Model of the Sabatier Reactor

3.5.1 Pressure Loss within the Reactor

In the following, the question of the extent of pressure loss within the reactor will prove to be crucial for the choice of the modeling method. In order to be able to answer this question, one can benefit from the work of [Blake, Kozeny, Carman, 1937] (for Re<10), [Burke, Plummer, 1922] (for Re>1000), and [Ergun, 1952] for the intermediate range.

We first define the following parameters:

The porosity of a packed bed is defined as

$$\varepsilon = \frac{V_{void}}{V_{total}} = \frac{V_{total} - V_{solids}}{V_{total}}$$

whereas:

- ε = porosity of the packed bed [-]
- V_{void} = volume of voids in the system [m^3]
- V_{solid} = volume of solids in the system [m^3]
- V_{total} = total volume of the system [m^3]

The superficial velocity[1] v_s:

$$v_s = \frac{\dot{V}}{A} = \frac{\dot{m}}{\rho \cdot A}$$

The Reynolds number for porous media Re_{PM} is defined as

$$\mathrm{Re}_{PM} = \frac{D_p \cdot v_s \cdot \rho}{\eta_{fluid} \cdot (1-\varepsilon)}$$

whereas:

- D_p = catalyst pellet diameter [m]
- η_{fluid} = dynamic viscosity[m^2/s]

[1] Care has to be taken in order to not confuse the superficial velocity v_s with the interstitial velocity v_i, where the volume flow is based on the area actually open to the flowing fluid. Thus, the latter can be derived from the from via the equation $v_i = \frac{v_s}{\varepsilon}$.

The equations used are:

$$\Delta p_{BKZ} = \frac{150 \cdot \mu \cdot L \cdot v_s \cdot (1-\varepsilon)^2}{{D_p}^2 \cdot \varepsilon^3} \quad \text{for } Re_{PM}<10$$

and:

$$\Delta p_{BP} = \frac{1.75 \cdot L \cdot {v_s}^2 \cdot \rho \cdot (1-\varepsilon)}{D_p \cdot \varepsilon^3} \quad \text{for } Re_{PM}>1000$$

and:

$$\Delta p_E = \Delta p_{BKZ} + \Delta p_{BP} = \frac{150 \mu L \cdot v_s \cdot (1-\varepsilon)^2}{{D_p}^2 \cdot \varepsilon^3} + \frac{1.75 L \cdot {v_s}^2 \cdot \rho \cdot (1-\varepsilon)}{D_p \cdot \varepsilon^3} \quad \text{for } 10<Re_{PM}<1000$$

whereas

L = bed length [m]

μ = dynamic viscosity [Ns/m²]

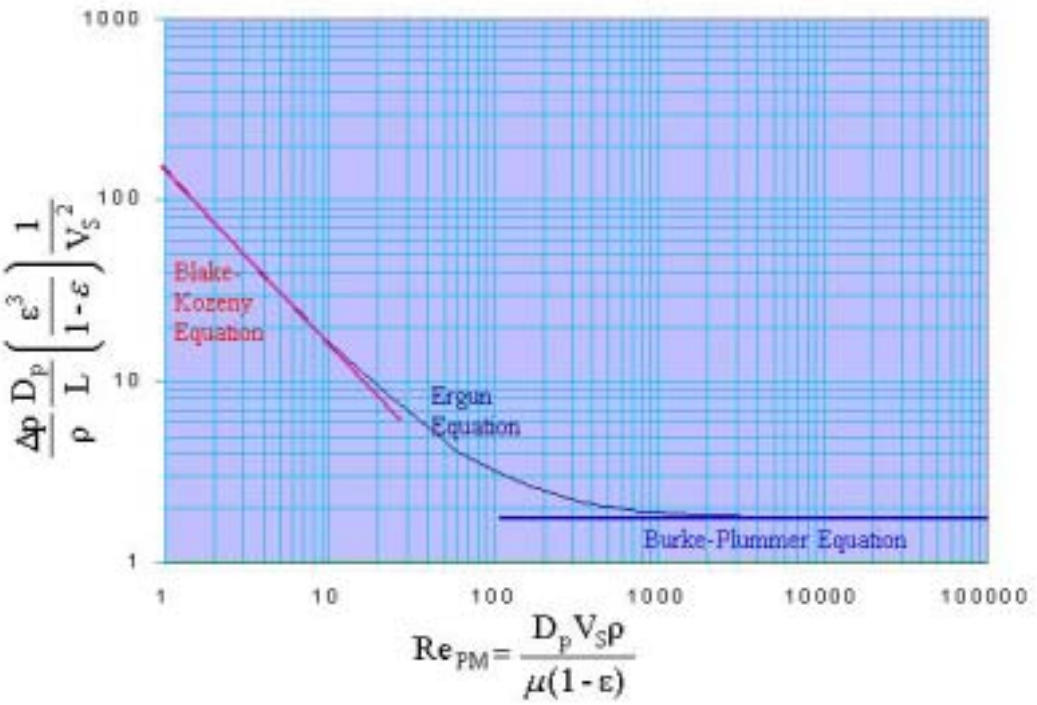

Figure 3-8: Pressure Loss Estimates [Subramanian, 2001]

With typical values for the Sabatier reactor:

p = 1.35bar, T = 600K, $\rho_{CH_4+2H_2O} = 0.47\frac{kg}{m^3}$, μ = 2.11·10$^{-5}\frac{Ns}{m^2}$, D_p = 3mm, D_i = 16mm, $\dot{m} = 0.58\frac{g}{\min}$, L = 100mm, and ε = 0.3 one ends up with Re_{PM} = 0.76 and an absolute pressure loss of Δp = 0.65mbar, which equals a relative pressure loss of $\Delta p / p = 0.65 mbar / 1.35 bar \approx 0.05\%$.

Therefore it is justified to assume constant pressure over the reactor.

3.5.2 Enthalpy, Heat of Reaction, Gibbs Energy

The work presented here is a first attempt to model a Sabatier / water electrolysis ISCP plant end-to-end, with all its essential chemical and physical processes, something that has not been tried yet in this form. It aims at serving as a stepping-stone for further work in this area.
Therefore, the models of the chemistry should be flexible to allow investigating other processes in the future, too. In order to achieve this, Gibb's method of free energy was chosen to calculate the reaction equilibria, which can be used – in opposition to other methods – for every reaction and every reactant. The analysis of equilibrium reactions described in this Ph.D. work is mainly based on Gibbs energy and heat of reaction.

In industrial practice chemical reactions are usually accompanied by physical processes (e.g. pressure, temperature changes, transfer of heat, etc.). Each of the vast number of possible chemical reactions may be carried out in many different ways, and each reaction carried out in a particular way is accompanied by a particular physical effect. Tabulation of all possible heat effects for all possible reactions is impossible. Thus, in chemical engineering effects like e.g. heat transfer for reactions carried out in diverse ways are calculated based on the data of reactions carried out in a standard way [Smith et al., 1996, p.117-135]. A consistent basis for the treatment of reaction heat effects results for example, when reactants and products of a reaction are all at the same temperature. Usually, state variables values are usually given at a temperature of T_0 = 298.15K and a pressure of p_0 = 1bar.

The following will describe how to derive good approximations of state variable values at any temperature and any pressure from the given data at standard conditions.

According to the Gibbs' phase rule in a system consisting of a homogenous substance of constant composition the molar or specific enthalpy (as well as other state variables, e.g. the internal energy U) may be expressed as a function of two other state variables. In the case of the enthalpy, with temperature T and pressure p as the two state variables, we can write:

$$H = H(T, p)$$

and thus:

$$dH = \left(\frac{dH}{dT}\right)_p dT + \left(\frac{dH}{dp}\right)_T dp$$

With the heat capacity at constant pressure C_P this becomes:

$$dH = C_P \cdot dT + \left(\frac{dH}{dp}\right)_T dp$$

The final term equals zero

- for any constant pressure process, regardless of the substance;
- whenever the enthalpy of the substance is independent of the pressure, regardless of the process. This is exactly true for ideal gases and approximately true for low-pressure real gases, for solids, and for liquids outside the critical region.

Dealing with chemical reactions, the enthalpy change caused by a chemical reaction is usually called the **heat of reaction**. In the case of the formation of a single compound from its constituent elements (e.g. formation of water from hydrogen and oxygen), the heat of reaction is also called **heat of formation**.

The standard-state[1] of enthalpy of a chemical compound is equal to its heat of formation plus the standard-state enthalpies of its constituent elements. **If we arbitrarily set the standard-state enthalpies of all elements equal to zero as the basis of calculation, then the standard-state enthalpy of each compound is its heat of formation. This considerably simplifies the calculations of chemical reaction heat effects.** This approach will be followed throughout this thesis.

Property values in the standard state are denoted with the degree symbol "°".

Thus, the standard heat of reaction of the Sabatier reaction is the sum of the standard heats of formation of the different species times their stoichiometric numbers:

$$\Delta H^o = \sum_i \upsilon_i \cdot H_i^o = \sum_i \upsilon_i \cdot H_{f\,i}^o \Rightarrow$$
$$\Delta H^o = (-1) \cdot H_{f\,CO_2}^o + (-4) \cdot H_{f\,H_2}^o + (+1) \cdot H_{f\,CH_4}^o + (+2) \cdot H_{f\,H_2O_{(g)}}^o$$

[1] The standard-state for liquids and solids is the actual pure liquid or solid at 1bar.
For gases, the standard-state is the ideal-gas state at 1bar.

In the case of the Sabatier reaction, this leads to:

$$\Delta H^{o}_{298K} = (-1)\cdot\left(-393509\frac{J}{mol}\right)+(-4)\cdot\left(0\frac{J}{mol}\right)+(+1)\cdot\left(-74520\frac{J}{mol}\right)+(+2)\cdot\left(-241818\frac{J}{mol}\right)=-164647\frac{J}{mol}$$

The fundamental equation that relates the heat of reaction to the temperature is:
[Smith et al., 1996]:

$$dH = C_P dT \Rightarrow \Delta H = \int_{T_1}^{T_2} C_P dT$$

or

$$d\Delta H^{o} = \Delta C_p^{o} dT$$

whereas

ΔC_p^o = standard heat capacity change of reaction

Integration gives

$$\Delta H^{o} = \Delta H_0^{o} + R\int_{T_0}^{T} \frac{\Delta C_p^{o}}{R} dT$$

ΔH^{o} and ΔH_0^{o} are the heats of reaction at the temperature T and at reference temperature T_0 respectively.

The heat capacity is a function of the temperature. Therefore, its practical use requires the knowledge of the dependence, which is usually given by an empirical equation of the expression:

$$\frac{C_p}{R} = A + B\cdot T + C\cdot T^2 + D\cdot T^{-2}$$

Values for the constants can be found in literature. The estimated values are in good accordance with the actual values as shown in Figure 3-9 (example: water, values as given by the National Institute of Standards and Technology):

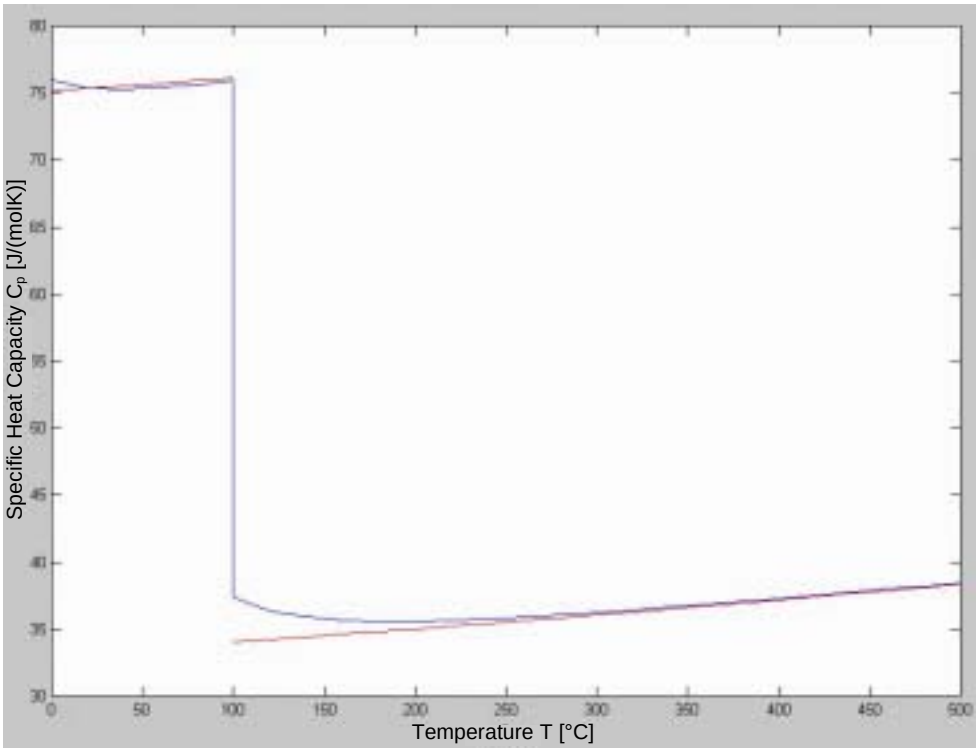

Figure 3-9: Modeled C_p (red) vs. actual C_p (blue)

With the last equation the standard heat capacity change of reaction integrated over the temperature can be calculated as:

$$\int_{T_0}^{T} \frac{\Delta C_p^o}{R} dT = \Delta A \cdot T_0 \cdot (\tau - 1) + \frac{\Delta B}{2} \cdot T_0^2 \cdot (\tau^2 - 1) + \frac{\Delta C}{3} \cdot T_0^3 \cdot (\tau^3 - 1) + \frac{\Delta D}{T_0} \cdot \frac{\tau - 1}{\tau}$$

whereas $\tau = \frac{T}{T_0}$ and $\Delta A = \sum_i \upsilon_i \cdot A_i$ with analogous definitions for ΔB, ΔC, and ΔD.

υ_i are the stoichiometric numbers, whereas $|\upsilon_i|$ are called the stoichiometric coefficients. The sign convention for υ_i is positive for products and negative for reactants. For the Sabatier reaction introduced in chapter 6

$$CO_2 + 4H_2 \rightarrow CH_4 + 2H_2O$$

the stoichiometric numbers are:

$$\upsilon_{CO_2} = -1;\ \upsilon_{H_2} = -4;\ \upsilon_{CH_4} = +1;\ \upsilon_{H_2O} = +2;$$

The necessary coefficient values can be obtained from [Smith et al., 1996] (see also Table 3-2):

Table 3-3: Heat Capacity Constants

Substance i	T_{max} [K]	A_i [-]	B_i [K^{-1}]	C_i [K^{-2}]	D_i [K^2]	υ_i [-]
CO_2	2000	+5.457	$+1.045 \cdot 10^{-3}$	±0	$-1.157 \cdot 10^{+5}$	-1
H_2	3000	+3.249	$+0.422 \cdot 10^{-3}$	±0	$+0.083 \cdot 10^{+5}$	-4
CH_4	1500	+1.702	$+9.081 \cdot 10^{-3}$	$-2.164 \cdot 10^{-6}$	±0	+1
H_2O	2000	+3.470	$+1.450 \cdot 10^{-3}$	±0	$+0.121 \cdot 10^{+5}$	+2
Total	1500	-9.811	$+9.248 \cdot 10^{-3}$	$-2.164 \cdot 10^{-6}$	$+1.067 \cdot 10^{+5}$	(-2)

Therefore we can write:

$$\Delta H^o(T) = \Delta H_0^o + R \cdot \int_{T_0}^{T} \frac{\Delta C_p^o}{R} dT =$$

$$= \Delta H_0^o + R \cdot \left[\Delta A \cdot (T - T_0) + \frac{\Delta B}{2} \cdot (T^2 - T_0^2) + \frac{\Delta C}{3} \cdot (T^3 - T_0^3) + \Delta D \cdot \left(\frac{1}{T_0} - \frac{1}{T} \right) \right]$$

$$= \Delta H_0^o + R \cdot \left[\left(\Delta A \cdot T + \frac{\Delta B \cdot T^2}{2} + \frac{\Delta C \cdot T^3}{3} - \frac{\Delta D}{T} \right) - \left(\Delta A \cdot T_0 + \frac{\Delta B \cdot T_0^2}{2} + \frac{\Delta C \cdot T_0^3}{3} - \frac{\Delta D}{T_0} \right) \right]$$

and thus

$$\Delta H^o(T) = -164647 \frac{J}{mol} + 8.314 \frac{J}{mol \cdot K} \cdot \left[\left(-9.811 \cdot T + 4.624 \cdot 10^{-3} K^{-1} \cdot T^2 - 7.213 \cdot 10^{-7} K^{-2} \cdot T^3 - 1.067 \cdot 10^{+5} K^2 \cdot T^{-1} \right) + 2891.1 K \right]$$

or

$$\Delta H^o(T) = - \begin{pmatrix} +8.8710 \cdot 10^{+5} \frac{J \cdot K}{mol} \\ +1.4061 \cdot 10^{+5} \frac{J}{mol} \\ +81.5687 \frac{J}{mol \cdot K} \\ -3.8444 \cdot 10^{-2} \frac{J}{mol \cdot K^2} \\ +5.9972 \cdot 10^{-6} \frac{J}{mol \cdot K^3} \end{pmatrix}^T \bullet \begin{pmatrix} T^{-1} \\ T^0 \\ T^1 \\ T^2 \\ T^3 \end{pmatrix}$$

Other sources propose different formulas, such as the one by [Jeng, 1995]:

$$\Delta H_R(T) = 68.6\frac{J}{mol \cdot K} \cdot T - 0.0233\frac{J}{mol \cdot K^2} \cdot T^2 + 46900\frac{J}{mol \cdot K} \cdot T^{-1} + 144900\frac{J}{mol}$$

and the one by [Lunde, 1974]:

$$\Delta H_R(T) = -68.52\frac{J}{mol \cdot K} \cdot T + 0.02327\frac{J}{mol \cdot K^2} \cdot T^2 - 46794\frac{J \cdot K}{mol} \cdot T^{-1} + 144698\frac{J}{mol}$$

which seem different at first look, but however are in good accordance with the one derived above as shown in Figure 3-10:

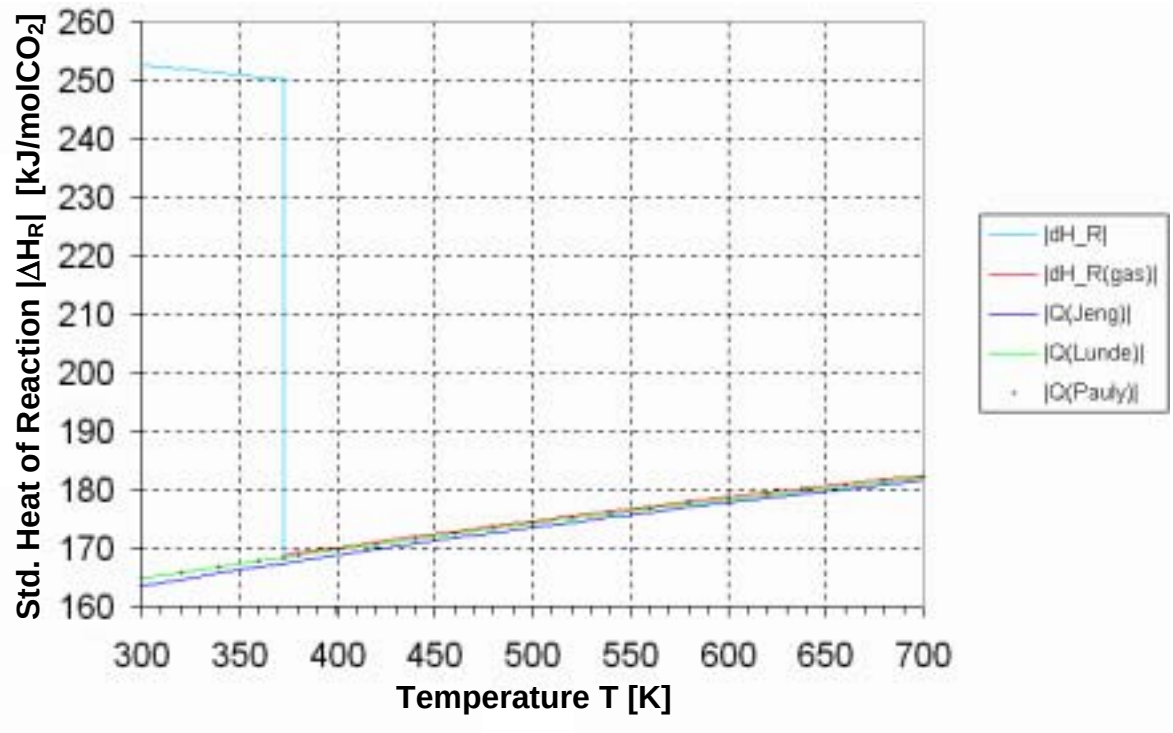

Figure 3-10: Comparison of different Approximations for the Standard Heat of Sabatier Reaction

The relative difference to the NIST data is below 1.0% for Jeng and below 0.4% for the other two. Assuming that the final (pressure dependent) term in the equation can be neglected, we can extent above formulas for the heat of reaction to pressures in the vicinity of p=1bar. Within this range (p=0.8 to 3.4bar for the computer model) we can estimate the heat of the Sabatier reaction as a function solely of temperature T, and not of the pressure.

In the computer model the enthalpies can either been taken from NIST data files or from the above approximation. The latter one is not as exact as the first one, however its inaccuracies are in the per mille order of magnitude, while it features an increased calculation speed.

When we calculate the heat capacity change of a reaction according to the above formulas, it makes sense to define a mean heat capacity change, so that we can write:

$$\Delta H = \int_{T_1}^{T_2} C_p \, dT = \langle C_P \rangle_H \cdot (T - T_0)$$

The subscript "H" signifies the mean value specific to enthalpy calculations. With a good approximation of the standard heat capacity change of reaction the standard Gibbs energy change of reaction can be calculated with:

$$\frac{\Delta G^o}{RT} = \frac{\Delta G_0^o - \Delta H_0^o}{RT_0} + \frac{\Delta H_0^o}{RT} + \frac{1}{T}\int_{T_0}^{T} \frac{\Delta C_p^o}{R} dT - \int_{T_0}^{T} \frac{\Delta C_p^o}{RT} dT$$

whereas

$$\int_{T_0}^{T} \frac{\Delta C_p^o}{RT} dT = \Delta A \ln \tau + \left[\Delta B \cdot T_0 + \left(\Delta C \cdot T_0^2 + \frac{\Delta D}{\tau^2 \cdot T_0^2} \right) \cdot \frac{\tau + 1}{2} \right] \cdot (\tau - 1) \qquad (15.21)$$

Again, the estimated values for Gibbs Energy and Enthalpy (curves) are in good accordance with the actual values (triangles and crosses) shown in Figure 3-11 (values as given by the National Institute of Standards and Technology):

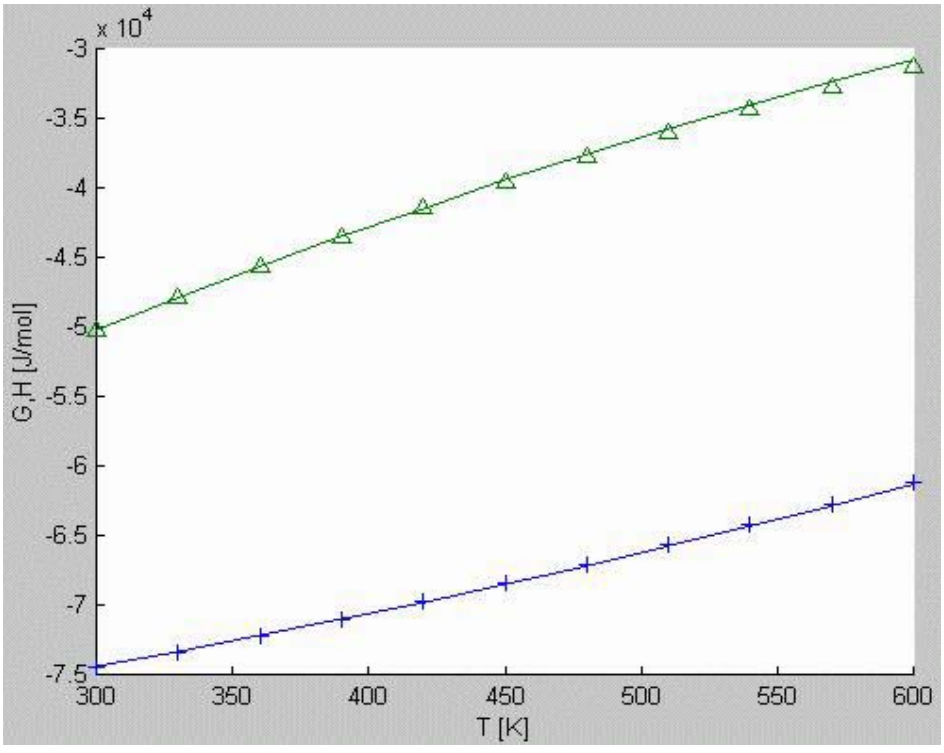

Figure 3-11: Modeled Gibbs Energy and Enthalphy vs. Actual Values

3.5.3 Actual Heat of Formation

The most convenient path to calculate the actual heat of formation at any temperature is *not* the direct path [Smith et al., 1996]. Instead we can take advantage of the fact that the enthalpy change is independent of path. Since all data available for the standard heats of reaction are based on standard conditions (25°C), it is actually more convenient to first calculate the enthalpy change from the actual reactants' condition to standard condition, then add the heat of formation at standard conditions as well as the enthalpy change from standard to products' conditions:

$$\Delta H = \Delta H_R^o + \Delta H_{298}^o + \Delta H_P^o$$

This working principle is shown in the following diagram:

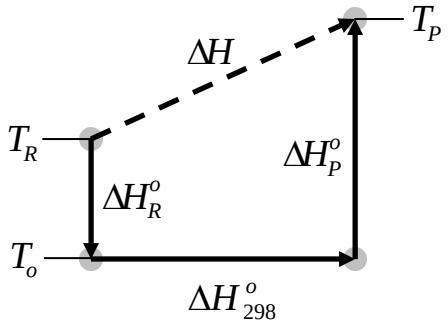

Figure 3-12: Principle of Enthalpy Calculation

With this working principle the reaction process in the reactor can be modeled as follows: Gases of the finite element (m,n-1) leave the element with the temperature $T_{m,n-1}$. A fraction of the molecules that leave the element react before they enter element (m,n), causing an enthalpy change of $\Delta H_{m,n}$. The mass stream that enters the finite element (m,n) therefore has an altered composition of constituents $n_{m,n}$ as well as an excess enthalpy $\Delta H_{m,n}$. This $\Delta H_{m,n}$ together with other factors, e.g. heat fluxes from neighboring elements is part of the (m,n) element's energy equilibrium equation. This equation results in this cells temperature, $T_{m,n}$. The cell (m,n+1) is treated accordingly. The modeling scheme is shown in the following diagram:

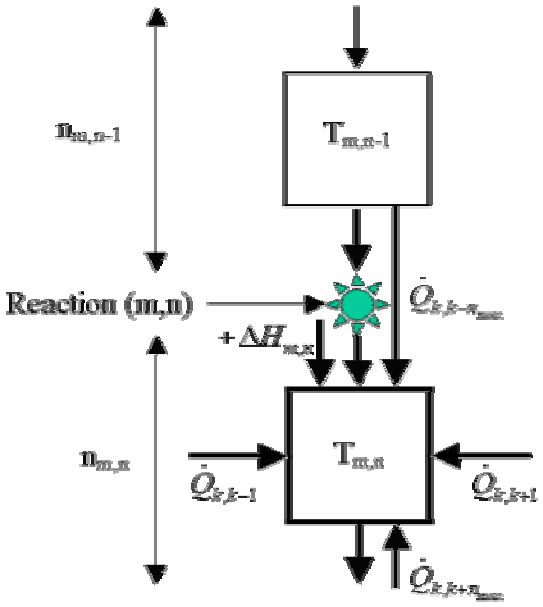

Figure 3-13: Working Scheme of Finite Element Modeling of Reactor

3.5.4 Lagrange's Undetermined Multipliers Method

In order to find the equilibrium state of a reaction, [Smith et al., 1996] derives the formula:

$$\Delta G_{f_i}^{o} + RT \cdot \ln \frac{f_i}{p^{o}} + \sum_k \lambda_k \cdot a_{ik} = 0$$

The fugacity f_i for a non-ideal gas like water vapor is shown in Figure 3-14. For ideal gases, the equation can be written as

$$\frac{\Delta G_{f_i}^{o}}{RT} + \ln \frac{n_i}{\sum_i n_i} + \sum_k \frac{\lambda_k}{RT} \cdot a_{ik} = 0$$

with λ being Lagrange multipliers and a_{ik} the number of the atoms of the element k per molecule of i. With the definition of

$$\Lambda_k = \frac{\lambda_k}{RT}$$

the formula can be further simplified to its final form:

$$\frac{\Delta G_{f_i}^{o}}{RT} + \ln \frac{n_i}{\sum_i n_i} + \sum_k \Lambda_k \cdot a_{ik} = 0$$

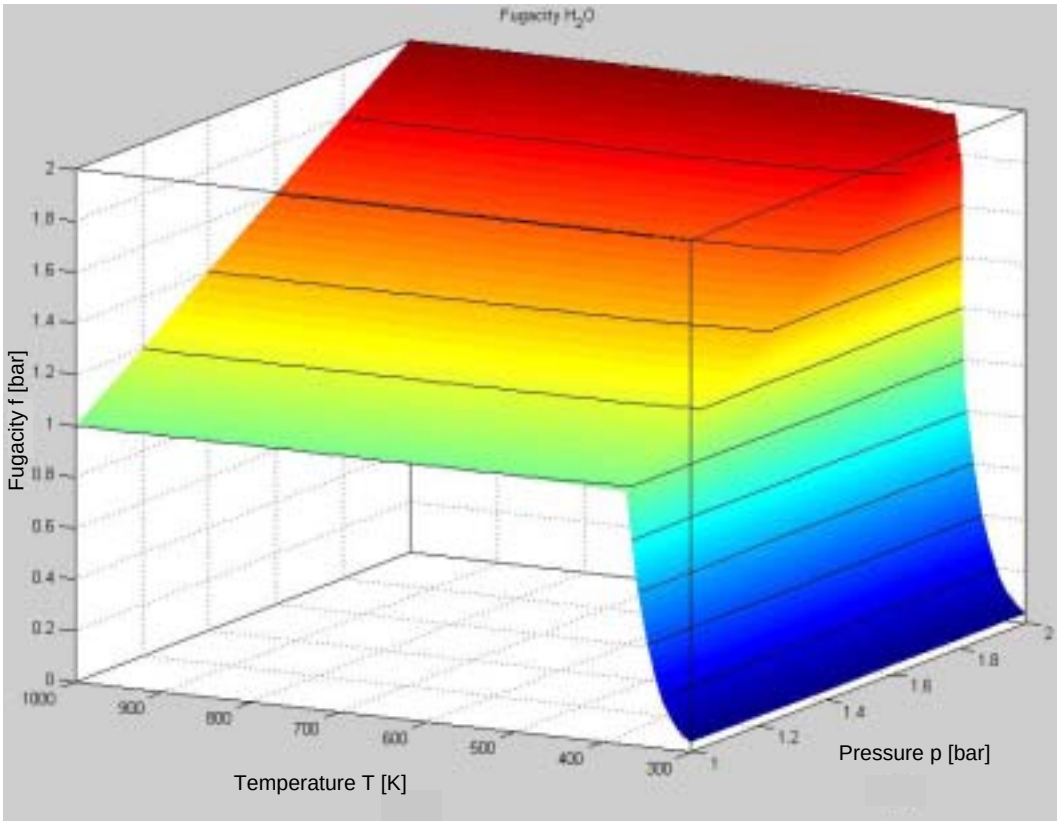

Figure 3-14: Fugacity of Water

The latter equation leads to a non-linear equation system of the order of i. For its solution, the Newton-Raphson method is used. This method is based on a Taylor series expansion of the nonlinear function f(x) around an initial estimate (x_0) of the root. With it, in the neighborhood of x_0, f(x) can be approximated by the tangent line drawn at $x=x_0$. The equation of the tangent line is given by:

$$f(x) = f(x_0) + \left.\frac{df(x)}{dx}\right|_{x=x_0} \cdot (x - x_0) + \left.\frac{d^2 f(x)}{dx^2}\right|_{x=x_0} \cdot \frac{(x-x_0)^2}{2!} + \left.\frac{d^3 f(x)}{dx^3}\right|_{x=x_0} \cdot \frac{(x-x_0)^3}{3!} + \ldots$$

However, the right side of this equation is an infinite series. Therefore, a finite number of terms must be retained and the remaining terms must be truncated. Retaining only the first two terms on the right side of the equation leads to an approximation g(x) (linearization) in the neighborhood of x_0:

$$g(x) = f(x_0) + \left.\frac{df(x)}{dx}\right|_{x=x_0} \cdot (x - x_0)$$

With this method, the non-linear equation system can be written as:

$$f_1 + \left(\frac{df_1}{dx_1}\right)\cdot\Delta x_1 + \left(\frac{df_1}{dx_2}\right)\cdot\Delta x_2 + \ldots + \left(\frac{df_1}{dx_i}\right)\cdot\Delta x_i = 0$$

$$f_2 + \left(\frac{df_2}{dx_1}\right)\cdot\Delta x_1 + \left(\frac{df_2}{dx_2}\right)\cdot\Delta x_2 + \ldots + \left(\frac{df_2}{dx_i}\right)\cdot\Delta x_i = 0$$

$$\ldots$$

$$f_i + \left(\frac{df_i}{dx_1}\right)\cdot\Delta x_1 + \left(\frac{df_i}{dx_2}\right)\cdot\Delta x_2 + \ldots + \left(\frac{df_i}{dx_i}\right)\cdot\Delta x_i = 0$$

which can than be solved – provided that good initial guesses were made. The result for a Sabatier reactor with stoichiometric feed $\left(\frac{n_{H_2}}{n_{CO_2}} = 4\right)$ is shown in Figure 3-15:

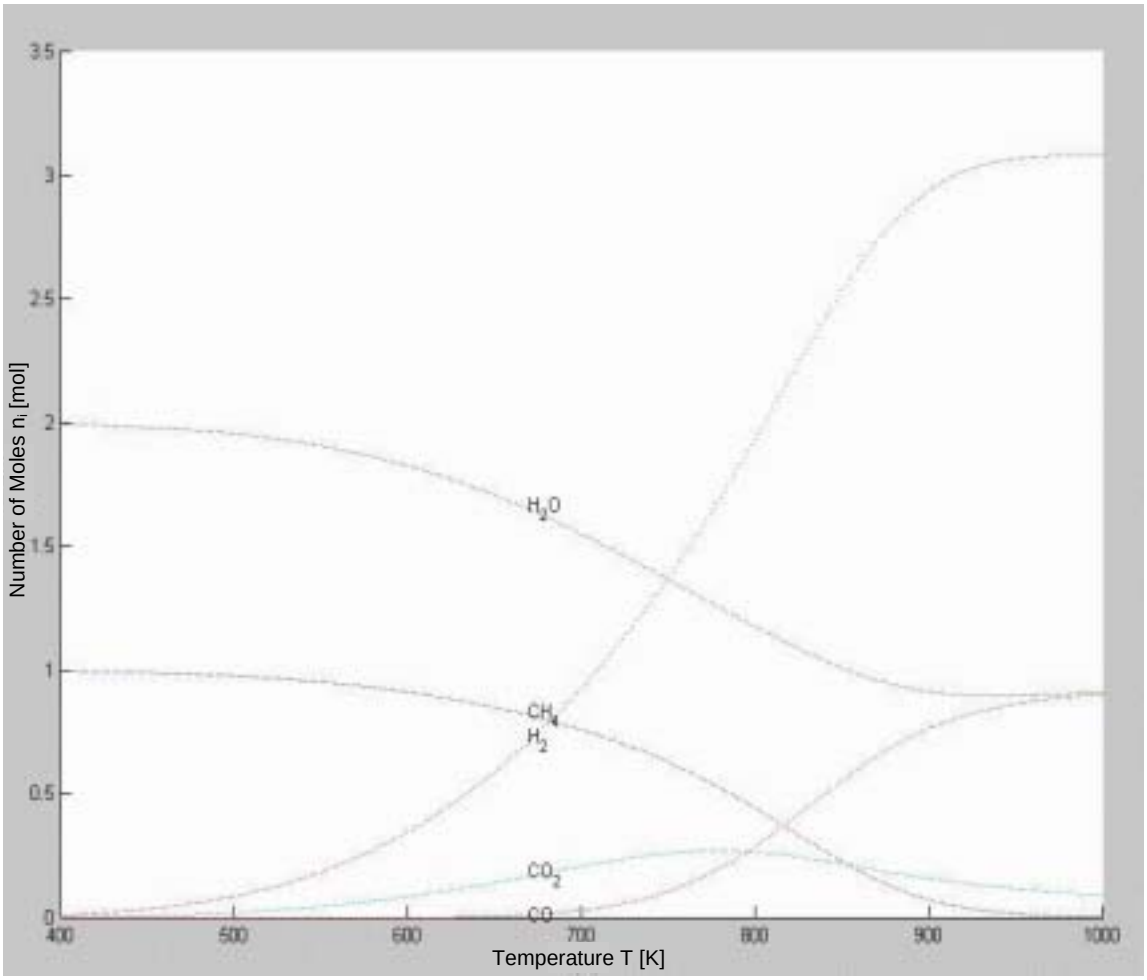

Figure 3-15: Reaction Equilibrium as a Function of Temperature

The same dependence, but with variant pressures from 1 to 2 bar, is shown in Figure 3-16 and Figure 3-17.

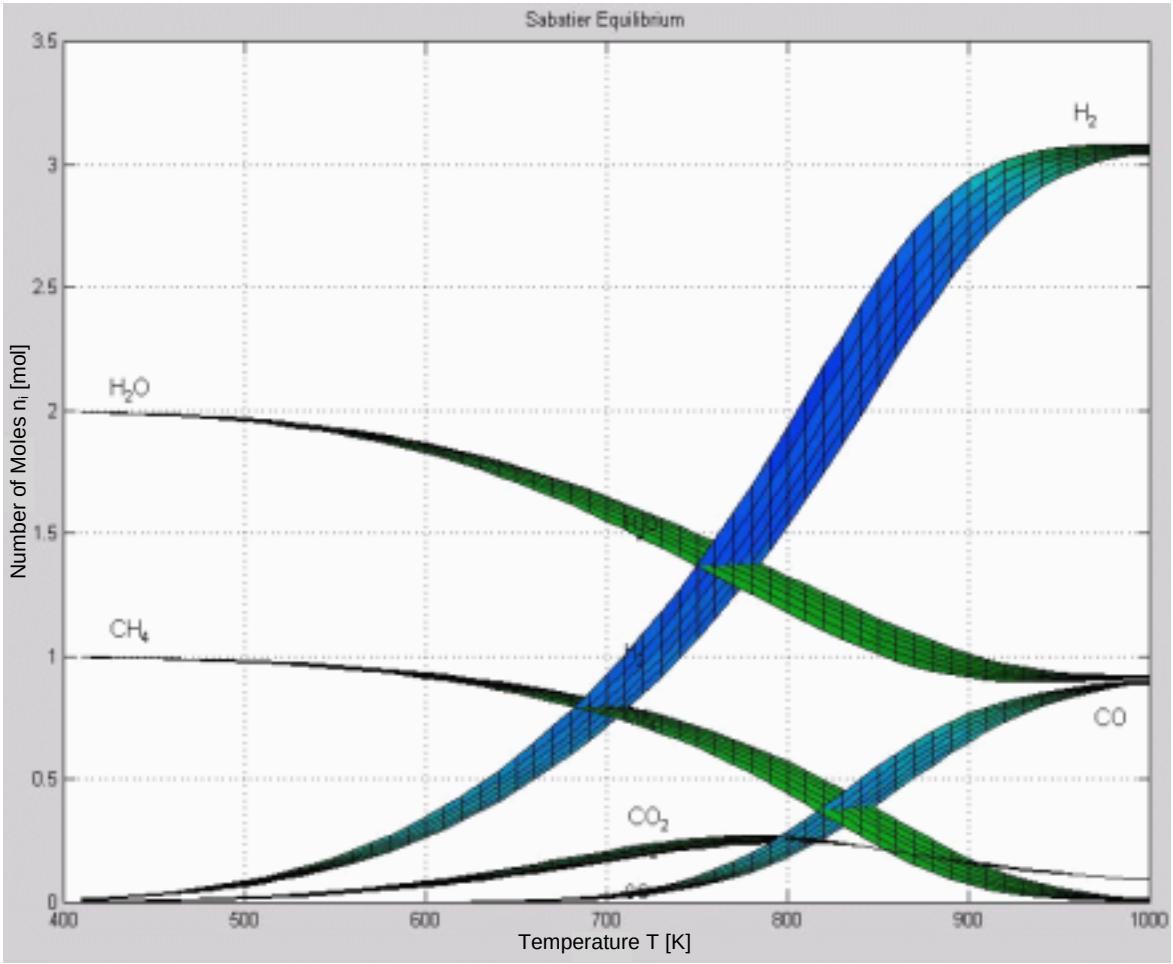

Figure 3-16: Reaction Equilibrium as a Function of Temperature and Pressure

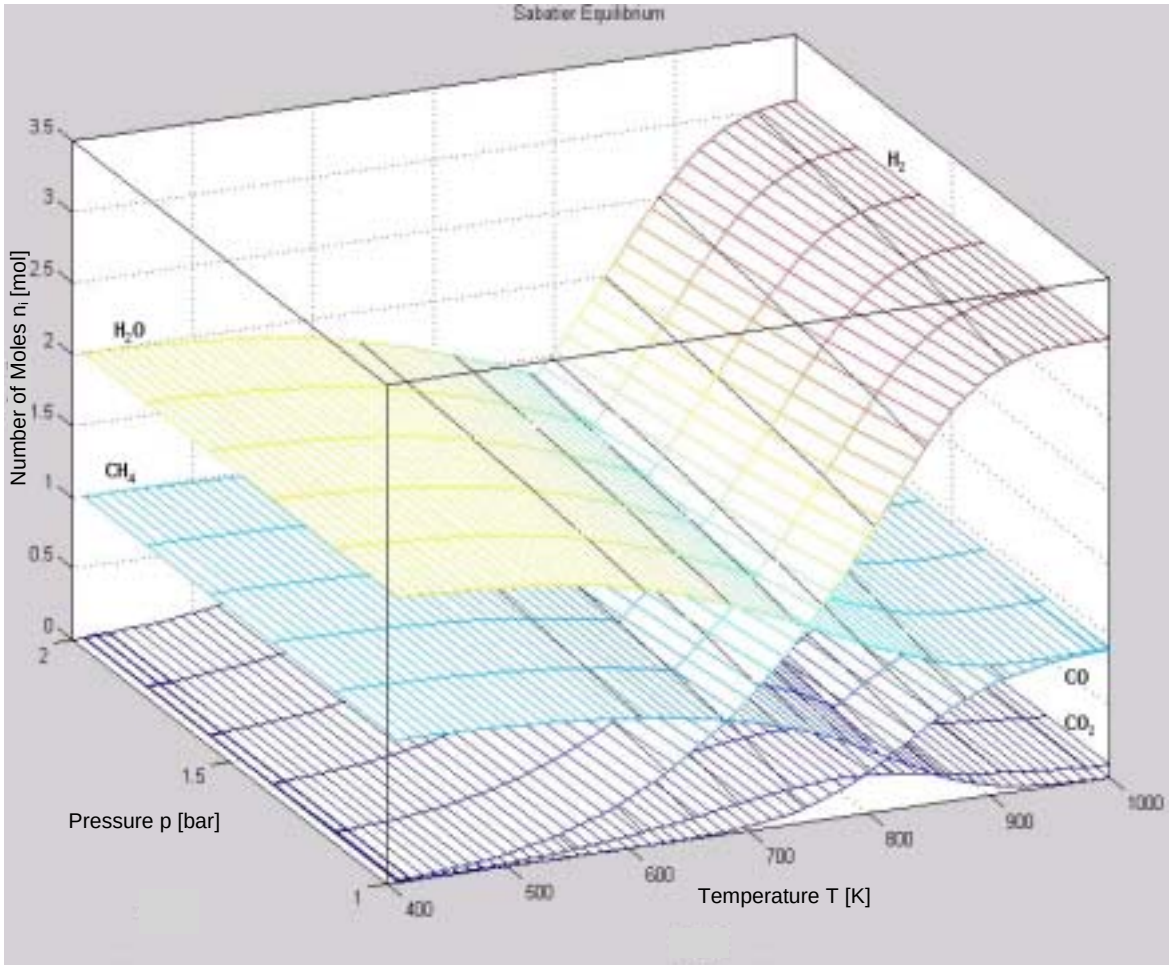

Figure 3-17: Reaction Equilibrium of Sabatier Reactor

3.5.5 Relaxation Method

Now the focus shifts from the away from the fluid and reaction properties towards the modeling of the heat flow within the system. During the thesis work, several different approaches were attempted and the utilized methods were ever improving. Some aspects of the employed methods and the model development steps will be discussed in this and in the succeeding subchapters.

[Meyers, 1971] and [Mayinger & Straub, 1988] suggest the "relaxation method" ("Relaxationsverfahren") as a numerical method to solve multi-dimensional stationary heat transfer problems. Since the cylinder shape of the reactor further complicates the situation, the method's working principles are first explained looking at the case of a two dimensional plate as shown in Figure 3-18:

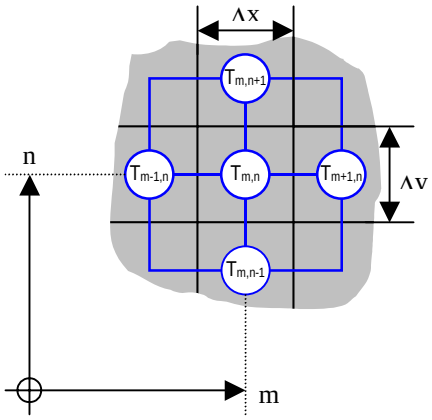

Figure 3-18: Two-Dimensional Finite Element Grid

In this scheme m and n are the element numbers in x and y direction. From Laplace's differential equation[1] for twodimensional (xy) thermal conduction

$$\Delta T = \frac{\partial^2 T}{\partial x^2} + \frac{\partial^2 T}{\partial x^2} = 0$$

(Δ in this formula being the Laplace-operator) we therefore derive via discretization (assuming λ=const. and equidistant grid $\Delta x=\Delta y$) of the homogenous area (in this case: the inner area – as opposed to the border area) the difference equation[2]:

$$T_{m,n-1} + T_{m-1,n} - 4T_{m,n} + T_{m+1,n} + T_{m,n+1} = \varphi_{m,n}$$

The "residual heat" $\varphi_{m,n}$ describes the difference between the heat flux resulting from the different temperatures and the theoretical value (which is zero in every finite element). The elements at the border obey slightly more complex formulas, e.g.

[1] Actually, we can obtain the same equation using other reflections as starting points (e.g. the energy balance of the finite element). The resulting difference equation is the same in any case.

[2] Special caution is required for the implementation of these formulas into a MATLAB® program code. In order to have a right hand x,y,z output of values z as functions of x and y, MATLAB® requires the values for one particular x to be stored in the same column, the values for one particular y in the same row. However, since the indices are ordered row then column, in order to get a certain value z(x,y) from the memory, in Matlab we actually have to enter z(y,z). Similarly, if the z=f(x,y) matrix has 3 different x values and 2 different y values, then the size of the array "size(z)" is according to MATLAB® "[2 3]". Of course we are free to store our values differently, however in that case graphic output commands like "surf(Z)" will display x,y, and z with a left hand coordinate system.

$$T_{m,n-1} + \frac{1}{2}T_{m-1,n} - (2 + Bi)T_{m,n} + \frac{1}{2}T_{m+1,n} + Bi \cdot T_0 = \varphi_{m,n}$$

for an (upper) edge point and

$$\frac{1}{2}T_{m,n-1} + \frac{1}{2}T_{m-1,n} - (1 + Bi) \cdot T_{m,n} + Bi \cdot T_0 = \varphi_{m,n}$$

for a corner (in this case the upper right corner). In both formulas, Bi describes Biot's number

$$Bi = \frac{\alpha \cdot \Delta x}{\lambda}$$

in that finite element.

The solution of multi-dimensional stationary heat transfer problems is therefore obtained by "minimizing the residual heats" in these formulas. To do so, after a supposition of a temperature distribution, the residual heats $\varphi_{m,n}$ in all finite elements are calculated. The temperature $T_{m,n}$ that corresponds to the maximum absolute residual heat $|\varphi_{m,n}|$ is then changed to a value that makes $\varphi_{m,n}$ disappear in that element. The residual heats are then again calculated based on the new temperature distribution. This algorithm is then iterated until the total residual heat

$$\Phi_{total} = \sum_m \left(\sum_n |\varphi_{m,n}| \right)$$

falls below a given accuracy after i iterations:

$$\lim_{i \to \infty} (\Phi_{total}) = \lim_{i \to \infty} \left(\sum_m \left(\sum_n |\varphi_{m,n}| \right) \right) = 0$$

[Mayinger & Straub, 1988] actually neglect the fact that the temperature of the element with the maximum of the ***absolute*** residual heat has to be altered; nevertheless it is imperative not to abstract the absolute, since otherwise negative residual heats do not lead to convergence towards the true value. Figure 3-19 shows the convergence of the relaxation method for a grid of 10x8 Elements.

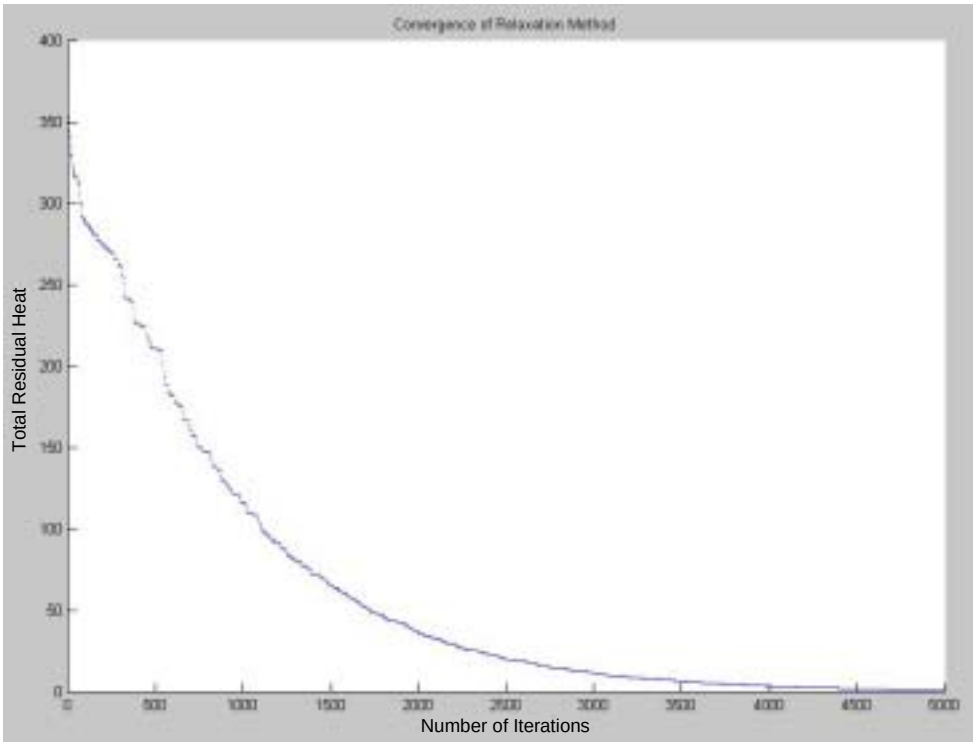

Figure 3-19: Convergence of Relaxation Method

In this example after 5000 iterations the total residual heat ϕ_{total} is typically in the order of 1.2K, meaning that (with 10x8 finite elements) the average difference between theoretical temperature and numerical result is some 15mK.

3.5.6 Modified Relaxation Method

With the relaxation method a solution is obtained in most cases – however (mostly due to the need for "WHILE"- and "FOR"-loops in the program code) it is quite slow, especially for high-resolution grids.

A modified approach to the problem is suggested by [Mayinger & Straub, 1988]:

With $\varphi_{m,n}$=0 for all k ($k := m \cdot n$) grid points we can obtain k first order equations of the form:

$$\begin{aligned} a_{11}T_1 + a_{12}T_2 + \ldots + a_{1k}T_k &= C_1 \\ a_{21}T_1 + a_{22}T_2 + \ldots + a_{2k}T_k &= C_2 \\ \vdots \quad\quad \vdots \quad\quad\quad \vdots \quad\quad\quad \vdots & \\ a_{k1}T_1 + a_{k2}T_2 + \ldots + a_{kk}T_k &= C_k \end{aligned}$$

or, written in matrix notation:

$$\underset{k\times k}{\begin{pmatrix} a_{11} & a_{12} & \cdots & a_{1k} \\ a_{21} & a_{22} & \cdots & a_{2k} \\ \vdots & \vdots & \ddots & \vdots \\ a_{k1} & a_{k2} & \cdots & a_{kk} \end{pmatrix}} \underset{k\times 1}{\begin{pmatrix} T_1 \\ T_2 \\ \vdots \\ T_k \end{pmatrix}} = \underset{k\times 1}{\begin{pmatrix} C_1 \\ C_2 \\ \vdots \\ C_k \end{pmatrix}} \quad \Leftrightarrow \quad \overline{\overline{a}}\,\overline{T} = \overline{C}$$

Therefore, we can easily calculate the temperature distribution $\overline{T}$ if we can obtain the matrix inverse of the coefficient matrix $\overline{\overline{a}}$:

$$\overline{T} = \overline{\overline{a}}^{-1}\,\overline{C}$$

Since programs like MATLAB® are optimized to obtain matrix inverses and to solve linear equation systems, this method proves to be much faster in practice than the original relaxation method.

3.5.7 Modified Relaxation Method in Cylinder Coordinates

The principles derived in the previous two chapters remain unchanged. We again start with the Laplace's differential equation for two-dimensional thermal conduction

$$\Delta T = 0$$

(with Δ in this formula again being the Laplace-operator). In cylinder coordinates (r,φ,z) this leads to:

$$\Delta T = \frac{\partial^2 T}{\partial r^2} + \frac{1}{r}\cdot\frac{\partial T}{\partial r} + \frac{1}{r^2}\cdot\frac{\partial^2 T}{\partial \varphi^2} + \frac{\partial^2 T}{\partial z^2} = 0$$

Taking into account the rotational symmetry, we obtain:

$$\frac{\partial^2 T}{\partial r^2} + \frac{1}{r}\cdot\frac{\partial T}{\partial r} + \frac{\partial^2 T}{\partial z^2} = 0$$

Note that this form is not dependent on the angle φ. With m and n this time being the element numbers in r and z direction, we can derive the difference equation for the homogeneous inner area via discretization accordingly (see the derivation in cartesian coordinates) as:

$$\frac{T_{m+1,n}-2T_{m,n}+T_{m-1,n}}{(\Delta r)^2}+\frac{T_{m+1,n}-T_{m-1,n}}{2r\cdot(\Delta r)}+\frac{T_{m,n+1}-2T_{m,n}+T_{m,n-1}}{(\Delta z)^2}=\frac{\varphi_{m,n}}{(\Delta r)^2}$$

whereas $\varphi_{m,n}$ is again the residual heats (not to be confused with the polar angle φ!). If we define

$$\psi := \left(\frac{\Delta r}{\Delta z}\right)^2 \Rightarrow (\Delta z)^2 = \frac{1}{\psi}\cdot(\Delta r)^2$$

as a ratio of element dimensions, and if we multiply the above difference equation with $(\Delta r)^2$, then we obtain:

$$(T_{m+1,n}-2T_{m,n}+T_{m-1,n})+\frac{\Delta r}{2r}\cdot(T_{m+1,n}-T_{m-1,n})+\psi\cdot(T_{m,n+1}-2T_{m,n}+T_{m,n-1})=\varphi_{m,n}$$

or, separated into the finite elements:

$$\left(1+\frac{\Delta r}{2r}\right)\cdot T_{m+1,n}+\left(1-\frac{\Delta r}{2r}\right)\cdot T_{m-1,n}-(2+2\psi)\cdot T_{m,n}+\psi\cdot T_{m,n+1}+\psi\cdot T_{m,n-1}=\varphi_{m,n}$$

If we take into account that $r(m)=m\cdot\Delta r$, then we can write:

$$\left(1+\frac{1}{2m}\right)\cdot T_{m+1,n}+\left(1-\frac{1}{2m}\right)\cdot T_{m-1,n}-(2+2\psi)\cdot T_{m,n}+\psi\cdot T_{m,n+1}+\psi\cdot T_{m,n-1}=\varphi_{m,n}$$

3.5.8 Relaxation Method with Internal Heat Sources

According to [Mayinger & Straub, 1988], Laplace's differential equation $\Delta T\cdot\lambda=0$ for homogeneous (constant) heat conductivity changes to:

$$\Delta T\cdot\lambda+\dot{w}=0$$

for an finite element with internal heat source density $\dot{w}$ (Δ in this formula being the Laplace-operator). The discretization (for cylinder coordinates) then changes to:

$$\left(\frac{T_{m+1,n}-2T_{m,n}+T_{m-1,n}}{(\Delta r)^2}+\frac{T_{m+1,n}-T_{m-1,n}}{2r\cdot(\Delta r)}+\frac{T_{m,n+1}-2T_{m,n}+T_{m,n-1}}{(\Delta z)^2}\right)\cdot\lambda+\dot{w}=\frac{\varphi_{m,n}}{(\Delta r)^2}\cdot\lambda$$

If we multiply the above difference equation with $\frac{(\Delta r)^2}{\lambda}$, then we obtain (with the same definition for ψ):

$$\left(T_{m+1,n} - 2T_{m,n} + T_{m-1,n}\right) + \frac{\Delta r}{2r} \cdot \left(T_{m+1,n} - T_{m-1,n}\right) + \psi \cdot \left(T_{m,n+1} - 2T_{m,n} + T_{m,n-1}\right) + \frac{(\Delta r)^2}{\lambda} \cdot \dot{w} = \varphi_{m,n}$$

or:

$$\left(1 + \frac{1}{2m}\right) \cdot T_{m+1,n} + \left(1 - \frac{1}{2m}\right) \cdot T_{m-1,n} - (2 + 2\psi) \cdot T_{m,n} + \psi \cdot T_{m,n+1} + \psi \cdot T_{m,n-1} = \varphi_{m,n} - \frac{(\Delta r)^2}{\lambda} \cdot \dot{w}$$

3.5.9 Influence of Catalyst on Mass and Heat Transport

Mass and heat transport in packed bed reactors has important ramifications for industrial applications. Hence, a wide range of literature exists that deals with this topic. Among the first to do significant work in this field was [Damköhler, 1936]. His work has been basis for research in this area for 65 years now. Models are used for calculating the influence of the catalyst pellets within the Sabatier reactor on its heat and mass flow. In these models, fluid velocity and porosity of the catalyst bed are usually assumed to be constant over the cross section. The heat transfer to the wall is calculated via the wall heat transfer coefficient α_w. This coefficient is also called a "lumped coefficient" since it incorporates a number of different phenomena which all occur at the wall (heat transfer from fluid to pellets and to the wall via convection and radiation; heat transfer from the pellets to the wall directly via heat conduction). While this works satisfactory for high Reynolds numbers (Re>1000), the accordance of theory and reality diverges for low Reynolds numbers [Vortmeyer et al., 1999].
In this context, the same authors suggest the so-called "Λ_r(r)-model", which is in better accordance with the data obtained in testing and practice, mainly because it avoids "the artificial temperature jump at the wall with temperatures" creating unrealistic reaction rates. The authors further expatiate that this new modeling approach …

"…uses locally varying radial dispersion coefficients due to the near-wall porosity and velocity changes and operates with the genuine boundary condition of the first kind at the wall (T(r) = T_w). […]
It may be concluded from this observation that the α_w-model is justified for large Reynolds numbers because the heat resistance at the wall can be reduced to a very thin "unmixed sublayer". The physical situation is different at small Reynolds because no kind viscous inhibition in the vicinity of the wall can be reasonably assumed, as hydrodynamic mixing is insignificant even in the bed core. Under these circumstances α_W becomes a pure lumping parameter, compensating every conceptional weakness of the model as well

as every experimental error. A similar, though not so erratic behavior characterizes also the second parameter of the a_W-model, namely the effective radial thermal conductivity. The latter is assumed to be constant over the bed, but appears to depend on D/d_p. […].
[In the modified $\Lambda_r(r)$-model] *bed porosities and flow profiles are calculated according to recent, well established methods, axial dispersion is taken into account functional relationships for the effective radial thermal conductivity and the effective radial dispersion coefficient in dependence of flow velocity and radial position are developed by comparison with an extended, comprehensive set of experimental data on heat and mass transport. Both the simplicity of resulting parameters and correlations and the good overall agreement with the experimental database underline the very satisfactory performance of the $\Lambda_r(r)$-model. Moreover, it is possible to describe the heat and mass transport in packed beds with and without chemical reaction by the same set of coefficients."* [Vortmeyer et al., 1999]

The applicability of the $\Lambda_r(r)$-model was also shown by [Hein, 1998].

Model Equations

The model equation for heat transport in a cylindrical packed bed **with** reaction can, according to [Vortmeyer et al., 1999], be written as:

$$\left\{\psi(r)\cdot\rho_f\cdot c_f+\left[1-\psi(r)\right]\cdot\rho_p\cdot c_p\right\}\cdot\frac{\partial T}{\partial t}=$$
$$\frac{1}{r}\frac{\partial}{\partial r}\cdot\left[\Lambda_r(r)\cdot r\cdot\frac{\partial T}{\partial r}\right]+\Lambda_{ax}(r)\cdot r\cdot\frac{\partial^2 T}{\partial z^2}-u_0(r)\cdot\rho_f\cdot c_f\cdot\frac{\partial T}{\partial z}+\frac{1-\psi(r)}{1-\overline{\psi}}\cdot\dot{r}(T,y)\cdot\left|\Delta H\right|$$

and

$$\psi(r)\cdot\frac{\partial y}{\partial t}=\frac{1}{r}\frac{\partial}{\partial r}\cdot\left[D_r(r)\cdot r\cdot\frac{\partial y}{\partial r}\right]+D_{ax}(r)\cdot r\cdot\frac{\partial^2 y}{\partial z^2}-u_0(r)\cdot\frac{\partial y}{\partial z}+\frac{1-\psi(r)}{1-\overline{\psi}}\cdot\frac{M}{\rho_f}\cdot\dot{r}(T,y)$$

for the mass transport. In these equations, the following parameters are used:

ψ	local bed porosity [-]
ρ_f, ρ_p	fluid / pellet density [kg/m^3]
c_f, c_p	fluid / pellet specific heat capacity [J/(kgK)]
T	temperature [K]
y	mass fraction [-]
t	time [s]
r, z	radial / axial coordinate [m]
Λ_r, Λ_{ax}	effective radial / axial thermal conductivity [W/(mK)]
D_r, D_{ax}	effective radial / axial mass dispersion coefficient [m^2/s]
u_0	local superficial velocity
$\dot{r}$	reaction rate [mol/(m^{3}s)]

ΔH reaction enthalpy [J/mol]

For the stationary case, the above equations simplify to:

$$0 = \frac{1}{r}\frac{\partial}{\partial r}\cdot\left[\Lambda_r(r)\cdot r\cdot\frac{\partial T}{\partial r}\right] + \Lambda_{ax}(r)\cdot r\cdot\frac{\partial^2 T}{\partial z^2} - u_0(r)\cdot\rho_f\cdot c_f\cdot\frac{\partial T}{\partial z} + \frac{1-\psi(r)}{1-\overline{\psi}}\cdot\dot{r}(T,y)\cdot|\Delta H|$$

and

$$0 = \frac{1}{r}\frac{\partial}{\partial r}\cdot\left[D_r(r)\cdot r\cdot\frac{\partial y}{\partial r}\right] + D_{ax}(r)\cdot r\cdot\frac{\partial^2 y}{\partial z^2} - u_0(r)\cdot\frac{\partial y}{\partial z} + \frac{1-\psi(r)}{1-\overline{\psi}}\cdot\frac{M}{\rho_f}\cdot\dot{r}(T,y)$$

The following equations are used to derive the required parameters:

The effective axial dispersion coefficients, conductivity and diffusivity without flow are calculated according to [Tsotsas, 1997] as

$$D_{ax} = \delta_{eff,v=0} + \frac{Pe_0}{2}\delta,$$

$$\Lambda_{ax} = \lambda_{eff,v=0} + \frac{Pe_0}{2}\lambda_f$$

wheras

δ molecular diffusion coefficient [m^2/s]

$\delta_{eff,v=0}$ effective bed diffusion coefficient without fluid flow [m^2/s]

Pe_0 molecular Péclet number for heat ($Pe_0 = \frac{\overline{u}_0\cdot d_p\cdot\rho_f\cdot c_f}{\lambda_f}$) and mass ($Pe_0 = \frac{\overline{u}_0\cdot d_p}{\delta}$) transfer [-]

$\lambda_{eff,v=0}$ effective thermal conductivity without fluid flow [W/(mK)].

The thermal conductivity and the effective diffusion coefficient of the packed bed without fluid flow are calculated from correlations provided by [Zehner & Schlünder, 1970] as a function of the local porosity ψ(r). [Zehner & Schlünder, 1970] suggest the equation:

$$\frac{\lambda_{eff,v=0}}{\lambda_f} = \left(1-\sqrt{1-\psi}\right)\cdot\left(1+\frac{\lambda_r}{\lambda_f}\right) + \sqrt{1-\psi}\cdot\left[\frac{2}{1-\frac{\lambda_f}{\lambda_s}B}\cdot\left[\frac{\left(1-\frac{\lambda_f}{\lambda_s}\right)\cdot B}{\left(1-\frac{\lambda_f}{\lambda_s}\cdot B\right)^2}\cdot\ln\frac{1}{\frac{\lambda_f}{\lambda_s}\cdot B} - \frac{B+1}{2} - \frac{B-1}{1-\frac{\lambda_f}{\lambda_s}\cdot B}\right] + \frac{1}{\frac{\lambda_f}{\lambda_r}+\frac{\lambda_f}{\lambda_s}}\right]$$

The deformation factor B takes into account the shape of the catalyst pellets. For spheres, this factor is written as

$$B = 1.25 \cdot \left(\frac{1-\psi}{\psi} \right)^{\frac{10}{9}}$$

whereas

ψ porosity of the reactor bed [-]

The above formula simplifies for $\frac{\lambda_r}{\lambda_f} \to 0$ (radiation effects neglected) to:

$$\frac{\lambda_{eff,v=0}}{\lambda_f} = \left(1 - \sqrt{1-\psi}\right) + \sqrt{1-\psi} \cdot \frac{2}{1-\frac{\lambda_f}{\lambda_s} B} \cdot \left[\frac{\left(1-\frac{\lambda_f}{\lambda_s}\right) \cdot B}{\left(1-\frac{\lambda_f}{\lambda_s} \cdot B\right)^2} \cdot \ln \frac{1}{\frac{\lambda_f}{\lambda_s} \cdot B} - \frac{B+1}{2} - \frac{B-1}{1-\frac{\lambda_f}{\lambda_s} \cdot B} \right]$$

as shown in Figure 3-20:

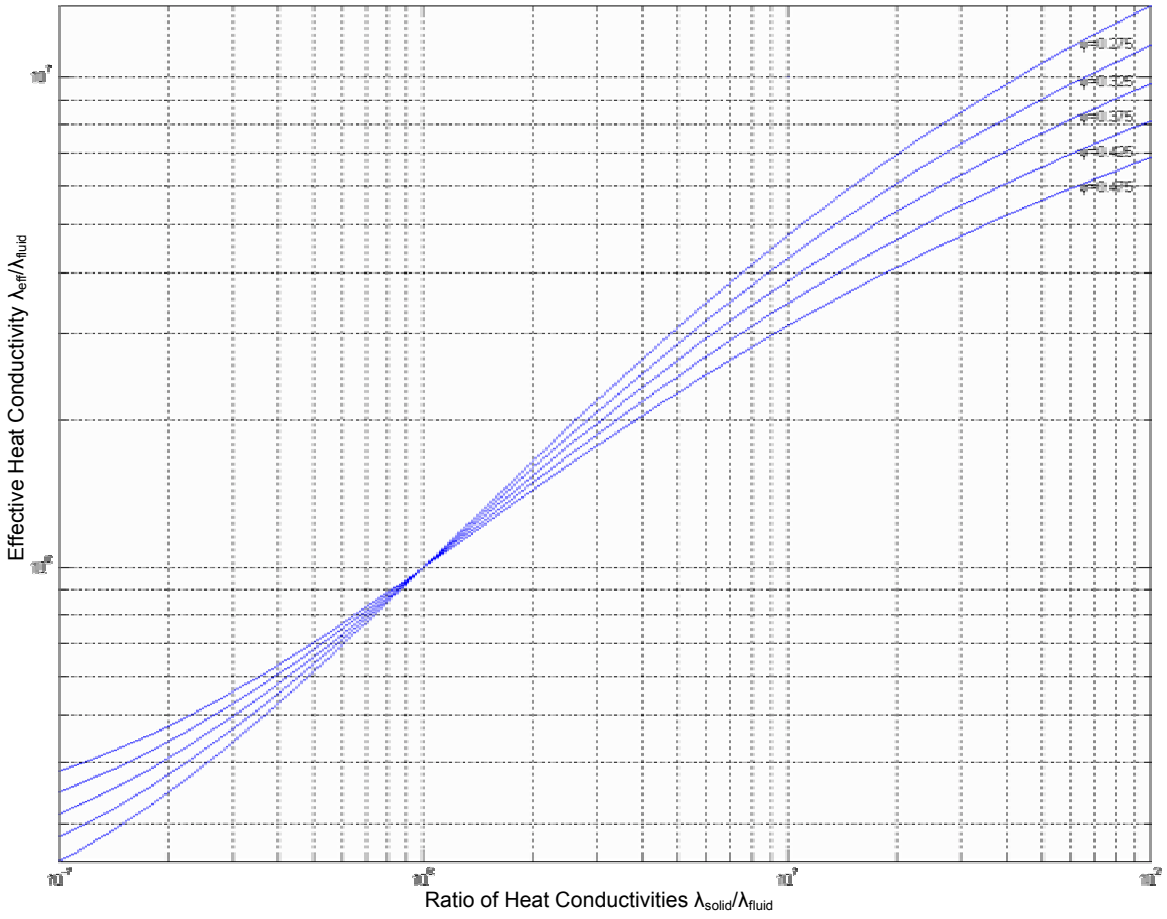

Figure 3-20: Effective Heat Conductivity as a Function of Porosity and $\lambda_{solid}/\lambda_{fluid}$

Thus, the question has to be answered whether the simpler one of the two equations for the effective thermal conductivity is sufficient or not. This will be done shortly. First however, a closer look on the bed porosity parameter.

In packed beds consisting of spheres of equal size, in practice the porosity (due to geometrical reasons) can only vary between 0.26 (densest sphere packing) and 0.476 (cubic packing). Therefore most equations aim for optimized accuracy in this area. However, in packed beds with pellets of a broad size spectrum as well as on a local scale (in particular close to the reactor wall) the porosity can significantly differ. [Zehner & Schlünder, 1970] e.g. therefore made an extra effort to ensure adequate model accuracy also outside of the porosity range stated above. For the approximation of porosity distribution over the radius for packed beds consisting of equally sized particles with small deviations from spherical shape the following equation is used [Giese, 1998]:

$$\psi(r) = \psi_c \cdot \left[1 + 1.36 \cdot \exp\left(-5.0 \cdot \frac{R-r}{d_p}\right)\right]$$

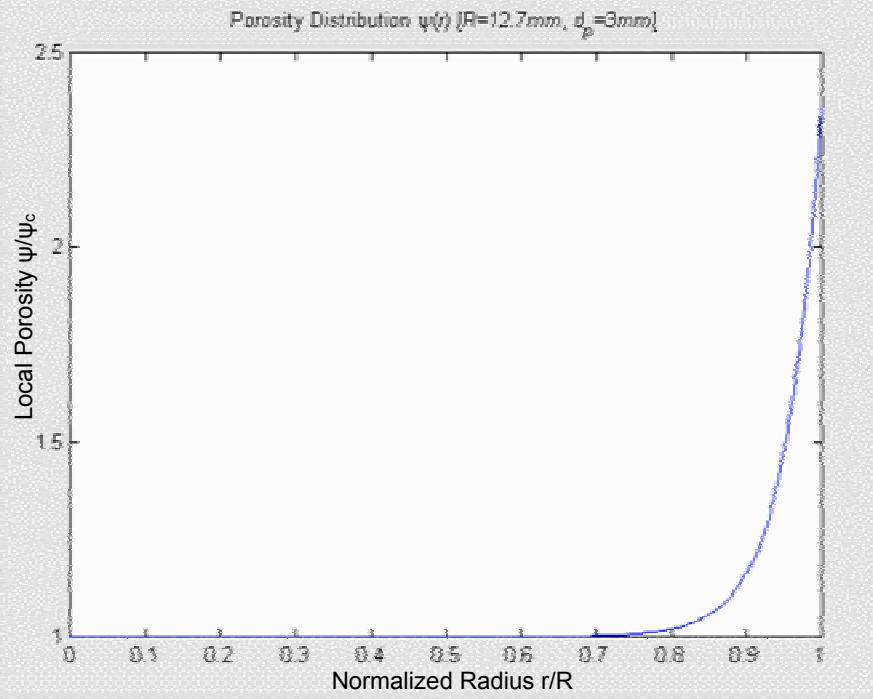

Figure 3-21: Reactor Bed Porosity Distribution

As it can be seen from Figure 3-21, the bed porosity changes only within the outer 10% of the reactor radius significantly. There however, the change is dramatic.

In order to evaluate the influence of the radiation, the Damköhler equation [Damköhler, 1937] is used as a first step:

$$\frac{\lambda_r}{\lambda_f} = \frac{0.04 \cdot \sigma_s}{\frac{2}{\varepsilon} - 1} \cdot \left(\frac{T}{100}\right)^3 \cdot d_p$$

whereas:

λ_f = thermal conductivity of the fluid phase [W/(mK)]
λ_r = thermal conductivity equivalent due to radiation [W/(mK)]
σ_s = Stefan-Boltzmann number [5.6697 · 10^{-8} W/(m^2K^4)]
T = Temperature [K]
d_p = catalyst pellet diameter [m]
ε = emissivity [-]

For temperatures around 600K, emissivities around 0.1, and pellet dimensions in the order of 3mm, the radiation is in the order of the thermal conductivity coefficient without (meaning neglecting) radiation. This means that radiation effects in the Sabatier reactor have to be included in the model, too, if we want to achieve an adequate accuracy.

With these preparations completed, the numbers for the effective radial thermal conductivity Λ_r, and the effective mass dispersion coefficient D_r can now be modeled (following the approach of [Vortmeyer et al., 1999]) as:

$$\Lambda_r(r) = \lambda_{eff,v=0} + \frac{Pe_0}{8} \cdot \frac{u_c}{\bar{u}_0} \cdot f(R-r) \cdot \lambda_f ,$$

$$\text{with } f(R-r) = \begin{cases} \left(\dfrac{R-r}{K_{2,h} \cdot d_p}\right)^2 & for \quad 0 < R-r \le (K_{2,h} \cdot d_p) \\ 1 & for \quad (K_{2,h} \cdot d_p) < R-r \le R \end{cases}$$

whereas

$K_{2,h}$ damping parameter for heat transfer $\left(K_{2,h} = 0.44 + 4 \cdot \exp\left(-\dfrac{\mathrm{Re}_0}{70}\right)\right)$

3.5.10 Reaction Rate

The determination of the reaction rate is a crucial part of the overall system modeling. The well-known general Arrhenius equation is the basis for the determination of the influence of temperature on the reaction rate:

$$k_f{}^n(T) = p \cdot Z \cdot \exp\left(\frac{-E_a}{RT}\right)$$

whereas:

Z = collision rate [1/s]
p = steric factor [-]
E_a = activation energy [J/mol]
T = temperature [K]
R = universal (molar) gas constant [8.31451 J/(molK)]

If we consider this equation in terms of changing temperature, the steric factor clearly does not depend on temperature. Z turns out to be only weakly dependant on temperature: changing T from 500 to 600 K changes Z by less than 10% [http://learn.chem.vt.edu/tutorials/kinetics/arrhenius.html]. It is therefore a reasonable approximation to assume that the $p \cdot Z$ part of the above equation is a constant, and we can write the better-known version of the Arrhenius equation:

$$k_f{}^n(T) = k \cdot \exp(-E_a / RT)$$

whereas k is called the reaction rate constant [s^{-1}].

Although (or rather because) crucial for modeling of the reactor behavior, information regarding catalyst production and performance are usually well-protected secrets in the chemical industry, since they mean cash money for its producers. On of the very few papers on this issued was published over a quarter of a century ago by [Luanda, Kestrel, 1973]. In the course of work in the life support area, a couple of publications have dealt with the work of Luanda and Kestrel in the last quarter of a century.
However, it seems that the lax handling of units especially in the States have caused a plethora of conversion mistakes in nearly all of these publications ([Lunde, 1974], [Strumpf et al., 1991], [Son & Barker, 1992], [Jeng, 1995]). Furthermore, all of these publications go back to [Lunde, Kester, 1974] for the determination of the reaction rate; they merely discuss the Lunde-derived coefficients and slightly higher or lower numbers are promoted. However, none of the papers presents anything new in terms of theoretical modeling.
In 1974, Lunde had introduced (based on the general work of [Dew et al., 1955]) the so-called catalyst coefficient n for the Sabatier reaction, about which he states that:

"Since the modification of [ideal] gas-phase kinetics from which this expression [the catalyst coefficient n] is derived has no theoretical justification, care should be taken that use is restricted over the range over which experimental data were collected." [Lunde & Kester, 1974]

Ironically, only the paper from the same year from the same author [Lunde, 1974], takes this into account, whereas all the other papers ([Strumpf et al., 1991], [Son & Barker, 1992], [Jeng, 1995]) present the equation of the reaction rate without discussion or even mentioning of n.

The Lunde paper from 1974 is nevertheless still the main basis for the determination of the reaction rate. In order to avoid previously made errors, the formulas are herewith converted into SI units.

The Sabatier reaction

$$CO_2 + 4H_2 \underset{k_r}{\overset{k_f}{\rightleftarrows}} CH_4 + 2H_2O$$

is an equilibrium reaction a forward and a reverse reaction represented by the reaction rate constants k_f and k_r. Thus,

$$-\frac{d[p_{CO_2}]}{dt} = {k_f}^n \cdot [p_{CO_2}]^n \cdot [p_{H_2}]^{4n} - {k_r}^n \cdot [p_{H_2O}]^{2n} \cdot [p_{CH_4}]^n$$

Equilibrium is achieved when the above equations equals zero and one can write

$$K_{eq} := \frac{k_f}{k_r} = \frac{[p_{H_2O}]^2 \cdot [p_{CH_4}]}{[p_{CO_2}] \cdot [p_{H_2}]^4}$$

and the empirical exponent applied to the partial pressures cancels so that the equilibrium constant K_{eq} is defined as in classical thermodynamics. With this definition of K_{eq}, we can rewrite the second to last formula to

$$-\frac{d[p_{CO_2}]}{dt} = {k_f}^n \cdot \left([p_{CO_2}]^n \cdot [p_{H_2}]^{4n} - \frac{[p_{H_2O}]^{2n} \cdot [p_{CH_4}]^n}{K_{eq}} \right)$$

The equilibrium constant is derived using methods described by [Pitzer & Brewer, 1961] as a function of the temperature:

$$K_{eq}(T) = \exp\left(\frac{1}{1.987} \cdot \left(\frac{56000}{T^2} + \frac{34633}{T} - 16.4 \ln T + 0.00557T \right) + 33.165 \right) \qquad [\text{atm}^{-2}]$$

or (according to [Strumpf et al., 1991]):

$$K_{eq}(T) = \exp\left(\frac{17700}{T} - 8.11 \cdot \ln T + 3.28 \cdot 10^{-3} T - 5.06 \cdot 10^{-3} T^{-8} + 31.7 \right) \qquad [\text{atm}^{-2}]$$

whereas

T	temperature [K]
K_{eq}	equilibrium constant in [atm^{-2}]

Note the use of atm^{-2} as opposed to a SI unit. Figure 3-22a shows the approximations plotted against each other over a temperature range from 350 to 700K, whereas Figure

3-22b shows the relative difference of the second approximation in relation to the first one.

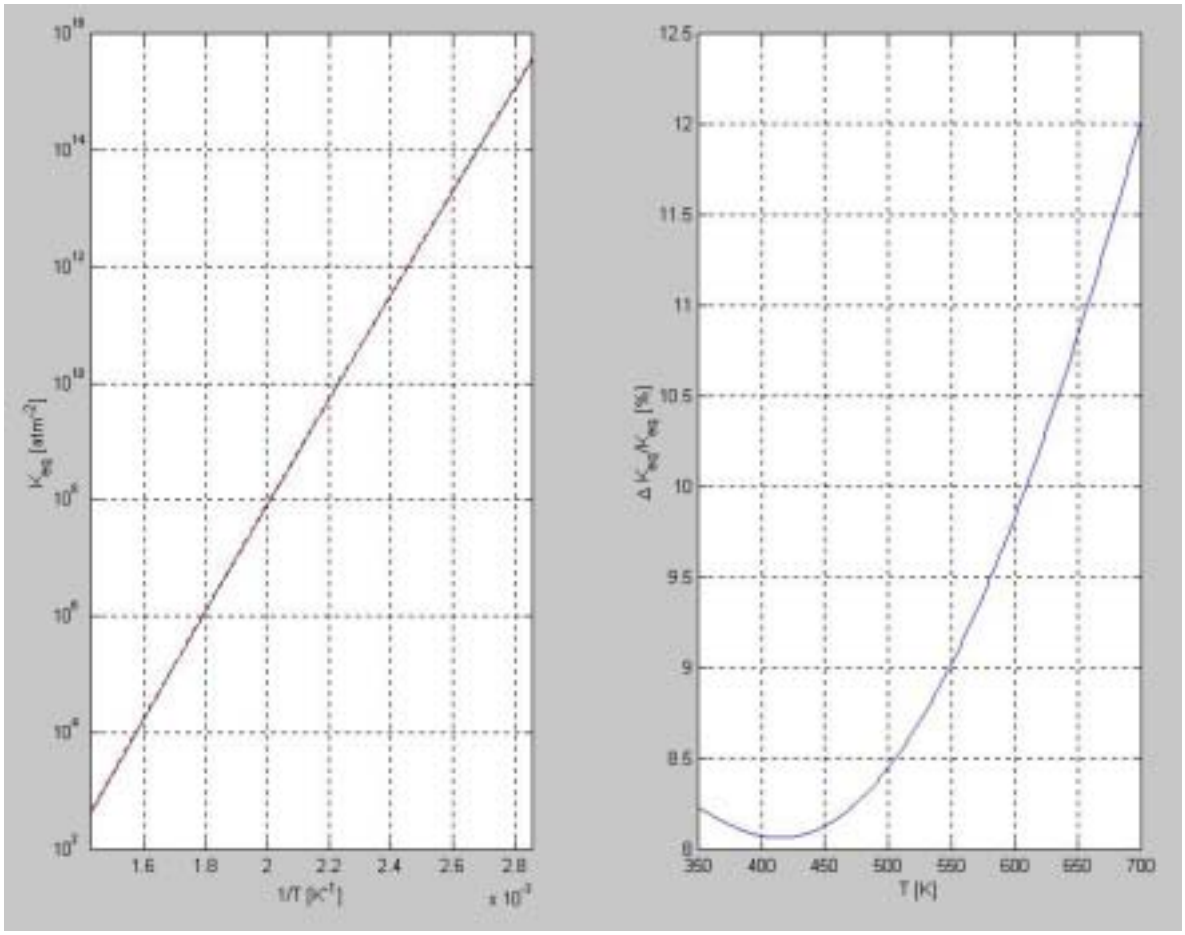

Figure 3-22: Sabatier Reaction Equilibrium Constant

With the Arrhenius equation, we can transform the rate expression into

$$-\frac{d\left[p_{CO_2}\right]}{dt} = k \cdot \exp\left(\frac{-E_a}{RT}\right) \cdot \left(\left[p_{CO_2}\right]^n \cdot \left[p_{H_2}\right]^{4n} - \frac{\left[p_{H_2O}\right]^{2n} \cdot \left[p_{CH_4}\right]^n}{K_{eq}}\right)$$

Again, k (the rate constant), E_a (the activation energy), and n (the catalyst coefficient) are constants determined from experimental data. Table 3-4 shows an overview over the numbers proposed by different papers (converted into SI units):

Table 3-4: Values for rate constant, activation energy, and catalyst coefficient

Source	Rate Constant A	Activation Energy E_a	Catalyst Coeff. n
[Lunde & Kester, 1974]	1.769×10^9 hr^{-1} $atm^{-0.125}$	30320 Btu/(lb mol CO_2)	0.225
[Lunde, 1974]	2.339×10^9 hr^{-1} $atm^{-0.25}$	31000 Btu/(lb mol CO_2)	0.25
[Strumpf et al., 1991]		16995 cal/mol	0.25
[Son & Barker, 1992]		16995 cal/mol	0.25

According to the constitutive equation of gases

$$pV = nRT$$

we can express the rate expression by writing

$$\frac{dp}{dt} = \frac{d(n/V)}{dt} RT = (-\dot{r}) \cdot RT$$

at constant temperatures. Thus, we can also determine r directly via:

$$\dot{r}_{CO_2} = -\frac{1}{RT} \cdot \frac{d\left[p_{CO_2}\right]}{dt}, \text{ and therefore}$$

$$\dot{r}_{CO_2}(T) = +\frac{k}{RT} \cdot \exp\left(\frac{-E_a}{RT}\right) \cdot \left(\left[p_{CO_2}\right]^n \cdot \left[p_{H_2}\right]^{4n} - \frac{\left[p_{H_2O}\right]^{2n} \cdot \left[p_{CH_4}\right]^n}{K_{eq}} \right)$$

or $(with\ A := k/R)$:

$$\dot{r}_{CO_2}(T) = +\frac{A}{T} \cdot \exp\left(\frac{-E_a}{RT}\right) \cdot \left(\left[p_{CO_2}\right]^n \cdot \left[p_{H_2}\right]^{4n} - \frac{\left[p_{H_2O}\right]^{2n} \cdot \left[p_{CH_4}\right]^n}{K_{eq}} \right)$$

whereas

$\dot{r}_{CO_2}$ = carbon dioxide reaction rate $\left[\frac{mol}{s}\frac{kg}{m^3}\right]$

A = pre-exponential factor $\left[1.094577 \cdot 10^9 \frac{kg}{m^3} \cdot \frac{mol\,CO_2}{s \cdot bar^{1.25}}\right]$

E_a = activation energy $\left[71110 \frac{J}{mol}\right]$

R = universal gas constant $\left[8.314 \frac{J}{mol \cdot K}\right]$

K_{eq} = equilibrium constant [atm^{-2}] (can be calculated via one of the methods described above)

T = catalyst bed temperature [K]
p_i = partial pressure [Pa]

3.6 MATLAB/SIMULINK Model of the Overall System

3.6.1 Modeling of Fluid Properties

many of the properties required in this work were acquired from the NIST database, like density and enthalpy as a function of pressure and temperature. However, the NIST database is currently still in the process of being assembled (see current research by [Wagner, 2000]), therefore not all the properties and not all the temperature ranges are available. Especially viscosity of hydrogen could not be provided by NIST at all. It therefore was necessary to get into contact with people working on the NIST database, who could fortunately provide the needed data [Bayazitoglu, 1999], [Wagner 2001].

[Wagner, 2001, to be published] suggests the following formula for modeling the dynamic viscosity of hydrogen between 180 and 2000 K:

$$\eta = AT + BT \cdot \rho + CT \cdot \rho^2$$

$$\begin{pmatrix} AT \\ BT \\ CT \end{pmatrix} \approx \overline{\overline{X}} \cdot \begin{pmatrix} 1 \\ T \\ T^2 \\ T^3 \\ T^4 \\ T^5 \\ T^6 \\ T^7 \end{pmatrix}$$

$$AT \approx X_{A0} + X_{A1} \cdot T + X_{A2} \cdot T^2 + X_{A3} \cdot T^3 + X_{A4} \cdot T^4 + X_{A5} \cdot T^5 + X_{A6} \cdot T^6 + X_{A7} \cdot T^7$$
$$BT \approx X_{B0} + X_{B1} \cdot T + X_{B2} \cdot T^2 + X_{B3} \cdot T^3 + X_{B4} \cdot T^4 + X_{B5} \cdot T^5 + X_{B6} \cdot T^6 + X_{B7} \cdot T^7$$
$$CT \approx X_{C0} + X_{C1} \cdot T + X_{C2} \cdot T^2 + X_{C3} \cdot T^3 + X_{C4} \cdot T^4 + X_{C5} \cdot T^5 + X_{C6} \cdot T^6 + X_{C7} \cdot T^7$$

with

$$\overline{\overline{X}} = \begin{pmatrix} 1.08455 \cdot 10^{-6} & 3.50549 \cdot 10^{-8} & -4.28810 \cdot 10^{-10} & 5.80119 \cdot 10^{-14} & -5.14103 \cdot 10^{-17} & 2.74444 \cdot 10^{-20} & -7.97104 \cdot 10^{-24} & 9.63843 \cdot 10^{-28} \\ 7.87549 \cdot 10^{-5} & -6.89732 \cdot 10^{-14} & 2.49124 \cdot 10^{-8} & -4.55024 \cdot 10^{-12} & 4.61888 \cdot 10^{-15} & -2.63710 \cdot 10^{-18} & 7.91719 \cdot 10^{-22} & -9.72039 \cdot 10^{-25} \\ -4.47336 \cdot 10^{-4} & 1.47342 \cdot 10^{-5} & -4.88172 \cdot 10^{-8} & 7.88985 \cdot 10^{-11} & -6.86010 \cdot 10^{-14} & 3.22297 \cdot 10^{-17} & -7.53365 \cdot 10^{-21} & 6.61819 \cdot 10^{-25} \end{pmatrix}$$

whereas the temperature is entered in K and the density in kg/m^3, resulting in a dynamic viscosity output in Poise (1 Poise = 0.1 Ns/m^2). Once the dynamic viscosity is derived, the kinematic viscosity in can be easily obtained using:

$$\upsilon = \frac{\eta}{\rho}$$

Figure 3-23 shows the high accuracy of this viscosity model (compared to data obtained in NIST laboratories). It shows, that in the area of interest (from 300K to 700K), the error is below 0.3%.

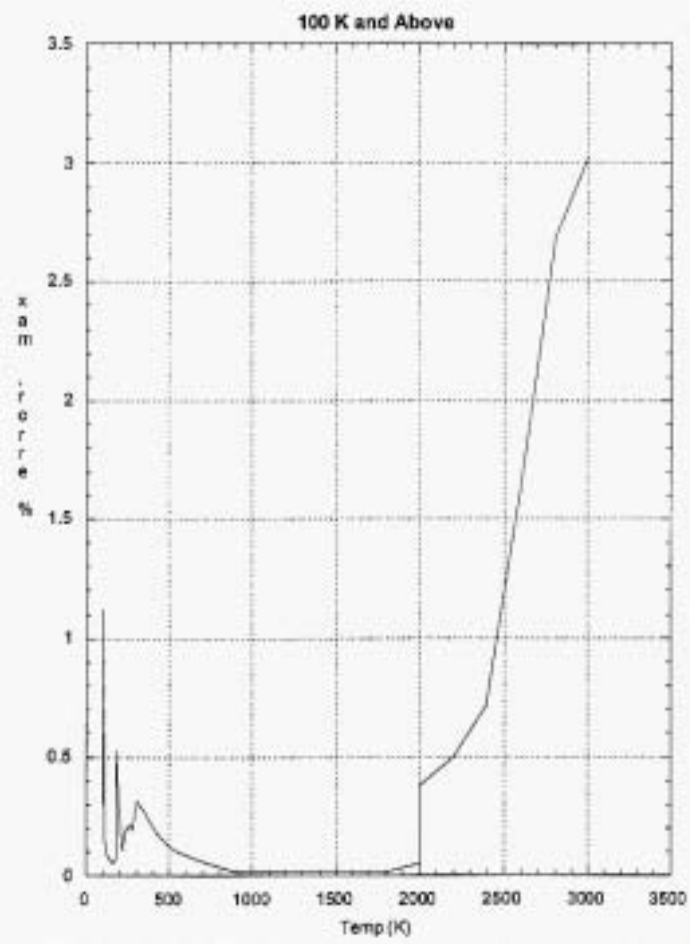

Figure 3-23: H_2 Viscosity Model – Accuracy [Wagner et al., 2000]

3.6.2 Atmosphere Acquisition System

The acquisition of carbon dioxide of the Mars atmosphere will be achieved via a sorption pump filled with a molecular sieve material ("Zeolite 13X"). Type 13X is produced synthetically, characterized by pores of uniform dimensions (pore diameter of 10Å), and used commercially for general gas drying, air plant feed purification (simultaneous removal of H_20 and CO_2) and liquid hydrocarbon and natural gas sweetening (H_2S and mercaptan removal). The Zeolite structure allows the water of crystallization to be removed, leaving a porous crystalline structure. These pores, or "cages", want to re-absorb water or other molecules [Plastic Services, 2001]. This property is used in the

breadboard atmosphere acquisition subsystem: at low temperatures, the Zeolite absorbs the carbon dioxide, which then can be released later through simply raising the bed temperature.
Type 13X can be regenerated by evacuating or purging at adequate temperatures. The desorption temperature of the breadboard was up to 450°F (505K). The degree of regeneration depends on the temperature and the pressure level.
To transfer this qualitative statement into an exact quantitative form the Langmuir isotherm [Smith et al., 1996] can be used, which is written:

$$q = \frac{c_m \cdot p}{c_m / k_{Henry} + p}$$

whereas:

- q = adsorbed CO_2 per adsorbent mass [m%] or [mol/kg], dependent on c_m.
- p = pressure [Pa]
- c_m = adsorbent constant
- k_{Henry} = Henry's constant

These Langmuir isotherms however can not fit the experimental data in general. The isotherms that are used more often in practice are derived from the Toth equation [Toth, 1979], which can be written in the form:

$$q = \frac{c_m \cdot p}{\sqrt[c_t]{c_b + p^{c_t}}}$$

whereas:

- q = adsorbed CO_2 per adsorbent mass in [m%] or [mol/kg], dependent on c_m.
- p = pressure [torr]
- c_m = adjustable constant for curve fit
- c_b = adjustable constant for curve fit
- c_t = adjustable constant for curve fit

Note that for $c_b = c_m/k_{Henry}$ and t=1, the Toth equation reduces to the Langmuir equation. For commercially available adsorbent materials, the values for the curve fit constants c_m, c_b, and c_t can usually be obtained from the manufacturer (e.g. Union Carbide for Zeolite 13X [UOP, 1996]), at least for moderate temperature and pressure ranges. However, temperatures and pressures found on Mars are sometimes below the ranges for which the curve fit constants are obtainable. Fortunately, the Langmuir equation's concurrence with empirical data increases for low temperatures and low pressures [Smith et al., 1996]. Thus, good approximation can be made over the full range of temperatures and pressures.

The isosteric heat of adsorption required for the energy balance in a flow system, can be determined as a function of loading by obtaining the slopes of plots of ln(p) versus reciprocal absolute temperature at constant loading [Smith et al., 1996]. The Toth equation can be used to interpolate between the data points. According to Langmuir equation, the heat of adsorption is independent of the adsorbent surface coverage for low pressures and temperatures and thus constant (some 44.9 kJ/mol according to the data).

3.6.3 Pipes

The following subchapters will deal with the modeling of the thermal budget of the breadboard's piping.

3.6.3.1 Heat Transfer at Inner Wall

The total heat flux lost by a substance flowing through a pipe is

$$\dot{Q} = \dot{m} \cdot c_p \cdot \left(T_{out} - T_{in} \right)$$

whereas

$\dot{Q}$ =heat flux [W]

$\dot{m}$ = mass flow [kg/s]

c_P = specific heat capacity [J/(kgK)]

The heat flux lost by the fluid must be equal to the heat flux going through the pipe wall. This flux is calculated with the help of the equation

$$\dot{Q} = A \cdot k \cdot \overline{\Delta T}$$

whereas

A	=	area through which the heat flows
K	=	the heat transition coefficient of the pipe related to the area A
$\overline{\Delta T}$	=	logarithmic average temperature difference the internal pipe temperature and the temperature of the atmosphere.

The reason for the fact that the average temperature difference is not a geometric average (but a logarithmic one) is that the temperature decreases exponential and not linear with the length of the pipe. The average is therefore defined as:

$$\overline{\Delta T} = \frac{T_{in} - T_{out}}{\ln \frac{T_{in} - T_{atm}}{T_{out} - T_{atm}}}$$

The strategy of the program in the design mode is basically to iterate the length of the pipe until the heat fluxes out of the fluid and through the pipe wall are equal. In order to be able to calculate the heat transition coefficient k, it is necessary to take a close look at the flow characteristics.

With standard normal conditions, according to Avogadro, 1 mol methane equals

$$V_{mn} = 22.4141 \text{ liters}$$

1 mol methane weighs approximately 16g, which results in a density at normal conditions of

$$\rho = \frac{m}{V} = \frac{16\,g}{22.4141 l} = 0.7143 \frac{kg}{m^3}$$

An required mass flow of for example 6.25 g/h therefore equals

$$\dot{V} = 2.431 \cdot 10^{-6} \frac{m^3}{s}$$

The Reynolds number of a flow through a pipe is defined by the formula

$$\mathrm{Re} = \frac{4\dot{m}}{D_i \cdot \pi \cdot \eta_{fluid}}$$

whereas:

- m = mass flow [kg/s]
- D_i = inner Diameter [m]
- η_{fluid} = dynamic viscosity

For Reynolds numbers below the critical Reynolds number R_c = 2300 the flow is laminar (Hagen-Poiseulle's law). Since the required mass flows are low, it is assumed that all flows are laminar.

The pipe's required inner diameter is:

$$D_i = \frac{4\dot{m}}{\mathrm{Re}_c \cdot \pi \cdot \eta_{fluid}} = \frac{4 \cdot 6.25 \frac{g}{h}}{2300 \cdot \pi \cdot 1.42 \cdot 10^{-5} \frac{m^2}{s} \cdot 0.7143 \frac{kg}{m^3}} \approx 0.1mm$$

Since the minimum diameter of the pipes available off the shelf is in the order of 2.5mm, the pipe is way oversized. With an inner diameter of 2.5mm the Reynolds number changes to:

$$\mathrm{Re} = \frac{4\dot{m}}{D_i \cdot \pi \cdot \eta_{fluid}} = \frac{4 \cdot 6.25 \frac{g}{h}}{2.5mm \cdot \pi \cdot 1.42 \cdot 10^{-5} \frac{m^2}{s} \cdot 0.7143 \frac{kg}{m^3}} = 87.172$$

The Reynolds number can also be written as:

$$\mathrm{Re} = \frac{v \cdot D_i \cdot \rho}{\eta_{fluid}}$$

Therefore the flow velocity v is:

$$v = \frac{\mathrm{Re} \cdot \eta_{fluid}}{D_i \cdot \rho} = \frac{87.172 \cdot 1.42 \cdot 10^{-5} \frac{m^2}{s}}{2.5mm} = 0.495 \frac{m}{s}$$

In order to estimate the temperature loss of a simple pipe, an example with a pipe length of 1 m is calculated.

For a stationary, one-dimensional flow in a pipe the flow of an incompressible fluid or with negligible pressure losses the differential equation for temperature is:

$$0 = -g \cdot v \cdot A \cdot c_p \frac{\partial T}{\partial z} + \frac{\partial}{\partial z}\left(\lambda \cdot A \cdot \frac{\partial T}{\partial z}\right) + \frac{\dot{q}_U \cdot U}{\cos\beta} + v \cdot \tau \cdot U$$

If the heat conduction in longitudinal direction is low compared to the heat transport due to mass flow and if the dissipation power is negligible, then the equation simplifies to:

$$0 = -g \cdot v \cdot A \cdot c_p \frac{\delta T}{\partial z} + \frac{\dot{q}_U \cdot U}{\cos\beta}$$

With the heat flux number k (related to the circumference U) for the heat flux between the fluid (temperature T) and the environment (with the temperature T_∞), the equation changes to the form:

$$0 = -g \cdot \nu \cdot A \cdot c_p \frac{\delta T}{\partial z} + \frac{k \cdot U}{\cos \beta}\left(T_\infty - T\right)$$

For a cylinder, the heat flux number k_i (related to the inner Diameter) is defined as:

$$k_i = \left(D_i \left(\frac{1}{\alpha_i D_i} + \frac{\ln \frac{D_o}{D_i}}{2\lambda} + \frac{1}{\alpha_o D_o} \right) \right)^{-1}$$

whereas

D_i = inner diameter [m]
D_o = outer diameter [m]
α_i = heat transition coefficient at the inner wall [W/m^{2}K]
α_o = heat transition coefficient at the outer wall [W/m^{2}K]
λ = heat conductivity [W/(mK)]

The smallest pipes used in NASA spacecrafts have an inner diameter D_i = 2.5 mm (1/10 inch) and an outer diameter D_a = 3.175 mm (1/8 inch). The heat conductivity of a pipe material like for example V2A steel is in the order of λ = 15 W/(mK).

The heat transition coefficient at the (inner and outer wall) can be calculated with the help of Nußelt's number Nu

$$\alpha = \frac{Nu \cdot \lambda}{d_i}$$

whereas

d_i = inner diameter of the cylinder [m].

Within the cylinder, Nußelt's number Nu can be calculated with the formula

$$Nu = \left[3.65 + \frac{0.19 \tilde{P}\tilde{e}^{0.8}}{1 + 0.117 \tilde{P}\tilde{e}^{0.467}} \right] \cdot K_{\mathrm{Pr}}$$

whereas

Peclet's number is defined as:

$$\widetilde{P}\widetilde{e} = \mathrm{Re}\cdot \mathrm{Pr}\cdot \frac{d_i}{L}$$

Prandtl's number being defined as:

$$\mathrm{Pr} = \frac{\nu \cdot \rho \cdot c_P}{\lambda}$$

With the heat transition coefficient at the inner wall α_{fluid}, the heat flux can be calculated according to the following formula. This second method is used for the iteration.

$$\overline{\Delta T_{fliid}} = \frac{T_{in} - T_{out}}{\ln \frac{T_{in} - T_{wall}}{T_{out} - T_{wall}}} = \frac{k}{\alpha_{fluid}} \cdot \overline{\Delta T}$$

Therefore a help variable ψ can be introduced:

$$\Psi = \frac{T_{in} - T_{wall}}{T_{out} - T_{wall}} = e^{\frac{T_{in} - T_{out}}{\overline{\Delta T_{fluid}}}}$$

With this, one can write:

$$T_{wall} = \frac{T_{in} - T_{out} \cdot \Psi}{1 - \Psi}$$

3.6.3.2 Heat Flow due to Convection

For a free convection with Prandtl numbers between 0.002 and 8000 and a constant wall temperature the Nußelt number is, according to [Mayinger, Straub, 1988], defined as:

$$Nu = Nu_0 + 0.668 \cdot K_F \cdot f(\mathrm{Pr}) \cdot Ra^{1/4}$$

whereas

Nu_0 = 0.36 for horizontal cylinders

K_F = $\sqrt{\frac{2}{\pi}} \approx 0.7979$ for horizontal cylinders, respectively 1.0 for vertical cylinders

Ra = Rayleigh's number.

The Prandtl function is defined as:

$$f(\mathrm{Pr}) = \left[1 + (2 \cdot \mathrm{Pr})^{-\frac{9}{16}}\right]^{-\frac{4}{9}}$$

with Prandtl's number being

$$\mathrm{Pr} = \frac{c_{P\,atm} \cdot \rho_{atm} \cdot \nu_{atm}}{\lambda_{atm}}$$

Rayleigh's number, which is also needed as input for the calculation of Nußelt's number, can be obtained from the equation:

$$Ra = Gr \cdot \mathrm{Pr}$$

whereas

Gr = Grashof's number [-]

Grashof's number is depending on the gravity factor as shown in the following formula:

$$Gr = \frac{g \cdot \beta_P \cdot L^3 \cdot \left(T_{wall} - T_{atm}\right)}{\nu^2}$$

whereas

g = gravity factor [m/s^2]

For a gas that behaves like an ideal gas, the following simplification can be made

$$\beta_P = -\frac{1}{\rho}\left(\frac{\partial p}{\partial T}\right)_{p=const.} \approx \frac{1}{T_{atm}}$$

3.6.3.3 Heat Transfer due to External Airflow

For an airflow caused by Martian winds with the mean velocity v_W the Nußelt number is written as

$$1 < \mathrm{Re} < 10^3 \quad : \quad Nu = \left(0.43 + 0.50\,\mathrm{Re}^{0.5}\right) \cdot \mathrm{Pr}^{0.38} \cdot \left(\frac{\mathrm{Pr}}{\mathrm{Pr}_V}\right)^{0.25}$$

$$10^3 < \mathrm{Re} < 2\ 10^5 \quad : \quad Nu = 0.25 \cdot \mathrm{Re}^{0.6} \cdot \mathrm{Pr}^{0.38} \cdot \left(\frac{\mathrm{Pr}}{\mathrm{Pr}_V}\right)^{0.25}$$

whereas:

Re = Reynold's number
Pr = Prandtl's number
Pr_V = Prandtl's number
Ra = Rayleigh's number.

The Reynolds number in this case is:

$$\mathbf{Re} = \frac{\mathbf{v_{atm} \cdot d_o \cdot \rho_{atm}}}{\boldsymbol{\eta}_{\mathbf{atm}}}$$

With the condition $T(z=0) = T_0$ the temperature changes over the length according to the formula

$$T = T_\infty + \left(T_0 - T_\infty\right) \cdot \exp\left(-\frac{k \cdot U}{\dot{m} \cdot c_p} \cdot z\right)$$

Therefore, at the end of the pipe, the fluid will have the temperature:

$$T_1 = T_\infty + \left(T_0 - T_\infty\right) \cdot \exp\left(-\frac{k \cdot U \cdot L}{\dot{m} \cdot c_p}\right)$$

The heat flux $\dot{Q}$ between the pipe and the environment of Mars due to radiation can be described with the help of the formula

$$\dot{Q} = \sigma_{12} \cdot d_o \pi \cdot \left({T_{atm}}^4 - {T_{wall}}^4\right)$$

whereas

σ_{12} = radiation constant $\left[\frac{W}{m^2 K^4}\right]$
d_o = outer diameter of reactor [m]
T_{atm} = temperature of surrounding atmosphere [K]
T_{wall} = temperature of reactor wall [K].

If a heat transition coefficient α_{rad} is defined, then it is a function of T_{atm} and T_{wall}:

$$\alpha_{rad} = \sigma_{12} \cdot \left(T_{atm} + T_{wall}\right) \cdot \left({T_{atm}}^2 + {T_{wall}}^2\right)$$

In these formulas σ_{12} is the radiation number of the layout, which is a product of the emission coefficient ε_1 of the pipe and the radiation constant of Stefan and Boltzmann σ_S:

$$\sigma_{12} = \varepsilon_1 \cdot \sigma_S$$

This formula is valid in the case of a thermal equilibrium.

The resulting heat transition coefficient α can be derived via the formula

$$\alpha_{out} = \alpha_{atm} + \alpha_{rad}$$

A summation of the calculations done for the pipe can be seen in Figure 3-24. This graphic also shows how e.g. the gravity factor g influences the overall system. The symbols that appear in Figure 3-24 and in Figure 3-24 are the following:

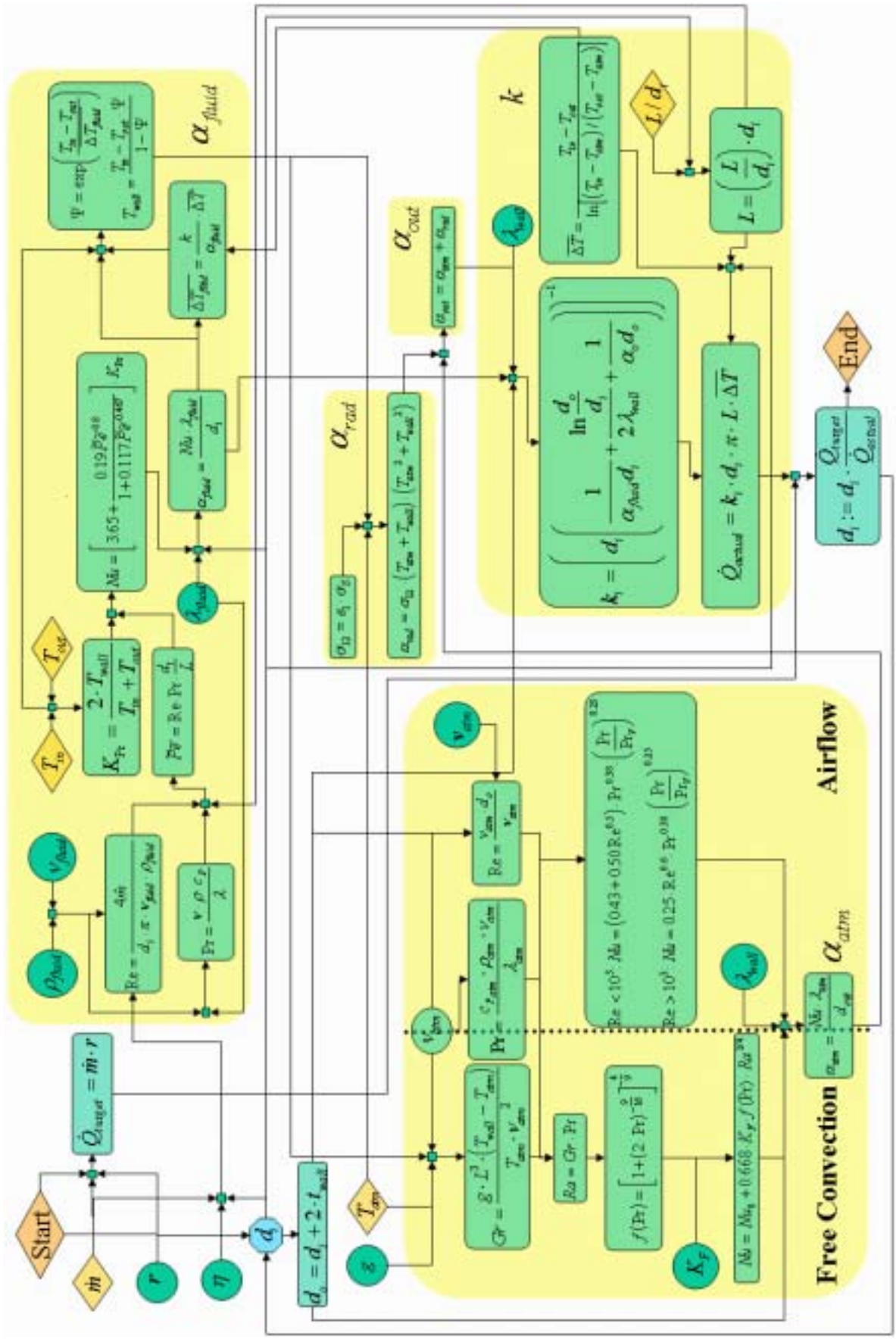

Figure 3-24: Pipe Temperature Loss Calculations Overview

3.6.4 Condenser

The purpose of a condenser is to change the condition of a gaseous substance to its liquid state. A common method to model a condenser is the "Nusselt's water film theory". It assumes that the content remains at its vaporization temperature during all time in the condenser. The input into the cell is solely gaseous, the outlet completely liquid. Therefore the needed heat flux can be written as:

$$\dot{Q} = \dot{m} \cdot r = \alpha_{cond} \cdot A_{cond} \cdot \left(T_V - T_W\right)$$

whereas

$\dot{Q}$	heat flux [W]
$\dot{m}$	mass flow [kg/s]
α_{cond}	heat transition coefficient [W/(m^{2}K)]
A_{cond}	area of cooled wall [m^2]
T_V	vaporization temperature [K]
T_W	wall temperature [K]

In order to be able to calculate the heat transition coefficient α_{cond}, the following formula is used:

$$\alpha_{cond} = Nu \cdot \frac{\lambda}{H} \cdot K_H$$

whereas

Nu = Nußelt's number [-]
λ = heat conductivity [W/(mK)]
H = height of the condenser wall [m]
K_H = film coefficient [-]

The heat conductivity λ of liquid water at 100°C is about 0.598 W/(mK) for water.

For Nußelt's number in condensers, four different formulas are available, depending on the Reynolds number:

		Re	<	10	:	$Nu = \sqrt[3]{\frac{0.943^4}{\mathrm{Re}}}$
10	<	Re	<	75	:	$Nu = \sqrt[3]{\frac{1.15^3}{\mathrm{Re}}}$
75	<	Re	<	1200	:	$Nu = 0.22$
1200	<	Re	<	10000	:	$Nu = \sqrt[3]{0.003^2 \cdot \mathrm{Re}}$

Since the pipe diameters used in the ISRU demonstrator missions are in the order of 1/10 in (2.54 mm), mainly the first formula of the four shown comes into use.

The required Reynolds number is obtained via the formula:

$$\mathrm{Re} = \frac{\dot{m}}{B \cdot \eta}$$

whereas

η = dynamic viscosity of the condense [Ns/m^2]
B = width of the condenser wall [m].

In the case of a circular cross-section, B can be written as:

$$B = \pi \cdot d_i$$

whereas

d_i = inner diameter of the condenser [m].

The film coefficient K_H can be calculated via the formula

$$K_H = H \cdot \left(\frac{\nu^2}{g} \right)^{-\frac{1}{3}}$$

whereas

H = height of the condenser wall [m]

K_H is the last input that is required in order to be able to calculate α_{cond}.

The wall temperature T_W, which is later needed for calculating the outer heat transition coefficients, can be calculated with the formula

$$T_W = T_V - \frac{\dot{Q}}{\alpha_{cond} \cdot B \cdot H}$$

whereas the flow velocities are

$$\nu = \frac{4\dot{m}}{d_i^{\,2} \cdot \pi \cdot \rho}$$

The film coefficient K_T, which is also needed as input, can be derived by solving the equation

$$K_T = \frac{\dot{Q}}{\alpha \cdot H \cdot B} \cdot \frac{\lambda}{\eta}$$

The conductivity and the outer heat transition coefficients are calculated exactly in the same way as it was done before for the pipe. Therefore, the overall heat flux number k_i (related to the inner Diameter) is:

$$k_i = \left(D_i \left(\frac{1}{\alpha_{cond} D_i} + \frac{\ln \frac{D_o}{D_i}}{2\lambda} + \frac{1}{\alpha_o D_o} \right) \right)^{-1}$$

The goal of the EXCEL® worksheet is to calculate the dimensions of the condenser for given temperatures. Therefore, the sheet starts with a starting value. After the first run, the actual obtained heat flux

$$\dot{Q}_{actual} = \alpha_{cond} \cdot A_{cond} \cdot \left(T_V - T_W \right)$$

is compared with the required target heat flux:

$$\dot{Q}_{target} = \dot{m} \cdot r$$

In order to meet the requirement, the diameter of the condenser is altered according to the formula:

$$d_i := d_i \cdot \frac{\dot{Q}_{target}}{\dot{Q}_{actual}}$$

Since d_i is not directly proportional to $\dot{Q}$, the next run will not result with the exact value for $\dot{Q}_{actual}$, but still with a value that is more accurate than the $\dot{Q}_{actual}$ in the first run. In a third run the accuracy increases again, and so on. The resulting iteration can calculate a value of sufficient accuracy very fast.
A summarization of the calculations for condenser simulation can be seen in Figure 3-25:

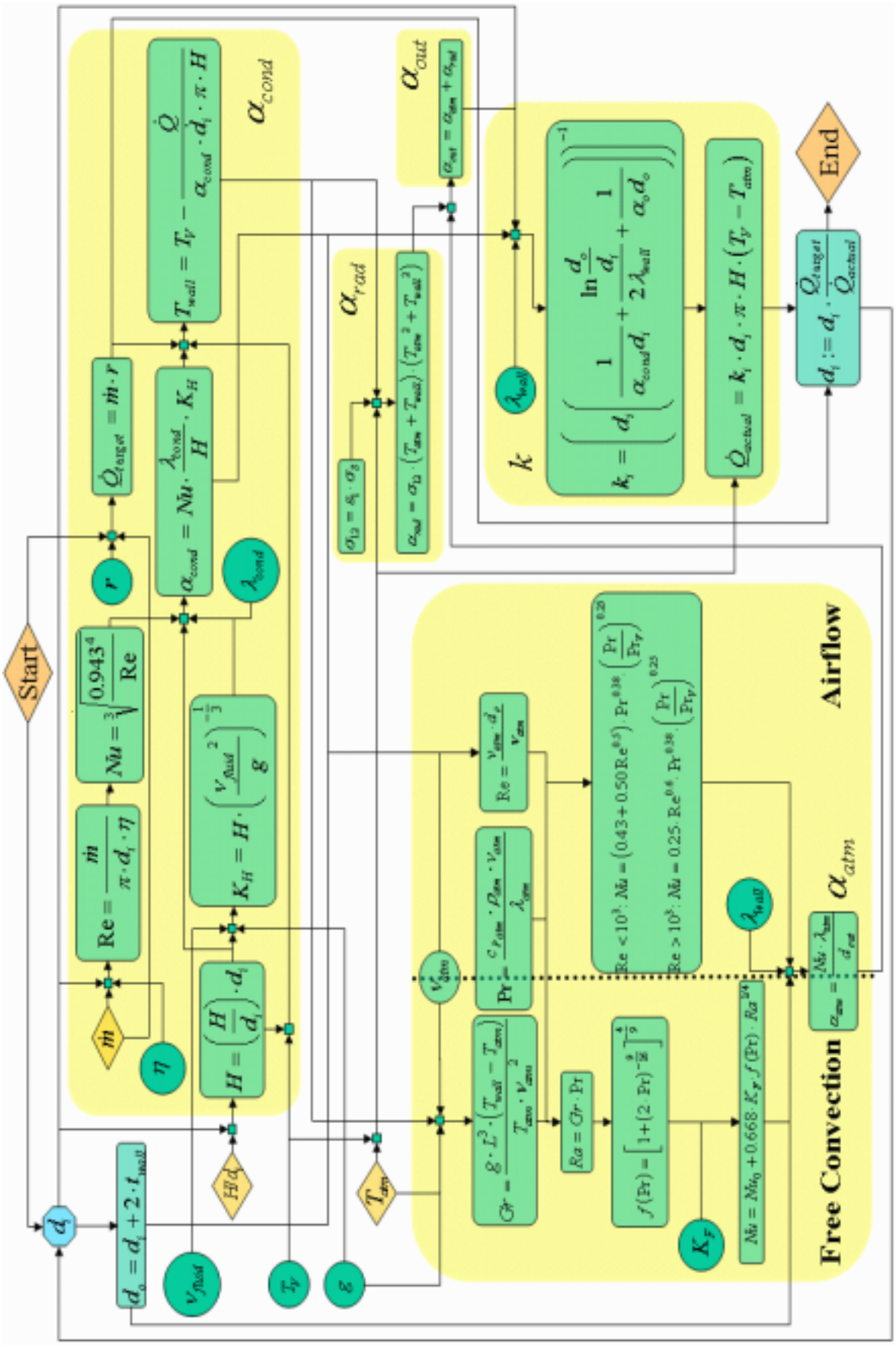

Figure 3-25: Condenser Calculations Overview

3.6.5 Electrolyzer

Hydrogen/oxygen fuel cells and electrolysis cells are familiar to astronautics since the Sixties. For many years electrolysis cells provided the crew of Mir with breathing oxygen. The chemistry and the physics that stand behind both fully understood, the modeling of the processes does not pose a significant challenge. Since the main focus of this thesis is on the Sabatier reaction and related phenomena, the electrolysis modeling was kept comparatively plain.

In an electrolyzer, a voltage between an anode and a cathode is applied, which causes the electrolysis reaction:

$$2H_2O_{(l)} \ (+ E) \rightarrow 2H_{2(g)}\uparrow \ + O_{2(g)}\uparrow$$

This reaction is strongly endothermic. The protons migrate from the anode towards the cathode, which are separated by the proton exchange membrane. An electrolysis cell thus actually consists of two half-elements, a hydrogen-producing half-element as well as an oxygen-producing half-element. These two half-reactions can be written as:

Anode:	$2H_2O_{(l)}$	$\rightarrow$	$O_{2(g)}\uparrow + 4H^+ + 4e^-$		
Cathode:	$4H^+ + 4e^-$	$\rightarrow$	$2H_{2(g)}\uparrow$		
Total:	$2H_2O$	$\rightarrow$	$2H_{2(g)}\uparrow + O_{2(g)}\uparrow$	E^o	= +1.229 V

The ion conductivity and thus the (voltage) efficiency of the membrane depends - among other things - on the water quality. Impure water decreases the membrane efficiency and results in a power loss. To avoid this, electrolyzers are typically filled with distilled water. In addition, before entering the electrolyzer, the water passes through an ion exchanger, which filters out undesirable metal ions. By doing so, the impurity level of the water can be kept low. Today's electrolyzers achieve voltage efficiencies from 70% up to and exceeding 85%. In practice, the voltage level differs from the number quoted above since it is a function of the operating pressures on both sides of the membrane, whereas the current I that is applied to the electrolyzer drives the mass flow rate through it.
For the modeling of these to interrelationships, two relations are employed; one being Faraday's first law:

$$\dot{m} = \frac{I \cdot M}{z \cdot F}$$

(with z representing the number of electrons that switch sides - in this case z=4 – and with F representing the product of Avogadro's constant and the elementary charge, also

called the Faraday constant $F = N_A \cdot e = 6.022 \cdot 10^{23} \frac{1}{mol} \cdot 1.602 \cdot 10^{-19} C = 9.648 \cdot 10^4 \frac{C}{mol}$)
and the other one being the Nernst equation:

$$E = E^o + \frac{R \cdot T}{z \cdot F} \cdot \ln \frac{[ox]}{[red]}$$

which takes into account the potential change due to non-standard conditions. Note that for the liquid water on the inlet side the activity is 1.

3.6.6 Overall Model

The overall model of the reactor is outlined in Figure 3-26:

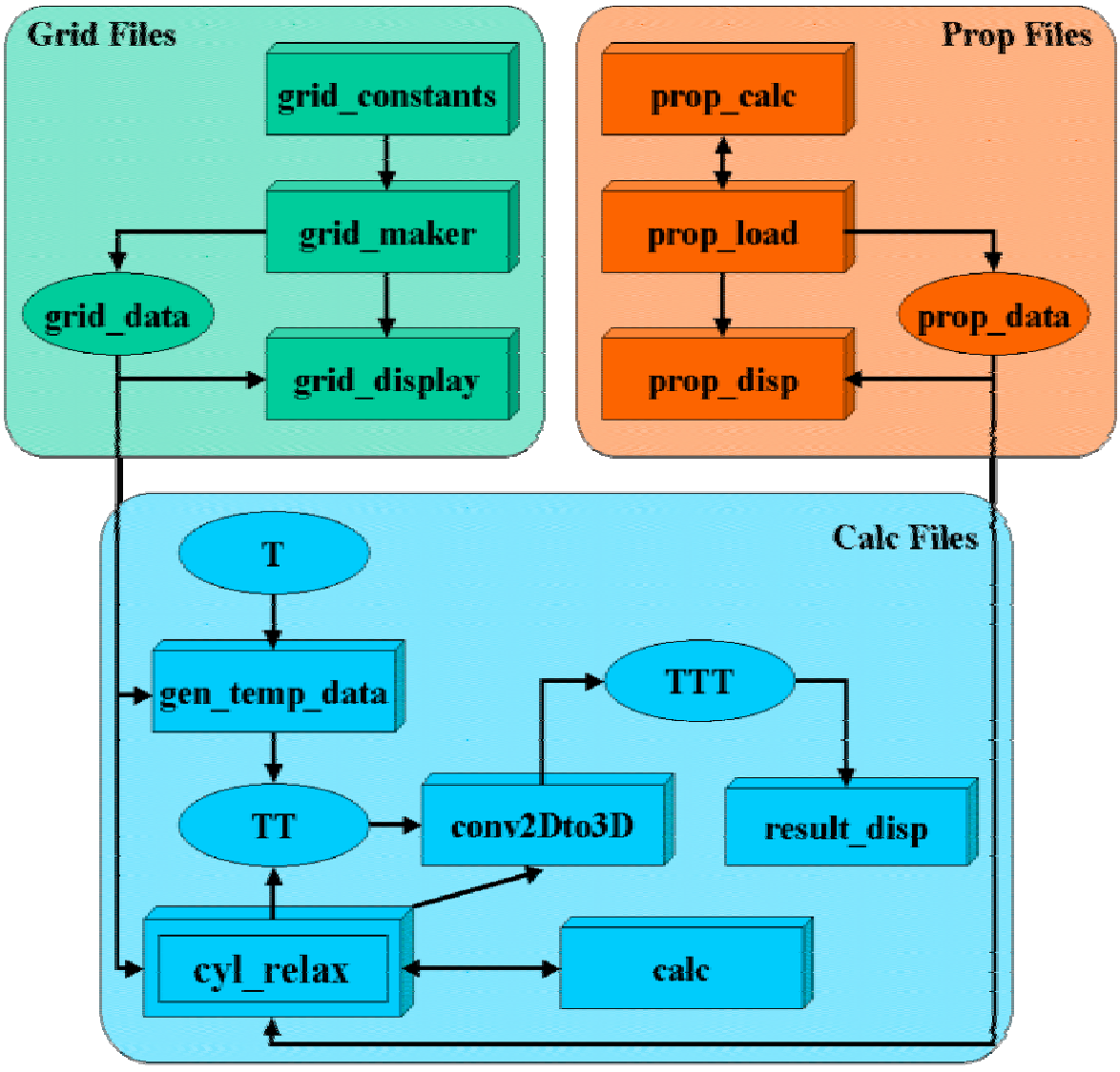

Figure 3-26: MATLAB Model - Overview over Simulation Program Elements

It consists of three main parts:

- the grid files block, in which the grid properties are created, displayed, saved, and loaded,
- the prop files block, in which the properties of the fluids are loaded, calculated, and displayed, and
- the calculations files block, the heart of then program. Based on the input of the two other blocks, here the temperature data is derived and displayed.

The Matlab Reactor Model is embedded in the Simulink model of the overall system. Utilizing the powerful features of Simulink, it allows the simulation of the operation with a user interface which allows the user to investigate the effect of inputs, similar to the reaction of the breadboard to the inputs of the test manager (see Figure 3-27). The contents of the various modules, functions and procedures where derived in the preceeding chapters.

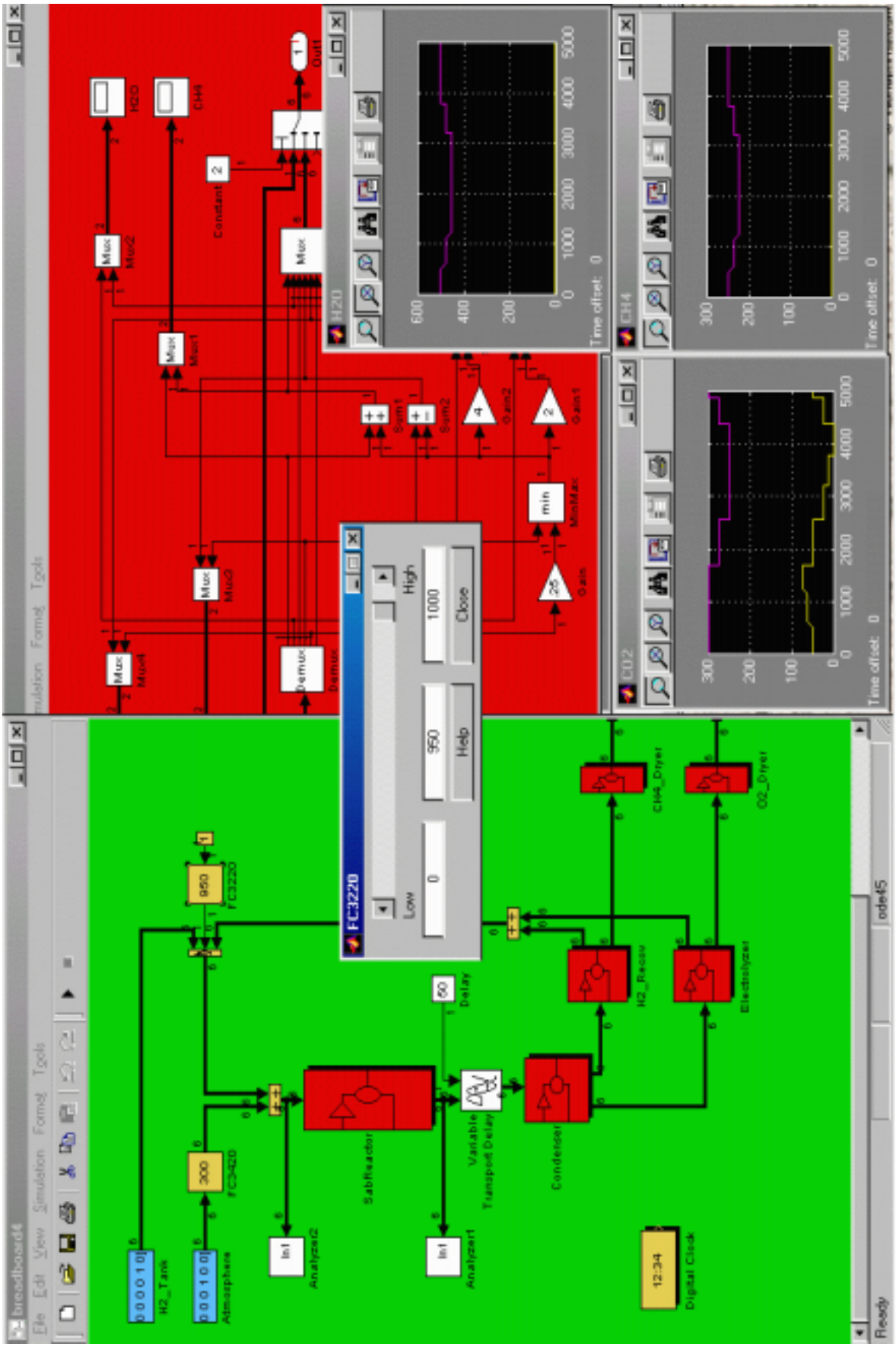

Figure 3-27: Simulink Model of the Overall Breadboard with User Interface

After first attempts using Excel and ChemCAD it was decided to use MATLAB as the basis for the programming of the computer models. This programming tool proved it self a very useful tool, which was – in opposition to the other two – up to the task.
In the course of the creation of the models, special attention was given to the heart of the system, the Sabatier reactor. The task is now to obtain experimental data (which will be done in the succeeding chapter) in order to be able to validate the model (which will be done in the chapter 5).

4 TESTING

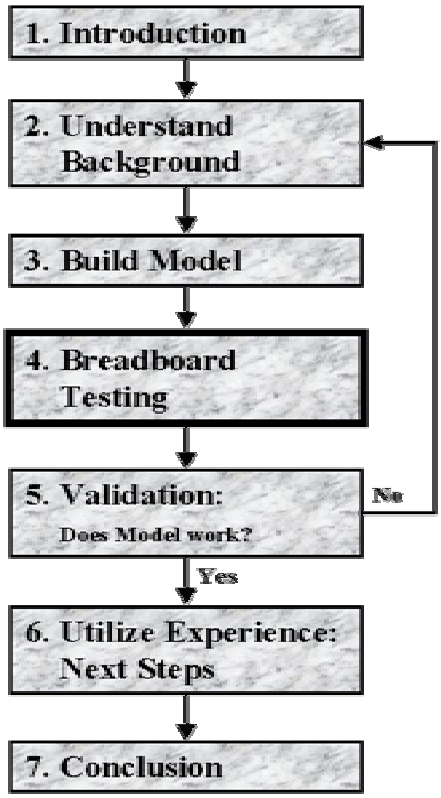

According to a quote of Wernher von Braun "one test is worth more than 1000 expert opinions". Consequently, in the course of this thesis, it is tried to verify the computer models that are based on theoretical deliberations derived in the preceding chapter with the help of Sabatier / water electrolysis breadboard tests.
The breadboard test campaign was conducted at the Mars ISRU Systems Test Facility of NASA Johnson Space Center under Earth ambient conditions on the one hand, as well as in simulated Martian environment on the other hand. These tests are subject of this chapter.
Once it is attained, the acquired test data will be compared to the computer model predictions in the succeeding chapter.

4.1 Outline

The goal of the Sabatier / water electrolysis system is to demonstrate its capability to convert (imported) hydrogen and Mars atmospheric carbon dioxide to methane and oxygen. This demonstration shall be end-to-end, meaning that it shall involve not only the core processes, but also the acquisition, the liquefaction, as well as the storage. The test can be conducted at Earth ambient temperatures as well as – with closed chamber and engaged liquid nitrogen thermal shroud cooling system – in simulated Martian environment including low temperatures, as they typically are encountered on Mars (chamber limit: –300°F/90K).
The Sabatier / water electrolysis breadboard (see Figure 4-3) was set up in the Mars ISRU Systems Test Facility (MISTF, see Figure 4-1) at the NASA Johnson Space Center in Houston, Texas, in Winter 1998/99. After the receipt of the various parts from the different suppliers and prior to their integration into the end-to-end breadboard test set-up, the various subsystems were each individually tested. The preparation of a test plan was commenced and in Spring 1999 the integrated end-to-end breadboard was turned on for the first time [McClean, 1999].

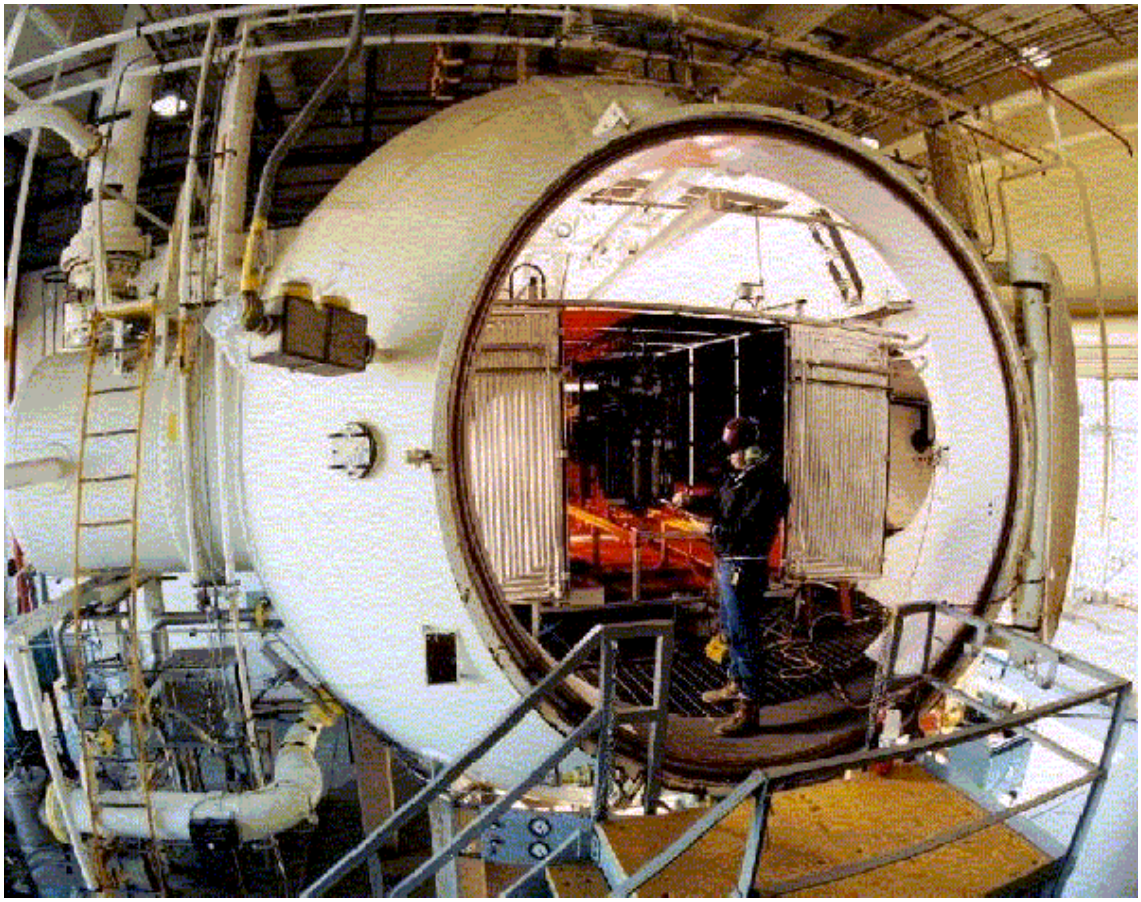

Figure 4-1: Sabatier / Water Electrolysis Breadboard in the 20ft Vacuum Chamber of the MISTF Facility [McClean, 2001]

4.2 Test Setup

The test article is a Sabatier / water electrolysis breadboard (see Figure 4-4 and Figure 4-3) whose function is to extract carbon dioxide from (simulated) Martian atmosphere, process the carbon dioxide together with hydrogen into methane and water, then split the water into hydrogen and oxygen, recycle the hydrogen, and liquefy and store the oxygen.

The breadboard consists of the same three subsystems that characterize every typical ISCP system and that were already outlined in chapter 2.1.4: acquisition, chemical processing, and liquefaction/storage. This can easily be seen by comparing Figure 2-1 with Figure 4-2 (all flow sheets are following [MISTF, 2000], which can also be found in Appendix A and B).

The details of the flow sheet are discussed later in the subsequent chapters. Sensors and controls of the breadboard are described separately in chapter 4.4.2 and in chapter 4.5.2.

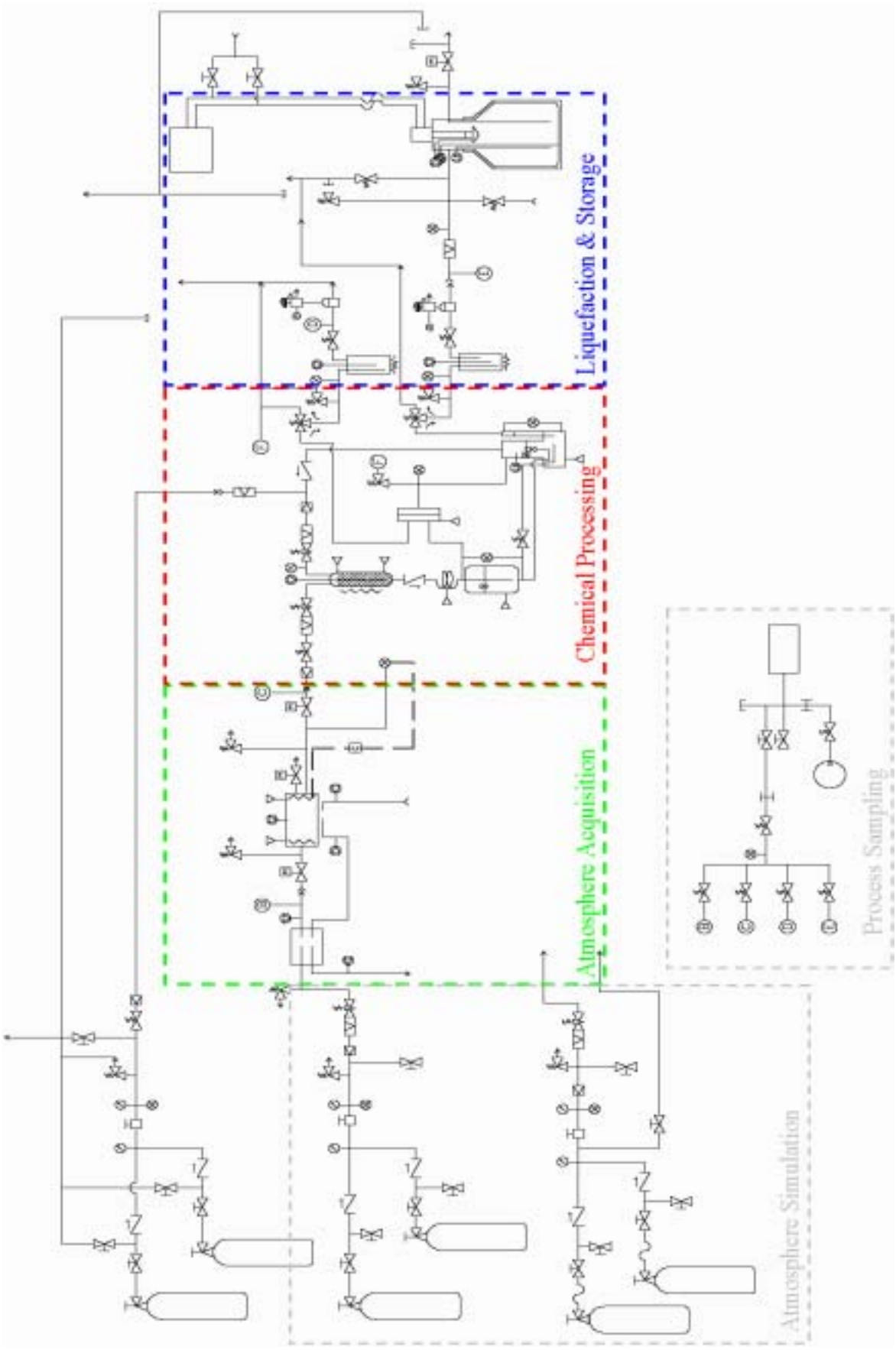

Figure 4-2: Breadboard Overview

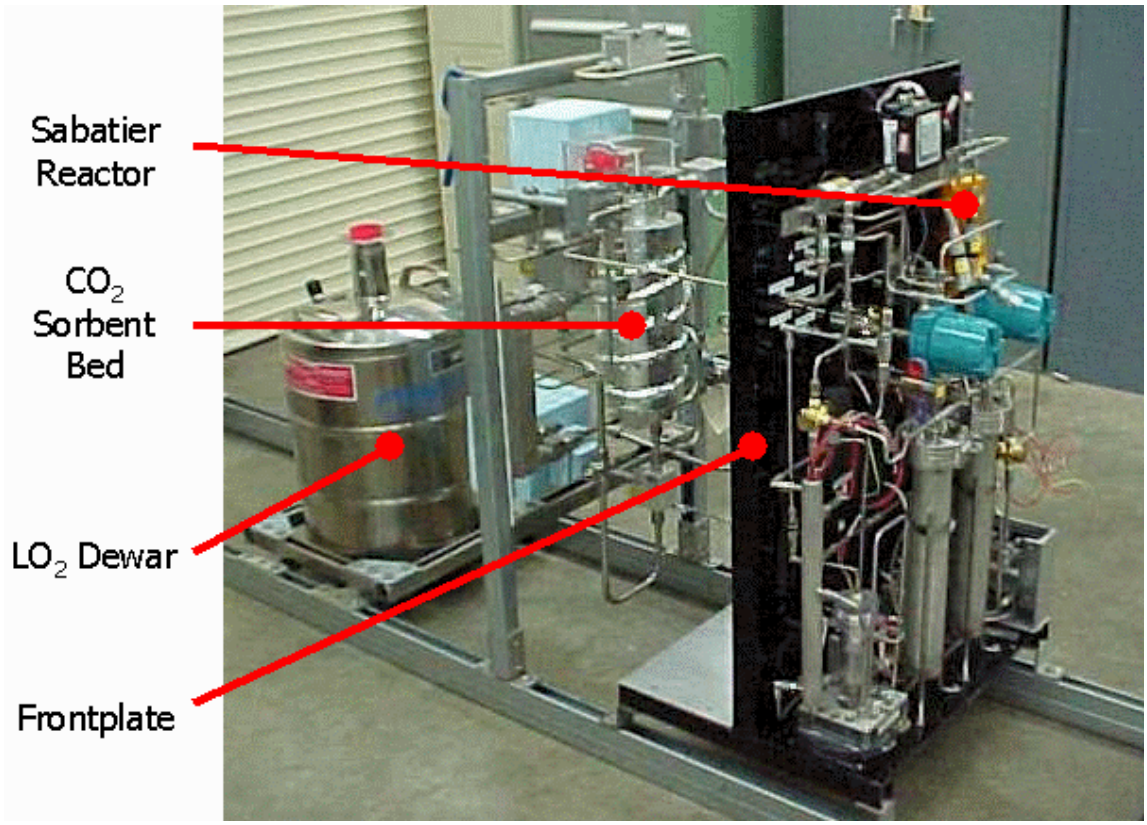

Figure 4-3: Overall Sabatier / Water Electrolysis Breadboard Layout

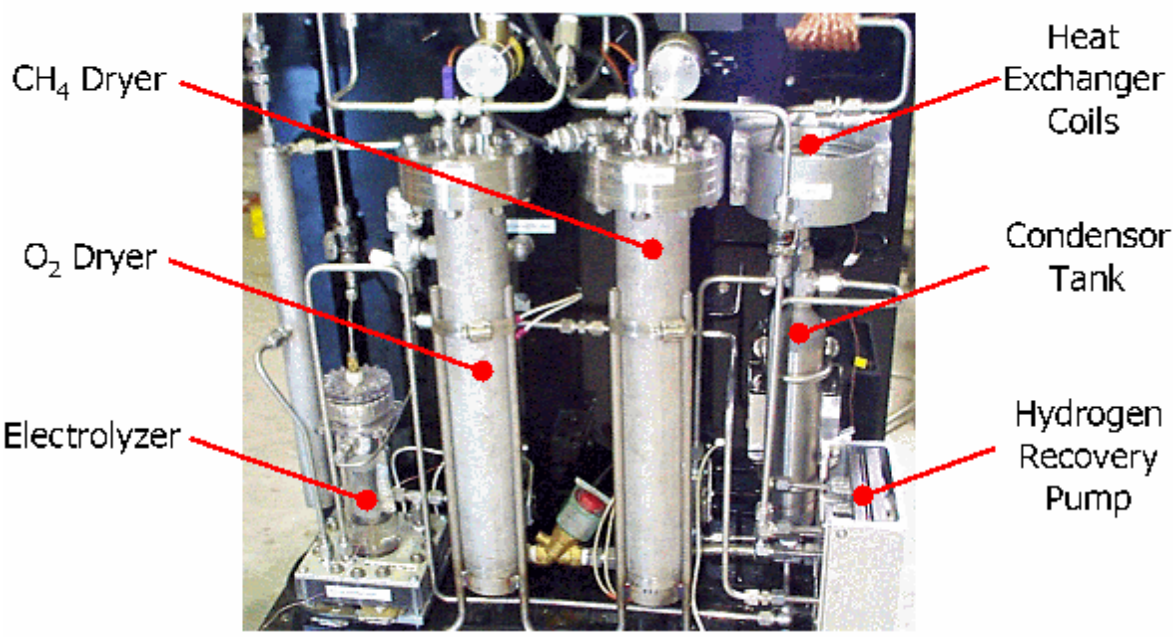

Figure 4-4: Breadboard Frontplate Subsystem Overview

4.2.1 Atmosphere Simulation and Acquisition

The acquisition of carbon dioxide will be performed by a sorption pump (see Figure 4-3) built by Lockheed Martin and tested in the Mars ISRU Systems Test Facility at NASA Johnson Space Center prior to the end-to-end breadboard tests.

On Mars, the carbon dioxide would be extracted from the CO_2-rich atmosphere, whereas the hydrogen would be imported in liquid form and recycled from the water electrolysis, respectively. In the Mars ISRU Systems Test Facility, the hydrogen is taken from standard hydrogen K-bottles, whereas the Martian atmosphere is simulated by "Mars Mix" K-bottles, basically a mix of carbon dioxide with a few percent of Argon (see Figure 4-5).

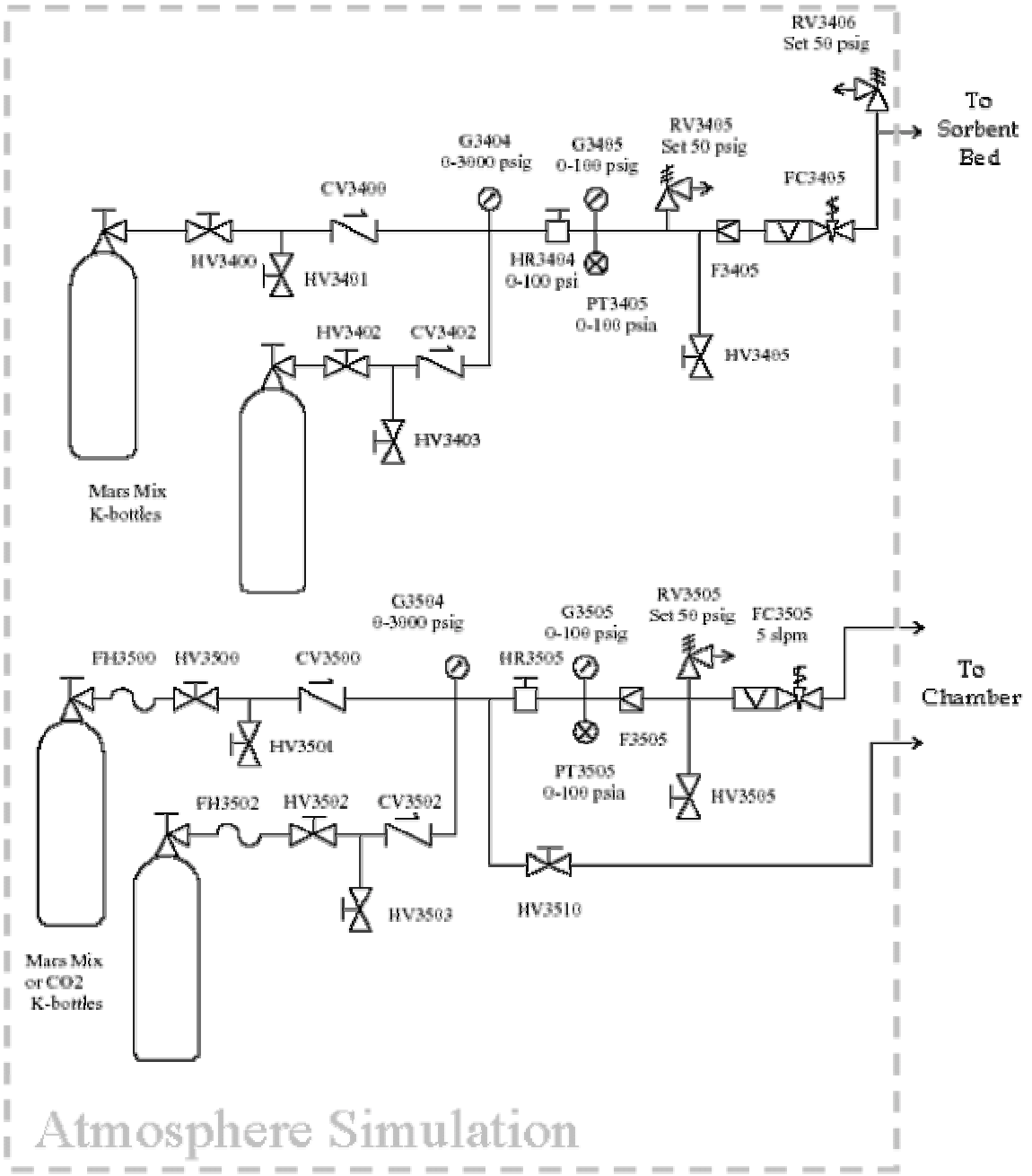

Figure 4-5: Flow Sheet of Breadboard Atmosphere Simulation Subsystem

During acquisition, the simulated (or rather emulated) Martian atmosphere flows through a heat exchanger into a sorbent bed (also called “sorption pump”, see flow sheet in Figure 4-6) filled with the molecular sieve material “Zeolite 13X”, described in chapter 3.6.2. At low temperatures, the Zeolite absorbs the carbon dioxide (external cold gas coils attached to the sorbent bed canister enable thermal conditioning), which then can be released later through simply raising the bed temperature. An internal heater raises the Zeolite’s temperature to provide pressurized carbon dioxide delivery through FC3420.
During simulated Mars environment testing, the content of the Mars-Mix (or CO_2) bottles is not only led to the sorbent bed, but also into the chamber (see Figure 4-5). The labels “B” and “C” mark the location of two of the four sample ports (see chapter 4.5.2).

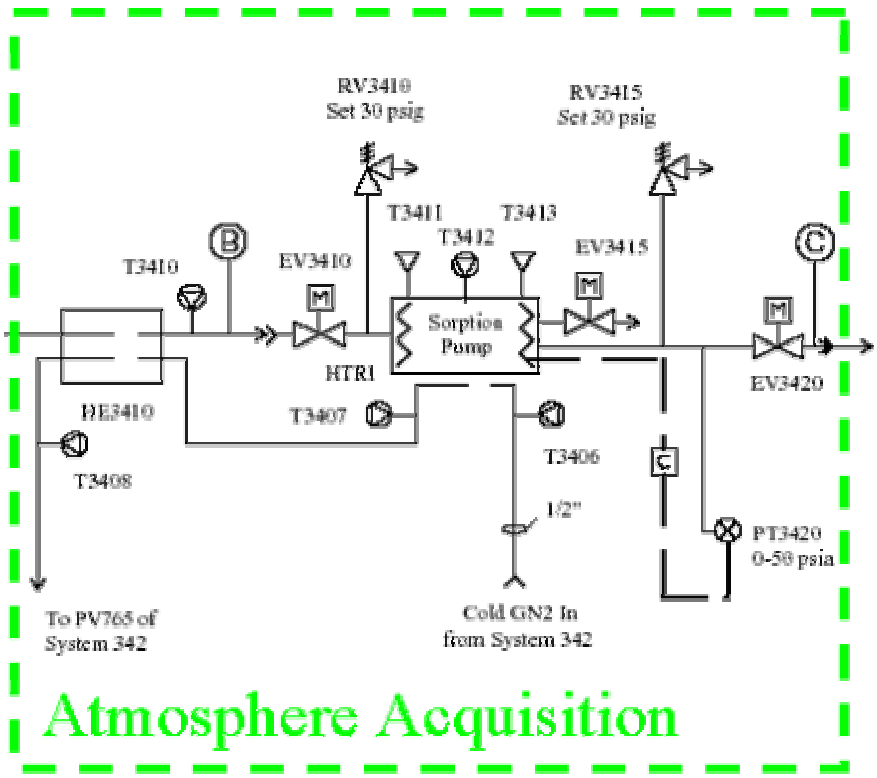

Figure 4-6: Flow Sheet of Breadboard Atmosphere Acquisition Subsystem

4.2.2 Chemical Processing

The chemical processing is performed within the Sabatier/water electrolysis subsystem, which is built by Lockheed-Martin. The core of the system is the Sabatier catalytic reactor (Figure 4-7).

Figure 4-7: Sabatier Reactor, with Copper Strap, with Insulation

This element of the breadboard will convert carbon dioxide and hydrogen to methane and water. The reactor basically is a pipe (outer length: 17.78mm) with to inlets at the top for carbon dioxide and hydrogen and one outlet for the reaction products. The reactor is insulated from its surrounding by approximately 2cm of insulation material. The temperature gradient that is needed for the reaction is achieved by a copper band attached to the lower end of the reactor which on the other end is connected to the breadboard support structure; thus the structure acts as a thermal sink. For an ideal reaction environment, the reactor core temperature should be slightly above 330°C (exact value dependent on feed ratio composition and reactor pressure). At this temperature, the reaction is stable and produces little or no unwanted reaction products. A lower temperature accelerates the reaction rate, however starting at 400°C the RWGS reaction outlined in chapter 3.2 sets in, which leads to an increase in carbon monoxide production. At a lower temperature however the reactants fails to achieve the activation energy needed to reach the “ignition point” at which the reaction stets in. Once established, the reaction is exothermic enough to sustain these temperatures without any requirements for active heating of the reactor. The heater elements that are placed between the outside of the reactor vessel and the insulation are only engaged during start-up, where they ensure sufficient temperatures for the reaction to start. Once the reaction has established itself within the reactor, the heater elements are turned off. The catalyst consists of 3mm diameter spheres of ruthenium on alumina (see also chapter 6.1.2).
Succeeding the Sabatier reactor is the check valve CV3320, the condenser tank, and the water electrolyzer (see Figure 4-4). While the water is condensed and separated from the

rest of the reactant stream, the other gases of the product stream (mostly methane, with traces of water, as well as unreacted hydrogen and carbon dioxide) leaves the condenser at the top and is led towards the hydrogen recovery pump (see Figure 4-8).

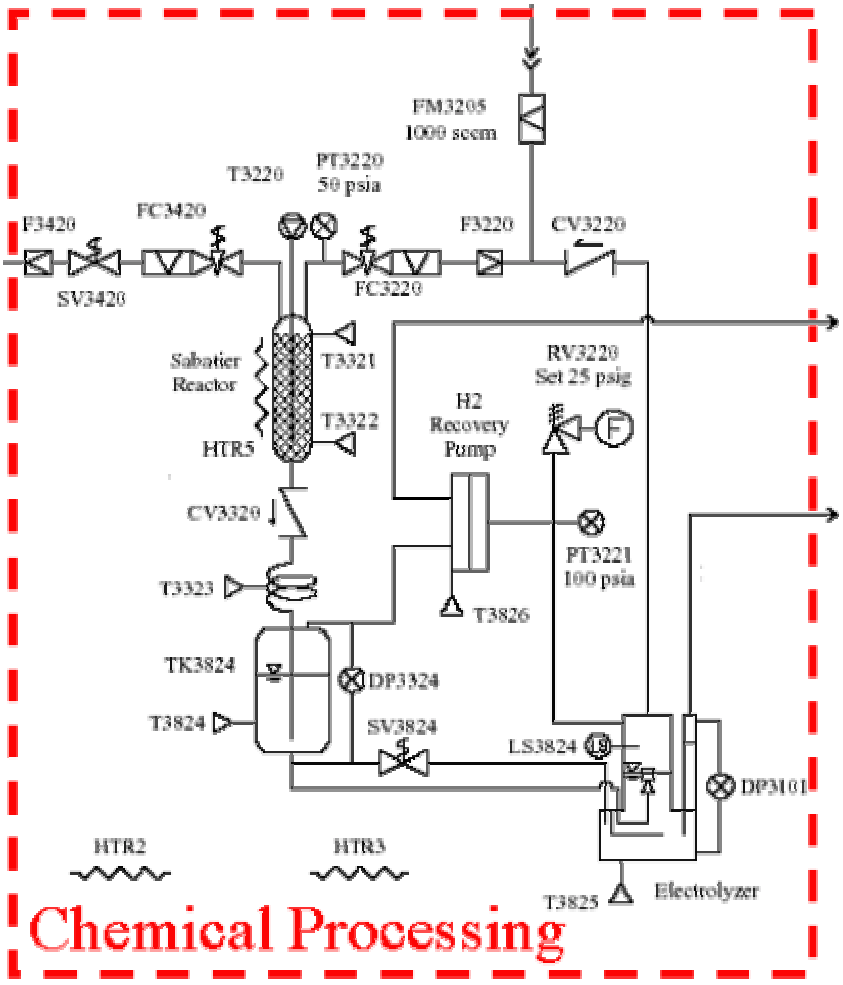

Figure 4-8: Flow Sheet of Breadboard Chemical Processing Subsystem

The water is led stepwise and manually (by opening and closing SV3824) into the electrolyzer in order to prevent a dry-running of the electrolyzer, which would damage it. Within the water electrolyzer the water is split into hydrogen and oxygen at a very high efficiency. The hydrogen from both, the hydrogen recycle pump as well as the electrolyzer is recycled back into the Sabatier reactor, thereby cutting the need for imported hydrogen in half.

4.2.3 Liquefaction and Storage

Upon leaving the chemical processing subsystem, both final product streams (methane and oxygen) are passed through their respective dryer in order to remove residual water vapor and carbon dioxide (see flow sheet in Figure 4-9). The labels “D” and “E” mark the location of two of the four sample ports (see chapter 4.5.2).

Both dryers are equipped with isolation valves and heaters to enable regeneration. Downstream of both dryers, the respective fluid streams are led through back pressure regulators which are employed to regulate the pressure throughout the breadboard. The liquefaction and storage itself is performed by a subsystem which was tested in the Mars ISRU Systems Test Facility at NASA Johnson Space Center prior to the end-to-end breadboard tests. A Gifford-McMahon cryogenic refrigerator built by Cryomech is mounted on top of a 25 liter dewar and provides a condensation surface for the oxygen. The cryogenic refrigerator power is adjusted in order to control the dewar internal pressure.

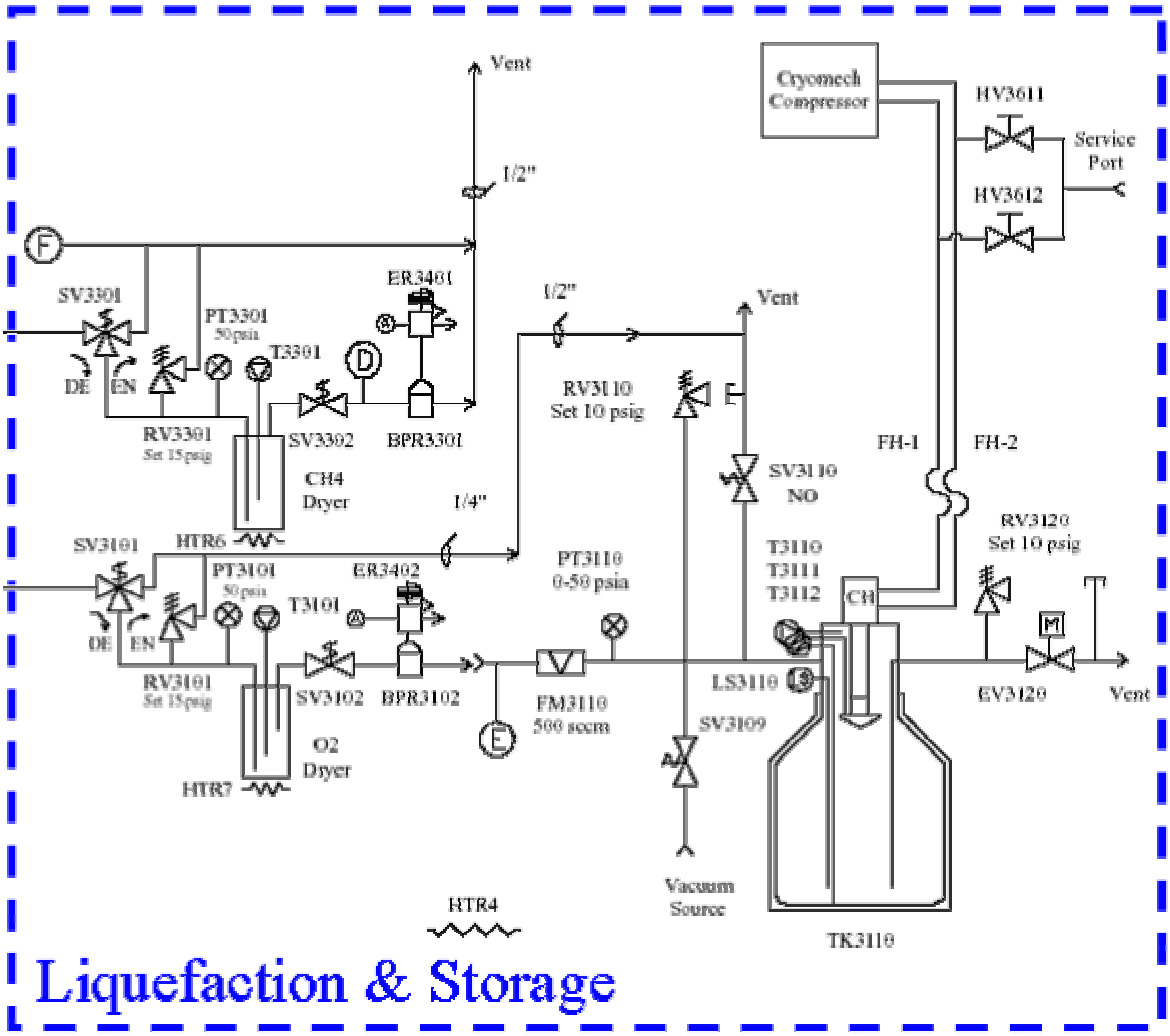

Figure 4-9: Flow Sheet of Breadboard Liquefaction and Storage Subsystem

Due to financial limitations, it was decided by NASA to only undertake the attempt to liquefy and store the oxygen, since this seemed to be the greater technological challenge (the boiling temperature of oxygen is lower than that of methane). It is therefore assumed that the demonstration of the feasibility of liquefaction and storage of oxygen validates the same also for methane. Therefore, as shown in the flow sheet, instead of liquefying and storing, the methane is released via the MISTF vent.

4.3 Safety and Environmental Impact

Before the commencement of the tests, the different potential hazards of the breadboard as well as the test setup had to be identified and mitigated in order to be in accordance with the strict safety standards of NASA.

One of the issues investigated was the potential **explosion risk**. During standard operation, the breadboard hosts massflows of less than 100g/h of hydrogen, oxygen and methane. It therefore has to be ensured that the hydrogen and the methane within the system always remain separated from the air during (and after) ambient testing (when the chamber door is open). In this respect, the Mars environment tests are of a lesser concern, since the Martian atmosphere consists mainly of carbon dioxide which is – as opposed to the Earth's atmosphere – is inherently safe, even if e.g. hydrogen should leak into the chamber. Nevertheless, during ambient *and* during Mars environment testing, methane and oxygen have to be separated from each other in order to mitigate the risk of explosions of methane/oxygen mixtures. The 20ft vacuum chamber in which the testing of the breadboard took place had already served as a test bench for the Apollo command module attitude control system in the Sixties. In order to be able to safely contain the firing tests of the attitude control thrusters, the chamber had thus been designed to withstand explosions of up to 10^8J. In the breadboard, at no point in the system do large amounts of any of the explosion sensitive fluids accumulate, so the chamber can ensure the safe containment of any explosions.

Of no lesser importance is the question of **elevated levels of potentially hazardous gases**, e.g. carbon dioxide. The 20ft vacuum chamber in which the testing took place (see Figure 4-1) can be entered. When people are in chamber, it has to be ensured that the local partial oxygen pressure is high enough to prevent suffocation and that the level of trace gases is low enough to not pose a hazard. This can be achieved by through and fan-supported airing of the chamber, in particular of course after Mars environment tests. The chamber must be cleared immediately if the portable CO_2 sensor, which is placed in the chamber, signalizes elevated harming CO_2 levels (via acoustic warning).

During the technical readiness review (TRR) for the environmental tests, the **environmental impact** of the breadboard was also evaluated. Of foremost interest is here the production of methane. For want of a methane dewar, the produced methane has been vented to the atmosphere. Methane is a greenhouse gas; the primary producer of methane in the Earth's atmosphere is cattle. Thus it was decided to compare the methane output of the breadboard with the methane production of an average cow. According to [MoA, 2000] an average cow produces 44kg of methane per year. That means that even by running the breadboard eight hours a day, it would still produce significantly (30%) less methane than a standard cow. Based on this calculation, the environmental impact of the breadboard was considered to be negligible. Other environmental impacts are described briefly in chapter 6.1.3; however none of these are within any reasonable closeness to real concern.

4.4 Integrated Tests under Ambient Conditions

4.4.1 Flow Schematic

The detailed flow schematic for tests under Earth ambient conditions can be found in Appendix A. The test setup of the Sabatier / water electrolysis breadboard was already discussed in chapter 4.2; this chapter discusses in particular the differences that characterize particularly the ambient tests.

During ambient testing, the door of the 20ft vacuum chamber of the Mars ISRU Systems Test Facility (in which the tests take place) remains open. In order to further simplify the access to the breadboard, the thermal insulation box around the breadboard frontplate system components (see Figure 4-3 and Figure 4-4) is not installed, which is possible since the surrounding temperature is not as cold as in the Mars environment tests. Furthermore, the chamber atmosphere simulation system is not engaged, the hand valves HV3500 and HV3502 remain close. The carbon dioxide supply to the sorbent bed is realized directly via the hand valves HV3400 and HV3402 from either “Mars Mix” or pure CO_2 K-bottles. Once the function of the sorption bed had been demonstrated, in some of the ambient tests both valves up- and downstream of the sorbent bed (EV3410 and EV3420) were opened in order to directly channel the carbon dioxide from the CO_2 K-bottles through the (not cooled) sorbent bed to the Sabatier reactor. Thus, the preparation time prior to the commencement of the tests could be shortened, since no down-cooling of the bed and no adsorption had to be undertaken.

4.4.2 Measurements and Controls

The breadboard is instrumented at various locations for pressure, temperature, flow rate, voltage and current. The controls consist of PID heater controls, solenoid valves, flow control valves, voltage and current controls, and backpressure regulators.

The temperature of the of the sorbent bed is measured at three locations with the thermocouples T3411, T3412, and T3413 located at the inlet, in the center, and at the outlet of the bed. Both reactant streams are controlled with a flow control valve in each stream. FC3420 is located on the carbon dioxide inlet and FC3220 is located on the hydrogen inlet. The flow control valves are also effective as shut off valves. The carbon dioxide inlet has also a redundant normally open solenoid valve (SV3420). The pressure of gases is measured with a single pressure transducer (PT3220) at the inlet of the Sabatier reactor.

The temperature of the Sabatier reactor is measured at one location internally (T3220) and two locations externally (T3321 and T3322). T3220 is internal to the reactor near the outlet. T3322 is co-located externally with the heater near the reactor near the outlet. T3321 is located externally near the reactor inlet. The reactor is heated with an electrical heater (HTR5) being PID controlled.

The heat radiator downstream of the reactor has a thermocouple (T3323) located on the 3rd coil of tubing. Another thermocouple (T3824) is located on the exterior of the

condenser tank. A differential pressure transducer (DP3324) provides a measurement of the water level in the condenser tank.
A normally closed solenoid valve (SV3824) controls the flow of water from the condenser tank into the electrolyzer. The water is led stepwise and manually (by opening and closing) into the electrolyzer in order to prevent a dry-running of the electrolyzer, which would damage it. The water level within the electrolyzer is monitored by the level sensor LS3824, and the temperature by the thermocouple T3825. The production of the electrolyzer is set by controlling input voltage and current, which are both measured.
The pressure of the electrolyzer and oxygen outlet is measured by PT3101 and set by a backpressure regulator (BPR3102). The backpressure regulator can be operated electronically as well as manually (see 6.1.5). The oxygen product passes through a dryer, which can be heated. The heater (HTR7) is PID controlled, with the temperature of the dryer being measured by T3101. The heater is used for regeneration of the dryer (as already mention in 4.2.3). During regeneration, the dryer outlet is isolated with SV3102, which is normally open.
The methane product stream is passed through the hydrogen recovery pump. The input voltage controls the pump output. The current draw is determined by the quantity of hydrogen available to pump.
The pressure of the methane stream after the recovery pump is measured by PT3301. A backpressure regulator (BPR3301) controls the pressure of the outlet along with the water reservoir and the Sabatier reactor. This backpressure regulator can also be operated electronically and manually. The methane passes through a dryer similar to the oxygen, with HTR6, T3301, and SV3302 being the heater, thermocouple, and solenoid valve for the methane branch.

4.4.3 Test Plan for Tests under Ambient Conditions

The entire test plan for tests under ambient conditions is listed in Appendix C. An overview over the different steps is given in Figure 4-10 (in brackets the reference to the respective corresponding subchapter in Appendix C which contains a more detailed description. The test plan is divided in three main phases: test preparation, test run, and shutdown.

Test preparation consists of:

- start up, where instrumentation is initialized and facility safety precautions are established,
- set up ambient test, where subsystems are checked for test readiness,
- set up oxygen dewar, where the dewar is emptied and prepared for liquefaction operation,
- establish GN_2 supply for the operation of the two backpressure regulators,
- service sorption pump, where the adsorbent material is loaded into the sorption pump and where the pump is prepared for operation,

- set up Mars atmosphere feed to establish the feed into the sorbent bed,
- set up hydrogen feed to establish the feed into the Sabatier reactor.

Test run is made up of:

- ambient adsorption, to fill the sorbent bed with carbon dioxide,
- RGA sampling, where the residual gas analyzer is set up and calibrated for sampling,
- propellant production, where the sorption pump is put into desorption mode, where the chemical conversion of CO_2 and H_2 in the Sabatier reaction is performed, where the oxygen is liquefied, and where the methane is vented,
- electrolyzer operation, where the water is split into hydrogen and oxygen,
- liquefaction operation, where the Gifford-McMahon cryo-cooler is started,
- process sampling, where the residual gas analyzer is employed for sampling,
- monitor, where the performance and the reactions of the overall system are examined.

Shutdown consists of:

- the shutdown electrolyzer, where the production of hydrogen and oxygen is turned off,
- shutdown propellant production, where the Sabatier reactor, the hydrogen recovery pump, as well as the sorption pump subsystems are turned off,
- shutdown liquefaction operation, where the oxygen liquefaction system and dewar are turned off and secured,
- shutdown hydrogen feed, where the hydrogen feed is turned off,
- shutdown Mars atmosphere feed, where the supply of hydrogen to the Sabatier reactor is stopped,
- shutdown ambient test and shutdown of breadboard, where the ambient test operations are ceased.

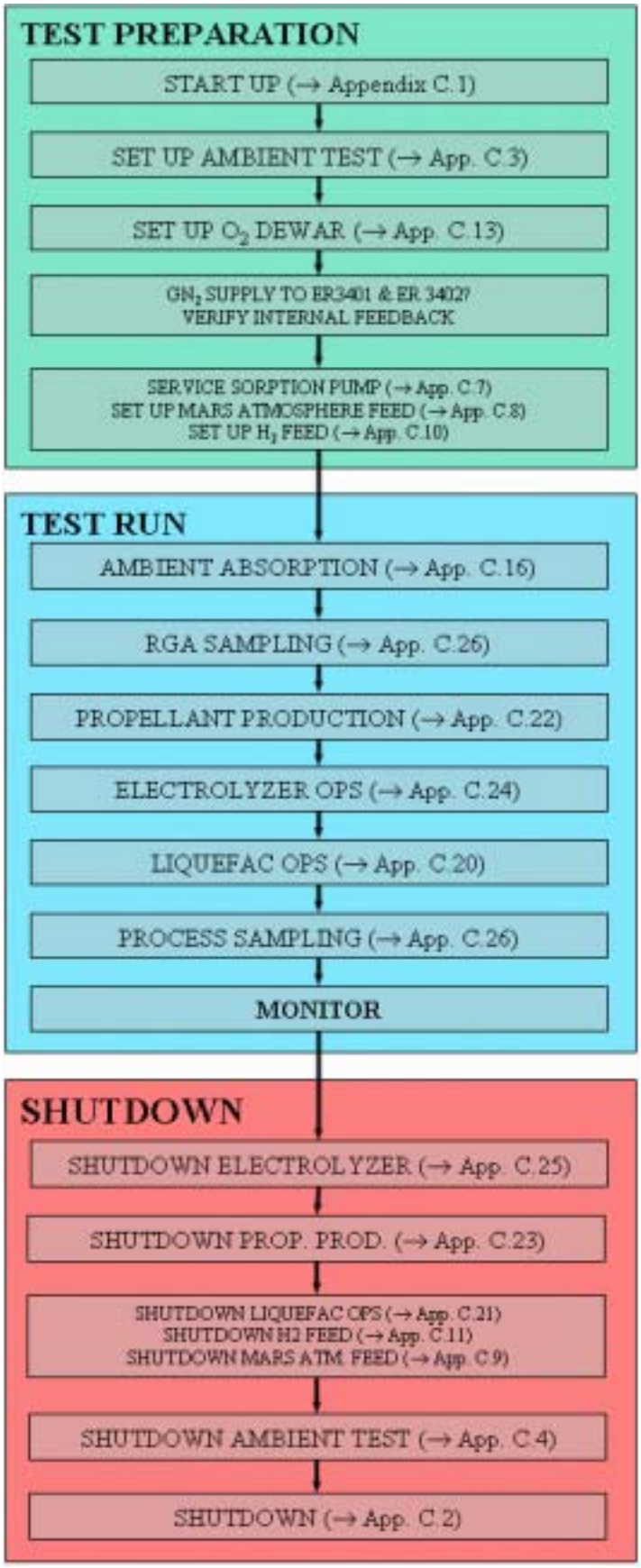

Figure 4-10: Test Procedure for Earth Ambient Tests
(with reference to the corresponding Appendix C subchapters)

4.5 Integrated Tests in Simulated Martian Environment

4.5.1 Flow Schematic

The detailed flow schematic for tests in simulated Martian environment can be found in Appendix B. The test setup of the Sabatier / water electrolysis breadboard was already discussed in chapter 4.2; this chapter discusses in particular the differences that characterize particularly the ambient tests.

Prior to the commencement of the environment tests, the door of the 20ft vacuum chamber of the Mars ISRU Systems Test Facility (in which the tests take place) is closed and hermetically sealed. In order to enable the chemical processing subsystem of the breadboard to endure the Mars environment, a thermal insulation box is installed which covers the breadboard frontplate system components (see Figure 4-3 and Figure 4-4). Furthermore, the chamber atmosphere simulation system is engaged, which is employed to fill the chamber with simulated Mars atmosphere from “Mars Mix” K-bottles via the valves HV3500 and HV3502. During the carrying out of the test run there are two options: the first one is to directly channel the CO_2 into the sorbent bed from the K-bottles. The other one is to divide the connection before EV3410 to allow the atmosphere in the chamber to enter the sorbent bed. In the latter case, the hand valves HV3400 and HV3402 remain closed; the flow controller FC3405 can also act as a shutoff valve.

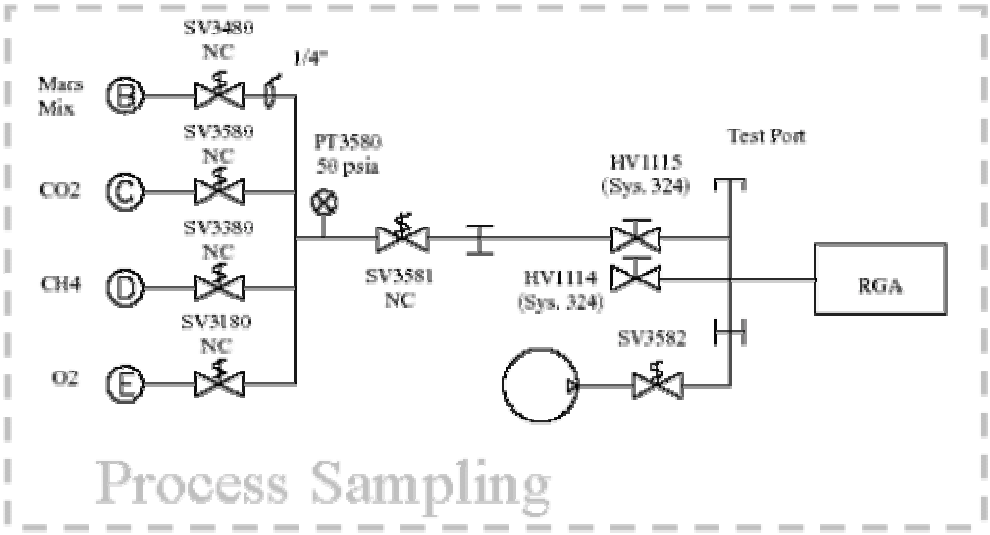

Figure 4-11: Flow Sheet of Breadboard Process Sampling Subsystem

4.5.2 Measurements and Controls

During the simulated Mars environmental tests, the set-up of the controls and sensors basically remained as they were for the Earth ambient test. They were however complemented by the environment controls and sensors.

During some of the environmental testing, the residual gas analyzer was also engaged, which allowed the analysis of the Sabatier reactor product stream. For that purpose, at four locations in the breadboard, sample ports are foreseen (see port “B” through “E” in Figure 4-11 as well as Appendix B), which allow the extraction of gas samples, which are then led to the residual gas analyzer, which features a simple interface to its users (see Figure 4-12).

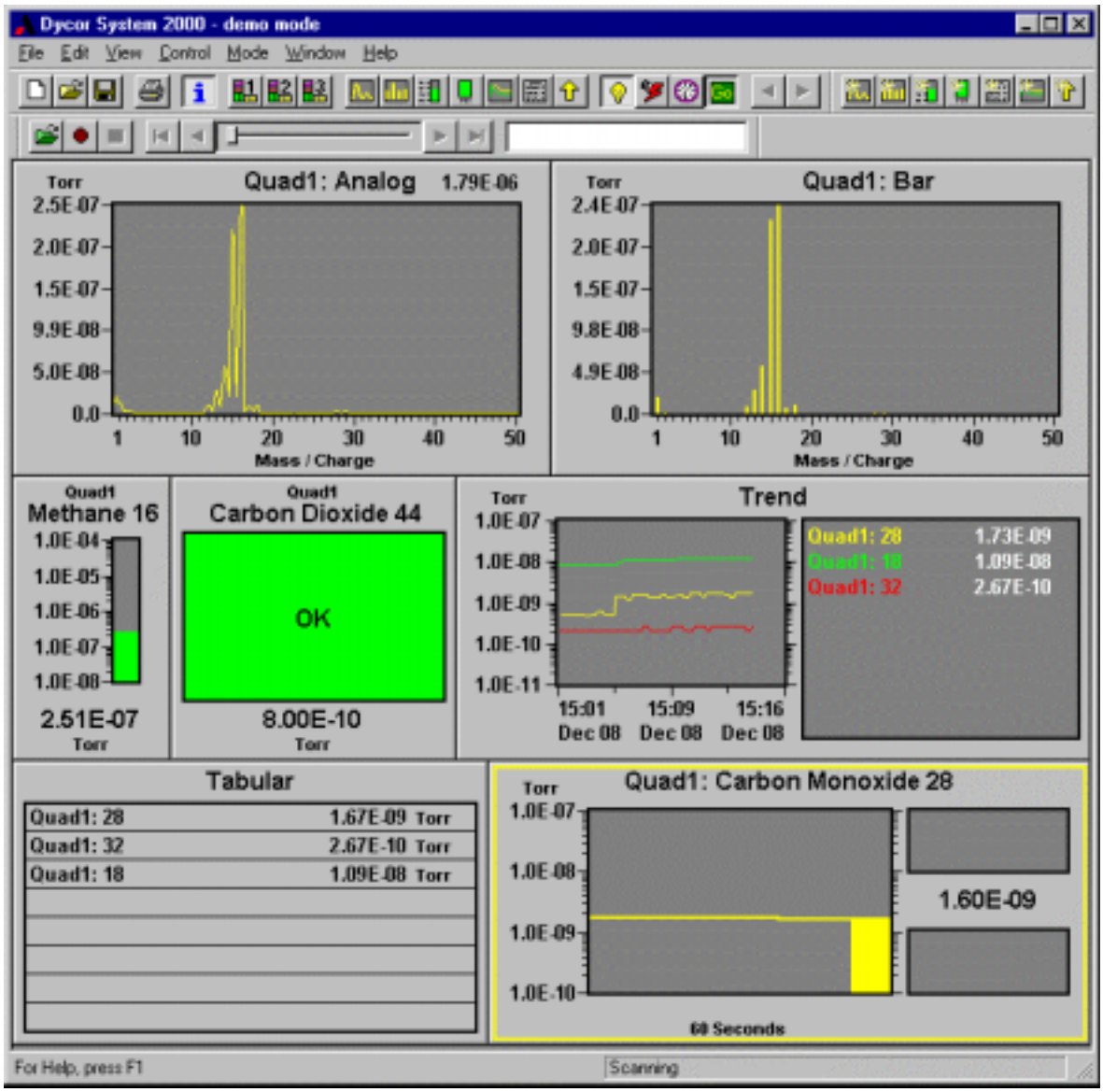

Figure 4-12: Residual Gas Analyzer User Interface

4.5.3 Simulation of Martian Environment

For the simulation of Mars environment conditions, the following parameters are controlled:

- atmosphere pressure,
- atmosphere composition, and

- temperature.

This is achieved by closing and evacuating the 20ft chamber, plus the engagement of the liquid nitrogen cooling panels which completely surround the breadboard (see Figure 4-1). The chamber is filled by the atmosphere simulation subsystem, which also ensures the provision of inlet gases of the sorbent bed. This system was already outlined in subchapter 4.2.1. In the near future, it is planned to equip the Mars ISRU Systems Test Facility also with the following features:

- dust,
- wind,
- solar flux (diurnal cycle)

These systems however were not yet available during the breadboard testing phase described in this thesis.

4.5.4 Test Plan for Tests under Simulated Martian Environment Conditions

The entire test plan for tests under simulated Martian environment conditions is listed in Appendix C. An overview over the different steps is given in Figure 4-13 (in brackets the reference to the respective corresponding subchapter in Appendix C, which contains a more detailed description). The test plan is also divided in three main phases: test preparation, test run, and shutdown.

Test preparation consists of:

- start up, where instrumentation is initialized and facility safety precautions are established,
- set up Mars environment test, where subsystems are checked for test readiness,
- set up oxygen dewar, where the dewar is emptied and prepared for liquefaction operation,
- establish GN_2 supply for the operation of the two backpressure regulators,
- service sorption pump, where the adsorbent material is loaded into the sorption pump and where the pump is prepared for operation,
- set up Mars atmosphere feed to establish the feed into the sorbent bed,
- set up hydrogen feed to establish the feed into the Sabatier reactor,
- set up thermal conditioning, where the liquid nitrogen chamber cooling system is set up.

Test run is made up of:

- ambient absorption, to fill the sorbent bed with carbon dioxide,

- set up chamber atmosphere feed, where the continuous supply of “Mars Mix” to the chamber is ensured,
- RGA sampling, where the residual gas analyzer is set up and calibrated for sampling,
- propellant production, where the sorption pump is put into desorption mode, where the chemical conversion of CO_2 and H_2 in the Sabatier reaction is performed, where the oxygen is liquefied, and where the methane is vented,
- electrolyzer operation, where the water is split into hydrogen and oxygen,
- liquefaction operation, where the Gifford-McMahon cryo-cooler is started,
- process sampling, where the residual gas analyzer is employed for sampling,
- monitor, where the performance and the reactions of the overall system are examined.

Shutdown consists of:

- the shutdown electrolyzer, where the production of hydrogen and oxygen is turned off,
- shutdown propellant production, where the Sabatier reactor, the hydrogen recovery pump, as well as the sorption pump subsystems are turned off,
- shutdown thermal conditioning system, where the operation of the thermal conditioning system is ended,
- shutdown chamber atmosphere feed, where the Mars atmosphere feed to the chamber (required for Mars environment test operations) is turned off,
- repress chamber, to equalize external and internal chamber pressure to allow the opening of the chamber door,
- shutdown liquefaction operation, where the oxygen liquefaction system and dewar are turned off and secured,
- shutdown hydrogen feed, where the hydrogen feed is turned off,
- shutdown Mars atmosphere feed, where the supply of hydrogen to the Sabatier reactor is stopped,
- shutdown Mars environment test and shutdown of breadboard, where the ambient test operations are ceased.

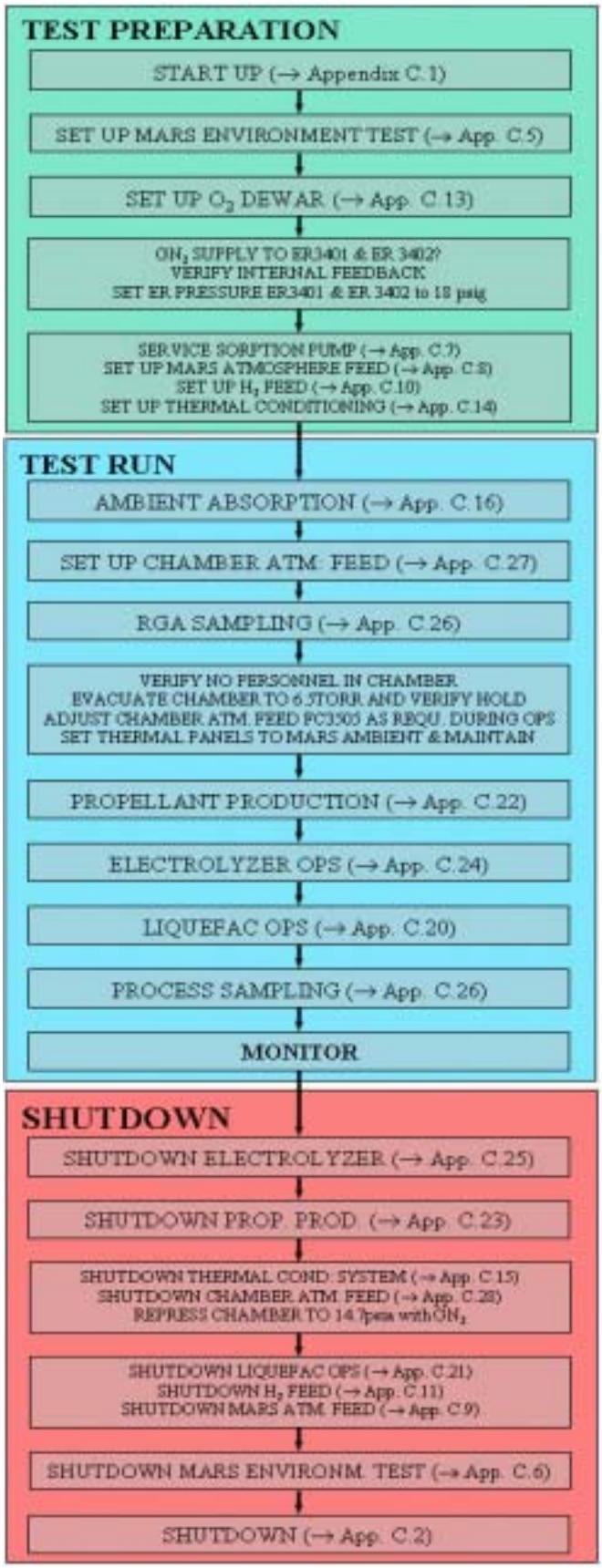

Figure 4-13: Test Procedure for Tests in Simulated Martian Environment
(with reference to the corresponding Appendix C subchapters)

4.6 Results of Integrated Tests under Ambient Conditions

During the carrying out of a typical ambient test, as in any test, the main goal is to attain and stabilize the Sabatier reaction. In order to achieve that, it is necessary to first ensure the provision of an adequate carbon dioxide flow to the reactor. This can be done by charging the sorption bed. Once that had been successfully demonstrated a couple of times, it was decided to run carbon dioxide directly from the bottles to the reactor. With this procedure, the lengthy sorbent bed charging period could be avoided and thus more time per day was available to the actual breadboard operation and propellant production respectively.

A second prerequisite of the Sabatier reaction is the attainment of an adequate reaction temperature. The exact minimum temperature is dependent on a variety of parameters, such as reactor pressure, feed ratio, etc., but it is always greater than 600K. Figure 4-14 represents a typical test run under ambient conditions. The test is started with the opening of the hydrogen inlet into the reactor (red line). Soon after that, the reactor heater is engaged, resulting in a sharp increase in temperature (black line). Once the minimum temperature is reached, both inlet streams are opened to their nominal values, 1000sccm for hydrogen (red line) and between 250 and 300sccm for carbon dioxide (blue line). The heater is programmed to maintain a certain reactor temperature, thus the setting in of the Sabatier reaction can not be identified by a temperature change. Hence, the attention is now on two parameters:

Firstly, the heater on/off intervals: the heater maintains the temperature within a set range by constantly turning on and off. Once the reaction sets in, the heater has to provide less power, resulting in a change in the turn on/off pattern.

Secondly, the commencement of the Sabatier reaction also results in a decreased volume flow (40% reduction), since the methane and the water vapor together require less space than the carbon dioxide and the hydrogen. The strong bubbling in the condenser vessel however obscures the measurement to some extent, a problem also outlined in chapters 6.1.4 and 6.1.12.

Once the reaction is established, it is possible to turn off the heating, since it is now able to sustain itself. The deactivation of the heater leads to a drop in temperature; the system then however stabilizes itself at the reaction temperature. At this point a definite answer is given to the question of whether the reaction has not been established or not: if the temperature falls unstopped to ambient temperatures as depicted in Figure 4-15, no reaction was attained. This can be due to a couple of different reasons, some of which are outlined in the “lessons learned” chapters, e.g. 6.1.2 or 6.1.15 respectively. The wild changes in this figures show that it was tried desperately to attain the reaction by changing various parameters, however none of them was successful (this special case is described in chapter 6.1.15).

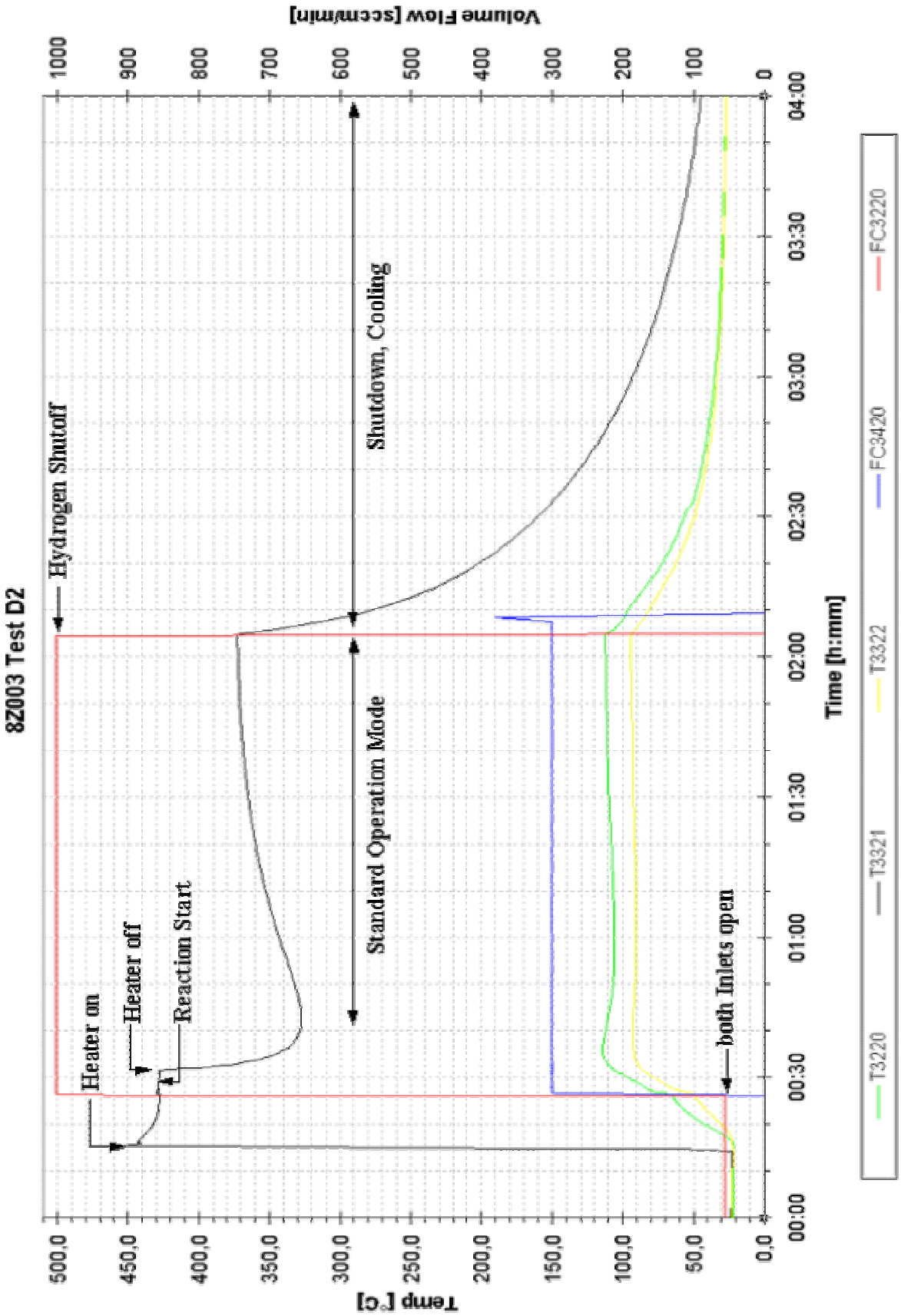

Figure 4-14: Successful Ambient Test Run
(Series D, Test 2, 22.09.1999 – Reaction Achieved)

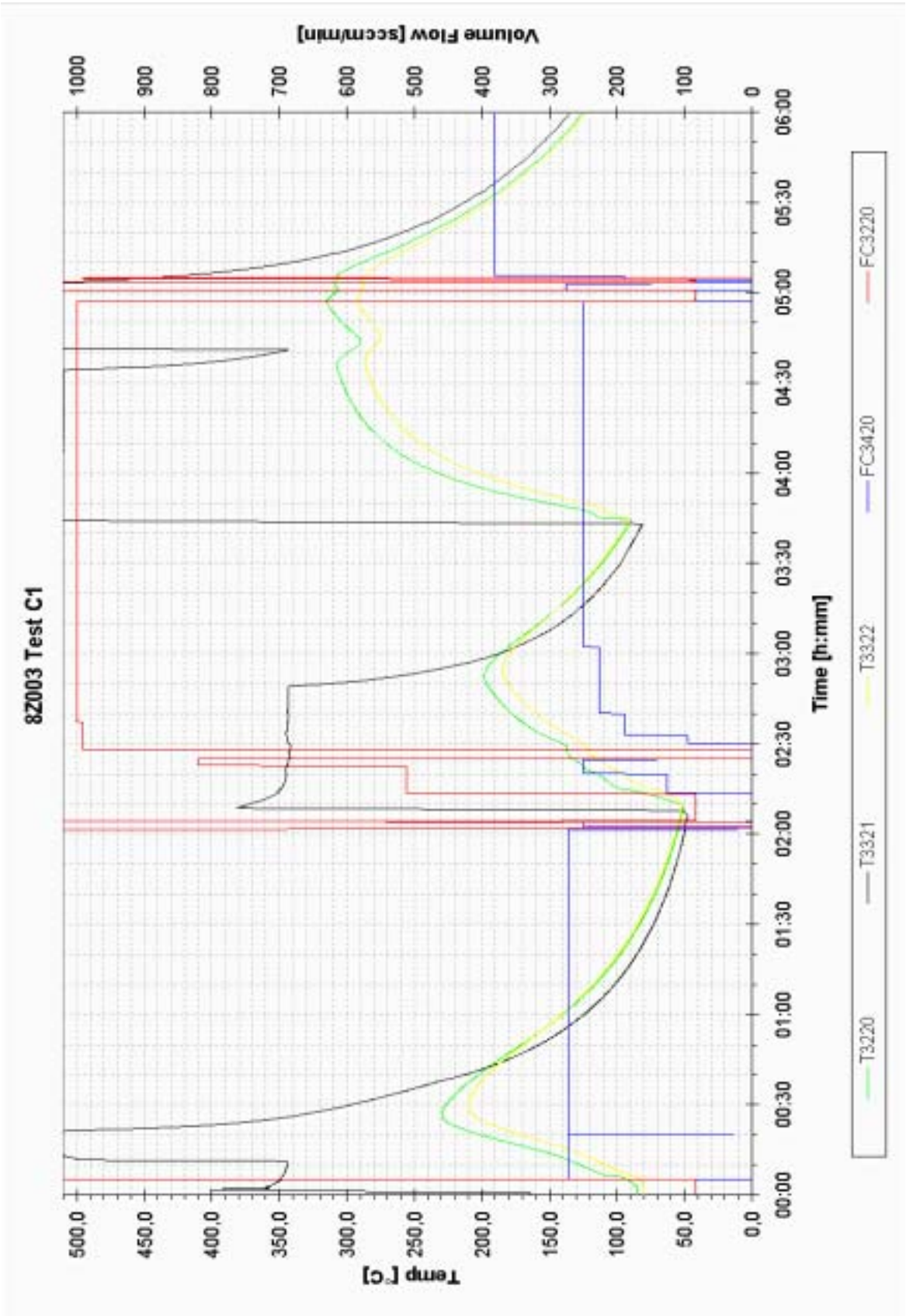

Figure 4-15: Failed Ambient Test Run
(Series C, Test 1, 16.09.99 – No Reaction)

In the hours following the establishment of the Sabatier reaction, typically different aspects of the breadboard performance behavior are investigated, such as propellant production, liquefaction, response to feed ratio changes, and so forth.
After completion of these tasks, the shutdown of the breadboard is initiated. This is managed by closing one of the two feed lines, either carbon dioxide or - as depicted in Figure 4-14 - hydrogen. This leads to a sudden drop in temperature to ambient temperature within a few hours. The lessons that were learned in the area of breadboard shutdown are subject of subchapter 6.1.2.

4.7 Results of Integrated Tests in Simulated Martian Environment

Like in ambient testing, the main goal of tests in simulated Martian conditions is to attain and stabilize the Sabatier reaction. As opposed to the ambient however, this is complicated mainly through the low temperatures that surround the breadboard. It was tried to mitigate this challenge by slightly altering the design of the breadboard during the environment tests, this design alteration is subject of subchapter 4.5.1. The idea is to decrease the temperature difference between the measurement and control hardware on the one side and the surrounding on the other side by introducing a thermal insulation box which shrouds the breadboard frontplate components. This box also incorporates some additional heating capability. However, as outlined in the learned lessons subchapter 6.1.4, it has to be stated, that the commercial of the shelf hardware which made up the breadboard were still challenged by the temperatures, and were only able to work properly for a comparatively short duration. The main problem was caused the flow meters, which were not qualified for low temperatures. Whereas the temperature in the center of the insulation box remained over 0°C at all times, it fell under that value at the corners of the box. Consequently, the systems in this area were the ones that caused the problems. The electrolyzer at the bottom end of the box could maintain an internal temperature exceeding the freezing temperature (freezing of the water would undoubtedly have destroyed the electrolyzer), however the inlet rubber fittings became brittle and started leaking. The flowmeters placed at the upper end of the thermal insulation box seized to work properly after a while, thus changing the inlet flows, which led to a change in temperature, so that some 20 minutes after the deactivation of the heaters the measurements as well as the results started to give false results. This faulty behavior is understandable, since the flowmeters that were used in the breadboard were based on the principle of conduction, which works of course only in the range for which the flowmeter is designed for. Outside this envelope, the fluid properties change considerably, thus leading to unreasonable results.

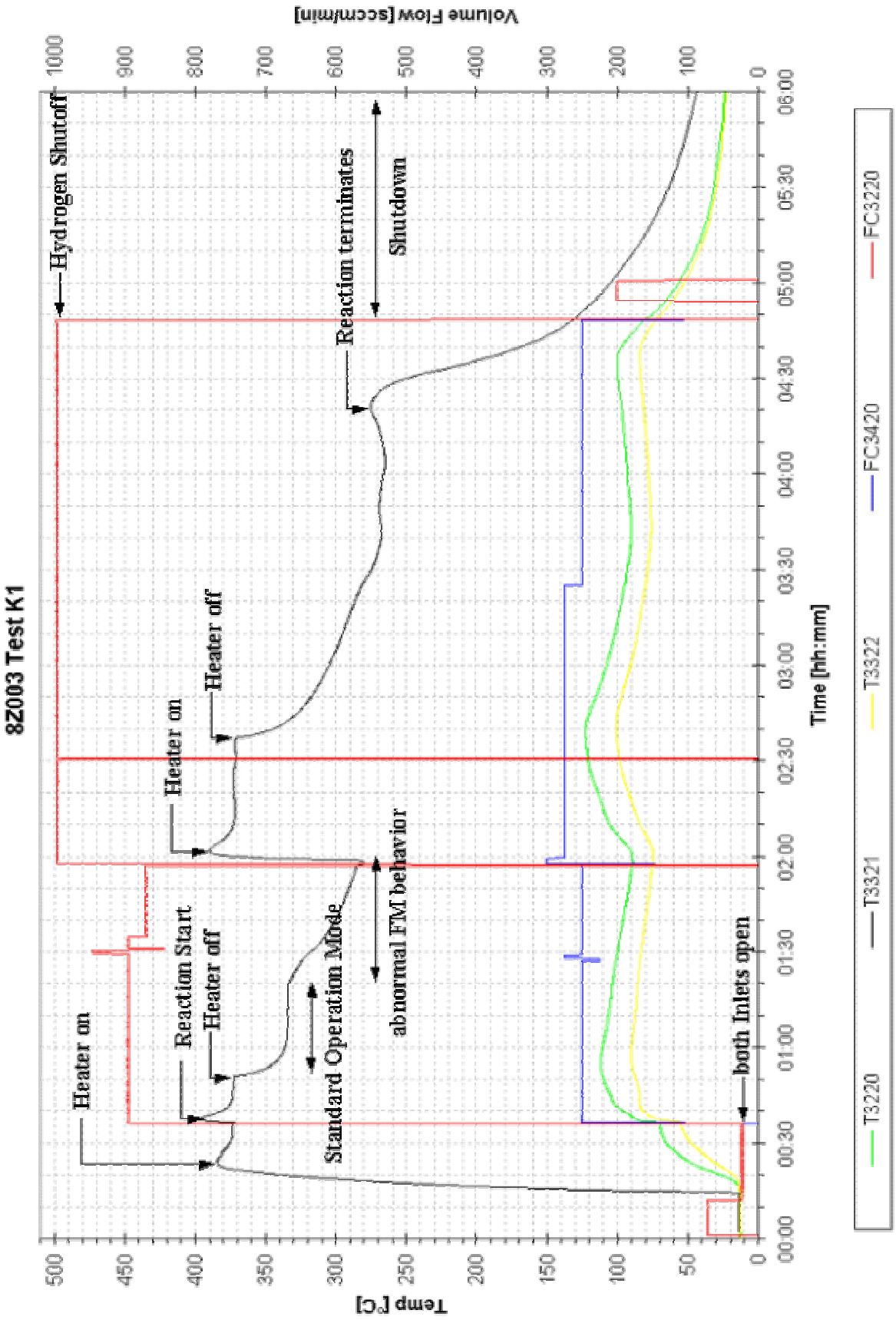

Figure 4-16: Successful Environment Test Run

(Series K, Test 1, 05.12.2000 – Reaction Achieved)

Despite these observations, it however remains a fact that these occurrences can all be attributed to the utilization of hardware that was not qualified for the given environmental conditions. The decision of JSC's Propulsion and Fluid Systems Branch to acquire these hardware components anyway was solely based on stringent budget limitations. Adequately specified hardware would have significantly increased the cost, since qualification campaigns are typically much more cost-intensive than the respective parts themselves. However, even under these less than optimal circumstances, a proof of concept could be achieved.

The usage of adequately qualified hardware will undoubtedly eliminate these effects.

In this chapter, the preparation, the test set up, the procedure and the results of the Sabatier / water electrolysis breadboard tests conducted in Earth ambient as well as in simulated Martian environment were described.
The tests were carried out at the Mars ISRU Systems Test Facility at NASA Johnson Space Center in Houston Texas from January 1999 to December 2001. During environment testing, the usage of not adequately qualified hardware components caused some mischief, however in summary no showstoppers or major technical hurdles were encountered.

5 VALIDATION / COMPARISON OF MODEL AND TESTS

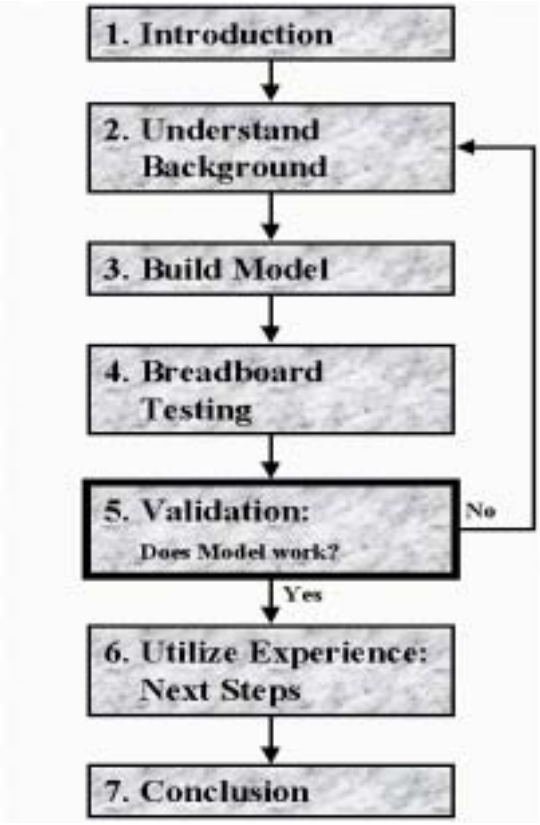

In this chapter, the predictions of the model derived from theory in chapter 3, as well as the results obtained in the test described in chapter 4 are brought together and are then evaluated in terms of accordance.
Only if it can be proven that reality is predicted right by the model, it can serve as a design tool. Consequently, it is the aim of this chapter to compare results of the two preceding chapters to look for divergences and inconsistencies between them, which would prevent that.
However, once this tool is available and validated, accurate predictions and estimates can be expected for follow-on designs and concepts in the future, some of which will be suggested and outlined in chapter 6.

5.1 Outline

During the testing in Earth ambient as well as in simulated Martian environment, the reactor temperature distribution was measured at three separate points with the help of thermocouples: one inside the reactor core (close to the reactor outlet), and two in between the outer reactor wall and the insulation (one at the top, close to the reactant inlet and one at the bottom, close to the reactor outlet). The data of these three sensors was collected every 1, 2, 5, or 10 seconds, depending on setting of the LabView® control. The temperatures are mainly dependent on the heater power, the reactant mixture ration, the inlet mass flow as well as the temperature of the surrounding. All these parameters were also modeled in the computer model as outlined in chapter 3.

Now the task will be to compare the temperature data obtained in the tests with the temperature curves calculated with the computer model. If the data is in accordance, than we actually hold a powerful design tool in hands, since the computer model can calculate the temperatures – as well as any other significant state parameter - at every place within the system, not just the temperatures at the three places mentioned before (see Figure 5-1).

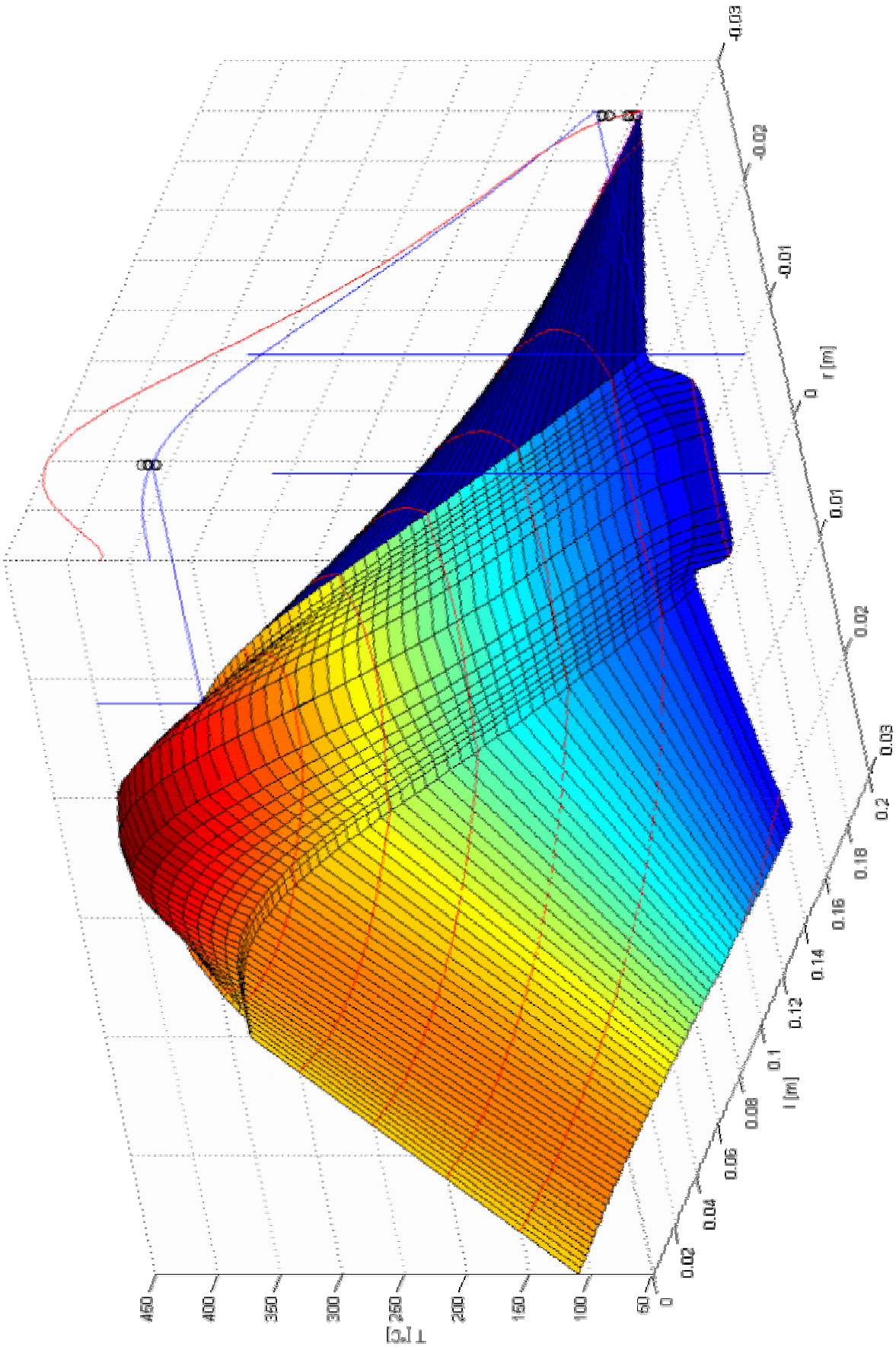

Figure 5-1: Temperature Distribution in the Reactor

5.2 Evaluation of Model Predictions of Atmosphere Acquisition

Upstream of the Sabatier reactor, the sorption pump described in chapter 4.2.1 fulfills it task of providing the subsequent elements of the breadboard with carbon dioxide which it extracts from the atmosphere. The atmosphere acquisition model is based on the formulas that were derived in chapter 3.6.2. Its heart are the Toth equation and the corresponding curve fit constants. The evaluation of model predictions and test results is summarized in Figure 5-2:

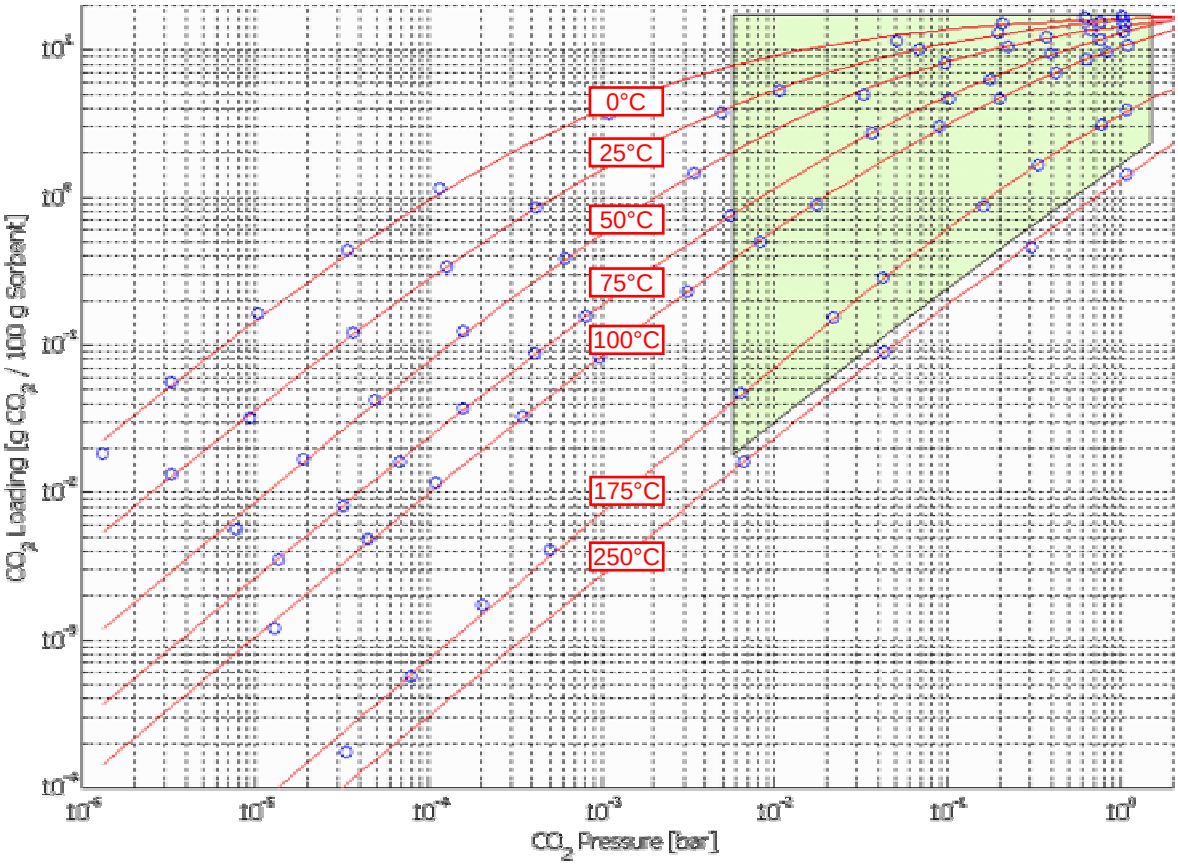

Figure 5-2: CO_2 Adsorption of Sorption Bed as a Function of Pressure and Temperature (in °C)

The accuracy of the sensors in the breadboard acquisition subsystem was not favorable to exact atmosphere adsorption measurements; the aim of the breadboard tests was more on the Sabatier reactor part of the overall system. Fortunately, exact measurements in the course of tests particularly focusing at the adsorption were conducted by Lockheed Martin [Mulloth & Finn, 1998] prior to the installation of the breadboard at JSC. These test results were therefore used for the validation of the adsorption model (all other modeling predictions were validated with breadboard test data). The blue circles in the graph represent the results of the Zeolite sorption bed tests. These tests extended over a

temperature range of 0 to 250°C and a pressure range of 10^{-6}bar to slightly over 1bar. The red lines in the graph show the corresponding computer model predictions for the different temperature levels at which the tests were conducted (red numbers, in °C). The shaded area signifies the envelope in which the breadboard sorption pump is operated in. It is bordered on the one hand by the minimum and the maximum sorption bed pressure, the former being the Mars surface pressure (between 4 and 6 mbars), the latter being slightly over Sabatier reactor pressure (typically around 1.35bar). On the other hand it is also limited by the maximum and the minimum temperature, meaning some 230°C for desorption and Mars ambient temperature for adsorption (or the sorption bed CO_2 load limit respectively).

As it can be seen from the graph, the model and the test results are in very good accordance.

5.3 Evaluation of Model Predictions of Tests under Ambient Conditions

Figure 5-3 shows the comparison of measured vs. predicted reactor temperatures under Earth ambient conditions. The red line shows the calculated temperature distribution at the reactor's symmetry axis (T_c) over the length of the reactor. The blue line represents the predicted temperature distribution at the reactor's vessels outer wall (T_w), a location that is still underneath the insulation. The third line is the temperature at the outside of the insulation, again predicted by the computer model.

The black circles represent test data achieved by the thermocouples at the respective locations: one internal temperature sensor at the outlet end of the reactor (on the symmetry line), as well as two external sensors, one near the inlet, the other near the outlet end of the reactor. The data was acquired during a series of tests, resulting in a distribution of data circles, which however all lie close to the corresponding points on the predicted temperature lines. It can thus be said that the model and the test data are in good accordance to each other.

This means that the model can now be used to estimate temperature levels at locations which are not accessible for thermal sensors. It also can give not just the temperature at a few discrete points, but over the full length and the full radius of the reactor. It can furthermore be used as a design tool for future apparatuses, some of which will be outlined in chapter 6.

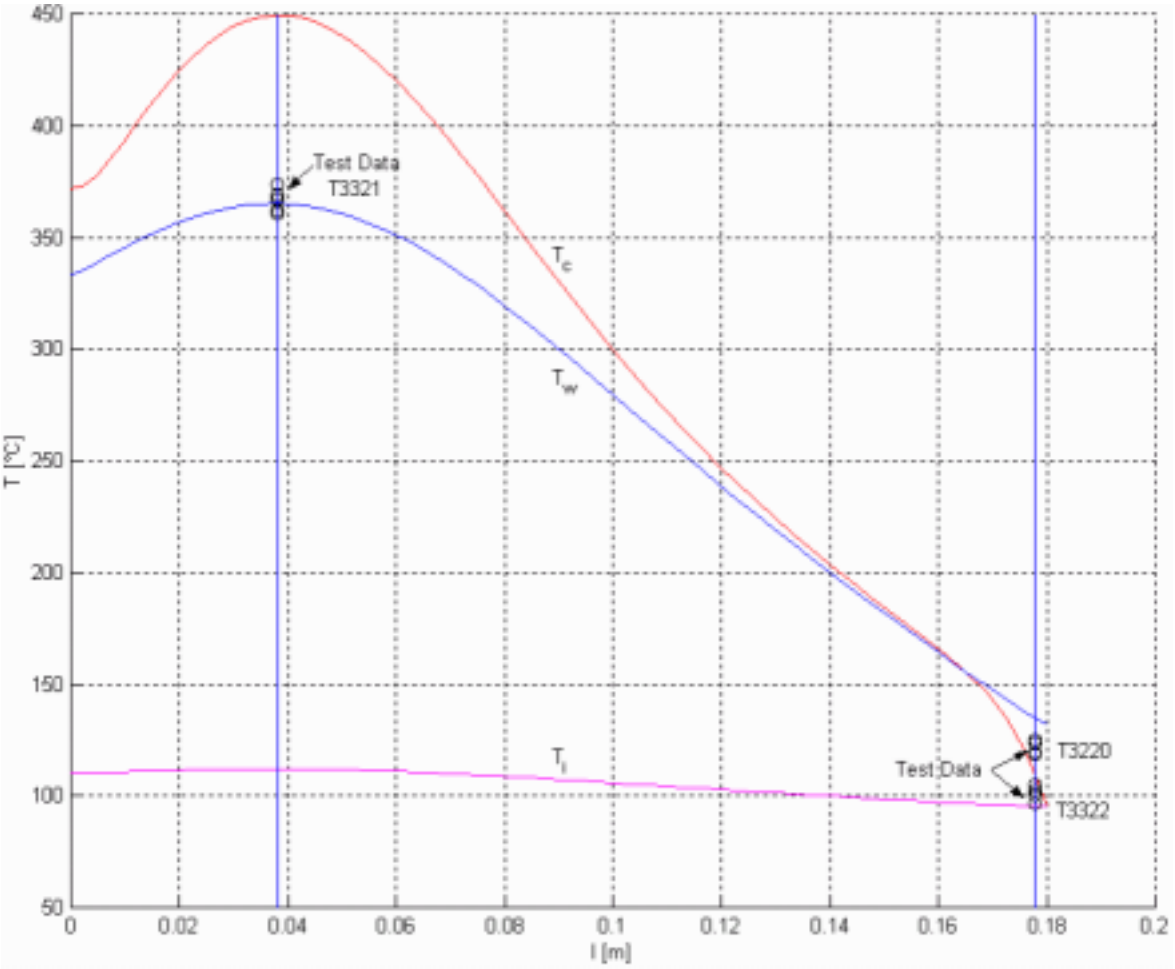

Figure 5-3: Comparison of measured vs. calculated Temperatures under Earth Ambient Conditions (at the **c**enter, **r**eactor wall, and **i**nsulation)

5.4 Evaluation of Model Predictions of Tests in Simulated Martian Environment

Figure 5-4 shows the comparison of measured vs. predicted reactor temperatures in Simulated Martian Environment. Again, similar to the previous chart, the red line symbolizes the calculated temperature distribution at the reactor's symmetry axis (T_c), the blue line the predicted temperature distribution at the reactor's vessels outer wall (T_w), the third line the temperature at the outside of the insulation, and the black circles the test data attained by the thermocouples. In summary, the locations of the sensors remained unchanged.

In chapter 4.7, the sensor problems that occurred during the test were discussed. As outlined, the sensors tended to deliver false results in the later phases of the test runs, so online data from early stages were put into considerations. With this in mind it can be stated, that – unlike the flowmeters - the interior of the reactor remained mainly oblivious

to the altered external temperatures. To draw a conclusion it can also here be said that the model and the test data are in good accordance to each other. This means that this aspect of the model is now also validated and available to be used as a design tool.

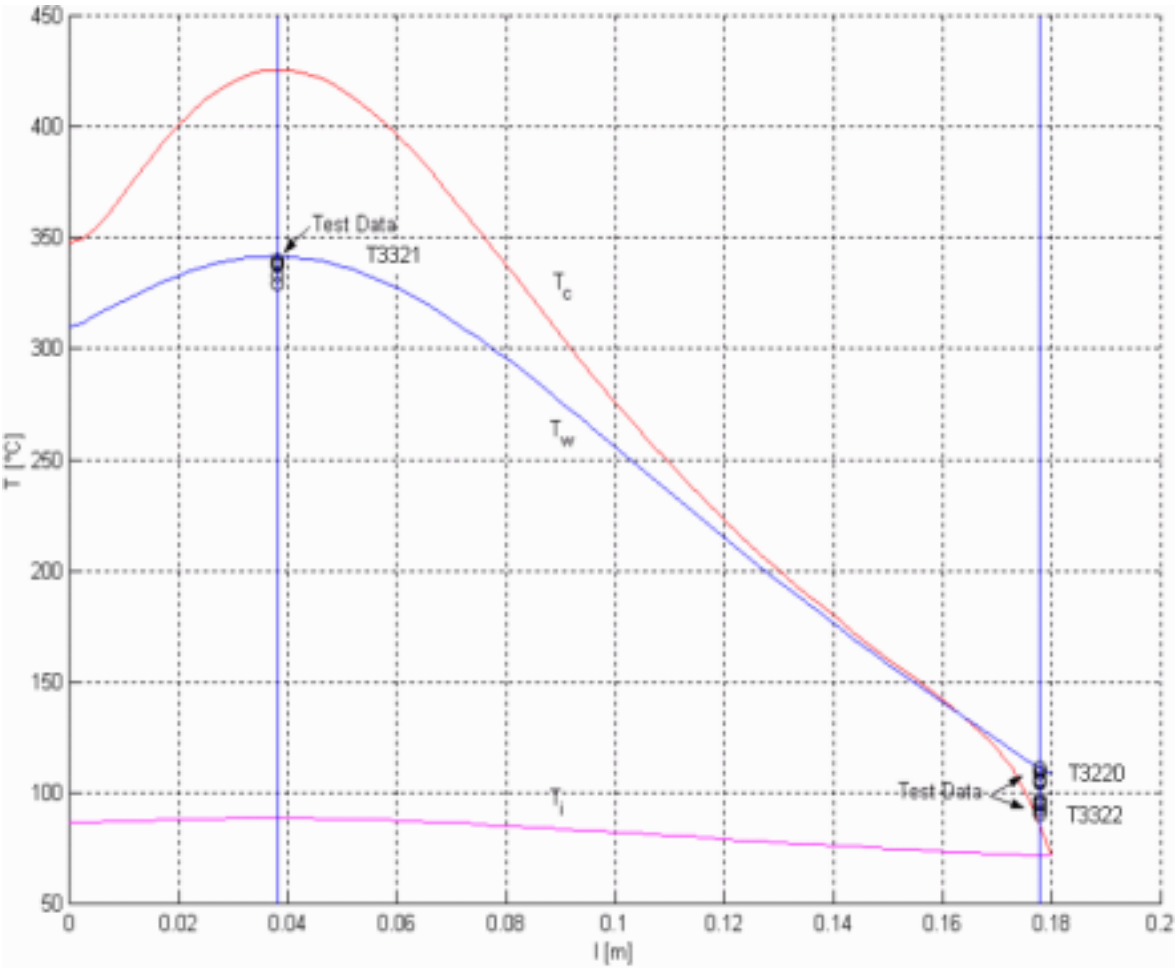

Figure 5-4: Comparison of measured vs. calculated Temperatures in simulated Martian Environment (at the **c**enter, **r**eactor wall, and **i**nsulation)

In this chapter the predictions of the model derived from theory in chapter 3, and the results obtained in the test described in chapter 4 were brought together and are evaluated in terms of accordance. Thereby, the model-based predictions were found to be in good accordance with the tests in ambient and Martian environment.
Using this tool, predictions and recommendations can be can derived, some of which are outlined in the preceding chapter.

6 NEXT STEPS

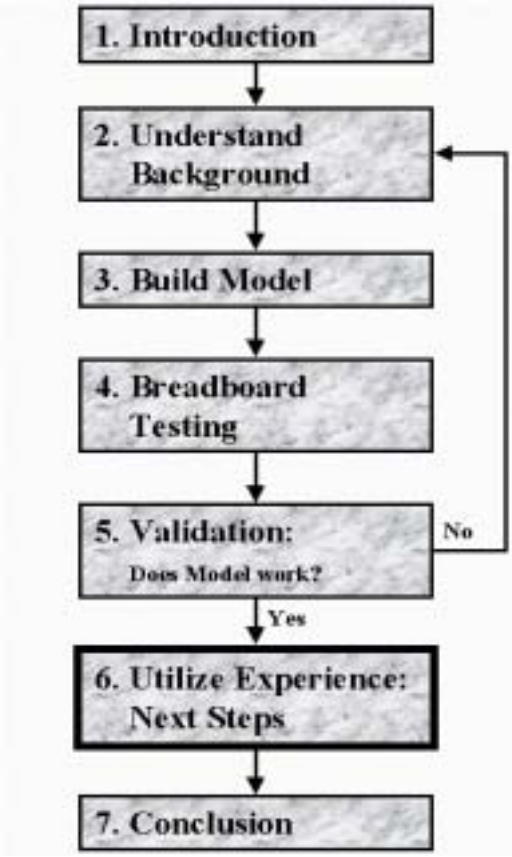

Based on the experience gained during the development of the computer models and during the carrying out of the tests under Earth ambient and under simulated Mars environment conditions, in the following chapter recommendations are given for the design of follow-on breadboards, of flight demonstrator experiments, as well as of hardware for robotic and human missions in the far future.
The chapter commences with a detailed summarization of the learned lessons of the Sabatier / water electrolysis hardware tests. Based on this summarization, suggestions intended to resolve the described problems are made; additionally, recommendations for the future are derived.

6.1 Learned Lessons of the 1st Generation Breadboard

As a first step before deriving recommendations and plans for the future, a look at the lessons that where learned during the testing of the breadboard shall now be taken.

6.1.1 Filling and Draining of Water into and from the Breadboard

Observation:

In the current setup the crew that sets up the test has to break a fitting in order to inject the water into the system. The removal of the system's water is even more difficult, since it not only involves breaking a fitting, but also soaking the water out (it is arduous to get all the water out of the system, if it has several low points where it can accumulate).

Recommendation:

Depending on whether there is a requirement for system flushing after operation, the system should be equipped with two or more valves throughout the system. Piping design

with lots of up and downs in the gravitational field should be avoided, since it complicates the introduction and removal of liquids to and from the system.

6.1.2 Flooding of Reactor

Observation:

As described in chapter 4 the flooding of the reactor caused quite some trouble and confusion. This usually occurs once the reaction in the reactor is ended. At that point, the reactor is filled with hydrogen and carbon dioxide (coming in as reactants for the reactions via the inlet) as well as methane and water vapor (which are produced in the reactor). According to the Sabatier Reaction

$$C0_2 + 4H_2 \rightarrow CH_4 + 2H_20 \ (+ E)$$

This reaction produces heat; therefore the reactor temperature drops significantly after termination of the reaction. This however leads to the following:

Two thirds of the volume of the reactant gas stream is water vapor. Upon temperature decrease this water vapor starts to condense *within* the reactor, thus decreasing the pressure in the reactor. This pressure drop now creates a pressure difference between reactor and the succeeding condenser tank, thus causing to suck the water back up the pipe and flooding the reactor. This actually became obvious in September 2000, when the reactor was taken apart to investigate the level of degradation of the catalyst. Surprisingly the catalyst was wet (see Figure) – a result of the prior testing.

Figure 6-1:
Wetted Catalyst

Also, during a couple of tests, a pressure difference (some 17kPa) was observed between reactor and condenser tank, which almost went to zero after reactor heat up. This can be explained by water that bedewed the filter at the bottom of the reactor casing (designed to filter small pieces of catalysts from wandering downstream). It also seems that a wet reactor under certain circumstances (if it was completely flooded) is not able to sustain a reaction without prior (extensive) drying by turning on the reactor heaters. This is certainly undesirable.

In one case, water vapor was even found in the $C0_2$ flow meter that precedes the reactor. The flow meter had been dismantled from the system since it showed abnormal behavior. Water can very well cause abnormal behavior in this kind of flow meters since they are based on heat flow measurements, which are different for different substances. Thus,

water (esp. liquid water) in a $C0_2$ flow meter will certainly lead to faulty control behavior. How the water got into the flow meter could not be explained yet.

Recommendation:
There are to possible solutions to this problem:

1. Purging:
   Upon test end, only one instead of both reactant streams is turned off. As result, the reaction still dies, however products which still reside within the reactor are "washed" out of the reactor, thus the pressure drop is smaller and not sufficient to lift the liquid water back up into the reactor. This however means that significant amounts (as opposed to just traces like during nominal operations) of either hydrogen or carbon dioxide attain downstream. The hydrogen could be filtered using the hydrogen recovery pump; the carbon dioxide could be released to the environment. The hydrogen flushing however will undoubtedly lead to an increased hydrogen loss in the system; the carbon dioxide flushing on the other hand could raise the problem of the creation of carbonic acid in the condenser tank. Both are undesirable.
2. Valve:
   An extra valve is added downstream of the reactor. This can either be a manual valve (which is closed at shutdown) or a check valve (which prevents the water from the condenser tank to re-enter the reactor). This however adds mass and risk of failure (CV3320 seemingly did not work).

Compare this issue also with the problem described in 6.1.3.

The issue of the increased pressure difference due to water in the filter could be solved by an additional heater at the bottom of the reactor vessel that would be used to dry the filter prior to reactor turn-on.

6.1.3 Vent Path for Trace Gases

Observation:
During startup, when the reaction has not yet started, but the reactants are already flowing, hydrogen attains downstream. This is comparable with the described drawback of the suggested purging solution of 6.1.2. Hydrogen gets downstream to the methane, when the recovery pump is on, to a much larger extent of course if the pump is not turned on. In any case, the system has to be able to cope with the fact that both, hydrogen and carbon dioxide, can accumulate in the methane storage tank[1]. During the

[1] In fact, the same is true for any other possible trace gases. The amount may be minute (as it has been shown in modeling and testing), however these gases will accumulate at the storage end of the system; thus the system has to be able to cope with them, e.g. by means of venting. On a lighter sight of the problem stands the fact that the environmental impact of this approach had to be evaluated during the TRR (test readiness review) as described in chapter 4.3.

1st Generation Breadboard Tests this was not an issue, since due to cost reduction reasons only the oxygen side actually had a storage tank (the methane was simply vented) – however this issue will come up once both propellants will be liquefied.

Recommendation:
Like in the case of turn off, a startup with both reactants is undesirable. One solution could be a recycling of the product stream back into the reactor – during startup, before the nominal temperature is reached, the outlet flow of the reactor is not led to the condenser tank, but rather recycled back to the reactor inlet. With that, the temperature increase would be much faster and the amounts of hydrogen and carbon oxide that attain downstream could be reduced. Once nominal reactor temperature is reached, a 3-way valve turns to reach nominal flow directions.
However, it is questionable whether a recycling can be achieved without a pump.

6.1.4 COTS vs. Martian Requirements

Observation:
Due to limitations in funding, most of the materials was commercial off the shelf (COTS) as well as residual material from other programs and tests. Although any of this material was ever intended to work on Mars or in simulated Martian environment, the testing in Martian environment resulted in the production of propellant and can be rated a success. The instruments chosen for the breadboard had to be chosen according to whether they seemed to be the right ones for the job – they were not chosen according whether they were certified for the job. Certainly this is not optimal, but limited money resources did not life other choices. Being a breadboard, it – per definition – cannot be flight ready hardware, this has to be kept in mind.
However, one should keep in remembrance the things in the design that certainly will have to be changed before it can sally forth to the Red Planet:

1. Flow meters:
   As outlined already in chapter 5.4, during the Mars environment testing the flow meters were fooled by water, as well as temperature and pressure changes. The flow meters used in the 1st Generation Breadboard are based on changes in thermal flux, which increases with increased mass flow. However, this is not the only variable it is a function offers. Other influencing factors are e.g. fluid thermal properties. These are listed in tables. However, being a black box, it is hard to reproduce how other factors come into play, namely different Martian environmental parameters (e.g. local gravitational acceleration g, atmosphere composition and pressure, etc.). For a flight unit these black boxes either have to be opened, understood and certified for Martian environment; or different ways to measure mass fluxes have to be employed which are better understood and/or less susceptible towards the environment they are in.
2. Sensors:
   This question of reliable sensors and controllers affects the question of whether

the system can be controlled effectively or not. No complex system can function if the parameters needed for the controller are faulty. It was not possible to see the indications for the commencement of the Sabatier reaction (see chapter 4.6), due to reasons connected with the software. This problem could not be identified (and thus solved) during the first seven tests. Failure Determination, Identification and Mitigation can only work if every element of it (the determination, the identification, and the mitigation) works. During the very first runs this became very clear: the provider of the Sabatier reactor subsystem had stated the initiation of the reaction could be clearly seen from a "rapid temperature increase and a raise in the water vapor content of the outlet stream". The problem with that was that the LabView, the software that is used to control the system, was configured to "auto scaling". Auto scaling is a software function that ensures, that the graph of a function does not "wander off the chart". If there is an increase, it automatically alters the axis. Another example of that is the water level indicator: the outlet pipe of the reactor in the 1st Generation Breadboard is led into the condenser tank. With methane being one of the constituents of the stream that enters the condenser tank through a submerged pipe, even with all the water in the stream already condensed, there is still a lot of bubbling going on in the reactor. The turbulences of the water level caused by these bubbles was in fact completely covered the effect of the slowly increasing water level – since the sensor only measures the height of the water level in the tank. Due to reasons like these two, the perceptions of the people operating this system was completely different compared with the impressions that the test team of the provider received who used a different sensor and control systems.

Recommendation:

For coming generations of breadboards as well as hardware it has to be made clear that COTS hardware is hardly up to the challenge of coping with the Martian environment. With special considerations it has to be made sure that the hardware used is not only designed, but also tested and certified to cope with Martian environment. This is not so much a engineering but rather a cost problem.

6.1.5 Pressure Control throughout the System

Observation:

The original concept in mind during the design process of the 1st Generation Breadboard was that the two backpressure regulators at the downstream ends of the system regulate the pressure upstream. However, in practice it showed that the attempted closed loop control these regulators were programmed for did not really succeed. The automatic pressure control seemed always to be bumpy, never really smooth; it proved in fact less inconvenient to regulate the system manually. In some cases, water even went the wrong way (upstream, compare issue 6.1.2). Certainly this needs to be worked on.

Recommendation:
No recommendation can be given at this point.

6.1.6 Check-Valve Problems

Observation:
Some of the check valves in the system didn't work, especially at places where they were supposed to hold back hydrogen (especially CV3220).

Recommendation:
This problem seems to occur especially when water is present in the area around the check valve. The mitigation should thus be attempted similar to that proposed in chapter 6.1.2.

6.1.7 Corrosion of Brass 3-Way Valve

Observation:
Within a month(!) after commencement of the breadboard testing, the pipe wall had not only corroded at the wall but all they way downstream to the O_2-dryer.

Recommendation:
A detailed analysis conducted by the chemistry lab of NASA Johnson Space Center of the problem uncovered an amazing plethora of different elements that led to this occurrence (accelerated corrosion due to oxygen solved in the water, occurrence of carbonic acid, local element). Therefore it was decided to not use brass elements throughout the system. The use of stainless steel solved those kinds of problems, and the cost difference between the two is marginal.

6.1.8 Carbonic Acid Production

Observation:
During Startup and Turn-off (whenever CO_2 *leaves* the reactor) there is a risk of carbonic acid (H_2CO_3) build-up in the condenser tank. This occurs when the CO2 in the condenser inlet stream dissolves in the liquid water of the condenser tank. This does not lead to any immediate problems, however it should be kept in mind - since the existence of acids in the system is hardly favorable.

Recommendation:
Compare with the recommendations for issue 6.1.3.

6.1.9 Loading of Reactor and Dryers

Observation:

The loading of the reactor as well as both dryers in the current configuration is inconvenient at best. Often, during loading both catalyst pellets and sorbent material get crushed. The act of loading also threatens the internal thermocouple (see Figure 6-2), which basically has to be forcefully pushed through the catalyst bed from the top.

Figure 6-2: Reactor Top with Thermocouple

Recommendation:

The new reactor design of the 2nd Generation Breadboard should separate the two functions of thermocouple fixture and reactor vessel closure. This can be achieved if the thermocouple penetrates the reactor vessel from the bottom whereas the reactor vessel can be filled, emptied and sealed from the top. Same principle can and should be employed for the dryers.

6.1.10 Sample Port Location

Observation:

With the current location of the sample ports after the dryers, it cannot be measured how much CO_2 leaves the electrolyzer, since it could be that this CO_2 gets absorbed by the O_2 dryer.

Recommendation:

It would be advantageous to place sample ports before the dryer. More preferably have sample ports before and after the dryers. Thus, the performance of the dryers can be evaluated, too.

6.1.11 Storage Vessel Evacuation

Observation:

During ambient testing, the O2 storage tank can be evacuated to the vent by opening valve SV3110. This is possible, since the storage pressure will be above or at atmospheric pressure (≈ 1 bar). However, during Mars environment testing, the system pressure was reduced to decrease the relative pressure between the subsystems and the low chamber pressure (≈ 6 torr). Thus, the storage vessel pressure actually was below atmospheric pressure. The product outlets should accommodate the evacuation of the storage vessels (see also 6.1.1).

Recommendation:

The decrease in system pressure was mainly aimed at reducing the stress for the not Mars environment certified hardware of the 1st generation breadboard. With coming generations of breadboards, less caution has to be taken, thus this problem should be eliminated.

6.1.12 Water Level Measurements

Observation:

The water level measurements in the condenser tank were usually very “noisy”.

Recommendation:

As already described in 6.1.4, the turbulences of the water level were caused by these bubbles was in fact completely covered the effect of the slowly increasing water level. It will be shown in 6.2, this problem will unfortunately intensify with the 2nd Generation Breadboard.

6.1.13 Over-sizing of Condenser Tank

Observation:

During ambient tests, by watching at the condenser inlet temperature and by touching the cooling loops between reactor and condenser tank, it could be noticed that both, cooling loops and condenser are considerably oversized for their job, at least for ambient condition, but probably also for operation in Martian environment.

Recommendation:

While a freezing of the condenser content certainly would be very damaging for the system, also too high water temperature (or even a not completely condensed water inlet stream into the electrolyzer) can damage subsystems in the vicinity, it should be no

problem to ensure operation within a certain range, provided that the thermal model of the electrolyzer is accurate enough. In this case, the 1st Generation Breadboard actually has to sustain higher stresses than the actual flight unit – since it has to operate in a wider temperature range (thermal flux varies considerably with decreased environment pressure and temperature). With the delivery of the 2nd Generation Breadboard's electrolyzer, it became obvious that staying within the input water temperature range and proper handling is crucial in order to prevent leaks in the seals – this explains the leakages in the 1st Generation Breadboard's electrolyzer (for which no maintenance guidelines and no temperature ranges were ever issued) after several months after the beginning of the tests.
During Martian night (since a condenser per se has to be connected to a thermal sink) heaters or a thermal shutter would have to prohibit freezing. Alternatively, evacuating the condenser tank over night could be considered.

6.1.14 Static Electricity Problems

Observation:

Some of the hydrogen recovery plumbing is connected via metallic pipes to the anode directly. This led to interferences with the data acquisition system.

Recommendation:

The solution that was employed in this case was a combination of non-conducting plastic plumbing interfaces and non-conducting Teflon insulation. This solution should be kept in mind for future breadboard and flight hardware generations.

6.1.15 Sabatier Reactor Heat Management

Observation:

Especially during the beginning of the tests the heat management was a major contributor to unsuccessful tests – mostly as a result of wrong interpretation of sensor data (compare with 6.1.4), also in this case. During routine work at the reactor, the copper removal strap was put back on the reactor, however at an altered location (higher, see Figure). By moving the reactor heat removal copper strap upwards on the reactor vessel, the thermal flux was altered to an extent that prohibited a sustained reaction.

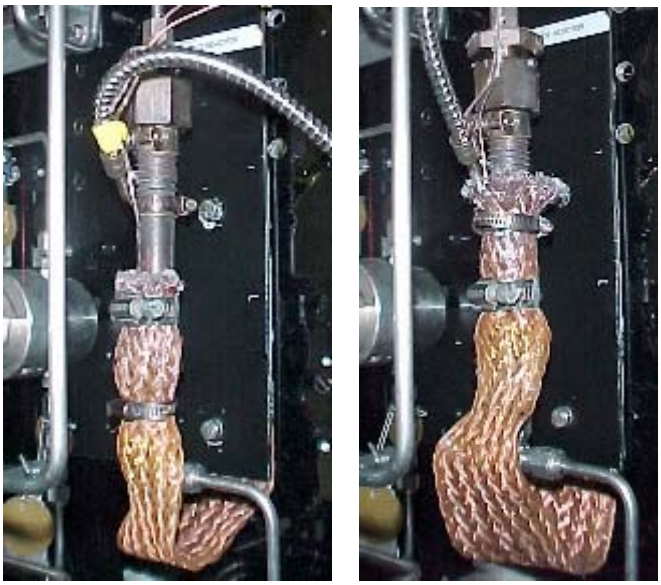

Figure 6-3: Installation of Copper Strap (Correct and Incorrect)

Recommendation:
The Sabatier reaction needs a certain minimum temperature to get started. This temperature depends on the pressure within the reactor vessel as well as the reactants. A clear understanding of these interrelations is one of the main aims of this thesis. Heat flux throughout the reactor as well as reaction kinetics modeling should be major design drivers from the beginning of the design process on. For future generation of breadboards and flight hardware, options like variable heat rejection, counter flow reactor vessel layouts as well as intensified temperature measurements throughout the system should be taken into consideration (see also 6.2).

6.1.16 Water Supply for Electrolyzer

Observation:
At a few occasions during operation, the inlet pressure into the electrolyzer fell short of the required level, resulting no or strongly reduced H_2/O_2 production

Recommendation:
Second storage vessel that ensures sufficient pressure difference, e.g. by a water column (however, the required pressure is equivalent to a 5m water column).

6.2 Second Generation Breadboard

Based on the experience gained during the modeling and testing of the first Sabatier / Electrolyses Breadboard and due to the circumstances described in chapter 2, it was decided to initiate a 2nd Generation Sabatier Electrolysis Breadboard as an interim step between the first one and spaceflight hardware. The core of the new system is a new,

counterflow reactor (see Figure 6-4), which has been iteratively optimized in the course of the design process based on the computer models that were validated with the test related to the first breadboard.

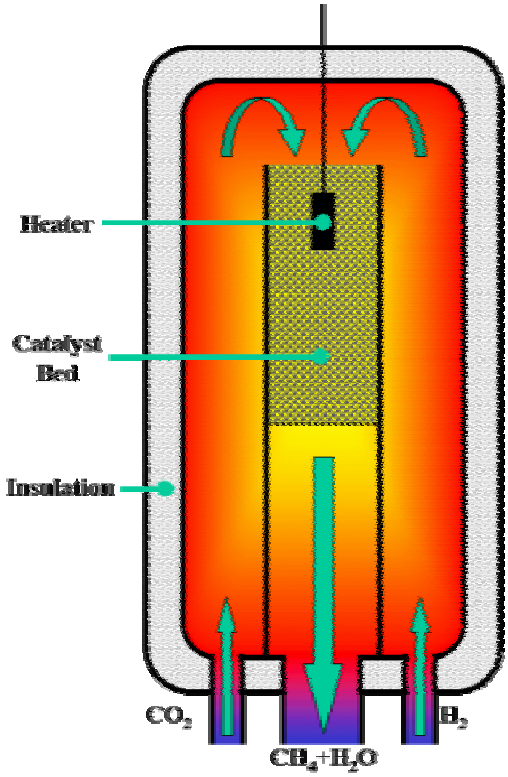

Figure 6-4: Conceptual Design of 2nd Generation Sabatier Reactor (Initial Design)

The new reactor will feature an augmented reactor pressure as well as a liquid cooled electrolyzer (see Figure 6-5). The computer model however has revealed that an increase in reactor pressure will lead to new problems, since the water vapor close to the cold end of the reactor already in the current 1st generation breadboard comes dangerously close to the point were it starts to condense. At the elevated pressures that are currently discussed in the context of the new breadboard condensation will become unavoidable. However, as the experience with the 1st generation breadboard has shown (see chapter 6.1.2), a flooding of the reactor bed is certainly not desirable.

There is also a second point, where the efficiency of the new breadboard is put at risk. In the course of the design of the follow-on breadboard, the propulsion branch issued an request for proposal for an electrolyzer out to industry. Unfortunately only for proposals were handed in, all of which did not really fit the requirements. The one that was selected worked at elevated intake pressures, which led to a need for a boost pump upstream.

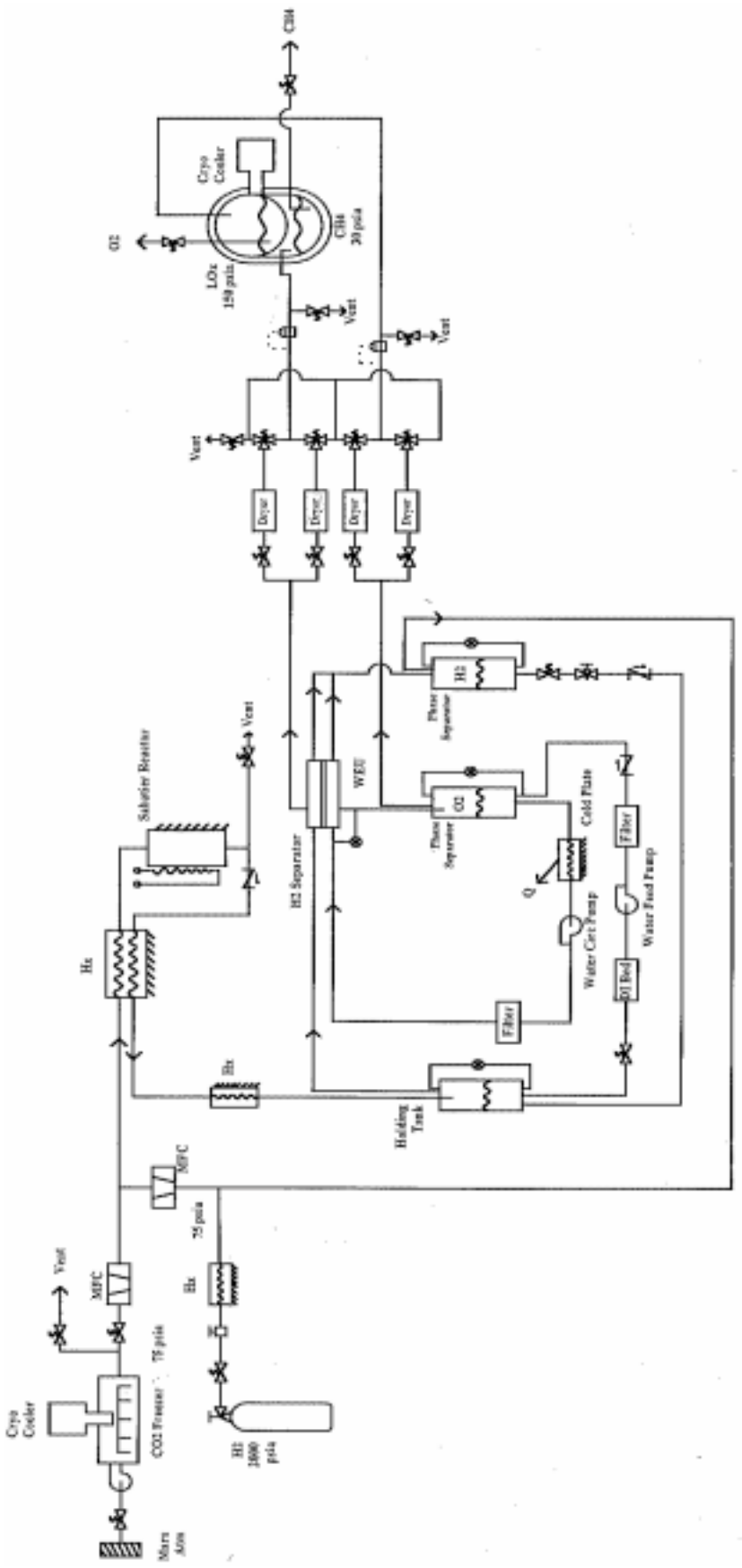

Figure 6-5: 2nd Generation Sabatier Breadboard - Draft Design [Trevathan, 2001]

Furthermore, the electrolyzer takes in water not only for electrolysis, but also for cooling. In fact, the intake for cooling water exceeds the electrolysis mass flow rate.

The overall system now is unfortunately driven to a great extent by these facts, which are mostly a result of limited financial resources, since they hardly leave room for dedicated designs but dictate the choice of COTS hardware[1].

Reactor Grid for 2nd Generation Breadboard

Part of the breadboard is the new layout featuring a counterflow reactor as outlined in Figure 6-4.

In order to derive an optimal design for the reactor, a detailed model of it was set up beforehand and different where emulated and tested electronically with the help of the computer. For this, the grid structure of the reactor had to be improved, as shown in the following picture (Figure 6-6).

[1] However, it should be noted that Astrium Friedrichshafen developed as part of their life support system for the ISS a dedicated, space-qualified electrolyzer which would well satisfy the requirements of the 2nd generation breadboard.

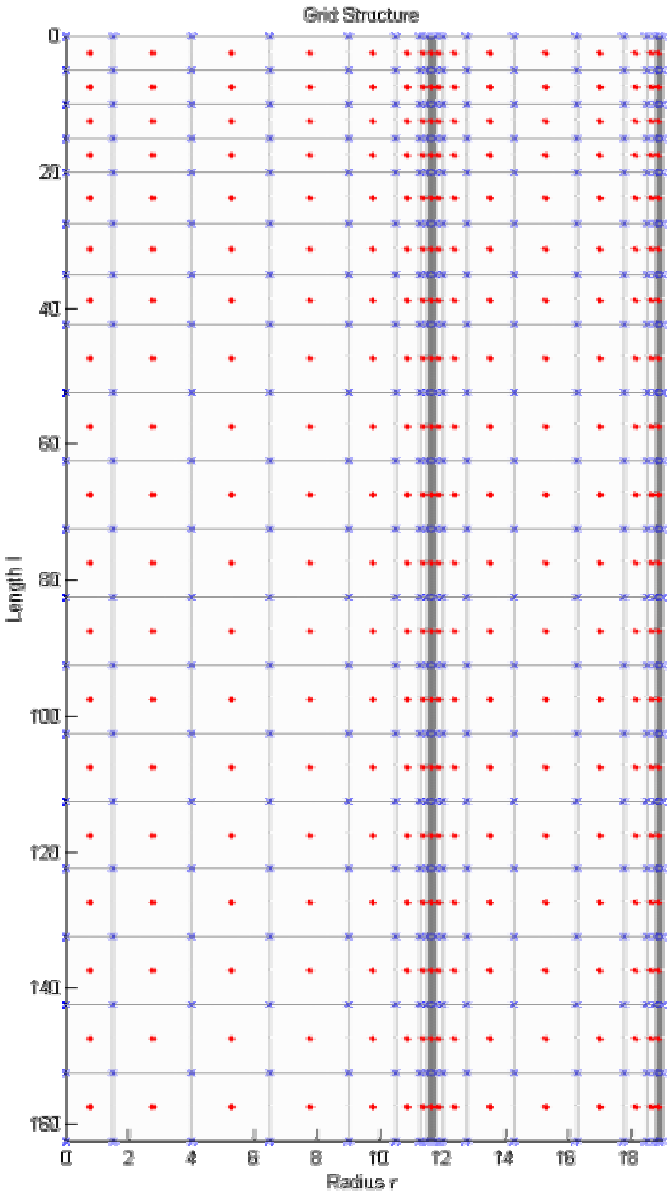

Figure 6-6: Grid Structure of 2nd Generation Breadboard Reactor

As a first step in the design of the 2nd Generation Breadboard, the fundamental parameters such as mass flows and pressures were evaluated, based on the EXCEL models presented in chapter 3.6.(see Figure 6-7).

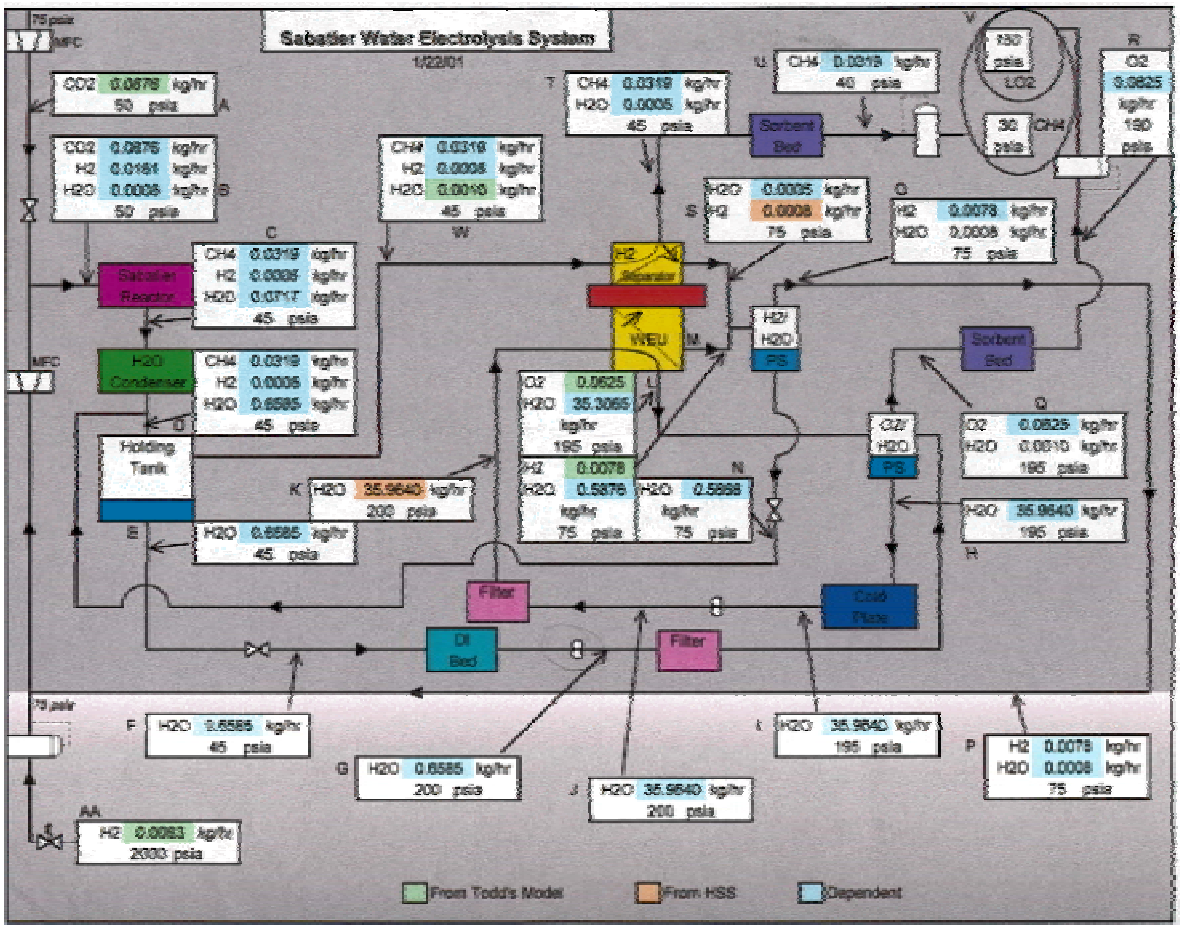

Figure 6-7: Massflow Analysis 2nd Generation Breadboard

According to these basic parameters, off the shelf hardware had to be found (example: electrolyzer); where that was not available, hardware had to be newly designed (example: Sabatier reactor). Based on this preliminary work, a first draft design was made (see Figure 6-5).

This draft design again was further analyzed and through iterative design steps, the design process was further pursued. Part of that process were the further refining and adaptation of the MATLAB® model as well as configuration concepts based on ProEngineer®. The latest status can be seen in Figure 6-8:

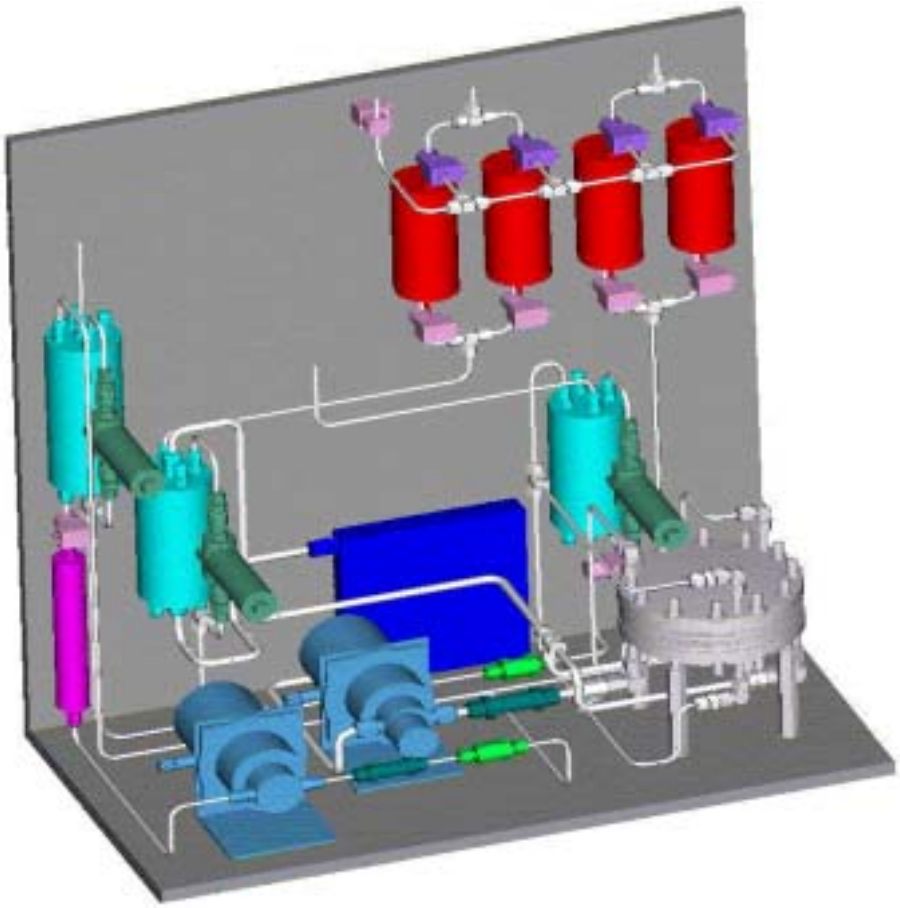

Figure 6-8: Latest Layout of 2nd Generation Breadboard [Simon, 2001]

In this drawing, the gray flat cylinder represents the electrolyzer, the four red cylinders in the upper right are the dryers for methane and oxygen; also shown are the two pumps in light blue, as well as the flat hydrogen separator in blue.
Based on the developed MATLAB® model, the user can (via the model's user interface) emulate the performance behavior of the reactor, as well as of the any vital parameter - anytime and anywhere within the reactor, long before it is actually built as shown in Figure 6-9 (the respective parameter values are color coded corresponding to their respective color bar):

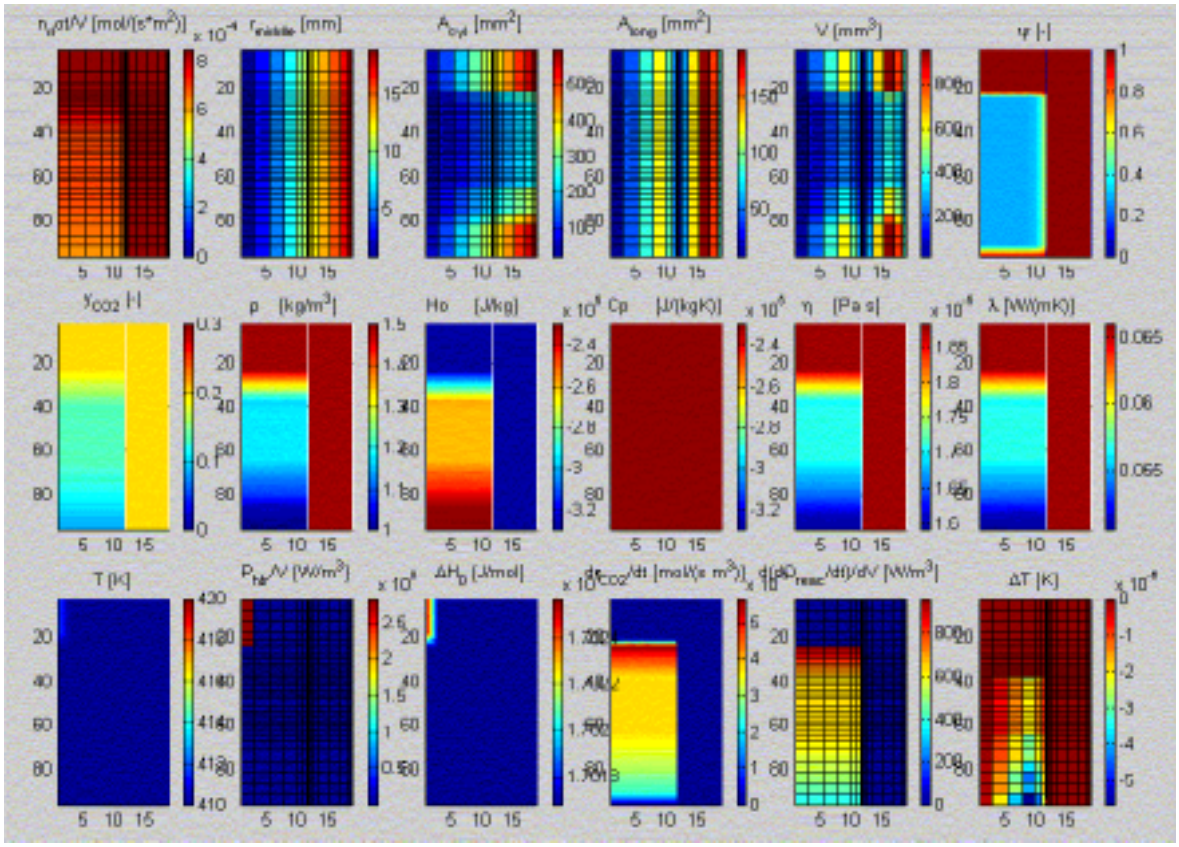

Figure 6-9: Model User Interface - Vital Parameters of 2nd Generation Breadboard

The adaptation of the model to the parameters of the new breadboard, as well as the hardware design process are still ongoing. The 2nd Generation Sabatier / Electrolysis Breadboard is scheduled to be turned on for the first time in early 2002.

6.3 Sabatier ISRU Demonstrator for Mars Surveyor Program Missions

As a next step after a 2nd generation breadboard, two new main goals should be set in order to facilitate the further development of ISRU systems:

1. Decrease system mass and size.
2. Transition from breadboard to flight hardware

It should be stated that the concepts proposed for the MIP follow-on experiments “PUMPP” (Propulsive Use of on Mars Produced Propellant) where certainly most efficient.

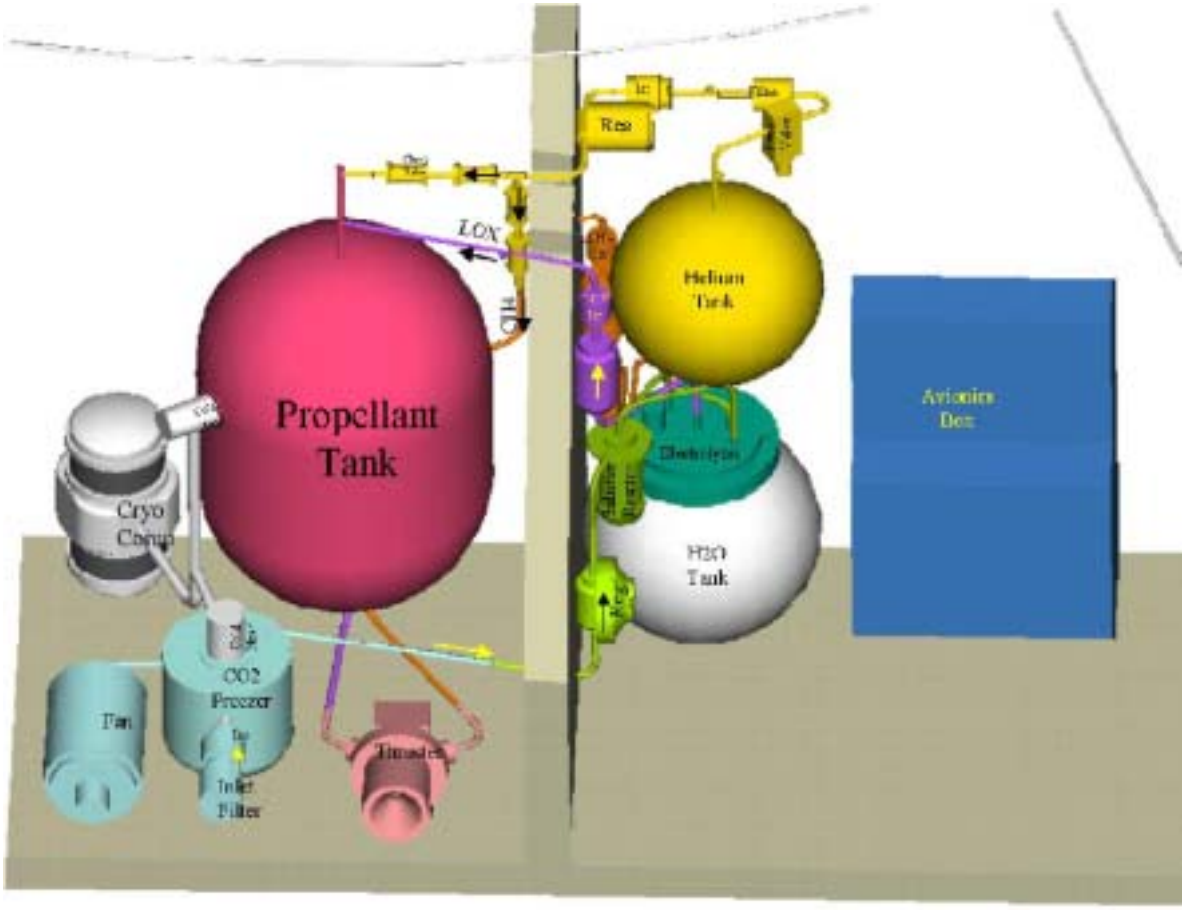

Figure 6-10: PUMPP ("Propulsive Use of on Mars Produced Propellant") Experiment - Preliminary Layout with Lander Shroud [Spencer, 2000]

One can only hope that the first decade of the new millennium sees a demonstrator mission featuring some of the proposed concepts.

Another concepts that should also be employed in order to aid to aid in achieving the two goals that were defined before is the so-called "micro-channel technology". This technology is patented by PNL Inc. from Sacramento, CA, and was until mainly focused at terrestrial applications such as e.g. methanol reformers for fuel cell cars. The idea is as simple as it is compelling: instead of choosing the classical way of chemical engineering where different parts of an overall system are connected with each other via pipes, pumps, and valves it is tried here to downscale and miniaturize all the subsystems and to integrate them into one element. The micro-channels are cut out of the ceramic using chemical edging (similar to that used in micro-circuit production). In the end, the system is thus reduced to a single block of ceramic material which consists of a stack of different layers, each providing a different function, such a e.g. Sabatier reactor, electrolysis, heat exchange, etc.
This concept is advantageous in many ways. First of all, validation is simplified greatly: instead of accepting the inaccuracies that often occur when flight systems are designed

that by up-scaling of their proof-of-concept predecessors, in the case of micro-channel technology in order to achieve higher flow rates, the amount of stack elements is simply increased, while the respective elements remain unchanged in size. Second, the mass (and also the power) requirements are reduced significantly. Furthermore, this technology holds great potential for commercially beneficial spin-off, since in twenty years the Earth might very well be covered with millions of fuel cell cars featuring methanol reformers.

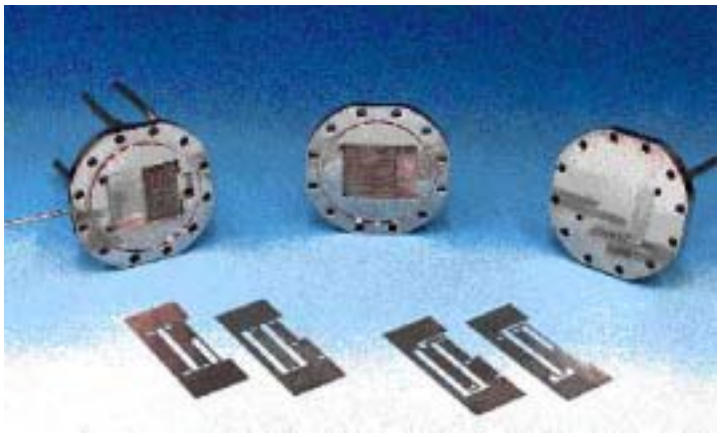

Figure 6-11: Micro-Channel Technology [PNL, 2001]

Along those lines, it can be stated that the emerging science of nanotechnology (lately portrayed in [SciAm, 2001]) holds a great potential for further improvements, not only - but in particular - in the area of in situ resource utilization. A detailed description of this goes beyond the scope of this thesis, however some of the concepts where already outlined in [Eckart, Pauly, et al., 2001].

6.4 ICONPROM - Integrated Consumables Production on Mars

The final step in the application of in situ resource utilization consists of human missions to Mars, which is the subject of this chapter.

6.4.1 Drawbacks of current Planning

In the current planning of the first human Mars missions, such in NASA's Design Reference Mission (see chapter) or in the Russian ITCP concept [ITCP, 2000], the different subsystems are often seen very isolated from each other; consequently, potential synergies are overlooked. A selection of characteristic elements of current program architectures is shown in Figure 6-12.

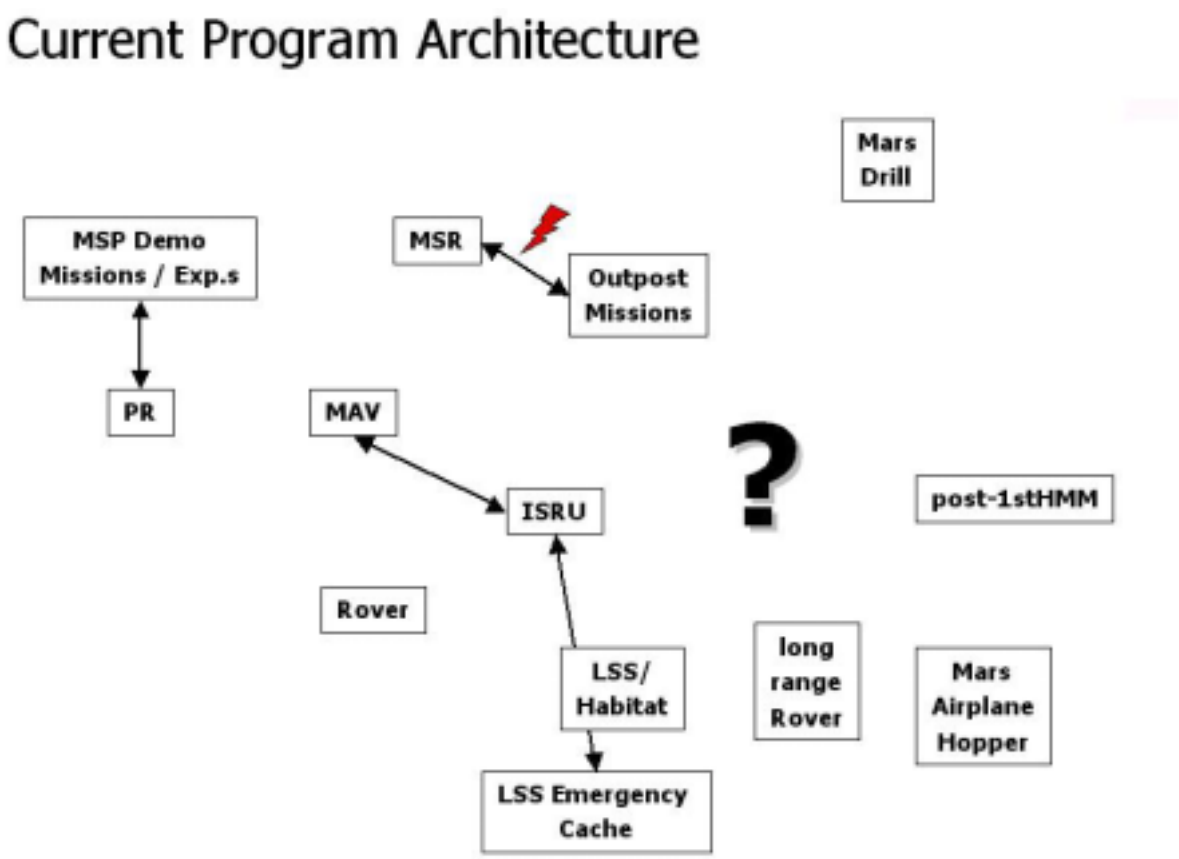

Figure 6-12: Elements of Current Program Architecture

The overall system "Mars program architecture" contains a number of precursor elements to a human Mars mission such as robotic spacecrafts, as well as sample return and outpost missions. They are succeeded by the preparatory elements of the human Mars missions which are pre-deployed to the Red Planet, such as in situ consumable production plants, as well as in Earth return and Mars ascent vehicles. These set the stage for the actual crewed missions, which require and consist of habitats for the astronauts with redundant life support systems, emergency caches, unpressurized (short-range) and pressurized (long-range) rovers, and experiments such as drills designed to explore depths up to a few kilometers. Follow-on missions, meaning 2nd generation missions that will take place after the first set of crewed missions, may involve also alternative transport systems, e.g. Mars hoppers.

These different missions can make up a valid, workable Mars architecture, which however fails to achieve optimum performance for a given input of effort.

6.4.2 IconProM – The Concept

In order to optimize the overall efficiency of the Mars program architecture, it is necessary to engage systems thinking rather than subsystem thinking. [Senge, 1990] defines systems thinking as follows:

"Systems thinking is a discipline for seeing wholes. It is a framework for seeing interrelationships rather than things, for seeing patterns of change rather than static 'snapshots'".

Based on this thinking, in the following a new approach for an Integrated Consumable Production on Mars (IConProM) is presented. IConProM connects the different subsystems and elements

- robotic spacecrafts (orbiters & landers)
- Mars sample return missions
- outpost missions
- in situ consumable production plants and mars ascent vehicles (pre-deployed)
- crew transfer vehicles and surface habitats
- redundant life support systems
- emergency caches
- (un)pressurized rovers,
- Mars drills
- Mars hoppers
- others

into an unified, integrated overall system in which the different subsystems avoid to lead isolated existences and attempt to identify and utilize synergy potentials (see also [Adams, Pauly, et al., 2000]. The facilitator of this integrated system is in situ consumable production (see Figure 6-13).

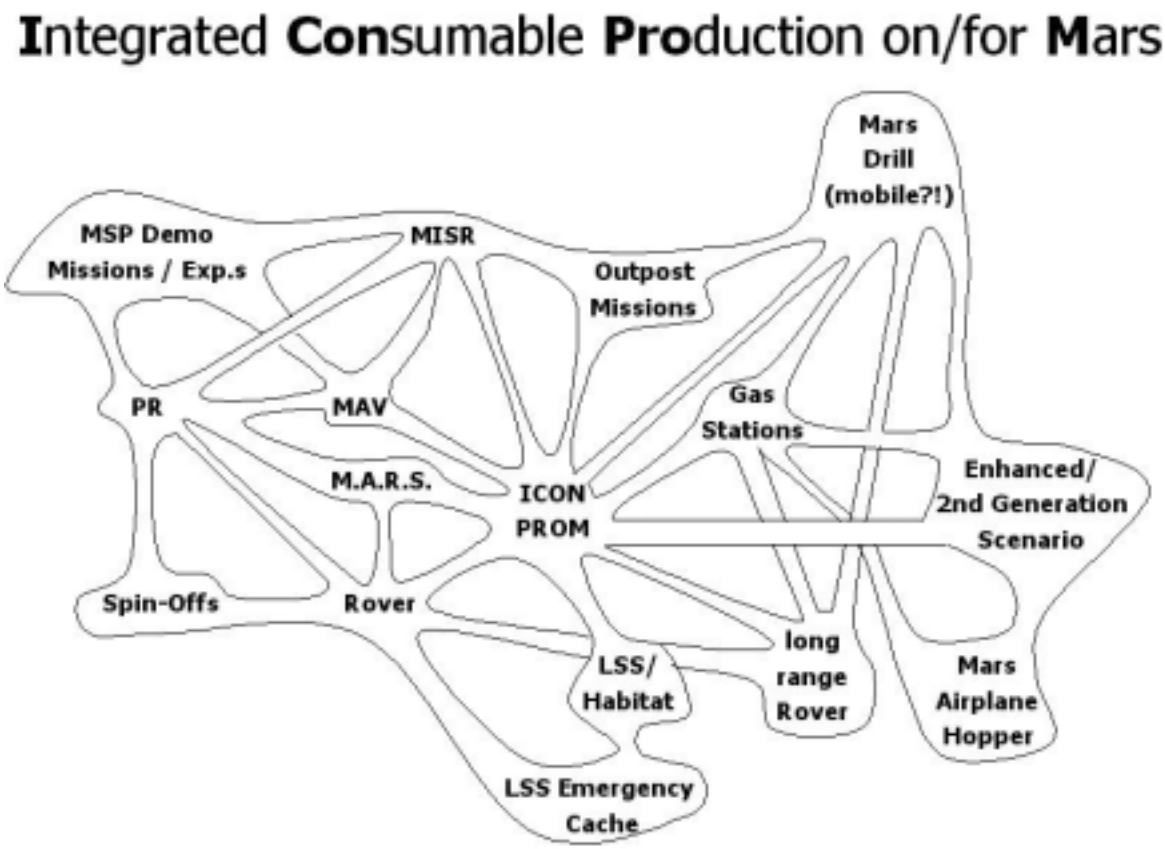

Figure 6-13: Integrated Consumable Production for/on Mars (IConProM)

How can this concept now be put into practice? On an engineering level, this can be achieved for example by the integration of the following subsystems into one integrated "big picture", as outlined in the example shown in Figure 6-14.

This graphic describes the application of IConProM in the context of a DRM-like scenario in which a cargo lander (in light red, right) with an ISCP plant aboard is pre-deployed on Mars prior to the manned mission (in light green, left). Before the latter one is sent to Mars, the former one produces life support system consumables, ascent vehicle and rover propellants, as well as an emergency consumables & energy cache. The cryogenic fluids (hydrogen, methane, oxygen) are liquefied and stored utilizing a coldhead ("C.H.") similar to the one employed during the testing of the 1st generation breadboard. The amount of required seed hydrogen mass that needs to be imported is decreased with the help of recycling using electrolysis, hydrogen recovery pump, and pyrolysis[1]. The production of chemical propellants avoids the drawbacks in performance that are inherent to the use of electrical rover propulsion, as well as the political impediments that are inherent to the use of plutonium radioisotope thermoelectric generators (compare with the demonstrations in the context of the Cassini/Huygens launch, described in [Simpson, 1998]). The re-use of landers as surface transportation systems ("hoppers") becomes conceivable now, too, whereas the use of cryogenic fluids can potentially open up the

[1] The pyrolysis is also employed to adjust the oxygen to methane ratio (compare chapter 2.4.1).

door to a drastic efficiency increase in combustion engines, since the turn obsolete the power lost usually connected to the compression cycle. It also significantly decreases the mass that has to be landed on the Martian surface in order to enable the crew to return to Earth[1].
Once the hab has landed, the crew can take full advantage of the pre-deployed logistics-infrastructure. The fluids that are needed and that are produced in the life support system part of the mission are the same that characterize its in situ propellant production part. The two systems are connected via the rover which can transport methane from and water to the hab. This philosophy of connecting ECLSS and ISPP leads to additional synergy opportunities. The methane – up to now a waste product in Sabatier-based life support systems - does not need to be vented anymore now, but can serve as a valuable resource, e.g. as a fuel for ascent vehicle and rover propulsion systems, as well as a contingency cache fluid, which provides the crew with energy and water in the case of an emergency. On the other hand, if the mission can be accomplished without contingencies, the unused emergency cache can provide the backup function for follow-on missions, eliminating the need for the import of significant amounts of mass for them; instead, in this case, additional payload capacity is made available, which would have not been obtainable normally.

But IConProM can be pushed even further, as outlined in Figure 6-15. Here the functions of life support and in situ propellant production are completely integrated. This can be done in renunciation of the DRM paradigm of a split scenario, in which ISPP systems are pre-deployed separate from the hab, or in the course of a follow-on human Mars mission, in which existing hardware on the Martian surface deployed by predecessor missions can be assumed. In this scenario, hab and ISCP plant are flown together, which allows for further synergies and simplification. Separate methane and water storage systems become obsolete, as well as parallel CO_2 acquisition systems, Sabatier reactors, condensors, electrolyzers, etc. for ECLSS and ISPP; and - not to forget - the transport requirement between them.

The power required to put IConProM into practice has to be made available by a surface power system with a power output in the order of 75 to 120kW. While recent and ongoing studies conducted by [Bailey, 2000] of NASA Glenn Research Center suggests that advanced solar power systems are able to provide these power levels, the problems with the automatic deployment of such large arrays will probably result in the need for an initial surface power source based on nuclear fission as outlined in [Eckart, Pauly, et al., 2001]. During follow-on missions succeeding the first cargo mission however, when astronauts can assist the deployment of ever increasing solar array areas on the surface of the Red Planet, solar power sources will allow for a stepwise increase of the non-nuclear percentage in the total power budget.

[1] Compare “Ticket Home Mass” in [Pauly, 1998a]

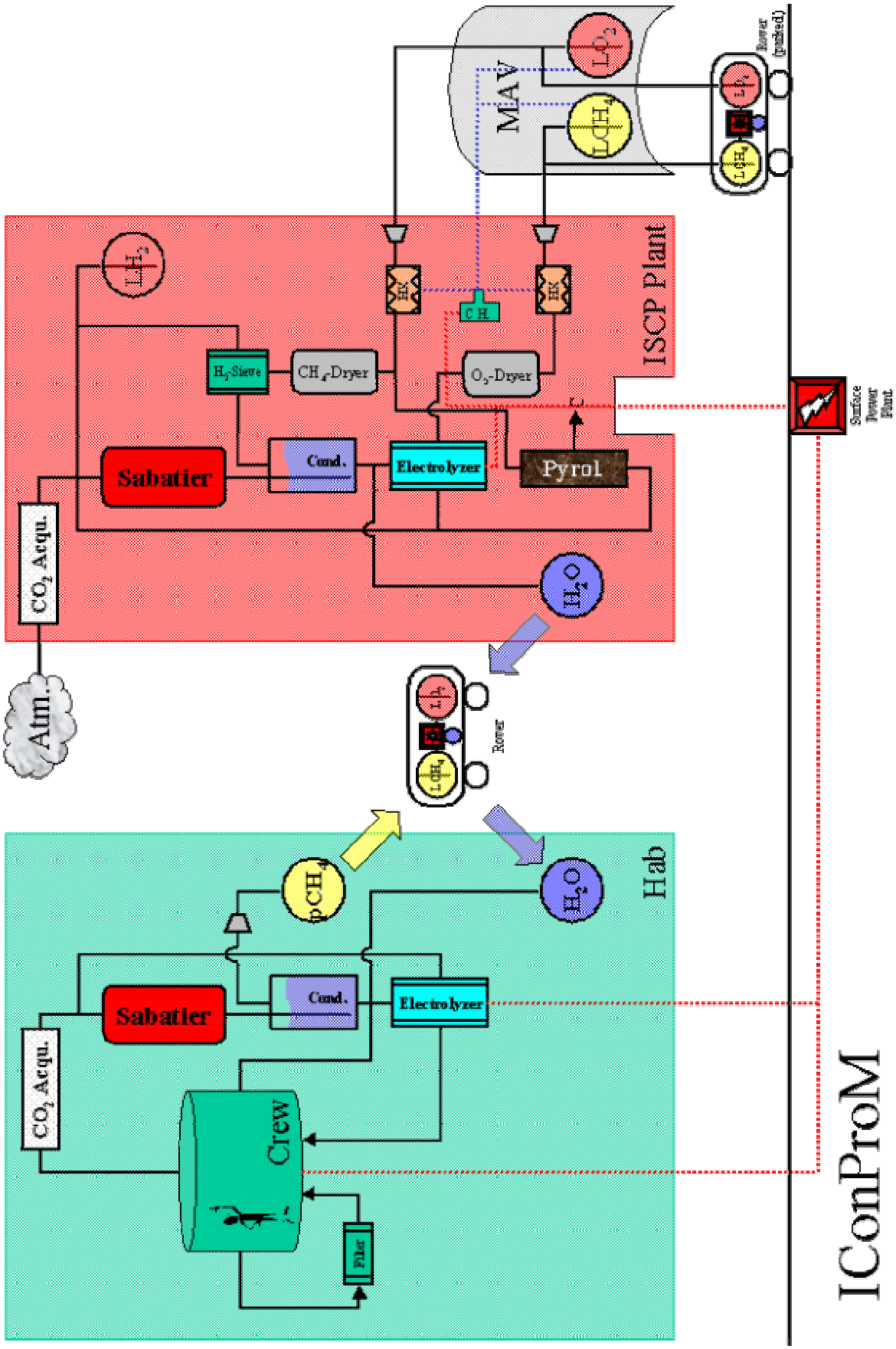

Figure 6-14: IConProM in Practice – Application in a DRM Scenario

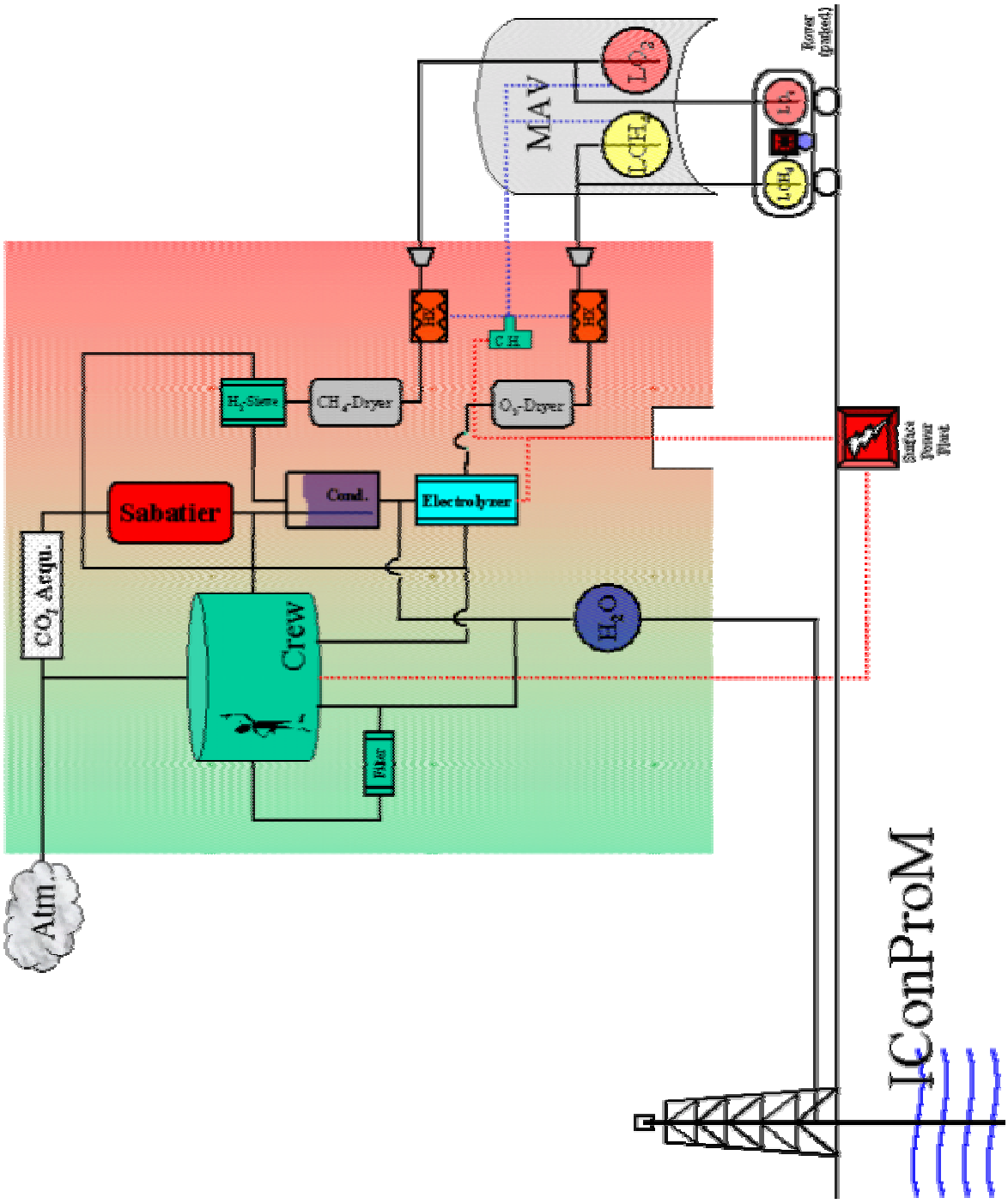

Figure 6-15: IConProM - Integrating ECLSS and ISPP Functions

6.4.3 Beyond Sabatier and Mars

Finally, it has to be noted that the concept of In Situ Resource Utilization should by all means not be limited to neither the Sabatier process nor the Martian Atmosphere. The offerings of resources on Mars available for use is rich, as can be seen in the list of potential sources for Martian water:

- The soil samples investigated by the Viking landers, in particular the GCMS, are likely to be good representatives of **average Martian soils**. In these samples, between 0.1% and 1% of the mass is water. In order to release this bound water, it takes some 10.3kWh of heat per kilogram of gained water [Stoker et al., 1993]. The actual water content of Martian soils however could be up to 10% or 15%, especially in buried soils, which of course would reduce the amount of heat to be invested per kilogram of water.
- If **permafrost** (underground ice) is found in shallow depths on Mars, this would represent a true gold mine for Martian exploration, since it would simplify human Mars missions in various aspects. Chances for finding permafrost in shallow depths are not bad, in particular in higher latitudes, as shown in Figure 6-16:

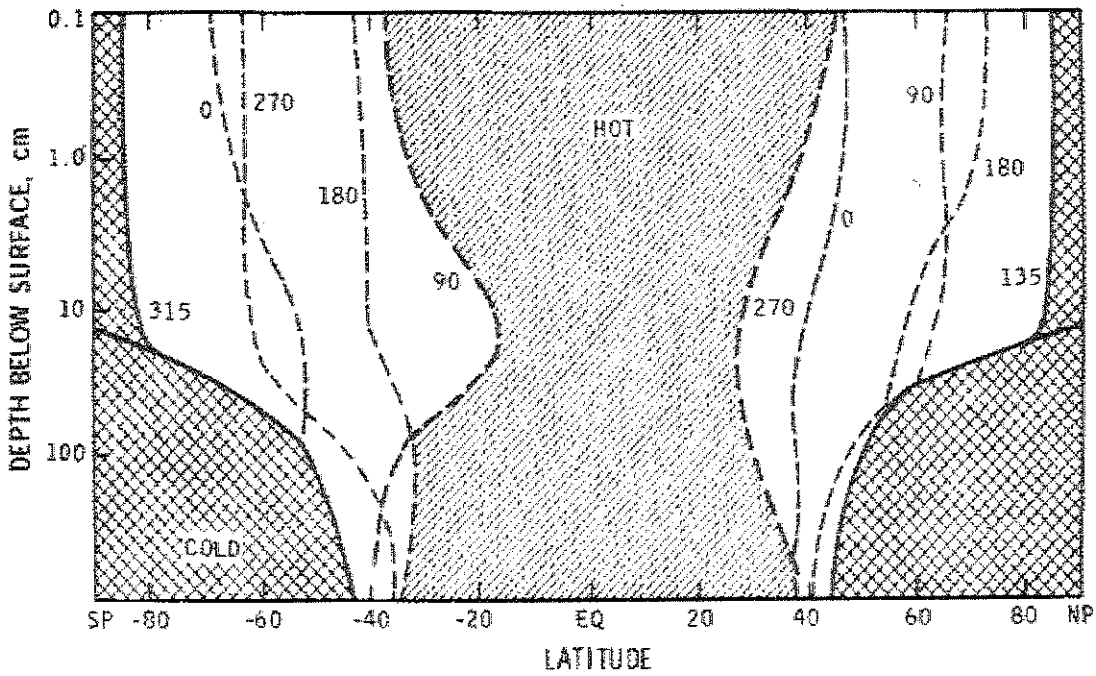

Figure 6-16: Stability of Sub-Surface Ice on Mars [Farmer & Doms, 1979]

The cross-hatched region is where sub-surface ice should be stable all year (the numbers represent the true anomaly in degrees). Hence, permafrost can be expected to be stable in near surface depths (deeper than approximately 10m) in latitudes around and higher than some 40°. [Squyres, 1999] points out that this may also vary greatly from site to site; ice could therefore also be stable in equatorial regions in greater depths (some 100m, exact depth depended on diffusion rates / porosity), or at so-called "hot-spots" respectively. This however has yet to be confirmed, e.g. by the radar experiment on Mars Express (to be launched in 2003).

- Even if free ice is not present, soil minerals like clays, oxyhydroxides, etc. could contain, in addition to absorbed water, several hydroxyl (-OH) groups. In the case of **hydrated clays**, this can be as much as and over 20% structurally bound

water [Baker et al., 1993]. Clays must be heated to 500°C, however due to the higher content, the amount of heat to be invested per kilogram of water could again be reduced.

- **Salt-rich solids** may contain as much as some 10% of water. Likely salts on the Martian surface include epsomite ($MgSO_4 \cdot 7H_2O$, 30.9m% water), gypsum ($CaSO_4 \cdot 2H_2O$, 33.3m% water), and hydrohalite ($NaCl \cdot 2H_2O$, 38.1m%) [Baker et al., 1993].
- **Clathrates** may contain significant amounts of water and/or methane (methane clathrates also have been found on terrestrial ocean floors and are considered a promising energy source for the future).
- But even in equatorial regions, water may be accessible in the vicinity of **hydrothermal systems** or "hot spots". The working principles of these systems are only poorly understood and remain an interesting subject for future investigation.

Concepts for the extraction of underground water were suggested by various authors. [Meyer et al., 1984] outline a simple, bulldozer-based scenario, in which only slightly less than 1% of the total energy is required to run the bulldozer and the conveyor; the major part is invested in the actual heating of the regolith. [Gwynne et al., 1991] suggest a microwave-based mining, which could increase the energy-efficiency of the water exploitation even further.

It might appear reasonable to ask whether it is possible to extract water directly from the Martian atmosphere as promoted e.g. by [Grover & Bruckner, 1998]. However, it is questionable whether the concept featured in this work will work as described. Based on more realistic assumptions, [Meyer et al., 1984] describe a system using successive cycles of cooling and compression. Here the difficulty is that the mixing ratio of water in Martian air is very small (<10ppm average) and thus huge volumes of air must be processed in order to obtain water at a energy cost of 102.8 kWh/kg, more than ten times higher than from regolith. A detailed analysis and evaluation of the atmospheric water acquisition concept in [Pauly, 1998a] shows that it is not competitive in comparison to other ISRU options such as SOEC or Sabatier / Water Electrolysis.

Water is of course not the only resource and oxygen can not only obtained from the atmospheric carbon dioxide. The regolith found on Mars is highly oxidized, and particularly iron oxides can serve as an valuable source for oxygen. The reduction of iron oxides, namely Fe_2O_3, can be achieved with hydrogen:

$$Fe_2O_3 + 3H_2 \rightarrow 2Fe + 3H_2O$$

The iron of course is everything but a waste product. It can be the basis for in situ produced steels, while the water can either be used directly or led into an electrolyzer which recycles the hydrogen and produces oxygen.

CO, the waste product of the oxygen producing solid oxide electrolysis cells can also put to good use here. -instead of directly venting it the atmosphere, it can also reduce the iron oxide according to the corresponding equation:

$$Fe_2O_3 + 3CO \rightarrow 2Fe + 3CO_2$$

The last to reactions where suggested by [Stoker et al., 1993]. The oxygen has not to be separated from the iron completely in order to be available for use. Reducing Fe^{III+} to Fe^{II+} according to the equation

$$2Fe_2O_3 \rightarrow 4FeO + O_2$$

requires no reducing agents and less energy than the reduction to pure iron.

The preceding formulas can however not be employed directly, since the Fe_2O_3 is not found in pure form, but mixed with other solids. The evaluation of these concepts is not subject of this thesis. They are just mentioned her in order to illustrate the fact that there is in fact a plethora of valid options for Martian ISRU conceivable, which all call for closer investigation.

Taking it a step further, it has to be stated that ISRU is of course not only limited to Mars alone after all. Future robotic and human exploration mission also aim at the moon, Near-Earth Objects, Europa, and others. At all these places, ISRU could potentially be employed to reduce the effort of going there, staying there, and returning from there.

Finding lunar water was one of the goals of the EuroMoon 2000 / LunarSat mission concepts, whereas suggestions for in situ resource utilization on Near-Earth Objects are currently under review in the course of ESA's Solar System Exploration Initiative "Aurora" as outlined in [Eckart, Pauly et al., 2001].

The application of ISRU on Mars as well as on other extraterrestrial bodies, holds a great and promising potential for new, innovative ideas which hopefully will help to open up the "final frontier".

Based on the experience gained during the development of the computer models and the conducting of tests under ambient and simulated Martian environment, recommendations were given for the design of follow-on breadboards and of flight demonstrator experiments, as well as of hardware for robotic and human missions in the far future.

7 CONCLUSIONS

Missions to Mars - in particular human missions - are among the most challenging endeavors ever attempted by man. They consist of a plethora of different subsystems, all together culminating in an effort of extraordinary size. In situ resource utilization (ISRU), in particular in situ consumable production (ISCP), can significantly reduce this effort. Goal of this thesis was to model such a system on the computer and to evaluate the performance of real hardware as well as the model with the help of tests in Earth ambient as well as simulated Martian environment, conducted during a research stay at NASA Johnson Space Center between January 1999 and May 2001.

Modeling

The ruthenium-catalyzed Sabatier reaction

$$CO_2 + 4H_2 \rightarrow CH_4 + 2H_2O\ (+ E)$$

was modeled taking into account both axial as well as radial heat transfer in the course of a two-dimensional computer model using the Gibbs free energy equilibrium analysis, as well as the "Λ_r method" introduced by [Vortmeyer et al., 1999] for a better calculation of the reaction and transfer phenomena within the reactor.

The Λ_r method has proven to be very useful, especially in combination with the chosen reaction rate determination method. The complexity of the involved chemical and physical processes prohibited the modeling in three dimensions (with time as the third dimension), however qualitative predictions for the transient behavior can certainly be made, and the approach to achieve a quantitative modeling of the transient behavior of the various processes is pointed out.

Testing

In the course of the tests conducted in the Mars ISRU Systems Test Facility of NASA Johnson Space Center, in situ consumable production (ISCP) has proven itself as an enabling technology. During the time period of the making of this thesis, no showstoppers or major technical obstacles were be found. The test were in accordance with the predictions given by the computer model. The Sabatier-based consumable production from the indigenous resources of Mars made a significant step towards its flight-readiness for a demonstrator experiment to be flown aboard a Mars lander; although more testing and development has to be accomplished in order to bring Sabatier to that technology readiness level, it can nevertheless undoubtedly be stated that ISCP in general and the Sabatier / water electrolysis in particular remain promising technologies that could and should play a crucial role in future space exploration - not only in the human exploration of Mars, but also of other celestial bodies.

Outlook

Based on the experience gained in the Mars ISRU Systems Test Facility at JSC, recommendations for the design of future breadboards, demonstrator experiments and other ISRU equipment have been given. At the commencement of the thesis work, the main aim of the efforts was the design of a demonstrator experiment to be flown aboard the 2003 Mars Lander. This plan was later postponed due to changes in the NASA Mars exploration program in favor of a follow-on ("2nd Generation") breadboard. Based on the experience and the modeling tools recommendations for its design were proposed and outlined – a design that is currently assembled at Johnson Space Center. Furthermore, the scope of this thesis engulfs a system layout for future Mars missions (both robotic and human) that opens up opportunities to use synergies between the different subsystems (e.g. between propulsion and life support) of such undertakings.

In situ consumable production can reduce mass, risk and cost. If the systems that are currently undergoing end-to-end testing (Sabatier / water electrolysis) and the systems that are flight-ready (Solid Oxide Electrolysis, as part of the Mars ISPP Precursor) can continue to prove their usefulness in the future, it is likely that the first human Mars missions will built upon these technologies.

ISRU is truly a generic, enabling technology; it can significantly enhance and expand robotic and human exploration by decreasing mass, cost, and risk of Mars missions. It can provide propellants for ascent and return vehicles, life support system consumables, increase surface mobility through production of Extra Vehicular Activity (EVA) consumables, reactants for fuel cell powered vehicles, propellants for hoppers, as well as emergency energy caches (for propellants, LSS consumables, as well electrical power and heat).

It is obvious that without in situ resource utilization a permanent presence of humans on Mars and beyond seems hardly feasible [James et al., 1998]. Consequently, ISCP is an integral part in the Mars exploration planning of both, NASA and ESA. The innovative concept of ISCP and "living off the land" is truly generic and certainly not limited to only Mars, but can also be employed at nearly every conceivable target of human space exploration, like for example moon, Near-Earth Objects, Europa, and others.

If man wants to explore deep space, he has to learn to use indigenous resources. Locking back, it has to be stated that this new concept of "living off the land" is in fact a very old one: the history of human exploration has always been a history of man utilizing his surrounding.

APPENDIX A: BREADBOARD FLOW SHEET FOR TESTS UNDER EARTH AMBIENT CONDITIONS

LTR	REVISION

CH4 and H2 out to
Cell 117 Fuel Vent Stack

O2 Vent Stack Cell 119

H2/CH4 Vent

3/8"

3/8"

HV3201

HV3205

G3204
0-3000 psig

G3205
0-60 psig

F3205

HV3200

C-3200

HR3204
0-100 psi

RV3205
Set 32 psig

SV3205

PT3205
0-50 psia

HV3203

HV3202

CV3202

GH2
K-bottles

To sys 324 PV1102 &
MV1106
(Vacuum Source)

RV3410
Set 32 psig

RV3415
Set 32 psig

RV3406
Set 50 psig

T3411

T3413

T3412

T3410

EV3410

EV3415

PT3410
0-10 torr

RV3220
Set 25 psig

T3220

PT3220

ER3401

SV3301

PT3301
0-60 psia

T3301

F3420

SV3420

FC3420

F3220

CV3220

EV3420

PT3420
0-50 psia

Sorption
Pump

T3407

T3406

HE3410

T3408

FC3405

RV3405
Set 50 psig

G3404
0-3000 psig

G3405
0-100 psig

CV3400

HV3400

HV3401

HR3404
0-100 psi

F3405

PT3405
0-100 psia

HV3405

HV3402

CV3402

HV3403

Mars Mix
K-bottles

To PV765 of
System 342

Cold GN2 In
from System 342

Sabatier
Reactor

T3321

T3322

T3323

H2 Recovery
Pump

T3826

TK3824

DP3324

T3824

SV3824

LS3824

DP3101

T3825

Electrolyzer

NO

SV3101

PT3101
0-60 psia

ER3402

T3101

RV3101
Set 15 psig

SV3102

BPR3102

O2
Dryer

NO

RV3301
Set 15 psig

SV3302

BPR3301

CH4
Dryer

RV3110
Set 10 psig

PT3110
0-50 psia

FM3110
0-5 SLPM

SV3110

T3110

T3111

T3112

CH

LS3110

SV3109

Vacuum
Source

Cryomech
Compressor

HV3611

Service
Port

HV3612

FH-1

FH-2

RV3120
Set 10 psig

EV3120

TK3110

SSC
Chamber &
Inside
Thermal Box

Process Sampling

SV3480

1/4"

SV3582

Mars Mix

SV3580

PT3580
50 psia

CO2

SV3380

3/8"

CH4

SV3581

To SSC
Chamber

RGA

SV3180

O2

Facility GN2 at 110 psig max

DR M.D.Reddington	4/22/99	TITLE	8Z003 ISRU Breadboard Assy		
ENG					
CH		DWG NO	353-8Z003-M1	REV A	SHEET 1 OF 1
APP					

ENERGY SYSTEMS TEST AREA

NATIONAL AERONAUTICS AND SPACE ADMINISTRATION JOHNSON SPACE CENTER HOUSTON, TEXAS

APPENDIX B: BREADBOARD FLOW SHEET FOR TESTS IN SIMULATED MARS ENVIRONMENT

LTR	REVISION

CH4 and H2 vented through vent stack on north side of building

1"
1/2"
3/8"
3/8"
HV3201
HV3205
G3204 0-3000 psig
G3205 0-60 psig
F3205
HV3200
C-3200
HV3203
HR3204 0-100 psi
PT3205 0-50 psia
RV3205 Set 32 psig
SV3205
HV3202
CV3202
GH2 K-bottles

RV3410 Set 30 psig
RV3415 Set 30 psig
RV3406 Set 50 psig
T3411
T3412
T3413
T3410
EV3410
EV3415
Sorption Pump
HTR1
T3407
HE3410
T3408
T3406
1/2"
To PV765 of System 342
Cold GN2 In from System 342
EV3420
F3420
SV3420
FC3420
T3220
PT3220 50 psia
F3220
FC3220
CV3220
FM3205 1000 sccm
Vent
1/2"
SV3301
DE
EN
PT3301 50 psia
T3301
ER3401
RV3301 Set 15 psig
SV3302
BPR3301
CH4 Dryer
1/4"
RV3110 Set 10 psig
Vent
O2 out to Cell 119 Vent Stack
1"
1/2"
Cryomech Compressor
HV3611
Service Port
HV3612
FH-1
FH-2
SV3110 NO
RV3120 Set 10 psig
T3110
T3111
T3112
CH
EV3120
Vent
LS3110
SV3109
Vacuum Source
TK3110

G3404 0-3000 psig
G3405 0-100 psig
RV3405 Set 50 psig
FC3405
CV3400
HV3400
HV3401
HR3404 0-100 psi
PT3405 0-100 psia
F3405
HV3405
HV3402
CV3402
HV3403
Mars Mix K-bottles

Sabatier Reactor
T3321
T3322
HTR5
CV3320
T3323
T3824
TK3824
DP3324
SV3824
T3825
Electrolyzer
LS3824
DP3101
PT3420 0-50 psia
H2 Recovery Pump
RV3220 Set 25 psig
PT3221 100 psia
T3826
SV3101
HTR6
PT3101 50 psia
T3101
ER3402
DE
EN
RV3101 Set 15 psig
SV3102
BPR3102
O2 Dryer
HTR7
FM3110 500 sccm
PT3110 0-50 psia
HTR2
HTR3
HTR4

SSC Chamber & Thermal Shroud

S/E Thermal Insulation box

G3504 0-3000 psig
G3505 0-100 psig
RV3505 Set 50 psig
FC3505 5 slpm
FH3500
HV3500
CV3500
HR3505
HV3501
F3505
PT3505 0-100 psia
HV3505
FH3502
HV3502
CV3502
HV3503
HV3510
Mars Mix or CO2 K-bottles

Process Sampling

Inside S/E Thermal Insulation box

SV3480 NC
1/4"
Mars Mix
SV3580 NC
CO2
SV3380 NC
CH4
SV3180 NC
O2
PT3580 50 psia
SV3581 NC
Test Port
HV1115 (Sys. 324)
HV1114 (Sys. 324)
SV3582
RGA

DR M.D.Reddington	11/15/00	TITLE 8Z003 ISRU Breadboard Assy		
ENG				
CH		DWG NO 353-8Z003-M1	REV F	SHEET 1 OF 1
APP				

ENERGY SYSTEMS TEST AREA

NATIONAL AERONAUTICS AND SPACE ADMINISTRATION JOHNSON SPACE CENTER HOUSTON, TEXAS

APPENDIX C: TEST PROCEDURE

C.1 Start Up

The following steps are performed each time test operations begin:

- Zero and span all instrumentation
- Synchronize breadboard and chamber computer clocks
- Set data recording interval
- Start data recording
- Announce area warning for operations in cell 116
- Contact operations controller and get authorization to switch facility status light.
- Verify/Set the facility status light to yellow.

C.2 Shutdown

The following steps are performed at the end of test operations:

- Verify/Perform the following:
  - Shutdown Propellant Production (see section C.23)
  - Shutdown Liquefaction Operations (see section C.21)
  - Shutdown Thermal Conditioning System (see section C.15)
- Verify/Set ER3401 and ER3402 to 0 psi
- Verify/Shut Off GN_2 supply to ER3401 and ER3402
- Verify all valve commands are off
- Set data recording interval to 5 or 10 seconds
- Verify O_2 dewar is empty of liquid and at ambient temperature
- Stop data recording
- Announce all clear in cell 116
- Notify operations controller of test completion to set the facility status light appropriately.

C.3 Set Up Ambient Test

The following steps prepare the test system and facility for breadboard operation with the subsystem chamber door open:

- Verify all system vents and relief valves outlets of O_2, H_2, CH_4 gases are routed out of the test cell
- Verify all LN_2 lines are insulated
- Verify the following monitoring equipment is in place, operational, calibrated, and set to the listed alarm levels (SMIP, H_2 1% max, CH_4 1% max, O_2 19.5% min and 23.5% max)
- Verify/Start forced ventilation of subsystem chamber

- Rope off the chamber doorway
- Verify/Perform the following:
  - Service Sorption Pump (see section C.7)
  - Set Up Mars Atmosphere Feed (see section C.8)
  - Set Up Hydrogen Feed (see section C.10)
  - Set Up Oxygen Dewar (see section C.13)
  - Set Up Thermal Conditioning (see section C.14)
- Set up GN_2 supply to ER3401 and ER3402 (<110 psig)
- Set up vacuum system to control to sorption pump vacuum (PT3410)
- Verify/Connect Sorption pump flow-through valve EV3415 to vacuum system.

C.4 Shutdown Ambient Test

Use these steps to perform a nominal shutdown from ambient test operations:

- Verify/Perform the following:
  - Shutdown Propellant Production (see section C.23)
  - Shutdown Liquefaction Operations (see section C.21)
  - Shutdown Thermal Conditioning System (see section C.15)
- Verify/Shutdown the following:
  - subsystem chamber vacuum system (system 324)
  - subsystem chamber thermal system (system 342)
  - 6000 gallon LN_2 Dewar (system 322)
- Remove rope from chamber doorway.

C.5 Set Up Mars Environment Test

The following steps prepare the test system and facility for breadboard operation with the subsystem chamber providing a partial Mars surface environment simulation:

- Verify all system vents and relief valves outlets for O_2, H_2, CH_4 are disconnected from their captured vents and the connections to the external vent stacks are capped
- Verify system and relief valve vents are directed out of the insulation box
- Verify H_2/CH_4 vents are separated from the O_2 vents
- Verify insulation on all LN_2 lines in the chamber is removed
- Verify/Install insulation box on S/E subsystem
- Set up vacuum system to control to subsystem chamber vacuum (PT tbd)
- Verify/Disconnect sorption pump flow-through valve EV3415 from the vacuum system.

C.6 Shutdown Mars Environment Test

The following steps perform a nominal shutdown from Mars environment test operations:

- Verify/Perform the following:
  - Shutdown Propellant Production (see section C.23)
  - Shutdown Liquefaction Operations (see section C.21)
  - Shutdown Thermal Conditioning System (see section C.15)
- Verify/Shutdown the following:
  - subsystem chamber vacuum system (see system 324)
  - RGA system.

C.7 Service Sorption Pump

These steps load adsorbent material into the sorption pump and prepare the pump for operations:

- Verify no pressure or vacuum is applied to sorption pump
- Remove sorption pump from test system
- Cap/Plug all open lines or ports
- Remove the top con-flat port on the sorption pump.
- Put on protective safety glasses and gloves prior to handling the adsorbent material (adsorbent material may cause skin irritation after prolonged skin contact).
- If replacing an adsorbent, remove the old adsorbent material from the sorption pump and store it in an appropriate container.
- Select the new adsorbent material to be used and record the type.
- Weigh approximately 3.0 kg or less of the adsorbent material in a small container and record the exact mass.
- Pour the adsorbent material into the sorption pump until filled.
- Record the exact final mass of the container.
- Repeat the last three steps until sorption pump is filled with adsorbent material.
- Calculate total weight of adsorbent in the sorption pump.
- Install the top con-flat port on the sorption pump.
- Install sorption pump according to drawing 353-8Z003-M1
- Leak check sorption pump subsystem.
- Perform Sorption Pump Bakeout (see section C.12).

C.8 Set Up Mars Atmosphere Feed

The following steps set up the Mars atmosphere feed required for ambient and Mars environment test operations:

- Verify/Close the following:
  - Mars atmosphere cylinder vent HV3401 & HV3403
  - Mars atmosphere feed purge/vent HV3405

  - Mars atmosphere cylinder isolation HV3400 & HV3402
  - Mars atmosphere feed controller FC3405
- Open one of the corresponding Mars atmosphere cylinder isolation valve HV3400 & HV3402
- Adjust HR3404 to G3405
- Cycle open then close HV3405 to purge the lines
- Verify HR3405 is still providing the pressure set above on G3405.

C.9 Shutdown Mars Atmosphere Feed

The following steps turn off the Mars atmosphere feed during shutdown of ambient and Mars environment test operations:

- Verify/Close
  - Mars atmosphere feed isolation FC3405
  - both Mars atmosphere cylinder valves
- Fully unload Mars atmosphere feed regulator HR3404
- Verify/Open the following:
  - Mars atmosphere cylinder vent HV3401 & HV3403
  - Mars atmosphere feed purge/vent HV3405
- Verify 0 psig indicated on the following:
  - Mars atmosphere supply pressure G3404
  - Mars atmosphere feed pressure G3405
- Verify/Close:
  - Mars atmosphere cylinder isolation HV3400 & HV3402
  - Mars atmosphere cylinder vent HV3401 & HV3403
  - Mars atmosphere feed purge/vent HV3405.

C.10 Set Up Hydrogen Feed

The following steps set up the hydrogen feed required for ambient and Mars environment test operations:

- Verify/Close the following:
  - H_2 cylinder vent HV3201 & HV3203
  - H_2 feed purge/vent HV3205
  - H_2 cylinder isolation HV3200 & HV3202
  - H_2 feed isolation SV3205
- Open one of the corresponding H_2 cylinder isolation valve HV3200 or HV3202
- Adjust HR3204 to G3205
- Cycle open then close HV3205 to purge the H_2 feed lines
- Verify HR3205 is still providing the pressure set above on G3205.

C.11 Shutdown Hydrogen Feed

The following steps turn off the hydrogen feed during shutdown of ambient and Mars environment test operations:

- Verify/Close:
  - H_2 feed isolation SV3205
  - both H_2 cylinder valves
- Fully unload H_2 feed regulator HR3204
- Verify/Open:
  - H_2 cylinder vent HV3201 & HV3203
  - H_2 feed purge/vent HV3205
- Verify 0 psig indicated on the following:
  - H_2 supply pressure G3204
  - H_2 feed pressure G3205
- Verify/Close:
  - H_2 cylinder isolation HV3200 & HV3202
  - H_2 cylinder vent HV3201 & HV3203
  - H_2 feed purge/vent HV3205.

C.12 Sorption Pump Bakeout

This section will be performed prior to the initial run with a new adsorbent material and as directed by the test manager:

- Close sorption pump inlet valve EV3410 and sorption pump outlet valve EV3420
- Verify/Connect sorption pump flow-through valve EV3415 to vacuum system
- Verify/Set up vacuum control on PT3410
- Verify/Set vacuum system to hold 6.5 torr
- Open the Sorption pump flow-through valve EV3415
- Set data recording interval to 5 to 10 seconds
- Turn on sorption pump heater (HTR1) and set T3412 to control to 350°F (the sorption pump may be damaged if the temperature exceeds 450°F).
- Verify internal temperature of the sorption pump T3412 reaches 350°F.
- Record time.
- Verify adequate bakeout time has elapsed.
- Turn off sorption pump heater (HTR1).
- Set data recording interval to 5 or 10 seconds
- Close Sorption pump flow-through valve EV3415.

C.13 Set Up Oxygen Dewar

The following steps evacuate the oxygen dewar and prepare it for liquefaction operations. Gifford-McMahon cryocooler set up procedure was derived from the Operation and Service Manual for the AL25 Cryomech Cryorefrigerator.

- Verify that dewar does not contain liquid oxygen.
- Verify dewar bottom temperature (T3112) indicates greater than -290°F
- Verify/Open O_2 dewar vent valve SV3110
- Verify dewar pressure (PT3110) indicates approximately 14.7 psia (ambient pressure)
- Verify/Close the following:
  - O_2 dewar liquid line valve EV3120
  - O_2 outlet isolation SV3102
  - O_2 dewar vent valve SV3110
- Connect vacuum pump to O_2 dewar vacuum isolation valve SV3109
- Verify/Open the following:
  - O_2 dewar vacuum isolation valve SV3109
  - vacuum pump isolation valve
- Evacuate dewar to less than reactor operating pressure on PT3110
- Close the following:
  - O_2 dewar vacuum isolation valve SV3109
  - vacuum pump isolation valve
- Verify/Connect cold head motor cord. Connecting/disconnecting motor cord when compressor is running may damage the connector, cold head motor, as well as the operator (high voltage arc).
- Verify/Connect all Aeroquip couplings securely
- Verify G-M Cryocooler compressor pressure is 205±5 psig on the Cryomech inlet and outlet gages
- Verify/Connect G-M cryo-cooler compressor to facility power.

C.14 Set Up Thermal Conditioning

The following steps configure thermal conditioning system 342 and the LabVIEW control for test operations:

- Verify/Open cell 116 doors
- Configure system 340 to supply actuation pressure for system 342 pneumatic valves
- Verify/Close all system 342 pneumatic valves:
  - Thermal system liquid control PV500
  - Thermal system gas control PV600
  - Thermal box front side control PV715
  - Thermal box front loop control PV725

  - Thermal box middle loop control PV735
  - Thermal box back loop control PV745
  - Thermal box back side control PV755
  - Martian atmosphere/sorption pump thermal control PV765
- Configure system 322 to supply 150 psig LN_2/GN_2 to PV500 and PV600, respectively
- Slightly Open HV500 to reduce pressure buildup from LN_2 boil-off.

C.15 Shutdown Thermal Conditioning System

Use these steps to perform a nominal shutdown of the thermal conditioning system 342:

- Shut off supply from system 322
- Open at least one of the system 342 pneumatic valves PV7x5
- Close the following:
  - Thermal system liquid control PV500
  - Thermal system gas control PV600
- Shut off supply from system 340.

C.16 Ambient Adsorption

The following steps charge the sorption pump with 100% CO_2 without use of thermal control:

- Verify/Perform Set Up Mars Atmosphere Feed (see section C.8)
- Verify/Set CO_2 inlet flow control FC3420 to 0 sccm
- Verify/Close Sorption pump flow-through valve EV3415
- Verify/Open the following:
  - Sorption pump inlet valve EV3410 / outlet valve EV3420
  - CO_2 feed isolation valve SV3420
- Set simulated Mars atmosphere flow (FC3405) to 770 sccm
- Verify PT3420 and PT3405 have equalized (FC3405 should indicate flow has stopped)
- Set simulated Mars atmosphere flow (FC3405) to 0 sccm
- Close sorption pump inlet valve EV3410
- Set sorption pump heater (HTR1) control to maintain sorption pump pressure (PT3420), but do not allow sorption pump temperature (T3412) to exceed 450°F.

C.17 Sorption Bypass Flow

The following steps set up 100% CO_2 flow through the sorption pump to the S/E subsystem; bypassing the sorption process:

- Verify/Perform Set Up Mars Atmosphere Feed (see section C.8)
- Verify/Set CO_2 inlet flow control (FC3420) to 0 sccm
- Verify/Close sorption pump flow-through valve EV3415

- Verify/Open the following:
  - Sorption pump inlet valve EV3410 / outlet valve EV3420
  - CO_2 feed isolation valve SV3420
- Set simulated Mars atmosphere flow (FC3405) to 770 sccm.

C.18 Full Adsorption

The following steps allow the simulated Mars atmosphere to flow through the sorption pump so that CO_2 is adsorbed:

- Verify/Perform Set Up Mars Atmosphere Feed (see section C.8)
- Verify/Set thermal system to control sorption pump external temperature (T3406) to -170 to -10 °F
- Verify/Set vacuum system to hold 6.5 torr
- Verify/Close sorption pump outlet valve EV3420
- Verify/Open the following:
  - Sorption pump inlet valve EV3410
  - Sorption pump flow-through valve EV3415
- Set data recording interval to 5 to 10 seconds
- Set simulated Mars atmosphere flow (FC3405) to 1000 sccm
- Monitor sorption process for some 1 to 2 hours to charge the sorption pump with CO_2
- Set simulated Mars atmosphere flow (FC3405) to 0 sccm
- Close the following:
  - Sorption pump inlet valve EV3410
  - Sorption pump flow-through valve EV3415 (the sorption pump is now charged with CO_2, thus increases of the sorption pump temperature may cause relief valves to open).
- Verify/Open the following:
  - Sorption pump outlet valve EV3420
  - CO_2 feed isolation valve SV3420
- Set sorption pump heater (HTR1) control to maintain sorption pump pressure (PT3420), but do not allow sorption pump temperature (T3412) to exceed 450 °F.
- Perform one of the following:
  - Desorption (see section C.19)
  - Propellant Production (see section C.22).

C.19 Desorption

The following steps desorb CO_2 from the sorption pump through the SE subsystem and out the CH_4/H_2 vent system. This section shall not be used for propellant production operations:

- Verify/Perform Shutdown Thermal Conditioning System (see section C.15)
- Verify/Close the following:
  - Sorption pump inlet valve EV3410

  - Sorption pump flow through valve EV3415
  - H_2 feed isolation valve SV3205
  - H_2 inlet flow control FC3220
  - Water transfer valve SV3824
- Verify/Open the following:
  - Sorption pump outlet valve EV3420
  - CO_2 feed isolation valve SV3420
  - CH_4 outlet valve SV3302
- Verify/De-energize CH_4 dryer regeneration valve SV3301
- Set data recording interval to 5 to 10 seconds
- Set the CO_2 inlet flow control (FC3420) to 1000 sccm
- Set sorption pump heater (HTR1) control to maintain sorption pump pressure (PT3420) at slightly over 20 psia (dependent on Sabatier reactor pressure) but do not allow sorption pump temperature (T3412) to exceed 450°F (505K).
- Adjust CH_4 back pressure BPR3301 to some 19 psia (exact value dependent on the Sabatier reactor pressure) on PT3220
- Verify sorption pump is exhausted.
- Turn off sorption pump heater (HTR1)
- Set the CO_2 inlet flow control (FC3420) to 0 sccm
- Verify/Close the following:
  - Sorption pump outlet valve EV3420
  - CO_2 feed isolation valve SV3420
  - CH_4 outlet valve SV3302.

C.20 Liquefaction Operations

The following steps start the G-M cryo-cooler. They were derived from the Operation and Service Manual for the AL25 Cryomech Cryorefrigerator.

- Verify/Perform Set Up Oxygen Dewar (see section C.13)
- Verify/Close the following:
  - O_2 dewar dump valve EV3120
  - O_2 dewar vent valve SV3110
  - O_2 dewar vacuum isolation valve SV3109
- Set data recording interval to 5 to 10 seconds
- At no time should the high pressure be allowed to exceed 270 psig. Pressures above 270 psig will overload the compressor module and cause possible failure.
- A pressure differential should be noticed immediately between high and low pressure gauges. The pressure differential will decrease as the cold head cools down.
- When the cold head first starts up, it will make a mechanical tapping sound. This sound will gradually diminish as the cold head cools down.
- Turn On G-M cryo-cooler or set control of power to the G-M cryo-cooler to maintain 18 psia in dewar (PT3110)
- Monitor compressor pressure periodically during operation for sudden changes.

C.21 Shutdown Liquefaction Operations

Use these steps to shutdown and secure the oxygen liquefaction system and dewar.

- Shut off power to G-M crycooler
- Verify O_2 dewar pressure (PT3110) is greater than 14.7 psia
- Verify/Open O_2 dewar vent valve SV3110.

C.22 Propellant Production

The following steps operate the sorption pump in desorption mode, perform the chemical conversion of CO_2 and H_2 in the Sabatier reaction, liquefy the O_2 product, and vent the methane product:

- Verify/Perform one of the following:
  - Ambient Adsorption (see section C.16)
  - Sorption Bypass Flow (see section C.17)
  - Full Adsorption (see section C.18)
- Verify/Perform Set Up Hydrogen Feed (see section C.10)
- Verify/Open the following:
  - H_2 feed isolation valve SV3205
  - Sorption pump outlet valve EV3420
  - CO_2 feed isolation valve SV3420
  - CH_4 outlet valve SV3302
- Verify/De-energize CH_4 dryer regeneration valve SV3301
- Verify/Close water transfer valve SV3824
- Set data recording interval to 5 to 10 seconds
- Set H_2 inlet flow control FC3220 to XXX sccm (50 to 200 sccm)
- Adjust CH_4 back pressure BPR3301 to XXX psia on PT3220
- Set Sabatier reactor heater (HTR5) to XXX °F on T3321 (500 to 800°F)
- Verify Sabatier reactor temperature (T3220) exceeds 150°F
- Set data recording interval to XXX seconds
- Set the following:
  - CO_2 inlet flow control FC3420 to XXX sccm
  - H_2 inlet flow control FC3220 to XXX sccm
- A rapid increase in T3220 indicates reaction is started.
- Verify water production by an increase in tank level (DP3324)
- If desired, power up hydrogen recovery pump HRP1 to ~0.8 to 1.0 volt
- Verify Sabatier reactor temperature (T3220) > 230°F / 110°C
- Turn off power to the Sabatier reactor heater (HTR5)
- Set data recording interval to XXX seconds
- Perform propellant production for XXX hours.

C.23 Shutdown Propellant Production

The following steps shutdown the Sabatier reactor, the hydrogen recovery pump, as well as the sorption pump subsystems:

- Adjust ER3401 to hold 15 psia on PT3301
- Verify 15 psia on PT3301
- Set the following:
  - CO_2 inlet flow control FC3420 to 0 sccm
  - H_2 inlet flow control FC3220 to 0 sccm
- Verify/Power off hydrogen recovery pump HRP1
- Turn off sorption pump heater (HTR1)
- Close the following:
  - H_2 feed isolation valve SV3205
  - Sorption pump outlet valve EV3420.

C.24 Electrolyzer Operations

The following steps operate the water electrolyzer to produce hydrogen and oxygen:

- Verify/Open O_2 outlet valve SV3102
- Verify/De-energize O_2 dryer regeneration valve SV3101
- Set data recording interval to XXX seconds
- Set electrolyzer voltage (V_{elec}) and current (I_{elec}) as needed until approximately 16A is obtained at the electrolyzer.
- Adjust electrolyzer output to match water production rate as indicated by steady water level (DP3324) indication
- Set ER3402 to hold PT3101 to PT3301 indication minus 0.5 to 1 psi
- If oxygen dryer pressure (PT3101) is greater than the methane dryer pressure (PT3301), water will be moved from electrolyzer to the water reservoir when the water transfer valve (SV3824) opens. This could cause electrolyzer to run dry and cause membrane damage.
- Set water transfer valve SV3824 to open for approximately 200 ms at 5 second intervals when DP3101 indicates less than 6 in. H_20.
- If water level gets high enough to press float against outlet filter, the vent hole is clogged and electrolyzer operations must be stopped until the vent can be cleared.
- Monitor H_2 side of electrolyzer and verify that excess water is vented out of chamber.

C.25 Shutdown Electrolyzer

The following steps turn off the electrolyzer:

- Set ER3402 to hold PT3101 to 15 psia
- Verify 15 psia on PT3101
- Power off the electrolyzer voltage and current

C.26 Process Sampling

The following steps operate the residual gas analyzer (RGA) sampling system to determine gas composition in various parts of the breadboard system:

- During the following operations only ONE of the following valves may be open at a time: Mars Mix sample SV3480, CO_2 sample SV3580, CH_4 sample SV3380, O_2 sample SV3180, and sample isolation SV3581.
- Verify/Calibrate the RGA sampling system
- Verify/Close the following:
  - Mars Mix sample valve SV3480
  - CO_2 sample valve SV3580
  - CH_4 sample valve SV3380
  - O_2 sample valve SV3180
- Verify/Open the following:
  - sample isolation valve SV3581
  - vacuum isolation valve SV3582
- Verify/Turn on the vacuum source at SV3582
- Verify XXX psia on sample volume pressure (PT3580)
- Close the following:
  - sample isolation valve SV3581
  - vacuum isolation valve SV3582
- Open one of the following:
  - Mars Mix sample valve SV3480
  - CO_2 sample valve SV3580
  - CH_4 sample valve SV3380
  - O_2 sample valve SV3180
- Verify stable pressure on sample volume pressure (PT3580)
- Close the sample valve again
- Verify/Close RGA isolation valve HV1114
- Verify RGA system is operating and ready to accept a sample
- Open sample isolation valve SV3581
- Record sample results
- Open the vacuum isolation valve SV3582.

C.27 Set Up Chamber Atmosphere Feed

The following steps set up the Mars atmosphere feed to the chamber required for Mars environment test operations:

- Verify/Close the following:
  - Chamber atmosphere cylinder vent HV3501 & HV3503
  - Chamber atmosphere feed purge/vent HV3505
  - Chamber atmosphere cylinder isolation HV3500 & HV3502
  - Chamber atmosphere bypass HV3510

  - Chamber atmosphere feed controller FC3505
- Open one of the following and the corresponding cylinder valve:
  - Mars mix cylinder isolation HV3500
  - CO_2 cylinder isolation HV3502
- Adjust HR3505 to XXX psig on G3505
- Cycle open then close HV3505 to purge the lines
- Verify HR3505 is still providing the pressure set above on G3505

C.28 Shutdown Chamber Atmosphere Feed

The following steps turn off the Mars atmosphere feed to the chamber required for Mars environment test operations:

- Verify/Close:
  - Mars atmosphere feed isolation FC3505
  - Chamber atmosphere bypass HV3510
  - both atmosphere cylinder valves
- Fully unload Mars atmosphere feed regulator HR3505
- Open the following:
  - Chamber atmosphere cylinder vent HV3501 & HV3503
  - Chamber atmosphere feed purge/vent HV3505
- Verify 0 psig indicated on the following:
  - Chamber atmosphere supply pressure G3504
  - Chamber atmosphere feed pressure G3505
- Verify/Close:
  - Chamber atmosphere cylinder isolation HV3500 & HV3502
  - Chamber atmosphere cylinder vent HV3501 & HV3503
  - Chamber atmosphere feed purge/vent HV3505

REFERENCES

Adams, C.M., M.R. McCurdy, K. Pauly, July 2000: “A proposal for Optimized Space Mission and Vehicle Design”, 00-ICES-2332, 30th International Conference on Environmental Systems, Toulouse, France.

Antonucci, V., P.L. Antonucci, A.S. Aricò, N. Giordano, 1996: “Partial Oxidation of Methane in Solid Oxide Fuel Cells”: An Experimental Evaluation”, Journal of Power Sources, Vol. 62.

Bequette, B.W.. 1998: “Process Dynamics: Modeling, Analysis, and Simulation”, Prentice-Hall, Inc., Upper Saddle River, NJ.

Bailey, Sheila, August 2001: Glenn Research Center, Personal Communication.

Baker, V.R., et al., 1993: "Water Resources and Hydrogeology of Mars", Resources of Near Earth Space, University of Arizona Press, Tucson, AZ.

Bayazitoglu, Y., et al., Sept. 1999: “Analytic Modeling of a Cryogenic Oxygen Tank and Curve Fitting H_2 Data”, Final Report, Mechanical Engineering & Materials Science Department, Rice University.

Becker, M., 1986: “Heat Transfer: A Modern Approach”, Plenum Press, New York.

Biran, A. & M. Breiner, 1999: “Matlab 5 for Engineers”, 2nd Edition, Addison-Wesley, Harlow, England.

Blake, F.C., B. Kozeny, P.C. Carman, 1937: “Fluid Flow Through Granular Beds”, Trans. Inst. Chem. Eng., 15, 150– 166.

Boyda, R.B., M.G. Lee, D.J. Grigger, July 1992: “The Sabatier Carbon Dioxide Reduction System for Space Station Freedom”, SAE Paper 921189, International Conference on Environmental Systems Seattle, WA.

Burke, A. & B. Plumme,r1922: “The Resistance of Packing to Fluid Flow” Trans. Am. Inst. Chem. Eng. **1**4, 415– 421.

Chambers, A., C. Park, R. Terry, K. Baker, N. Rodriguez, May 1998: “Hydrogen Storage in Graphite Nanofibers”, Journal of Physical Chemistry, Vol. 102, Nr. 22.

Connolly, John, 27. May 1998: “Mars Surveyor Program Update”, Johnson Space Center Contact Person to JPL Mars Surveyor Program Office, handout accompanying the briefing given to the Exploration Office, Houston.

Constantinides, A. & N. Mostoufi, 1999: “Numerical Methods for Chemical Engineers with Matlab”, Book News Inc., Portland, OR.

Crow, Steven C., July 6-9, 1997: “The MOXCE Project: New Cells for Producing Oxygen on Mars”, AIAA 97-2766, AIAA/SAE/ASME/ASEE 33rd Joint Propulsion Conference, Seattle.

Cyr, Kelly, 1998: Cost Estimation Group, Johnson Space Center Houston, Personal Correspondence.

Damköhler, G., 1936: “Einflüsse der Strömung, Diffusion und des Wärmeüberganges auf die Leistung von Reaktionsöfen”, Zeitschr. Elektrochem., 42(12), p. 846-862.

Damköhler, G., 1937: “Einfluß von Diffusion, Strömung und Wärmetransport auf die Ausbeute bei chemisch-technischen Reaktionen”, in “Der Chemie-Ingenieur”, Vol. III, A. Eucken & M. Jakob, Leverkusen.

Dennis, J.E. & R.B. Schnabel, 1983: “Numerical Methods for Unconstrained Optimization and Nonlinear Equations”, Prentice-Hall Inc., Englewood Cliffs, NJ.

Dew, J.M., R.R. White, C.M. Sliepcevitch, 1955: In. Eng. Chem., 47, 140.

Drake, Bret, 1998: Exploration Office, Johnson Space Center Houston, Personal Correspondence.

Drake, Bret, May 1998: “Reference Mission Version 3.0 / Addendum to the Human Exploration of Mars: The Reference Mission of the NASA Mars Exploration Study Team”, JSC Publication 28208, Houston.

DRM V3.0, 1993: NASA Design Reference Mission, Version 3.0:
http://exploration.jsc.nasa.gov/HumanExplore/Exploration/EXLibrary/docs/MarsRef/addendum/A3.htm

Eckart, P., K. Pauly, et al., 2001: “Framework of Human and Robotic Solar System Exploration”, ESA Contract # , Division of Astronautics, Technische Universität München.

Eckart, Peter, 1996: “Spaceflight Life Support and Biospherics”, Kluwer / Microcosm, Dordrecht, Netherlands / Norwell, MA.

Ergun, S., 1952: Chem. Eng. Progress, Vol. 48, p.89.

Ertl, G., H. Knözinger, J. Weitkamp, 1997: “Handbook of Heterogeneous Catalysis”, Vol. 1 through 5, VCH Verlagsgesellschaft mbH, Weinheim.

Exploration Design Project Team, 1999: “Out of the Cradle: An International Strategy for Human Exploration away from the Earth”, Final Report of the International Space University Summer Session 1999, hosted at Suranaree University of Technology, Nakhon Ratchasima, Thailand.

Frassanito, John & Associates, 1993: “Propellant Production from Mars Atmosphere”, NASA/JSC Image #S93-050643, Technical Concept Studies, NASA Planetary Missions and Materials Office, Johnson Space Center.

Frisbee, R.H., June 29 - July 23 1987: “Mass and Power Estimates For Mars In-Situ Propellant Production Systems”, AIAA 87-1900, AIAA/SAE/ASME/ASEE 23rd Joint Propulsion Conference, San Diego.

Gebhard, S.C., G. Alptekin, B. Hitch, J.D. Wright, June 1999: “Production of Liquid Hydrocarbon Propellants on Mars”, Contract No. NAS 9-99013, Phase 1 Final Report, TDA Research Inc., Wheat Ridge, CO.

Giese, M., 1998: “Strömung in porösen Medien unter Berücksichtigung effektiver Viskositäten”, Dissertation, Technische Universität München.

Giola, G., W. Chew, D. Ryder, December 1989: “Propulsion Systems Hazards Evaluation and Liquid/Gel Propulsion Componenet Development Program”, Volume IV - Executive Summary, TRW Inc., Final Report, Contract Number DAAH-01086-C-0114, Technical Report CR-RD-PR-90-1.

Grover, M. R. & A. P. Bruckner, July 13-15, 1998: “Water Vapor Extraction from the Martian Atmosphere by Adsorption in Molecular Sieves”, Paper No. AIAA 98-3302, 34th AIAA/ASME/SAE/ASEE Joint Propulsion Conference, Cleveland, OH.

Gwynne, O., et al., 1991: "Getting Water from Water of Hydration", Resources of Near Earth Space, Proceedings of the 2nd Annual Symposium, Tucson, AZ.

Hamilton Sundstrand, 2000: “Methanol Production Study”, prepared for NASA Johnson Space Center, Contract Ref.: T5272W.

Hanselman, D. & B. Littlefield, 1998: “Mastering Matlab 5”, Matlab Curriculum Series, Prentice Hall Inc., Upper Saddle River, NJ.

Hein, S., 1998: “Modellierung wandgekühlter katalytischer Festbettreaktoren mit Ein- und Zweiphasen-modellen”, Dissertation, Technische Universität München.

Himmel, S.C., J.F. Dugan, R.W. Luidens, and R.J. Weber, January 23-25, 1961: "A Study of Manned Nuclear-Rocket Missions to Mars," IAS Paper No. 61-49, paper presented in New York City at the 29th Annual Meeting of the Institute of Aerospace Sciences.

Himmelblau, D.M. & K.B. Bischoff, 1968: “Process Analysis and Simulation: Deterministic Systems”, John Wiley and Sons Inc., New York.

Hoffmann, S. & D. Kaplan, July 1997: “Human Exploration of Mars: The Reference Mission of the NASA Mars Exploration Study Team”, NASA Special Publication 6107, Houston.

Hsu, C.T. & P. Cheng, 19XX: “Thermal dispersion in a porous medium”, International Journal of Heat & Mass Transfer”, Vol. 37(6),p. 1587-1597.

James, G., G. Chamitoff, D. Barker, April 1998: ”Resource Utilization and Site Selection for a Self-Sufficient Martian Outpost”, NASA/TP-98-206538, Houston.

Jeng, F., 1995: “Modeling and Analysis of Test Data of the LSSIF CRS Subsystem”, Technical Memorandum, Contact NAS9-19100, Job Order 061-EC-CAA, Lockheed, Houston, TX.

Jeng, F., 1995: “ Modeling and Analysis of Test Data of the LSSIF CRS Subsystem”, Technical Memorandum, Lockheed, Contract NAS9-19100, Houston, TX.

Joosten, Kent, Ryan Schaefer, Stephan Hoffman, August 1997: “Recent Evolution of the Mars Reference Mission”, AAS/AIAA Astrodynamics Specialist Conference, Sun Valley.

Justus, C.G., B.F. James, D.L. Johnson: “Mars Global Reference Atmospheric Model (Mars-GRAM 3.34): Programmer’s Guide”, NASA Technical Memorandum 108509, May, 1996.

Kelley, C.T., 1995: “Frontiers in Applied Mathematics: Iterative Methods for Linear and Nonlinear Equations”, Society for Industrial and Applied Mathematics, Philadelphia, PA.

Kendall, K., 16.03.2000: “Hydrocarbon fuels: Hopes for a flame-free future”, Nature, Vol. 404.

Kuchling, H., 1996: “Taschenbuch der Physik”, 16. Auflage, Fachbuchverlag Leipzig.

Larson, Wiley J., 1999: “Human Spaceflight Mission Analysis and Design”, McGraw-Hill Inc., New York.

Larson, Wiley J., James R. Wertz (ed.), 1993: “Space Mission Analysis and Design”, 2nd Printing, Kluwer / Microcosm, Dordrecht, Netherlands / Norwell, MA.

Lauterbach, Jochen, 1998: Professor at the School of Chemical Engineering, Purdue University, Personal Correspondence.

Lewis, J., 1999: “Mining the Sky: Untold Riches from the Asteroids, Comets, and Planets”, Book News Inc., Portland, OR.

Lewis, J.S., et al. (ed.), 1993: "Resources of Near Earth Space", University of Arizona Press, Tucson.

Linden, D., 1984: “Handbook of Batteries and Fuel Cells”, McGraw-Hill, New York.

Lunde, P.J. & F.L. Kester, 1973: “Rates of Methane Formation from Carbon Dioxide and Hydrogen over a Ruthenium Catalyst”, Journal of Catalysis Vol. 30, p. 423-429.

Lunde, P.J. & F.L. Kester, 1974: “Carbon Dioxide Methanation on a Ruthenium Catalyst”, Ind. Eng. Chem., Proc. Des. Develop., Vol. 13, No. 1.

Lunde, P.J. , 1974: “Modeling, Simulation, and Operation of a Sabatier Reactor”, Ind. Eng. Chem., Proc. Des. Develop., Vol. 13, No. 3.

Malek-Madani, R., 1998: “Advanced Engineering Mathematics with Mathematica and Matlab”, Vol. 1, Addison-Wesley, Reading, MA.

MATLAB, 2000: “Matlab Online Manuals”, http://www.ee.siue.edu/HELP/matlab/fulldocset.html, Southern Illinois University.

Matthews, M.A. & P.S. Fedkiw, April 1997: “Workshop on Hydrogen Storage and Generation for Medium-Power and –Energy Applications”, Final Report, Workshop on Hydrogen Storage and Generation for Medium-Power and –Energy Applications, Orlando, FL.

Mayinger, F. & J. Straub, 1988: “Arbeitsunterlagen zur Vorlesung Wärme- und Stoffübertragung”, Lehrstuhl A für Thermodynamik, Technische Universität München.

McClean, Martin, 2001: Photo Collection of the MISTF Test Manager, Johnson Space Center, Source: Internal JSC Server, with friendly permission of NASA.

McClean, Martin, 1999: “Test Procedure In Situ Resource Utilization Breadboard”, NASA Doc. No. ESTA-T-8Z003, Rev. 0 (Draft), Energy Systems Branch, Johnson Space Center, Source: Internal JSC Server, with friendly permission of NASA.

Meyberg, K. & P. Vachenauer, 1991: “Höhere Mathematik 1”, Springer Verlag, Berlin.

Meyberg, K. & P. Vachenauer, 1991: “Höhere Mathematik 2”, Springer Verlag, Berlin.

Meyer, T.R. & C.P. McKay, 1984: "The Atmosphere of Mars – Resources for the Exploration and Settlement of Mars", The Case for Mars, ed. P.J. Boston, Univelt, San Diego, CA.

Meyer, T.R. & C.P. McKay, 1989: "The Resources of Mars for Human Settlements", Journal of the British Interplanetary Society42, 147-160, London.

Meyer, Tom, 1997: http://spot.colorado.edu/~meyertr/rwgs/rwgs.html

Meyers, G.E., 1971: “Analytical Methods in Conduction Heat Transfer”, McGraw-Hill, New York.
Minkowycz, W.J. & E.M. Sparrow, 1997: “Advances in Numerical Heat Transfer”, Vol. 1, Taylor and Francis, Washington, DC.

MISTF, 2000: Flow sheets of the Mars ISRU Systems Test Facility, Internal Document of NASA Johnson Space Center, Source: Internal JSC Server, with friendly permission of NASA.

Mitchell, K.L., December 1993: "Technical Assessment of the MIR-1 Life Support Hardware for the International Space Station", NASA Technical Report, NASA-TM-108441, NASA Marshall Space Flight Center, Huntsville, AL.

MoA, 2000: Homepage of the Ministry of Agriculture, Province of Alberta, Canada: http://www.agric.gov.ab.ca/research/researchupdate/97beef13.html

Mueller, P. & D. Rapp, April/May 1998: "Transportation of Hydrogen to Mars for In Situ Propellant Production", Draft, Paper for the 3rd IAA International Conference on Low-Cost Planetary Missions.

Mulloth, Lila M., John E. Finn, 1998: "Carbon Dioxide Adsorption on Zeolite for CO_2 Removal", Prepared for NASA by Lockheed Martin Moffett Field, NASA Technical Memorandum #NASA/TM-1998-208752.

Murray, E.P., T. Tsai, S.A. Barnett, 12.08.1999: "A direct-methane fuel cell with a ceria-based anode", Nature, Vol. 400.

Nernst, W., 1899: "Electrical Glow-Light", United States Patent No. 623811.

Nobel Foundation, 2000: Homepage on Nobel Laureates: http://www.nobel.se/chemistry/laureates/1912/sabatier-bio.html

Olson, Lynn, January 1997: "Boston NSS December Lecture Summary", Spaceviews, National Space Society, Boston Chapter, http://www.seds.org/spaceviews/9701/nss-news.html#1.

Palaszewski, B. & J.S. Zakany, July 1996: "Metallized Gelled Propellants: Oxygen/RP-1 Aluminum Rocket Heat Transfer and Combustion Measurements", NASA Technical Memorandum 107309, AIAA-96-2622, 32nd Joint Propulsion Conference, Lake Buena Vista, FL.

Palaszewski, Bryan, 1997: "Gelled Liquid Hydrogen", http://www.grc.nasa.gov/WWW/TU/launch/GELLED.htm, Lewis Research Center, Cleveland.

Palaszewski, Bryan, February 1997: "A Persuasive Wave of Future Propulsion Benefits", http://www.grc.nasa.gov/WWW/TU/launch/Propellant.htm, Lewis Research Center, Cleveland.

Palszewski, Bryan, 1998: Lewis Research Center, Personal Correspondence.

Pauly, Kristian, 1998a: "Mars Mission Scenarios Involving In-Situ Resource Utilization", Diplomarbeit 98/10 am Fachgebiet Raumfahrttechnik, Technische Universität München, in Cooperation with the Exploration Office, Johnson Space Center Houston.

Pauly, Kristian, August 1998b: „A Comparison of ISRU Options for the first Human Mars Missions", Mars Society Founding Convention, Boulder, Colorado.

Pauly, Kristian, October 1998c: „A Comparison of ISRU Options for the first Human Mars Missions", ExploSpace Workshop of Resource Utilization and Space Exploitation, Cagliari, Sardinien (ESA Outreach Programme Award).

Pitzer, K.S. & L. Brewer, 1961: "Thermodynamics, Lewis and Randall", 2nd ed., McGraw-Hill, New York, NY.

Plachta, David, 1998: Lewis Research Center, Personal Correspondence.

Plastic Services & Equipment, 2001: http://www.plasticservices.com/MoldingAcces/desicant.htm

PNL, 2001: http://www.pnl.gov/microcats/aboutus/research.html

Portree, David, Feb. 2001: “Humans to Mars: Fifty Years of Mission Planning”, Monographs in Aerospace History Series, No. 21, NASA SP-2001-4521.

Prado, M., 1998: “P.E.R.M.A.N.E.N.T. – Projects to Employ Resources of the Moon and Asteroids Near Earth in the Near Term”, Fong Tong Enterprise Co., Ltd., Bangkok.

Reichert, M., 1996: “Rahmenbedingungen für Kostenvorteile zukünftiger Raumfahrtprogramme bei Verwendung von Mond- und Marstreibstoffen”, Forschungsbericht 96-31, Deutsches Zentrum für Luft- und Raumfahrt, Köln.

Richter, R., 1981: “Basic Investigation into the Production of Oxygen in a Solid Oxide Electrolyte Process”, AIAA 81-1175, American Institute of Aeronautics and Astronautics.

Robinson, D.E. et al., July 1970: “System Analysis of Gelled Space-Storable Propellants”, Final Report, Contract No. NAS 7-473, SA-3, Prepared for NASA-HQ.

Ruppe, Harry O., June 6-7, 1963: "Data for Vehicle Design for Earth Orbit to Mars Orbit and Return," Exploration of Mars, George Morgenthaler, editor, pp. 151-173; proceedings of the American Astronautical Society Symposium on the Exploration of Mars, Denver, Colorado.

Ruppe, Harry O., 1982: “Die grenzenlose Dimension: Raumfahrt”, Econ Verlag, Düsseldorf.

Sabatier, Paul & J.B. Sendersen, 1902: Acad. Sci., 134, 689.

Sanders, G.B., J.R. Trevathan, D.I. Kaplan, T.A. Peters, R.S. Baird, J.S. Cook, M. McClean, K. Pauly, July 2000: “Development of In Situ Consumable Production (ISCP) for Robotic and Human Exploration at NASA Johnson Space Center”, 00-ICES-168, 30th International Conference on Environmental Systems, Toulouse, France.

Satterfield, C.N., 1991: “Heterogeneous Catalysis in Industrial Practice”, 2nd Edition, McGraw-Hill Inc., New York.

Schaefer, Ryan, June 1997: “Addendum to Mars Reference Mission V1.0”, Houston.

Schucan,, T.H., 2000: Paul Scherrer Institut, Zürich, Switzerland, Personal Correspondence.

SciAm, September 2001: “Nanotech – The Science of the Small gets down to business”, Scientific American, Special Issue.

Scott, Baird, April 2001: “In Situ Resource Utilization Primer”, Presentation to the Engineering Division Head, Johnson Space Center, Source: Internal JSC Server, with friendly permission of NASA.

Seborg, D.E., T.F. Edgar, D.A. Mellichamp, 1989: “Process Dynamics and Control”, John Wiley and Sons Inc., New York.

Seyfert, W., 1984: “Kinetische Untersuchungen zur Methanolsynthese im verbesserten Treibstrahlreaktor unter höheren Drücken”, Dissertation, Technische Hochschule Darmstadt.

Simpson, H., 1998: “Nuclear Safety Issues”, Burns Inc., Springfield, MA.

Simon, Thomas, 2001: 2nd Sabatier / Water Electrolysis Breadboard, Pro Engineer® Design Concept, Johnson Space Center, Source: Internal JSC Server, with friendly permission of NASA.

Smith, J.M., H.C. van Ness, M.M. Abbott, 1996: “Introduction to Chemical Engineering Thermodynamics”, 5th Edition, McGraw-Hill, New York.

Son, C.H. & R.S. Barker, 1992: ”Comparative Test Data Assessment and Simplified Math Modeling for Sabatier CO2 Reduction Subsystem”, SAE Technical Paper Series No. 921228, 22nd International Conference on Environmental Systems, Seattle, WA.

Starkovich, J., S. Adams, B. Palaszewski, July 1996: “Nanoparticulate Gellants for Metallized Gelled Liquid Hydrogen With Aluminum”, NASA Technical Memorandum 107280, AIAA-96-3234, 32nd Joint Propulsion Conference, Lake Buena Vista, FL.

Steinhoff, Ernst A., June 6-7, 1963: "Use of Extraterrestrial Resources for Mars Basing", in “Exploration of Mars”, George Morgenthaler, editor; Proceedings of the American Astronautical Society Symposium on the Exploration of Mars, Denver, Colorado, pp. 468-500.

Stoker, C.R., et al., 1993: "The Physical and Chemical Properties and Resource Potential of Martian Surface Soils", Resources of Near Earth Space, University of Arizona Press, Tucson, AZ.

Strumpf, H., C. Chin, G. Lester, S. Homeyer, 1991: “Sabatier Carbon Dioxide Reduction System for Long-Duration Manned Space Application”, SAE Technical Paper Series No. 911541, 21st International Conference on Environmental Systems, San Francisco, CA.

Subramanian, M., 2001: “Fluid Mechanics - Lecture Notes”, Department of Chemical Engineering, Sri Venkateswara College of Engineering, Sriperumbudur, Tamil Nadu, India, http://mca.svce.ac.in/~msubbu/FM-WebBook/Unit-IV/PresDropThroPackedBed.htm.

Toth, J. , 1971, Acta Chim. Acad. Sci. Hung., 69, 311.

UOP, 1996: “UOP / Union Carbide Technical Data Sheets”, UOP Molecular Sieve Division, Toronto.

von Braun, Wernher, 1956: “Start in den Weltraum”.

von Puttkamer, Jesco, 1996: “Jahrtausend Projekt Mars”, Umschau Verlag, Hamburg.

von Puttkamer, Jesco, 1997: “Der Mensch im Weltraum”, Umschau Verlag, Frankfurt am Main, p.132-142.

Vortmeyer, D., A. Krischke, E. Tsotsas, M. Winterberg, 1999: “A simple and coherent set of coefficients for modeling of heat and mass transport with and without chemical reaction filled with spheres”, Chemical Engineering Science, Vol. 55 (2000), p. 967-979.

Wagner, H., G. Tunc, and Y. Bayazitoglu, Sept. 2000: “A Model for Hydrogen Thermal Conductivity and Viscosity Including the Critical Point”, *Thermal Science and Engineering*, Vol. 8, No. 5.

Wagner, Howard, 2001a: Johnson Space Center, Personal Communication.

Wagner, Howard, 2001b: “Critical Point Pressure Sensitivity”, PhD Thesis Rice University, to published by UMI Dissertation Services, Houston.

Weber, R., 1988: “Wasserstoff: Wie aus Ideen Chancen werden”, Reportage der Informationszentrale der Elektrizitätswirtschaft (IZE), Frankfurt.

Wegeng, R.S., August 1999: “Definition Study for 2005 Mars Surveyor Program: Compact ISPP Plant based on micro chemical / thermal systems”, Batelle No. 32299, Battelle Institute, Richland, WA.

Wong, W., J. Starkovich, S. Adams, B. Palaszewski, June 1994: "Cryogenic Gellant and Fuel Formulation for Metallized Gelled Propellants: Hydrocarbons and Hydrogen with Aluminum", AIAA-94-3175, 30th Joint Propulsion Conference, Indianapolis, IN.

Worlund, A.L. et al., October 1968: "A Study of Hydrogen Slush and/or Hydrogen Gel Utilization. Volume I: Saturn S-IVC Manned Mars Flyby Vehicle Application Study", Final Report, Contract No. NAS 8-20342, Prepared for NASA-MSFC.

Zehner, P. & E.P. Schlünder, 1970: "Wärmeleitfähigkeit von Schüttungen bei mäßigen Temperaturen" in "Chemie-Ingenieur Technik", 42, p. 933-941.

Zubrin, R. & B. Frankie, T. Kito, 1997: "Mars Methanol In-Situ Propellant Production SBIR Phase I Study", NAS 9-97082, Pioneer Astronautics, Lakewood, CO.

Zubrin, R. & R. Wagner, 1996: "The Case for Mars", Simon & Schuster Inc., New York.

Zubrin, R., S. Price, L. Mason, L. Clark, 1995: "Phase III Final Report: An End-to-End Demonstration of a full scale Mars In-Situ Propellant Production Unit" Contract NAS 9-19145, Martin Marietta Astronautics, Denver, CO.